Investigation Of Neuronal Dysfunction In Parkinson's Disease Using Advanced Physiological Induced Pluripotent Stem Cells.

Thesis submitted for the degree of Doctor of Philosophy



Quyen Do

Lincoln College

Department of Physiology, Anatomy and Genetics

University of Oxford

Michaelmas Term 2022

Abstract

The study of Parkinson's Disease (PD) pathogenesis has been greatly facilitated by the revolutionary induced pluripotent stem cells (iPSC) technology which permits modelling of PD using human neurons and with human-specific genetics. However, current iPSC-derived models are still largely dependent on adherent monoculture of a single cell type with limited capacity to capture the complex neuronal microenvironment and the resulting plethora of cell-cell interactions evident *in vivo*. Here, I described attempts at establishing three different strategies of advanced culturing of iPSC-derived neurons, namely i) the striatal presynaptic microcircuit consisting of iPSC-derived medium spiny neurons (MSN), cortical and dopaminergic neurons , ii) human midbrain-like organoids (hMLO) and iii) the fluid-walled microfluidic-based corticostriatal pathway. The striatal microcircuit recapitulated the directed connectivity of the presynaptic landscape of MSN wherein both cortical and dopaminergic axons converged on the MSN. Electrophysiological recordings of the MSN of the striatal presynaptic microcircuit delineated the pro-maturational roles of cortical and dopaminergic inputs on MSN physiology, as well as the pathological effect of DaN harbouring PD-related *GBA N370S* mutation on inducing early and transient immature and hyperexcitable-like phenotype of the connected healthy MSNs. On the other hand, characterisation of the hMLO suggested expression of DaN of floor-plate origin surrounded by diverse subsets of neuronal and neural cells. However, hMLO derived from PD patients carrying the triplication of *SNCA* or the *N370S GBA* mutation lacked phenotypic DaN degeneration or synucleinopathy. Lastly, I recreated the corticostriatal pathway on the novel fluid-walled microfluidic platform. This provided the proof-of-concept of the possibility to recapitulating any neuronal circuits of interest in an open-access fashion free of the obstructive barrier apparent in conventional microfluidic approach, rendering it suitable for direct physical manipulation such as directed axotomy. Live monitoring of axon growth post directed axotomy suggested the positive effect of permissive

environment such as that induced by exogenously supplied brain-derived trophic factor (BDNF) or endogenous post-synaptic target (i.e. MSN) on cortical axon regeneration. Taken together, this work offers frameworks of novel advanced culture strategies that could be employed to improve neuronal maturation in *in vitro* modelling as well as to facilitate studies of network-dependent biological phenomena.

Acknowledgment

This DPhil has been an amazing journey not only of academic growth but also of personal development throughout which I have always been blessed with generous supports and encouragements from friends, families and colleagues.

First and foremost, I would like to extend my sincerest gratitude towards Prof Richard Wade-Martins for the opportunity to join the lab and to pursue a very stimulating project. His wealth of knowledge and incredible patience in dealing with my many simultaneous ideas and last minute requests have been very valuable to the blossoming and smooth sail of this work. I feel incredibly privileged to be able to learn a great deal from him. I am also indebted to Dr Nora Bengoa-Vergniory who has constantly supported me throughout my DPhil. Her resourcefulness, exceptional attention to details, and tenacity are purely inspirational to me. A huge thanks to Dr Ricardo Marquez Gomez for his invaluable support in the last year. His experience, positivity and remarkable creativity have always livened up our discussions to an unexpected note, both in and out of the lab.

The Wade-Martins lab has been a wonderful home for my last four years of research work and I cannot possibly express enough my gratitude towards everyone, past and present members, for having created such an academically stimulating and socially exuberant working environment. I am especially thankful to Dayne for breaking the thick ice of electrophysiology which becomes one of the dearest techniques of my work; to Naroa and Charmaine for their generous donation of dopaminergic neurons used in this work, to Natalia for advices on striatal differentiation; to Bryan for his help with the cortical differentiation protocol; to Maria Claudia, Kaitlyn, Mindaugas, Billy, Sandor, John, Ajantha and Fe for sharing experimental resources; to Stewart for his help with cloning and viral packaging; to Sarah and Milena for all logistic support, to Gabriela for general lab life advices and keeping my early Saturday morning

fencing routine fulfilled; and to Mootaz for the numerous life/science lessons and banters alike and all the beautiful memories spent in Oxford and elsewhere.

To my collaborator, Federico, I am grateful for being able work with and learn a great deal of bioengineering from him. His positivity and quirky sense of humour have made every working moment together thoroughly enjoyable and I feel honoured to have his friendship.

Thank you to the Agency of Science, Technology and Research (Singapore) for the National Science Scholarship (NSS) that made my DPhil pursuit financially bearable. A huge thanks to my fellow NSS friends, both in Oxford and across the Atlantic, who are always by my side throughout the decade-long academic pursuit ever since high school.

To those friends who have made my years in Oxford unforgettably one of the best chapters of my life, with all my love: Sam, Nina, Ewa, Wearn Xin, Bernie, Aniq, Valerian, Jieyan, Jingyi, Anh, Rashmi, Richie, Koichi, Amalie, Scott, Shu, Carl, Mika, Max and Natasha (of course not in any particular order).

And last, but by no means least, special thanks and enormous gratitude go to my dearest family, to Dad and Mum for their unconditional love and sacrifice, and my sister for her unshakeable faith and pride. To them, all my love.

Declaration

I hereby confirm that the work presented in this thesis is of my own and performed by the author at the University of Oxford. Where information has been derived from other sources or from collaboration, I confirmed that this has been indicated in the thesis. This work has not been submitted for any other degree in this or any other University

Collaboration

Part of this work (described in chapter 7) was done in collaboration with Federico Nebuloni, a DPhil candidate in Engineering jointly supervised by Prof. Peter Cook and Dr Edmond Walsh from the University of Oxford. Federico provided expertise developed in his lab and together with me, we performed the culture work on fluid-walled microfluidic platform.

Conference presentations

ARUK Dementia Research Day, *In vitro* modelling of neural circuits affected in Parkinson's Disease from induced pluripotent stem cells, 2019. *Poster*

The Cajal Advanced Neuroscience Training Programme – Advanced techniques for Synapse Biology, Modelling Parkinson's Disease using human iPSC-derived midbrain-like organoid, 2019. *Poster*

Ion channels in Synaptic and Neural Circuit Physiology, Cold Spring Habours Laboratory, Modelling human MSN using induced pluripotent stem cells, 2021. *Poster*

AD/PD 2022, An all iPSC-derived cortico-striato-nigral minicircuit on custom microfluidics, 2022. *Poster.*

FENS Forum 2022, Electrophysiological dysfunction of medium spiny neurons in in vitro human striatal circuit of Parkinson's Disease, 2022. *Poster.*

ISN-APSN 2022, iPSC-derived in vitro human striatal micro-circuit to understand *GBA-N370S* variant-associated Parkinson's Disease. *Poster.*

Europe SLAS 2023, Microfluidic Palette for in vitro Modelling Human Neuronal Circuit. *Selected talk.*

GRC Physics and Chemistry of Microfluidics 2023, In vitro modelling of human neuronal microcircuits on microfluidics revealed emerging neuronal properties. *Poster.*

Manuscripts

Do, Q. B., Ng, B., Gomez, R. M., Beccano-Kelly, D., Ibarra-Aizpura, N., Caiazza, M.-C., … Wade-Martins, R. (2023). Early striatal hyperexcitability in an in vitro human striatal microcircuit model carrying the Parkinson's GBA-N370S mutation. *BioRxiv*, 2023.03.01.530566. https://doi.org/10.1101/2023.03.01.530566 (Under review)

Do, Q[*]; Nebuloni, F[*].; Cook, P.R.; Walsh, E.J.; Wade-Martins, R. A fluid-walled microfluidic platform for human neuronal microcircuit and axotomy. *Contributed equally. In preparation.

Contents

Abstract **3**

Acknowledgement **5**

Declaration **7**

Collaborations **9**

Conference presentations **10**

Publications **11**

List of figures **18**

List of tables **20**

Abbreviation **20**

Chapter 1: Introduction

1.1. Parkinson's Disease

1.1.1. Clinical manifestation 27

1.1.2. Pathophysiology of Parkinson's Disease 28

1.1.3. Genetics of Parkinson's Disease

1.1.1.1. Identification of rare familial PD 29

1.1.1.2. Risk loci from genome-wide association study (GWAS) 31

1.2. The basal ganglia in Parkinson's Disease

1.2.1. Anatomy and neurophysiology of the basal ganglia and human striatum 34

1.2.2. Basal ganglia pathology in Parkinson's Disease 39

1.3. Induced pluripotent stem cell (iPSC) technology 41

1.4. iPSC-derived Parkinson's Disease modelling 43

1.5. Advanced modelling approaches of Parkinson's Disease 45

1.6. Aims 46

Chapter 2: Materials and Methods

2.1. Materials

2.1.1. Mammalian cells 49

2.1.2. Media formulations 51

2.1.3. Electrophysiological buffer and solution 52

2.1.4. Drugs 52

2.1.5. Lentiviral vectors 53
2.1.6. RT-qPCR primers 53
2.1.7. Primary antibody for immunofluorescence 55
2.1.8. Secondary antibody for immunofluorescence 56

2.2. Methods

2.2.1. Lentivirus packaging 56
2.2.2. Maintenance and expansion of iPSC 57
2.2.3. Coverslip preparation 58
2.2.4. Differentiation of iPSC into medium spiny neurons 58
2.2.5. Differentiation of iPSC into dopaminergic neurons 60
2.2.6. Differentiation of iPSC into cortical neurons 60
2.2.7. Differentiation of iPSC into human-like midbrain organoid (hMLO) 62
2.2.8. Rat cortical astrocyte expansion 63
2.2.9. Microfluidic fabrication 63
2.2.10. Immunofluorescence and imaging 64
2.2.11. Fontana-Mason staining 67
2.2.12. RNA extraction and RT-qPCR 67
2.2.13. Electrophysiology 68
2.2.14. Dendritic spine visualisation and quantification 70
2.2.15. Quantifying relative PKA activity 70
2.2.16. Cloning
i. Vector linearisation 71
ii. Insert polymerase chain reaction 72
iii. In-Fusion HD reaction 73
iv. Transformation 73
v. Colony screening 74
vi. Sequencing 75
2.2.17. Axotomy on fluid-walled microfluidics (FWM)
i. Fabrication of fluid-walled microfluidics 75
ii. Establishment of corticostriatal pathway 76
iii. Directed axotomy on FWM 77
2.2.18. Statistics 77

Chapter 3: Investigating effects of an all iPSC-derived cortico-striato-nigral micro-circuit on the functional maturation of MSN using custom 3-chamber microfluidics.

3.1. Introduction

3.1.1. *In vivo* development of medium spiny neurons (MSN) 79

3.1.1. Architecture of the striatal presynaptic microcircuit 80

3.1.2. Microfluidic technology for cell culture 81

3.1.3. Aims 81

3.2. Results

3.2.1. Generation and characterisation of iPSC-derived MSN from iPSC 82

3.2.2. Establishment of the striatal presynaptic microcircuit

i. Directed coculturing of iPSC-derived cortical neurons, MSN, and dopaminergic neurons on open 3-chamber microfluidic platform 94

ii. Effects of cortical glutamatergic inputs on MSN maturation *in vitro* 98

iii. Effects of dopaminergic projections on corticostriatal neuron maturation *in vitro* 102

3.3. Discussion

3.3.1. Generation of iPSC-MSN 106

3.3.2. Modular microcircuit model to dissect neurotransmitter functions 108

Chapter 4: Investigating temporal changes of striatal electrophysiological properties circuited with dopaminergic neurons habouring PD-related *GBA-N370S* mutation.

4.1. Introduction

4.1.1. Mutant *GBA-N370S*-habouring DaN 113

4.1.2. Striatal pathology in Parkinson's Diseases 114

4.1.3. Protein kinase A and striatum and PD 115

4.1.4. Aims 117

4.2. Results

4.2.1. Establishment of striatal presynaptic triad with mutant *GBA-N370S* dopaminergic neurons 117

4.2.2. Impact of mutant *GBA-N370S* dopaminergic neurons on MSN functional properties 118
4.2.3. Involvement of protein kinase A signalling in modulating striatal pathology 121

4.3. Discussion 125
4.3.1. Putative compensative mechanism of striatal micro-circuit 125
4.3.2. Putative pathological mechanism of *GBA-N370S* mutation 128

Chapter 5: Generation and characterisation of healthy control and familial PD-patient iPSC-derived hMLO

5.1. Introduction
5.1.1. Cerebral organoid 130
5.1.2. Midbrain organoid 131
5.1.3. α-synuclein pathology in familial Parkinson's Diseases 132
5.1.4. Aims 132

5.2. Result
5.2.1. Characterisation of iPSC-derived hMLO 133
5.2.2. Disease-modelling of familial PD patients-specific hMLO 140

5.3. Discussion 143
5.3.1. Generation of hMLO from iPSC 144
5.3.2. Synucleinopathy inn hMLO-based modelling of PD 146

Chapter 6: Generation and charaterisation of a custom human tyroxine-hydroxylase promoter-specific reporter in a viral expression system

6.1. Introduction
6.1.1. Biology of human tyrosine hydroxylase promoter 147
6.1.2. Current status quo of human TH promoter-driven reporter 148
6.1.3. Aims 149

6.2. Results

6.2.1. *In silico* generation of a custom human TH promoter 149

6.2.2. Generation and characterisation of a custom human TH promoter-specific reporter in lentiviruses 152

6.3. Discussion 155

Chapter 7: Advanced modelling neuronal microcircuit with fluid-walled microfluidic (FWM) platform

7.1. Introduction

7.1.1. Axon pathology and its relevance to PD 157

7.1.2. Axon injury and regeneration models on microfluidic platform *in vitro* 159

7.1.3. Fluid-walled microfluidic technology 160

7.1.4. Aims 160

7.2. Results

7.2.1. Fabrication and principles of fluid-walled dumbbell-shaped microfluidics 161

7.2.2. Recapitulation of human corticostriatal pathway on fluid-walled dumbbells 162

7.2.3. Independency of cortical axon outgrowth on target-derived signals 164

7.2.4. Effect of target-derived signals on the regeneration of axotomized iPSC-cortical axon 166

7.3. Discussion 169

7.3.1. Fluid-walled circuit for neuronal circuit modelling 170

7.3.2. Automatic axotomy assay using micro-jet on FWM 171

7.3.3. Target-dependent axonal physiology in health and PD 172

Chapter 8: Discussion 175

8.1. Advanced iPSC-derived cultures *in vitro*

8.1.1. Neuronal circuits on open-chambered microfluidics 175

8.1.2. Human midbrain-like organoid (hMLO) 176

8.1.3. Neural circuit on fluid-walled microfluidics (FWM) 178
8.1.4. Adoption of bioengineered tools to improve neural culture model 180
8.1.5. Future directions 180

8.2. Striatal pathology in PD

8.2.1. Early human striatal pathology in PD 182
8.2.2. Future directions 183

References **186**
Appendix **228**

List of figures

Figure 1.1: Schematic diagram of the intrinsic circuity of the motor circuit……
Figure 1.2: Schematic diagram of basal ganglia circuitry in healthy and Parkinson's Disease state in the classical model……

Figure 2.1: Map of lentiviral backbone used in the production of custom human TH promoter……

Figure 3.1: Schematics of iPSC-derived MSN differentiation paradigms……
Figure 3.2: Relative expression profile of cultures from different differentiation paradigms at DIV 5, 12 and 14. ……
Figure 3.3: Relative expression of selected genes between differentiation condition A versus B……
Figure 3.4: Effect of Activin A at DIV 12 on expression of selected genes on DIV 14 cultures……
Figure 3.5: DIV 35 MSN characterisation by CTIP2 and DARPP32 co-expression across different healthy control iPS cell lines……
Figure 3.6: Characterisation of DIV 35 MSN derived from four different healthy control iPS cell lines across various differentiation conditions by expression of Dopamine 1 receptor (D1R), Calbindin (CB), and GAD67……
Figure 3.7: Generation and characterisation of iPSC-derived MSN.……
Figure 3.8: Characterisation of MSN subtypes……
Figure 3.9: Characterisation of iPSC-derived cortical neurons……
Figure 3.10: Characterisation of iPSC-derived dopaminergic neurons……
Figure 3.11: *In vitro* recapitulation of directed striatal presynaptic triad using microfluidics……
Figure 3.12: Co-culturing with iPSC-derived cortical neurons improved synaptic activities and dendritic spine morphology of iPSC-derived MSN……
Figure 3.13: Dopaminergic neurons triggers the intrinsic maturation of iPSC-derived MSN during a critical period……
Figure 3.14: Developmental timeline of corticosynaptogenesis in mouse……

Figure 4.1: Early but transient current deficits and altered excitability of MSN circuited with *GBA-N370S* DaN……
Figure 4.2: PKA antagonist rescued early current deficits of MSN circuited with *GBA-N370S* DaN……

Figure 5.2: Representative immunostaining image of hMLO differentiation batch 1 at DIV 46……
Figure 5.2: Schematics of differentiation conditions of iPSC-derived human midbrain-like organoid……
Figure 5.3: Immunohistochemical characterisation of midbrain origin by Foxa2 expression in paraffin-embedded hMLO on DIV 46……
Figure 5.4: Quantification of differential TH expression in corresponding differentiation conditions at DIV 96……
Figure 5.5: Characterisation of the optimised differentiation paradigm of hMLO……
Figure 5.6: Representative ICC images of DIV 96 hMLO reflecting their diverse neuronal and neural make-up……

Figure 5.7: Neither overt neurodegeneration nor alpha-synuclein pathology observed in hMLO of different genetic burden……

Figure 6.1 Characterisation of transduction efficiency of different viral vector
Figure 6.2: human TH promoter annotations……
Figure 6.3: Generation of custom human TH promoter reporter……
Figure 6.4: Characterisation of mApple expression driven by pcTH v2.0 in transduced iPSC-neurons 7 days post-transduction……

Figure 7.1: Generation of fluid-walled microfluidic-based circuit……
Figure 7.2: Recapitulation of the human cortiostriatal pathway on fluid-walled microfluidics……
Figure 7.3: Cortical axon outgrowth is independent of target-derived signals…..
Figure 7.4: Directed axotomy and regeneration of human cortical neurons……
Figure 7.5.: Dependency of axon regeneration on target-derived signals post axotomy……

List of tables

Table 1.1. PARK-assigned genes involved in familial PD
Table 2.1. Demographics and reprogramming methods of all iPSC lines used
Table 2.1.6. List of primers used in RT-qPCR
Table 2.1.7. List of primary antibodies
Table 2.1.8. List of secondary antibodies
Table 5.2.2. Quality control on robustness of hMLO differentiated from various iPS cell lines of various genetic background across differentiations

Abbreviations

AMM = Astrocyte maintenance medium

ANOVA = Analysis of variance

ANOVA = Analysis of variance

AP = Action potential

AraC = Cytosine arabinoside

BDNF = Brain-derived neurotrophic factor

cAMP = 3',5'-cyclic adenosine monophosphate

cDNA = Complementary deoxyribonucleic acid

CGE = Caudal ganglionic eminence

CN = Cortical neurons

DaN = Dopaminergic neurons

dMSN = Direct pathway medium spiny neuron

DIV = Days in vitro

EB = Embryoid body

ESC = Embryonic stem cell

EPSC = Excitatory post-synaptic current

EPSP = Excitatory post-synaptic potential

FC40 = Fluorocarbon 40

FGF2 = Fibroblast growth factor 2

FMW = Fluid-walled microfluidics

GABA = γ-aminobutyric acid

GBA = Glucocerebrosidase

GFAP = Glial fibrillary acidic protein

GWAS = Genome wide association studies

iPSC = human induced pluripotent stem cell

hMLO = human midbrain-like organoid

hPSC = human pluripotent cell

iMSN = Indirect pathway medium spiny neurons

IPSC = Inhibitory post-synaptic current

LGE = Lateral ganglionic eminence

MGE = Medial ganglionic eminence

MSN = Medium spiny neurons

NMM = Neural maintenance medium

PBS = Phosphate buffered saline

PCR = Polymerase chain reaction

pcTH = Custom human TH promoter

PD = Parkinson's Disease

PDMS = Polydimethylsiloxane

PKA = protein kinase A

PP1 = Protein phosphatase 1

RMP = Resting membrane potential

RT = Room temperature

RT-qPCR = Reverse transcription- quantitative polymerase chain reaction

SNP = Single nucleotide polymorphism

sIPSC = Spontaneous inhibitory post-synaptic current

AMY = Amygdala

GCase = Glucocerebrosidase

sEPSC = Spontaneous excitatory postsynaptic current

SNCA = Synuclein Alpha

Chapter 1: Introduction

1.1. Parkinson's Disease

1.1.1. Clinical manifestations

Parkinson's Disease (PD) is the second most common neurodegenerative condition which affects 1 every 500 people in the U.K. and over 8.5 millions globally (as per WHO statistics in 2019). More worryingly, PD is the world's fastest growing neurological disorder. Its prevalence doubled over the last 25 years and is projected to double again to reach above 12 millions in 2040 in light of the increasingly aging population (Dorsey *et al.*, 2018). While juvenile PD exists (Schrag *et al.*, 2003; Köroğlu *et al.*, 2013), most people are diagnosed with PD later in life at the age of 50 years old and above, starting with 0.50 per 100,000 in the 30- to 39-year category, 11 per 100,000 in the 50- to 59-year group and up to 119.01 per 100,000 in the 70- to 79-year group (Van Den Eeden *et al.*, 2003). In America with the prevalence of approximately one million cases of PD, the total economic burden, including direct medical cost and indirect loss of income, amounted to $51.9 billions and was conservatively estimated to exceed $79 billions in 2037 (Yang *et al.*, 2020).

First described in 1817 by James Parkinson in his essay entitled *"An essay on the shaking palsy",* PD was detailed with the characteristic involuntary resting tremors of the limbs and bradykinesia without apparent loss of visceral senses or cognitive ability. Although definitive test for the diagnosis of PD is still missing, modern clinical diagnosis of PD involves identification of four cardinal features grouped under the acronyms TRAP: Tremor at rest, Rigidity, Akinesia (or bradykinesia), and Postural stability (Jankovic, 2008). Clinical assessments, however, needs to be further validated by histopathological identification of α-synuclein-

containing Lewy bodies (LBs) or Lewy neurites. Patients with PD can also develop secondary motor impairments such as microphagia, shuffling gait, dysphagia, hypomimia, freezing, dystonia and sialorrhoea to name a few. The severity of motor disability varies among individuals and often should be evaluated within the context of the patient's personal profile. Importantly, PD patients also suffer from a wide array of non-motor impairments including autonomic dysfunction, cognitive disorders, sensory and sleep abnormality. Interestingly, non-motor symptoms often precede motor impairments, emerging early in the pre-motor or prodromal phase of PD (Poewe, 2008; Postuma *et al.*, 2012). As the result, whilst these non-motor signs were historically under-appreciated, their consistent occurrence preceding motor disability and with advancing disease could render them attractive targets of early preclinical diagnosis of PD.

1.1.2. Pathophysiology of Parkinson's Disease

The human midbrain is made up two major subclasses of dopaminergic neurons (DaN) categorised based on their molecular signatures and projection patterns: A9 neurons in the substantial nigra pars compacta (SNpc) which project to the striatum and A10 neurons in the ventral tegmental area (VTA) projecting to the limbic and cortical areas. While neuronal loss in some other brain regions has been noted (Giguère, Burke Nanni and Trudeau, 2018), PD is characterised by the preferential degeneration of SNpc DaN (Wakabayashi *et al.*, 2007), first noticed 100 years since James Parkinson's report in 1817, while glia cells are largely spared. Much of ongoing effort at understanding PD pathogenesis has centered around understanding molecular determinants of selective vulnerability of SNpc A9 DaN in relative comparison to the resistant VTA A10 DaN with some current evidence pointing towards A9 characteristic lack of calcium binding protein Calbindin and intrinsic enrichment of cell-autonomous pathways (Brichta and Greengard, 2014; Kamath *et al.*, 2022).

Significant loss of SNpc DaN causes reduced nigrostriatal projections towards the dorsolateral striatum and consequently, reduced dopamine (DA) release onto striatal medium spiny neurons (MSN) in the dorsal striatum, the post-synaptic targets of SNpc DaN. Disturbance of this pathway was shown to cause classical motor signs including bradykinesia and rigidity in PD patients (Parr-Brownlie and Hyland, 2005; Parker *et al.*, 2018). Studies in toxin-based mouse models of PD reported dendritic atrophy, altered spine morphology and neuronal excitability of MSN following DA depletion (Fieblinger *et al.*, 2014; Parker *et al.*, 2018; Graves and Surmeier, 2019). Similar reduction in dendritic arborization and spine density was reported in post-mortem brain tissues of PD patients (Zaja-Milatovic *et al.*, 2005) and MPTP-treated monkeys (Villalba, Lee and Smith, 2009). Furthermore, previous findings also suggested that striatal axonal terminal loss preceded nigral DaN loss (Villalba, Lee and Smith, 2009), suggesting that synaptic alterations of MSN might be early pathology leading to SNpc DaN degeneration. However, these findings were restricted to animal models with abrupt chemically induced degeneration of DaN or late-stage PD postmortem brains. Whether similar synaptic alterations occur in human neurons carrying PD-related mutations remains unknown. Better understanding of synaptic changes could provide insight to early pathophysiology of PD and might inform early interventions to delay aberrant motor behaviours.

1.1.3. Genetics of Parkinson's Disease

1.1.3.1. Identification of rare familial PD

PD is a multifactorial disease with genetics and environmental factors both playing a role although the exact cause of PD remains unknown. 10-15% of cases are of familial origin, 5% have a known Mendelian inheritance and the remaining of PD cases are idiopathic (Deng,

Wang and Jankovic, 2018). The first report of genetic linkage in PD was found in 1996 on chromosome 4q21-q23 (*SNCA* locus) following genetic linkage analysis of kindreds identified by a familial aggregation of the disease (Polymeropoulos *et al.*, 1996). Reports in the following years identified new chromosomal regions associated with rare genetic PD (Muñoz *et al.*, 1997; Scott *et al.*, 1997; Farrer *et al.*, 1998), cementing the idea that PD is genetically linked and heterogenous with rare variants. Later studies employing also functional gene candidate approach and exome sequencing further revealed more disease-causing variants (*HtrA2 and UCHL1* from candidate gene approach; *SYNJ1, VPS35, DNAJC6,* and *VPS13C* from exome sequencing) (Leroy *et al.*, 1998; Strauss *et al.*, 2005; Zimprich *et al.*, 2011; Edvardson *et al.*, 2012; Quadri *et al.*, 2013; Lesage *et al.*, 2016). Putative PD-causing genes have been historically termed 'PARK' and chronologically numbered in the sequence of their discovery. Until today 23 PARK loci have been found associated with rare form of PD (see Table 1.1.). However, it is noteworthy that not all of the reported loci contain identified causative genes, nor do all identified genes contain causative mutations (and hence, deemed only as risk factors predisposing to PD, e.g. *PARK3, PARK10, PARK12, PARK16,* and *PARK22*.). As the result, only 18 specific chromosomal regions have been linked to rare familial form of PD, accounting for approximately 30% of the familial and 3-5% of the sporadic cases (Klein and Westenberger, 2012). Among them, highly penetrant mutations producing monogenic form either in the autosomal dominant manner such as *SCNA, LRRK2*, and *VPS3* or in the autosomal recessive manner such *PRKN, PINK1*, and *DJ-1* are rare. Rather, PD aetiology has long been thought to exist in a continuum ranging from rare monogenic Mendelian inheritance to complex polygenic inheritance influenced by many common variants each confers relatively small risk.

1.1.3.2. Risk loci from genome-wide association studies (GWAS)

Variants of several PARK-designated (*SNCA, UCHL1, LRRK2, PARK 16, GAK*) and a few other genes (*MAPT, GBA, NAT2, INOS2A, GAK, HLA-DRA*, and *APOE)* have been found to predispose carriers to the increased risk of developing PD (Hernandez, Reed and Singleton, 2016). Among them, both genome wide association (GWAS) and candidate gene association studies consistently highlighted the common variants on *SNCA, LRRK2, MAP2* and *GBA* as the most significant and common risk factors associated with PD (Nalls *et al.*, 2011, 2019; Chang *et al.*, 2017). Taken together, a total of more than 75 risk loci of more than 90 common risk variants have been identified to significantly mediate PD risk, accounting for 16-36% of the variance in PD liability in individuals of European ancestry (Nalls *et al.*, 2019), pointing to a large segment of variance which remains to be identified. Considering the complex and multifactorial nature of PD pathogenesis, genetic PD provides an excellent model to better understand pathophysiology of general PD and idiopathic PD both of which often display remarkably similar clinical pathology.

Among the variants, *GBA* is the most common risk factor PD, found in 5-15% of all PD patients (Sidransky *et al.*, 2009). The GBA gene encodes for glucocerebrosidase (GCase), a lysosomal enzyme which is involved in regulating glycosphingolipid homeostasis by converting glucosylceramide into ceramide and glucose. Up to date, approximately more than 400 pathogenic mutations, both common and rare mutations found only in individual families, have been reported in the *GBA* gene, including substitutions, deletions, insertions, and complex alleles (Horowitz and Zimran, 1994; Hruska *et al.*, 2008). Homozygous GBA mutation is well characterized in Gaucher's disease, a rare autosomal recessive disease, although heterozygous carriers do not develop Gaucher's (Lu *et al.*, 2010). Among them, the L444P (p.L483P) mutation is one of the most commonly found world-wide, and is frequently associated with neuronopathic Gaucher disease. The mutation N370S (p.N409S), found exclusively in patients with type 1 Gaucher disease, is the most frequent mutation among patients in the United States, Europe and Israel. GBA mutations result in reduction in GCase

enzymatic activity, albeit to variable extent depending on the specific mutation, subsequently leading to accumulation of glucosylceramide (Gegg *et al.*, 2012). Interestingly, only a very small percentage of GBA mutation carriers end up developing PD, and Gaucher's disease patients are as likely to develop PD as heterozygous mutation carriers. The odds of developing PD and the severity of PD pathogenicity vary according to the specific mutation and are thought to inversely correlate with GCase activity (Huh *et al.*, 2020).

Table 1.1: *PARK*-assigned genes involved in familial PD (Adapted and modified from Antonina Kouli et.al., 2018) (Kouli, Torsney and Kuan, 2018)

PARK	Gene	OMIM Reference	Inheritance	Description	Clinical features
PARK1 and PARK4	*SNCA*	168601	AD	α-synuclein	Ranging from classical PD to early-onset cases with dementia
PARK2	*PRKN*	600116	AR	parkin RBR E3 ubiquitin protein ligase	Early-onset PD, slow progression, often features of dystonia
PARK5	*UCHL1*	613643	AD	ubiquitin C-terminal hydrolase L1	Classical PD—only one family, findings not since replicated
PARK6	*PINK1*	605909	AR	PTEN-induced putative kinase 1	Early-onset PD, slow progression
PARK7	*DJ-1*	606324	AR	Parkinsonism-associated deglycase	Early-onset PD, slow progression
PARK8	*LRRK2*	607060	AD	Leucine-rich repeat kinase 2	Classical PD with less frequent dementia and slower progression
PARK9	*ATP13A2*	606693	AR	Cation-transporting ATPase 13A2	Early-onset (adolescence), atypical parkinsonism with dementia, spasticity and supranuclear palsy
PARK11	*GIGYF2*	607688	AD	GRB10 interacting GYF protein 2	Classical PD
PARK13	*HTRA2*	610297	AR	HtrA serine peptidase 2	Classical PD
PARK14	*PLA2G6*	612593	AR	Calcium-independent phospholipase A2 enzyme	Early onset with atypical features (dystonia parkinsonism)
PARK15	*FBX07*	260300	AR	F-box protein 7	Early onset with atypical features (pallido-pyramidal syndrome)
PARK17	*VPS35*	614203	AD	Vacuolar protein sorting-associated protein 35	Classical PD
PARK18	*EIF4G1*	614251	AD	Eukaryotic translation initiation factor 4 gamma 1	Classical PD
PARK19	*DNAJC6*	615528	AR	HSP40 Auxilin	Early-onset PD, slow progression
PARK20	*SYNJ1*	615530	AR	Synaptojanin 1	Parkinsonism with dystonia and cognitive decline
PARK21	*DNAJC13*	616361	AD	Receptor-mediated endocytosis 8 (RME-8)	Classical PD
PARK23	*VPS13C*	616840	AR	Vacuolar protein sorting-associated protein 13C	Early-onset PD, rapid progression

OMIM: Online Mendelian Inheritance in Man database, AD: autosomal dominant, AR: autosomal recessive. PARK3 PARK10, PARK12, PARK16, and PARK22 are considered risk factors or the genes have not been identified yet and are not included in this table.

1.2. The basal ganglia and Parkinson's Disease

1.2.1. Anatomy and neurophysiology of the basal ganglia and the striatum

The striatum is a subcortical nuclei structure located in the basal ganglia of the forebrain, the neuronal circuit that is primarily responsible for voluntary movement regulation, together with a variety of other functions such as learning, executive functions, and emotion. Anatomically, the basal ganglia and its constituent nuclei can be categorised into i) input nuclei, ii) output nuclei and iii) intrinsic nuclei. The striatum receives and processes information from different brain regions, mainly the cortex, thalamus and the midbrain, and is considered the major input nuclei. The output nuclei consist of the internal segment of the globus pallidus (GPi) and the substantia nigra pars reticulata (SNr) both of which are responsible for forwarding basal ganglia output to the thalamus which in turn projects to the frontal cortex. Intermediate structures including the external segment of the globus pallidus (GPe), the STN and the substantia nigra pars compacta (SNpc) are intrinsic nuclei relaying information between the input and output nuclei. These different structures are arranged into segregated subcircuits, altogether forming parallel re-entrant loops that service between multiple areas of the cerebral cortex and the similarly specific portions of the thalamus and back to the same cortical areas from which the loops originate (Alexander, DeLong and Strick, 1986; Kelly and Strick, 2004). Important features of the basal ganglia-thalamocortical circuitry are demonstrated schematically in Figure 1.1.

Details of the subcircuits projecting to and departing from the striatum have also been identified (Figure 1.2). In primate, the striatum is divided into a ventral and dorsal striatum. The former contains the nucleus accumbens (NAc) while the latter consists of the caudate nucleus and the putamen. Anatomically, a white matter nerve tract between brain cortex and

brainstem also known as the internal capsule runs between and hence, separates the dorsal and ventral striatum. The dorsal and ventral regions of the striatum are also distinguished according to their intrinsic and extrinsic connections which consequentially determine their differential fundamental functions as the major control center of motor and reward/motivation, respectively (Di Martino *et al.*, 2008). NAc receives convergent glutamatergic inputs from ventral hippocampus (vHIP), medial prefrontal cortex (mPFC) and basolateral amygdala (AMY), in addition to other regions such as the thalamus (French and Totterdell, 2003; Britt *et al.*, 2012; MacAskill *et al.*, 2012), with dopaminergic modulation from the ventral tegmental area (Sesack and Grace, 2010). Meanwhile, the majority of the glutamatergic projections onto the dorsal striatum originate from distributed regions of the cerebral cortex and the thalamus, as well as the AMY and other subcortical structures (Alexander and Crutcher, 1990; Di Martino *et al.*, 2008; Pan, Mao and Dudman, 2010; Choi, Yeo and Buckner, 2012; Guo *et al.*, 2015), with dopaminergic modulation from the SNpc (Haber, Fudge and McFarland, 2000; Björklund and Dunnett, 2007; Matsuda *et al.*, 2009).

Microscopically, the striatum is made up of GABAergic neurons of more thann 90% medium spiny neurons (MSN) identity (i.e. mid-sized projection neurons) and less thann 10% interneurons. The classical model of basal ganglia function further subdivides MSN into two main categories according to their molecular signatures in addition to their axonal projection patterns. This model of the motor circuit mediated by the basal ganglia circuitry and mostly involved the putamen is predicated on the separation of cortical information flow via functionally opposing pathways, namely the direct and indirect pathway, spearheaded by each of the two distinguishable MSN subtypes, the striatonigral and striatopallidal MSN, respectively. The direct pathway constitutes of striatonigral MSN (dMSN) preferentially expressing dopamine 1 receptor and projecting directly to output nuclei GPi and SNr (Deng, Lei and Reiner, 2006). Hence, activation of striatonigral MSN following inputs from the cortex

would reduce the overall basal ganglia output, resulting in disinhibition of the excitatory thalamocortical projections and subsequently activation of the topographically mapped regions in the cortex. The indirect pathway, on the other hand, constitutes of striatopallidal MSN (iMSN) preferentially expressing dopamine 2 receptor and relayed through the GPe then STN which in turn sends axons to the GPi and SNr (Deng, Lei and Reiner, 2006). As the result, activity of the indirect pathway is thought to lead to the net inhibition of the thalamocortical projections, suppressing cortically induced motor drive. The balanced activity of the two diametrically modulated pathways has been proposed to play the key role in regulating movement initiation and selection. Details of the intricacy of the motor circuit circuitry is depicted in Figure 1.1.

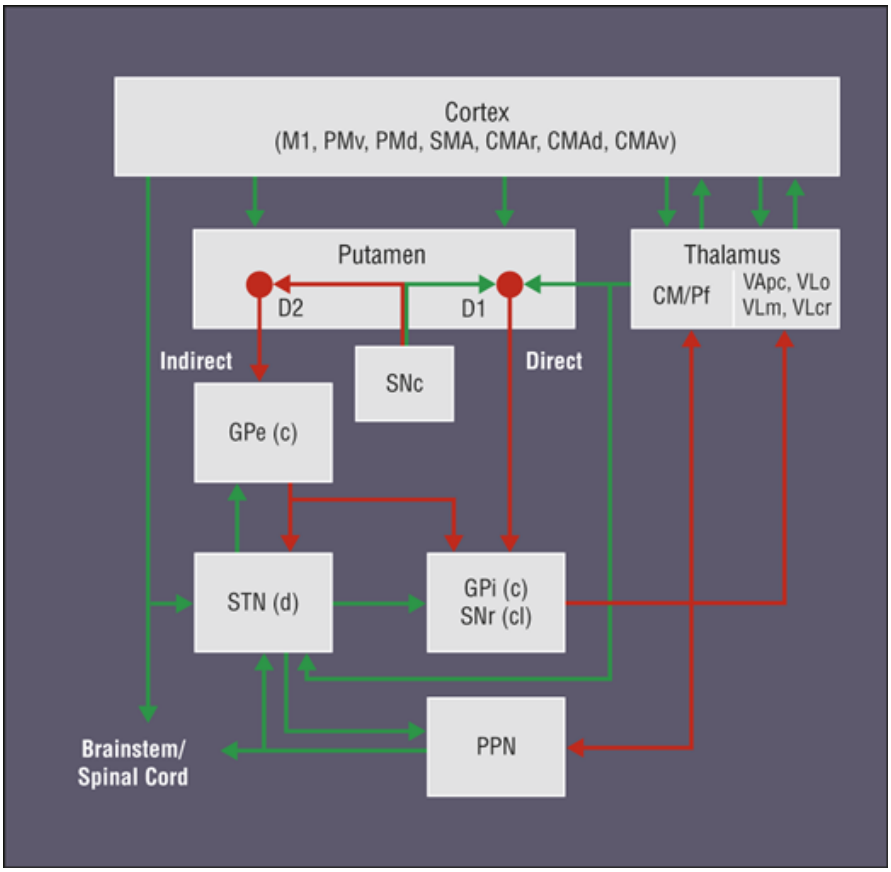

Figure 1.1: Schematic diagram of the intrinsic circuity of the motor circuit mediated by the cortico-basal ganglia-cortical loops. Green arrows indicate excitatory (glutamatergic) connections; red arrows indicate inhibitory (γ-aminobutyric acid [GABA]–ergic) connections. Abbreviations: CMAr, rostral portion of cingulate motor area; CMAd, dorsal portion of

cingulate motor area; CMAv, ventral portion of cingulate motor area; D1, dopamine 1 receptor; D2, dopamine 2 receptor; GPe, external segment of globus pallidus; GPi, internal segment of globus pallidus; M1, primary motor cortex; Pf, parafascicular nucleus of the thalamus; PMd, dorsal premotor cortex; PMv, ventral premotor cortex; PPN, pedunculopontine nucleus; SMA, supplementary motor area; SNc; substantia nigra pars compacta; SNr, substantia nigra pars reticulata; STN, subthalamic nucleus; VApc, ventral anterior nucleus of thalamus pars parvocellularis; VLm, ventrolateral nucleus of thalamus pars medialis; VLo, ventrolateral nucleus of thalamus pars oralis; VLcr, ventrolateral nucleus of thalamus rostral pars caudalis; c, caudal; cl, caudolateral; and d, dorsal. Adapted from DeLong et al., 2007 (DeLong and Wichmann, 2007)

While the classical premises suggested functionally opposed roles of dMSN and iMSN in regulating action, more recent observations of co-activation of both pathways at the initiation of movement have challenged this view (Cui *et al.*, 2013; Jin, Tecuapetla and Costa, 2014; Tecuapetla *et al.*, 2014) . An idea first proposed by Mink (Mink and Thach, 1993; Mink, 1996) and later supported by more recent studies, this novel 'center-around' model hypothesises that disinhibition of the thalamocortical neurons following dMSN transmission permits action initiation while concurrent activation of iMSN is critical in suppressing simultaneously occurring and competing action, allowing action selection (Schmidt *et al.*, 2013; Barbera *et al.*, 2016; McGregor and Nelson, 2019).

MSNs receives glutamatergic inputs from cortical neurons arising from 2 main subtypes (1) upper layer 5 intratelencephalic (IT) neurons that are involved in pre-movement planning and sensory signal; and (2) lower layer 5 pyramidal tract (PT) neurons that transmit motor commands to hindbrain and spinal cord (Turner and DeLong, 2000; Beloozerova *et al.*, 2003) and more recently identified (3) layer 4 pyramidal neurons that controls auditory sensory (Bertero, Verrillo and Apicella, 2022) . Rabies virus retrograde transneuronal labeling suggests selective and specific cortical sources to different classes of MSNs (Deng *et al.*, 2015). Layer 5 IT-type CNs preferentially make synapses with dMSNs while a higher percentage of layer 5 PT-type CNs make synapses on iMSN spines than dMSN ones. Bertero and colleagues recently

reported a novel corticostriatal connecitivity, suggesting direct excitatory inputs from layer 4 pyramidal neurons to MSNs in the ipsilateral striatum (Bertero, Verrillo and Apicella, 2022) .

Other than MSN, 10% of striatum are interneurons of five major classes: i) cholinergic interneurons (ChINs), ii) GABAergic calretinin-expressing neurons, iii) GABAergic parvalbumin-expressing neurons (or fast-spiking interneurons), iv) GABAergic neuropeptide Y (NPY)/somatostatin (SOM)/nitric oxide synthase (NOS)-expressing neurons (or low threshold spiking interneuron), and v) the more recently discovered tyrosine hydroxylase (TH)-expressing interneurons (THINs). Among them, ChINs makes up only 10%, and the remaining interneurons are of GABAergic interneurons subtypes. Despite their small presence, ChINs forms dense terminal field with both MSN subtypes and provides a tonic acetylcholine tone at about 5Hz modulating striatal outflow (Kitai and Surmeier, 1993; Zhou, Wilson and Dani, 2002; Dorst *et al.*, 2020; Laverne *et al.*, 2022). Mid-sized GABAergic interneurons is distinguished from their GABAergic MSNs as being aspiny with varicose dendrites (Bolam *et al.*, 1983) and exhibited significantly stronger glutamate decarboxylase (GAD) activity (Bolam *et al.*, 1985; Cowan *et al.*, 1990; Kita, 1993; Kubota, Mikawa and Kawaguchi, 1993; Gasser, 2005). GABAergic interneurons can be further categorized according to expression of calcium binding proteins, each with different molecular and electrophysiological properties (see review (Tepper *et al.*, 2010, 2018)). Each subtypes display highly selective and specific connection among themselves and with MSN, exerting specific local inhibitory inputs on MSN firing activities (Tepper *et al.*, 2018; Hjorth *et al.*, 2020).

1.2.2. Basal ganglia pathology in Parkinson's Disease

In PD, degeneration of DaN in the SNpc leads to secondary depletion of dopaminergic innervation in the striatum. Multimodal imaging studies employing advanced functional imaging techniques such as positron emission tomography (PET) and magnetic resonance imaging (MRI) in PD patients demonstrated the apparent reduction of striatal dopamine content, striatal dopamine intake and associated PD-related motor disabilities (Bohnen *et al.*, 2006; Nandhagopal *et al.*, 2009; Drori, Berman and Mezer, 2022). Notably, loss of nigrostriatal dopaminergic terminal field is most pronounced in the putamen and found associated with motor impairments (Ma *et al.*, 2002; Kish *et al.*, 2008) while dysfunction of the dopaminergic transmission in the caudate has been linked to cognitive impairments (Carbon *et al.*, 2004; Jokinen *et al.*, 2009; Ekman *et al.*, 2012; Polito *et al.*, 2012). Several theoretical frameworks have been proposed to stipulate the basal ganglia circuit dysfunction in motor disorders: i) the firing rate mode, ii) the firing pattern model, and iii) the dynamic activity model.

The firing rate model follows the classical model of motor circuit organisation and hence, emphasizes the imbalance of neural discharge between the direct and indirect pathway as causative mechanism of PD-related motor dysfunction (Figure 1.2). This model presumes the bidirectional regulation of dopaminergic signalling on dMSN and iMSN considering the differential expression of endogenous dopamine receptors (Gerfen *et al.*, 1990). Dopamine release from the nigrostriatal projections is proposed to facilitate dMSN output via Gs-coupled D1-like dopamine receptors but inhibit iMSN firing via the inhibitory Gi-coupled D2-like dopamine receptors. Therefore, loss of striatal DA content in the context of PD would result in a net increase in basal ganglia output via excessive activation of the iMSN and concurrent reduced activity of the dMSN (DeLong and Wichmann, 2007; Parker *et al.*, 2018). Such diametrical changes in neuronal firing rate in PD lead to an overall increase in GPI/SNr activity and hence inhibition of the thalamus and cortex, resulting in akinesia. Optogenetic activation

of dMSN in the dorsomedial striatum indeed thoroughly rescued motor dysfunctions in the bilateral 6-hydroxydopamine (6-OHDA)-lesioned mice model of PD while that of iMSN induced parkinsonian-like locomotor state in healthy mice. (Kravitz *et al.*, 2010). However, several studies reported conflicting observations and hence, called into question the robustness of the idea of firing rate abnormality in PD. For example, recordings from primate model of 1-methyl-4-phenyl-1,2,3,6-tetrahydropyridine (MPTP)-induced PD found no changes in MSN (Deffains *et al.*, 2016) or thalamic activity (Pessiglione *et al.*, 2005). Also in primate model of PD, GPi has been found to show reduced activity, opposite to what was predicted by the model (Tachibana *et al.*, 2011).

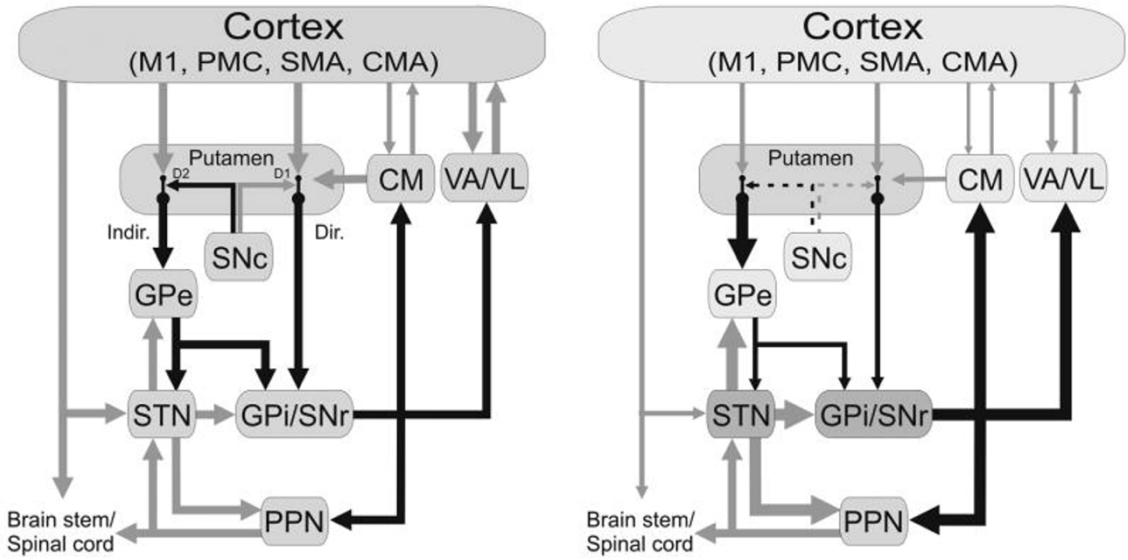

Figure 1.2: Schematic diagram of basal ganglia circuitry in healthy and Parkinson's Disease state in the classical model. Loss of SNpc dopaminergic projections results in imbalanced activity between the direct and indirect pathway MSNs. The net effect is an increased basal ganglia output which suppresses firing of excitatory thalamocortical neurons. Abbreviations: CMA, cingulate motor area; D1, dopamine 1 receptor; D2, dopamine 2 receptor; Dir, direct; GPe, external segment of globus pallidus; GPi, internal segment of globus pallidus; Indir, indirect; M1, primary motor cortex; PMC, premotor cortex; PPN, pedunculopontine nucleus; SMA, supplementary motor area; SNc; substantia nigra pars compacta; SNr, substantia nigra pars reticulata; STN, subthalamic nucleus; VA, ventral anterior nucleus of thalamus; VL, ventrolateral nucleus of thalamus. Adapted from Galvan et al., (2008) (Galvan and Wichmann, 2008).

The firing pattern model, on the other hand, points toward alteration of single-cell activity and synchronized firing of the basal ganglia as the potential sources of failure for properly integrated and coordinated motor information. Bursting and synchronisation were commonly reported in PD patients (Magnin, Morel and Jeanmonod, 2000) as well as animal models of PD (Levy *et al.*, 2000; Goldberg *et al.*, 2004; Wichmann and Soares, 2006; Tachibana *et al.*, 2011). Changes of the local field potential, particularly of the low beta frequency range, across various basal ganglia nuclei have also been implicated in parkinsonism (Brown and Williams, 2005; Brittain, Sharott and Brown, 2014; Little and Brown, 2014; Oswal *et al.*, 2021). Despite the strong correlation between observed perturbed neuronal firing pattern and parkinsonism, their direct causal link remains to be determined.

More recently, Nambu et al., (2015) proposed the novel 'dynamic activity model' presuming on the 'center-surround' model of functional organization of the basal ganglia (discussed in Chapter 1.3.1) (Nambu, Tachibana and Chiken, 2015). It was argued to offer a more unified explanation for observations of both firing rate and pattern abnormalities. However, this model remains highly hypothetical and requires further empirical evidence in support.

1.3. Induced pluripotent stem cell (iPSC) technology

Pioneered by Takahashi and Yamanaka (Takahashi and Yamanaka, 2006), the breakthrough of reprogramming somatic cells into stem cells of self-renewal and differentiation potential has revolutionised research of human-related conditions. Yamanka and colleagues showed that terminally differentiated somatic cells such as mouse fibroblast could be converted back to the embryonic pluripotent state following exposure to four transcription factors Oct3/4, Sox2, c-Myc, and Klf4 (Takahashi and Yamanaka, 2006). These converted cells displayed embryonic

stem (ES) cell-like features, maintained their pluripotency in cultures and were able to generate into cells from all three germ-layers (Takahashi and Yamanaka, 2006). Continuing on with success from the mouse fibroblast, it was later demonstrated that similar outcome could be applied in reprogramming human somatic cells into pluripotent stem cell-like entities (Yu *et al.*, 2007). The reprogramming process historically involved the traditional delivery followed by integration of retroviruses carrying reprogramming transcription factors (Takahashi and Yamanaka, 2006). However, this strategy runs a high risk of transgene reactivation and/or insertional mutagenesis (Nakagawa *et al.*, 2008). Today, alternative methods employing non-integrating methods of transgene delivery such as the use of RNA-based Sendai virus or synthetic mRNA has been developed to overcome the initial reprogramming risk with retroviruses (Fusaki *et al.*, 2009; Warren *et al.*, 2010; Okita *et al.*, 2013). Sendai virus-based approach is also commercialised into user-friendly kits to allow wider and standardized adoption of this technology.

The iPSC technology is of particular significance in neuroscience research due to the inaccessibility to human tissues other than those acquired in post-mortem which offer limited snapshot windows into disease pathogenesis. Hence, human-derived model is critical to study human-specific features in both healthy and disease state which has long been deemed the bottleneck to clinical trial success. iPSC are expected to retain their unique genetic landscape post-reprogramming process and are hence valuable to be used to model the genetic aspect of their sources, particularly in the modelling of genetic disorders. iPSC technology could also be coupled with advanced gene editing technology to generate isogenic lines of the same origin, enabling study of one or a few specific mutation-associated pathology whilst controlling for potential individual-specific genetic variations.

1.4. iPSC-derived Parkinson's Disease modelling

The two most widely used animal models of PD are toxin-induced and genetic-based approach. Historical animal models of PD mainly involve treating healthy animal of neurotoxic chemicals, for example the chemically induced 1-methyl-4-phenyl-1,2,3,6-tetrahydropyridine (MPTP) and 6-hydroxydopamine (6-OHDA), or agrochemicals such as the pesticide rotenone, the herbicide paraquat, and the fungicide maneb. These treatment model DaN degeneration resulted from environmental risk factors implicated in PD. They induces rapid and substantial cell loss in the substantia nigra pars compacta (SNpc), permitting investigation of subsequent behavioural changes as well as molecular signatures of the surviving striatum (Parker *et al.*, 2018; Graves and Surmeier, 2019; Valsky *et al.*, 2020). On the other hand, genetic-based animal models, be it transgenic mouse or via viral transfection, demonstrate more variable cell loss as well as offer insights into the role of PD-related mutations (Janezic *et al.*, 2013; Taguchi *et al.*, 2017; Vanan *et al.*, 2020; Hendrickx *et al.*, 2021; Tian *et al.*, 2021). Both strategies complement each other and offer windows to deepen our understanding of the heterogeneity and multifaceted pathology of PD, albeit at the lack of human-specific materials. Meanwhile, iPSC has revolutionized our capacity to model PD with human cells eliciting patients' specific genomic signature.

The majority of current iPSC-derived PD modelling place emphasis on modelling SNpc DaN, the principal cell types preferentially degenerated in the course of PD progression. Current development of iPSC towards the SNpc DaN lineage successfully generated robust and reproducible DaN monolayer culture to study PD pathophysiology (Kriks *et al.*, 2011; Hartfield *et al.*, 2014). Whilst each protocol differs slightly in the detailed sequence of growth factor application, they all mimic similar developmental trajectory of neurogenesis, followed by floorplate patterning and then terminal differentiation towards postmitotic DaN. These neurons displayed the molecular profile characteristic of SNpc DaN expressing particularly dual marker tyrosine hydroxylase (TH) and hepatocyte nuclear factor 3-beta (FOXA2). Comparison

of DaN derived from healthy controls to those derived from PD patients with specific genetic mutations offered mechanistic insights into the causative role of those specific mutations in PD and potential pathophysiology including susceptibility to oxidative stress (Lin *et al.*, 2016), lysosomal and mitochondria dysfunctions (Fernandes *et al.*, 2016; Prots *et al.*, 2018; Zambon *et al.*, 2019), endoplasmic reticulum stress (Fernandes *et al.*, 2016; Heman-Ackah *et al.*, 2017; Lang *et al.*, 2019), synaptic dysfunctions (Oliveira *et al.*, 2015), dopamine release perturbation (Woodard *et al.*, 2014; Lang *et al.*, 2019).

While DaN is the primary research focus of neurodegeneration , more recent endeavours have also extended their research interest into non-cell autonomous mechanisms involving glial cells such as astrocytes (Leventoux *et al.*, 2020; Sonninen *et al.*, 2020; de Rus Jacquet *et al.*, 2021) and microglia (Svoboda *et al.*, 2019; Xu *et al.*, 2020; Dräger *et al.*, 2022). Modelling of mutant astrocytes carrying *LRRK2-G2019S* and *GBA-N370S* mutation, for example, revealed altered polyamine metabolism, increased sensitivity to inflammation and dysregulated Ca^{2+} release from the ER (Sonninen *et al.*, 2020). *LRRK2-G2019S* astrocytes demonstrated aberrant metabolic activity that eventually hindered its proper role in neuroprotection (Ramos-Gonzalez *et al.*, 2021). Likewise, idiopathic PD patient-derived microglia displayed higher phagocytic capacity under basal condition which flared up upon neuroinflammatory stimulation with lipopolysaccharide (Badanjak *et al.*, 2021). Co-culture of iPSC-astrocytes and iPSC-neurons further consolidated the crucial supporting role of astrocytes in neuroprotection by active clearing of toxic metabolites released from mutant neurons and hence, safeguarding the healthy living environment surrounding DaN (di Domenico *et al.*, 2019; Tsunemi *et al.*, 2020).

1.5. Advanced modelling approaches of Parkinson's Disease

The majority of current monoculture models in research are i) often of a single cell type and/or ii) two-dimensional (2D). Both represent an over-simplification of neuronal architecture *in vivo,* and hence pose concerns about the relevance of this model to recapitulate *in vivo* SNpc DaN. While reductionistic monoculture has proven to be a useful platform to learn of cell autonomous functions, many neuron-specific features such as electrophysiological features and synaptic properties emerge only in sophisticated microenvironment capturing a diverse range of essential cell-cell interactions. Hence, it is often assumed that the apparent delayed or lack of neuron functional maturation *in vitro* originates from the dearth of important non-autologous signals. In fact, iPSC-cortical neurons co-cultured with iPSC-astrocytes exhibited enhanced excitability and synaptic maturation (Hedegaard *et al.*, 2020). Immature neurons could eventually result in loss or alteration of potentially meaningful phenotypes in an aging-related disorder like PD.

In vitro coculture has been more actively pursued recently in the effort to better mimic the *in vivo* physiological conditions. Such physiological representation of neurons *in vitro* is thought to facilitate emergence of not only more physiological manifestations of individual neurons in both basal and stimulated state (Hedegaard *et al.*, 2020) but also network-dependent phenotypes such as synaptic pathology, electrophysiological properties and neuronal cross-talk. While co-culture has been more widely developed and adopted in recent years, it is often restricted between neurons and glial cells. Coculture of different neuronal populations is rarer, mostly due to the dearth of appropriate tools to facilitate neuronal coculture with similar spatial organization as the *in vivo* environment. Fortunately, bespoke co-culture is recently facilitated by the parallel development of microengineered devices e.g. microfluidic devices. Chambers housing neuronal subtypes are connected by microgrooves, providing a customized platform to recapitulate microcircuits of interest in a controlled manner (Gladkov *et al.*, 2017;

Virlogeux *et al.*, 2018). This microcircuit modelling, hence, should enable investigation of synaptic and microcircuit changes in a broad context of many diseases. In the context of PD, recapitulation of the cortico-striato-nigral microcircuit reminiscent of the *in vivo* corticostriatal and nigrostriatal pathway in which both iPSC-derived cortical neurons (CN) and DaN synapse onto iPSC-derived MSN might allow investigation of synaptic alterations of nigrostriatal synapses in the early stage of PD caused by a PD-relevant mutation.

On the other hand, three-dimensional (3D) self-assembly culture, known as organoid, represents another exciting physiologically relevant *in vitro* models of the human brain (Lancaster *et al.*, 2013). Conceptualised from the similar need to reconstruct the complexity of various endogenous inputs *in vitro*, organoid offers a 3D reductionist replica that mimics the cellular diversity of brain sub-regions assembled within a naturalistic tissue micro-environment with abundant spatial interactions (Lancaster *et al.*, 2013; Muguruma *et al.*, 2015; Jo *et al.*, 2016). The potential of organoid to reproduce both the functional and cellular complexity of different brain regions provides an exciting avenue for studies of both physiological neural development (Li *et al.*, 2017; Uzquiano *et al.*, 2022) as well as neural pathophysiology (Park *et al.*, 2018; Paulsen *et al.*, 2022).

1.6. Aims

Considering various limitations of the traditional monoculture *in vitro* in modelling human neuronal conditions, together with apparent promises heralded by the co-culture platform, the overarching aim of this thesis is to establish advanced circuit-based neuronal cultures using iPSC-derived cells and subsequently investigate potential mechanisms associated with neuronal dysfunctions in the context of PD. Such advanced co-culture would not only leverage on the human-specific strength of the iPSC technology but also incorporate to a certain extent

the endogenous neuronal network element critical for a better recapitulation of neuronal physiology as evident *in vivo*. This effort will be detailed in five result chapters documenting my attempts at three different advanced culture strategies:

1. To generate and establish the cortico-striato-nigral presynaptic microcircuit from healthy control individuals and assess functional significance of the microcircuit-based culture on iPSC-medium spiny neurons (MSN) (Chapter 3).
2. To investigate debilitating effect of *GBA-N370S* DaN on healthy control iPSC-MSN electrophysiology in the microcircuit and potential rescue mechanism (Chapter 4).
3. To generate and assess human midbrain-like organoid from healthy control individuals and familial PD patients (Chapter 5).
4. To develop a custom human tyrosine hydroxylase promoter useful for labelling of human DaN cultures (Chapter 6).
5. To establish the human cortiostriatal network on fluid-walled microfluidics from healthy control iPS cell lines and develop directed axotomy assay on corticostriatal tract. This work was done in collaboration with Federico Nebuloni jointly supervised by Prof Peter Cook (Dunn School of Pathology) and Dr Edmond Walsh (Department of Engineering) (Chapter 7).

Chapter 2: Materials and Methods

2.1. Materials

2.1.1. Mammalian cells

iPSC lines were acquired from the OPDC-StemBANCC consortium cell repository (https://www.stembancc.org/). All iPSC were derived from human skin biopsy fibroblast obtained with informed consent and ethical approval (Ethics committee: National Health Service, Health Research Authority, NRES Committee South Central, Berkshire, UK, REC 10/H0505/71). All control lines were derived from healthy individuals with no history of dementia, mental health problems, diabetes, or migraine. All *GBA-N370S* iPSC were derived from *GBA-N370S* PD patients who exhibited akinetic-rigid parkinsonism and responsiveness to levodopa treatment for the first 5 years of treatments in the absence of significant fall and dementia. Demographic details of all iPSC used are included in table 1. Reprogramming was performed by transducing low passage donated fibroblast with either reprograming Cytotune 2.0 or 1.0 Sendai viruses (SeV) or reprogramming retroviruses (RV).

.

Table 2.1: Demographics and reprogramming methods of all iPSC lines used. M = male, F = female, RV = retrovirus, SeV = Sendai virus.

Genotype	Cell Line	Clone	Sex (F/M)	Age	Reprogramming method
Healthy controls	SFC067-03	1	M	72	Cytotune 2 (SeV)
	SFC156-03	1	M	75	Cytotune 2 (SeV)
	SFC856-03	4	F	78	Cytotune 2 (SeV)
	JR053	1	M	68	RV
	MK071	3	F	81	RV
GBA-N370S	SFC871-03	9	F	70	Cytotune 2 (SeV)
	MK082	26	M	51	RV
	MK088	1	M	46	RV
	SFC828-3	6	F	51	Cytotune 1
SNCA A53T	SFC830-4	9	M	51	Cytotune 1
	SFC829-03	6	M	46	Cytotune 1
	SFC831-03	1	F	55	Cytotune 1
SNCA Triplication	SFC831-03	3	F	55	Cytotune 1
	SFC831-03	5	F	55	Cytotune 1

2.1.2. Media Formulation

All media components were purchased from Life Technologies unless otherwise stated.

2.1.2.1. Cortical neural maintenance medium (cNMM)

50% v/v Neurobasal, 50% v/v DMEM/F12 Glutamax medium containing 0.5x N2, 0.5x B27 Plus + Vitamin A, 5 µg/ml insulin, 2 mM L-glutamine, 1x non-essential amino acids, 100 µM β-mercaptoethanol (Merck), 1mM sodium pyruvate, 50 U/ml Penicillin-Streptomycin.

2.1.2.2. Astrocyte maintenance medium (AMM)

85% v/v DMEM high glucose, 15% v/v fetal bovine serum containing 2 mM L-glutamine and 50 U/ml Penicillin-Streptomycin. Gibco primary rat cortical astrocytes were purchased from ThermoFisher (Cat No.: N7741500)

2.1.2.3. Organoid neural maintenance medium (oNMM)

50% v/v DMEM/F12 and 50% v/v Neurobasal medium containing 1x N2, 1x B27, 1% GlutaMax, 1x non-essential amino acids, 100 µM β-mercaptoethanol (Merck), 50 U/ml Penicillin-Streptomycin.

2.1.2.4. Striatal neural maintenance medium (sNMM)

100% v/v DMEM/F12 Glutamax medium containing 1x N2, 1x B27, 2 mM L-glutamine, 1x non-essential amino acids, 100 µM β- mercaptoethanol (Merck), 50 U/ml Penicillin-Streptomycin.

2.1.3. Electrophysiological solution

All chemicals were purchased from Sigma unless otherwise stated. Solutions were made in ddH20.

2.1.3.1. Extracellular recording solution (ECS)

2.4 mM KCl, 167 mM NaCl, 10 mM Glucose, 10 mM HEPES, 1 mM $MgCl_2$, and 2 mM $CaCl_2$ adjusted to 300 mOsmol/L and pH 7.36 with NaOH. ECS was made fresh to be used within 2 weeks and kept at 4°C.

2.1.3.2. Intracellular recording solution (ICS)

For current-clamp and channel current recordings: 140 mM $C_6H_{11}KO_7$, 6 mM NaCl, 1 mM EGTA, 4 mM MgATP, 0.4 mM Na_3GTP, 10 mM HEPES, and 0.01% Neurobiotin (SP-1120) adjusted to 290 mOsmol/l and pH 7.3 using KOH.

For post-synaptic current recordings: 140 mM $C_6H_{11}CsO_7$, 6 mM NaCl, 1 mM EGTA, 4 mM MgATP, 0.4 mM Na_3GTP, 10 mM HEPES, and 0.01% Neurobiotin adjusted to 290 mOsmol/l and pH 7.3 using CsOH. ICS was made in big batch of 50 ml on ice and frozen in single-use aliquots.

2.1.4. Drugs

All drugs were purchased from Tocris unless otherwise stated.

Drug	Function	Diluents	Final concentrations
SB431542	Inhibitor of the TGF-β/Actiivn/NODAL pathway	DMSO	10 μM
Puromycin	aminonucleoside antibiotic	ddH2O	1 μg/ml
Doxycycline	road-spectrum tetracycline class antibiotic	ddH2O	1 μg/ml
PD0332991	selective inhibitor of CDK4/6	ddH2O	2 μM

GABA	γ-Aminobutyric acid, inhibitory neurotransmitter	ddH2O	300 μM
LM22A4	partial agonist of TrkB	ddH2O	1 μM
H89	Protein kinase A inhibitor	ddH2O	10 μM
8-Br-cAMP	cAMP analogue	ddH2O	500 μM
DAPT	γ-secretase inhibitor	DMSO	10 μM
AraC	cell cycle G1/S arrest	ddH2O	100 nM
CHIR99021	Inhibitor of GSK-3	DMSO	3 μM
$CaCl_2$	Calcium salt	ddH2O	0.6 μM
Ascorbic acid	Vitamin C	ddH2O	200 μM
LDN193189	selective ALK2 and ALK3 inhibitor	DMSO	0.118 μM
Y27632 dihydrochloride	ROCK inhibitor	ddH2O	10 μM
SAG	SHH agonist	ddH2O	100 nM

2.1.5. Lentiviral vectors

Plasmids	Virus	Source	Cat No.
psPAX2	Encodes viral packaging	Addgene	12260
pMD2.G	Encodes viral envelop	Addgene	12259
pAdVantage	Increases translation initiation in cells	Promega	E1711
pTet-O-Ngn2-puro	LV-TetO-mNgn2-T2A- Puro	Addgene	52047
pLV-TetO-hNGN2-eGFP-Puro	LV-TetO-hNGN2-eGFP Puro	Addgene	79823
FUdeltaGW-rTA	LV-Ubiq-rtTA	Addgene	19780

2.1.6. RT-qPCR primers

Table 2.1.6.: List of primers used in RT-qPCR

Gene	Forward primers	Reverse primers
PAX6	aggccagcaacacacctagt	agccagatgtgaaggaggaa

DLX2	gcctcaacaacgtcccttact	tcactatccgaatttcaggctca
GSX2	atgtcgcgctccttctatgtc	atgccaagcgggatgaagaaa
DLX5	ttcagaagactcagtacctcgc	gagttacacgccattgggtc
ASCL1	gtcctgtcgcccaccatctc	ccctcccaacgccactgac
MEIS2	gatgaaagagacggcagctcc	gggttgaggttgcatcatcg
NKX2.1	aggacaccatgaggaacagc	cccatgaagcgggagatg
FOXP1	ctaccgcttccatgggaaatc	ctgttgtcactaaggacaggg
GAPDH	ctgacttcaacagcgacccc	atgaggtccaccaccctgt
ISL1	caggttgtacgggatcaaatgc	cacacagcggaaacactcgat
CTIP2	atcctcagccccttttgttt	gccgttgttcctgaattgtt
GAD1	ccaaggtgctggactttcat	aaatcgaggatgacctgtgc
DARPP32	cctgaaggtcatcaggcagt	ggtcttccacttggtcctca
TH	tgaggagaaggaggggaagg	ccgggtctctagatggtgga
FOXP	ctaccgcttccatgggaaatc	ctgttgtcactaaggacaggg
EBF1	aatgtaagcaaggtggacgc	tcaaggtctaagccggacac
D1R	agggacatgtctttggcttcag	gggaacagtgttagcacctgtt
PDYN	caccacagcggactgcctgt	agcagggcagcctggcattg
D2R	ctggagaggcagaactggag	gaagacgatgacagcgatga
ADORA2A	aggagggctgtcaggtgaa	gttctggcagcagcatcat
PENK	atcctcgccaagcggtatg	ggttgtcccctgtttccaga

2.1.7. Primary antibodies for immunofluorescence

Antibodies	Supplier	Catalogue #	Raised in	Dilution factor for immuno-histochemistry	Dilution factor for immuno-cytochemistry
Calbindin D28K	Abcam	Ab1778	Rabbit	1:100	1:200
Ctip2	Abcam	Ab18465	Rat	NA	1:250
D1R	Abcam	Ab20066	Rabbit	NA	1:200
Darpp32	Abcam	Ab40801	Rabbit	NA	1:250
Darpp32	Sigma	HPA061142	Rabbit	NA	1:250
DAT	Millipore	Mab369	Rat	1:100	NA
Foxa2	R&D System	AF2400	Goat	1:150	NA
Gad67	Millipore	Mab5406	Mouse	1:250	1:250
GFAP	Agilent	Dako	Rabbit	1:200	NA
Girk2	Abcam	Ab65096	Goat	1:100	NA
Ki67	Abcam	Ab15508	Rabbit	1:500	NA
Map2	Abcam	Ab92434	Chicken	1:250	1:1000
Nestin	Millipore	Mab5326	Mouse	1:250	NA
Parvalbumin	Abcam	Ab11427	Rabbit	1:200	NA
Smi-312	Biolegend	837904	Mouse	NA	1:500
S100β	Sigma	SAB4200671	mouse	1:200	NA
Sabt2	Abcam	Ab51502	Mouse	NA	1:250
Tbr1	Abcam	AB23345	Rabbit	NA	1:250
TH	Abcam	Ab152	Rabbit	1:100	NA
TH(F-11)	Santa Cruz	Sc-25269	Mouse	1:100	1:250
Synaptophysin	Synaptic System	101004 x	Guinea pig	NA	1:1000
Homer1	Synaptic System	160003	Rabbit	NA	1:500
Pdyn	Sigma	HPA053342	Rabbit	NA	1:250
Pken	Sigma	HPA013138	Rabbit	NA	1:250

Substance P	Sigma	sc21715	Rat	NA	1:250

2.1.8. Secondary antibodies for immunofluorescence.

All secondary antibodies were purchased from Life Technologies unless otherwise stated.

Table 2.1.8.: List of secondary antibodies.

Antibody	Conjugate	Raised in	Dilution factor	Catalogue #	Supplier
Anti-mouse	Alexa Fluor 488/555/647/680	Donkey	1:1000	A21202/A31570/ A31571/A10038	
Anti-rabbit	Alexa Fluor 555/647/680	Donkey	1:1000	A31572/31573/ A10043	
Anti-guinea pig	Alexa Fluor 488	Goat	1:400	A11073	
Anti-rat	Alexa Fluor 488	Goat	1:1000	A11006	
Anti-chicken	Alexa Fluor 488	Goat/Donkey	1:1000	A11039/ 703-545-155-JIR-0.5mg	Stratech Scientific Ltd
Streptavidin	Alex Fluor 488	NA	1:1000	S32354	Thermo Fisher Scientific
Streptavidin	Alex Fluor 488	NA	1:1000	S11223	Thermo Fisher Scientific

2.2. Methods

2.2.1. Lentivirus packaging

Low passage Lenti-X HEK 293T cells were seeded at 2.5 x 10^6 cells/15cm petri dish, maintained in growth medium containing 90% vol/vol DMEM (Life Technologies) and 10% vol/vol FBS (Life Technologies), and grown to 90% confluence at the point of transfection. On the day of transfection, 2 tubes of Lipofectamine mix and DNA mix were made separately. The former

consisted of 30 µl Lipofectamin™ 3000 (Invitrogen) mixed in 2.4 ml of pre-warmed Opti-MEM (Life Technologies) and incubated for 5-20 mins at room temperature. DNA mix was made up of 2.4 ml pre-warmed Opti-MEM, 80 µl P3000, 26.3 µg psPAX2, 9 µg pMD2G, 3.6 µg pAdVantage, and 39 µg vector of interest. DNA mix was then added to Lipofectamin mix with 8 flickings to ensure even mixing. After 20 min-incubation, the final mix was added dropwise into HEK culture, accompanied by constant gently swirling of the plate to ensure even mixing. Cell media was changed afresh the next morning and supplemented with 6 µl ViralBoost (Alstem). From this step onwards, all materials in contact with viral particle-containing media needed to be treated with Chemgene prior to autoclaving.

After 2 days, viral particle-containing media was collected in full, centrifuged at 10,000 g to pellet cell debris for removal and the supernatant was kept at 4°C. If no ViralBoost was used, smaller volumes of media were collected daily and pooled after 3 days. The final pooled media was either centrifuged at 10,000 g or filtered with low-protein binding 0.45um filter to remove cell debris. The supernatant was further concentrated using Lenti-X ™ concentrator as per manufacturer's instructions (Takara Bio). Viral particle concentrates were aliquoted in single-use volumes into Eppendorf tubes and stored at -80ºC.

2.2.2. Maintenance and expansion of human induced pluripotent stem cells (iPSC).

All iPSC were maintained on hECS-qualified Matrigel™ (Corning)-coated plates under feeder-free culture condition with mTSER1™ (StemCell Technology) supplemented with 1% penicillin/streptomycin (P/S) (Life Technologies). Coating Matrigel was thawed from -80°C frozen stock and resuspended in cold KO DMEM (Life Technology) to make a final concentration of 0.16 mg/ml. Coated plates were incubated at 37°C for at least 1 hour or overnight prior to cell plating. Medium was changed daily. Cultures were passaged 1:2 every

other day using TrypLE Express™ (Life Technologies) when they reached 90-100% confluency. Passaged cells were collected in and fed with in mTSER1™ (StemCell Technology) supplemented with 1% penicillin/streptomycin (P/S) (Life Technologies) and 10 µM Y-27632 (Tocris) for 24 hours.

2.2.3. Coverslip preparation

13 mm or 19 mm glass coverslips (VWR) were submerged and sterilised in 70% ethanol overnight before being dried in the tissue culture hood. For monoculture, 100 µg/ml poly-D-lysine was applied in droplet of 100 µl directly on to the surface of 13 mm glass coverslip and incubated overnight at 37°C. Afterwards, coverslips were washed with PBS three times. PBS was applied in droplets of 90 µl directly onto coverslip surface to prevent potential spillage. Thereafter, coverslips were coated with Matrigel ™ droplets of 80 µl and incubated at 37°C for at least 1 hours prior to plating.

For microfluidic-based cultures, microfluidic devices were first placed on top of 19 mm coverslips using point tip tweezers such that the entire area of the microfluidic chambers was covered. Subsequent coating sequence followed that of monoculture with the only difference being that only the area of coverslips circumscribed by the microfluidic devices will be coated. Importantly, coating volume between different chambers was also different to create a volume gradient permitting fluid flow and hence, coating of the microgrooves.

2.2.4. Generation of iPSC-derived medium spiny neurons (MSN)

iPSC were differentiated into MSN using condition modified from previously established protocols (Telezhkin *et al.*, 2016) as follows. iPSC were passaged onto Matrigel-coated plates at 70,000 cells/well of a 6-well plate and maintained until 80-90% confluence (after approximately 24 hours). Culture was then switched to striatal neural induction medium

(sNIM) made up of sNMM supplemented with 1 µM LDN193189 (Sigma), 10µM SB431542 (Abcam) and 4 µM XAV (Tocris). On DIV 04, culture was pre-incubated with ROCK Inhibitor (Y-27632) for 1 hour, washed with PBS once, incubated in Accutase for 5-10 min and then passaged in 1:2 ratio (Life Technologies) onto freshly Matrigel-coated plates. Note that cell detachment with Accutase was milder than that with TrypLE Express™ and hence, more desirable post-iPSC stage. Required incubation time varied depending on culture stage, cell types and cell density and therefore, constant visual check for determining appropriate end time was necessary. DIV 04 culture was continued to maintained in sNIM and passaged again in the ratio of 1:2 on DIV 08 following the same steps as DIV 04 passaging. 100 nM of SAG could be added depending on differentiation paradigms. From DIV 08 till DIV 12, culture was maintained in sNMM supplemented with 200 µM LDN193189 (Sigma) and 4 µM XAV (Tocris). Between DIV 12-16, 25 ng/ml Activin A was added to the previously used (i.e. DIV 08-12) culture media. At this stage, cells could be further differentiated or cryopreserved in clumps (and not in single cells) in cryostore CS10® (Stem Cell Technology) at 5x10e6 cells/1 ml. When cryostore CS10 ® was not available, progenitors were frozen down in DIV 15 medium supplemented with 10% DMSO.

Frozen progenitor vials were fast-thawed at 37°C, centrifuged at 350 g for 5 mins, and plated on pre-coated plates (immunohistochemistry) or coverslips (electrophysiology) at 70,000 and 150,000 cells/cm^2, respectively. Coating included 10 and 100 µg/ml Poly-d-lysine (Sigma-Aldrich) overnight for plastic plates and glass coverslips, respectively, followed by 1:100 Matrigel™ for at least 1 hour. Neuronal progenitor cells were cultured in the maturation medium SynaptoJuice® previously reported (Telezhkin *et al.*, 2016). Culture was treated with 100 nM AraC (Tocris) on DIV 18 to arrest proliferation of non-neuronal cells capable of DNA synthesis. AraC concentration in the culture was gradually diluted with subsequent media changes. Medium was changed every other day till further experiments.

2.2.5. Generation of iPSC-derived dopaminergic neurons.

DaN used in microcircuit was generously donated in cell suspension at DIV 35-40 on their final replating dates from Charmaine Lang and Naroa Ibarra Aizpurua. iPSC were differentiated into DaN as previously described (Lang *et al.*, 2019) with an additional 3-week expansion stage started on DIV 10. In brief, iPSC were first exposed to neural induction media containing NNB media supplemented with 1 µM LDN193189 (Sigma), 10µM SB431542 (Abcam), 100 ng/ml SHH-C24II (Biotechne), 2 µM Purmorphamine (Biotechne), 100 ng/ml FGF8a (Stratech) for 6 days. 3 µM CHIR99021 is added in the induction media from day 3. Between Day 6 and 10, cell cultures were exposed to a mixture of decreasing amount of NNB and increasing amount of KO DMEM KSR supplemented with 1 µM LDN193189 (Sigma) and 3 µM CHIR99021. Day 10 precursors were further expanded with weekly passaging in the ratio of 1:2 in the DIV 10 media for the subsequent 20 days. Post-expansion precursors were further differentiated and matured as previously reported (Langet al., 2019) in NB media supplemented with 20 nng/ml BDNF (Peprotech), 20 ng/ml GDNF (Peprotech), 1 ng/ml TGFb3 (Peprotech), 10 µM DAPT (Abcam), 200 µM Ascorbic acid (Sigma) and 500 µM cAMP (Sigma). I finally replated DIV 40 DaN on microfluidic devices at 170,000 cells/ cm^2 and subsequently matured them into post-mitotic midbrain neurons as previously described (Lang *et al.*, 2019).

2.2.6. Generation of iPSC-derived cortical neurons.

Generation of cortical neurons from iPSC was adapted from previously detailed protocol (Hedegaard *et al.*, 2020) and redescribed as follows. iPSC was passaged and grown till 90% confluence at which point the culture medium was switched into cortical neural induction medium (NIM) i.e. cNMM supplemented with 100 nM LDN193189 (Sigma) and 10µM SB431542 (Abcam). Media was changed daily for 12 days. At DIV 12, the cells formed a

dense neurepithelial sheets which were enzymatically lifted using 10 mg/ml Dispase (Life Technologies). Incubation of Dispase™ at 37°C was regularly monitored and on average took about 15-20 mins to completely detach cell sheets. Cells were broken lightly into slightly smaller clumps and collected into pre-warmed NMM. They were let to settle by gravity to the bottom of the containing falcons, media was then removed from cell pellet and replaced with fresh pre-warmed NMM and this step was repeated 3 times to wash out Dispase. Following that, cells clumps were plated in onto fibronectin-coated plates with NIM and 10 μM ROCK Inhibitor (Y-27632 dihydrochloride) in 1:2 ratio to encourage development of neural rosettes. Media was removed after 24 hours and replaced with NMM with 20 ng/ml FGF2 (Peprotech) on DIV 13. Same media was changed again on DIV 15. On DIV 17, cultures were passaged with Dispase again, as previously described on DIV 12, at the surface ratio of 1:2 or 1:3, depending on cell density and proliferation rate, onto freshly laminin-coated plates. Cells were cultured in NMM with media change every other day until DIV 25. Neurogenesis should be obvious at this stage where axons could be visibly seen projecting out from the clumps. Between DIV 25-30, progenitors were either replated or cryopreserved. If the latter, cells were lifted with Accutase, spin down at 300 g for 5 mins and frozen at 5-6x10^6 cells/ml of Cryostore CS10™.

Upon fast-thawing vials of cortical progenitors at DIV 30 cortical neurogenesis, cells were centrifuged at 350 g for 5 mins and plated onto Poly-L-orthinite (Sigma) plus laminin-coated plates in NMM supplemented with 10 ng/ml FGF2, 10 μM ROCK Inhibitor, LV-TetO-mNgn2-T2A- Puro, and LV-Ubiq-rTA. This viral co-transduction strategy permitted Dox-dependent overexpression of NGN2 of cells in the cultures. Fresh NMM was removed and replaced with basal NMM in the following 8 hours. Cells were incubated for 2 days before both NGN2 and rTA expression being initiated with Dox-containing maturation media (DcMM) for another 2 days. This media was made up of 100% v/v Neurobasal containing 1x B27 Plus (with vitamin A), 1x Glutamax, 50 mg/ml penicillin-streptomycin, 1 μg/ml doxycycline, 10 ng/ml BDNF, 10 ng/ml NT-3, and 200 μM ascorbic acid. For the following 48 hours fresh DcMM supplemented with 1

μg/ml puromycin was fed to the culture to allow selection of only successfully transduced cells prior to final replating. Surviving cortical progenitors were subsequently lifted with Accutase and replated as single cells onto cortical rat astrocytes for future experiments. Media from now on was changed every 3-4 days and supplemented with Laminin. Single neurons were replated at the density of 65 - 100,000 cells/cm^2 with 10 μM ROCK Inhibitor.

2.2.7. Generation of iPSC-derived human midbrain-like organoid (hMLO)

iPSC differentiated into hMLO according to previously published protocol (Jo *et al.*, 2016) with several modifications as follows. 90% confluent iPSC were lifted using TrypLE™ and seeded onto round-bottom Costar® ultra-low attachment 96-well plate (Corning) at the density of 20,000 cells/well to form uniform embryoid bodies (EBs). EBs were maintained in oNMM supplemented with 1 μg/ml heparin (Sigma-Aldrich), 100 nM LDN193189 (Sigma) and 10 μM SB431542 (Abcam), 0.8 μM CHIR99021 (Reagents directs), and 10 μM ROCK Inhibitor Y27632. After 48 hours, medium was changed afresh in the absence of ROCK Inhibitor Y27632. On DIV 4, 100 ng/ml SHH-C25II (R&D System) and 100 ng/ml FGF8 (R&D System) were added into the culture medium to induce midbrain patterning. After 3-4 days, cell medium was removed completely, hMLO were immediately embedded in 30 μl of Matrigel™ and incubated for 30 mins at 37ºC. Pipette tip was pre-chilled and Matrigel was always kept cold to prevent solidification of Matrigel prior to embedding. After 30 mins, Matrigel-embedded hMLO were maintained in oNMM topped with 2.5 μg/ml insulin (Sigma), 200 ng/ml laminin (Sigma), 100 ng/ml SHH-C25II (R&D System) and 100 ng/ml FGF8 (R&D System) overnight. At this stage, a sizeable spheroid with extensive budding and neurite outward projection was visible. hMLO were then transferred to ultra-low attachment 6-well plates (Costar) using wide-bore 1000 μl pipette tips and induced toward greater growth and terminal differentiation in maturation medium made up of 100% v/v Neurobasal medium containing 1x N2, 1x B27, 1% GlutaMax, 1x non-essential amino acids, 100 μM β-mercaptoethanol (Merck), 50 U/ml Penicillin-

Streptomycin, 125µM db-cAMP (Sigma), 10 ng/ml BDNF (Peprotech), 10 ng/ml GDNF (Peprotech) and 100 µM ascorbic acid (Sigma). From now on, the medium was changed every 3-4 days.

2.2.8. Rat cortical astrocyte expansion

P1 primary cortical rat astrocytes purchased from ThermoFisher were plated on fresh sterile T75 flasks and grown in AMM for approximately 2 weeks till confluency. The medium was changed every 3-4 days. Once reaching confluency, P1 astrocytes were passaged with Accutase™ in the ratio of 1:7 to fresh sterile T75 flasks and grown for another 2-3 weeks till confluency. Once P2 astrocytes reached 100% confluency, they were cryopreserved in AMM supplemented with 10% DMSO at the density of 2x10^6 cells/1ml.
Fast-thawed vials of astrocytes were resuspended in AMM, plated at 50,000 cells/cm^2 and grown in AMM for 2 days before cortical neurons were plated on top of the astrocytic monolayer.

2.2.9. Microfluidic fabrication

Custom design of the master mould containing both duo- and trio-chambers was manufactured by Microliquid (Spain). Casting mixed was made from silicon elastomer (PDMS, SylGARD 184, Dow Corning ©) with its curing agent in the ratio of 1:10. The final mix was poured into the master mould which was then incubated for 3 hours at 60ºC for polymerisation to take place. Final devices were manually cut out from the negative cast using a sharp blade and soaked with 100% ethanol. Cut-out devices were air-dried in tissue culture hood and subsequently placed on ethanol –sterilised 19mm-diameter coverslips to form an instantaneously tight seal. Both the chambers and microchannel area were coated with poly-

D-lysin (0.1mg/ml) overnight, followed by three PBS washes and subsequently Geltrex™ (ThermoFisher) prior to cell culturing.

2.2.10. Immunofluorescence and imaging

For immunocytochemistry, culture was fixed with 2% PFA for 20 mins at room temperature (RT), rinsed with PBS, and antigen retrieved in citrate buffer pH 6.0 (ThermoFisher) in water bath at 80ºC for 5 mins. For staining with antibodies not DARPP32, antigen retrieval was omitted. Samples were left to rest for 10 mins at RT before being permeabilised and blocked in PBS, 10% donkey serum and 0.01% of Triton X-100 for 10 mins. Incubation of primary antibody in PBS and 10% donkey serum was performed overnight at 4ºC. Samples were washed with PBS and subsequently incubated in species-appropriate Alexa Fluor© secondary antibody in PBS with 10% donkey serum for 1 hour at RT.

To prepare for immunohistochemistry, hMLO were fixed in 4% PFA solution for 30 mins, followed by dehydration with a series of decreasingly diluted ethanol solutions of 100% for 30 mins, 95% for 30 mins and 70% for 60 mins. hMLO were then soaked in Histoclear for 30 mins twice to clear out tissue so as to attain uniform density of scatterers, minimise lateral scattering and ensure more efficient light penetration through the tissue. Lastly, hMLO were incubated in melting paraffin solution for 30 mins before being embedded using HistoStar™ embedder (Thermo Fisher Scientific). Paraffin-embedded hMLO were sliced into sections of 5 μm thick using HM 325 microtome (Thermo Fisher Scientific). Sections were mounted sequentially on pre-labelled and numbered slides such that each slide consisted of 5 sections that are each 150 μm. Slides were left to dry at RT before immunohistochemistry.
For immunohistochemistry, hMLO slides were first dewaxed in xylene followed by Histoclear, and rehydrated in 100%, then 95% and 70% ethanol, each for 2 mins, being washed in ddH2O for at least 5 mins. hMLO slides then were treated with 10% H2O2 (diluted in PBS) for 5 mins

to quench endogenous peroxidase and then washed again with RO water for 5 mins. After that, hMLO were antigen retrieved with citrate buffer pH 6.0 in microwave in a sequence as follows: 4 mins in microwave followed by 5 min rest, three times of 1.5 mins in microwave followed by 5 min rest, and lastly 1.5. mins in microwave. Heat-treated slides were incubated on ice to cool for 20 mins and area encompassing hMLO sections was subsequently marked out by hydrophobic ImmEdge pen and washed with TBS (200 ml tris 1M pH 7.5, 80 g NaCl, MiliQ® H2O to 1 L) plus 0.05% Tween (TBS-T). hMLO sections were then blocked with 130 µl blocking buffer made up of TBS, 10% normal donkey (or goat) serum and 0.1% of Triton X-100 for 60 mins. After 3 times TBS-T washes, slides were incubated in primary antibody solution overnight made up of TBS, 10% normal donkey (or goat) serum, and relevant dilution of primary antibody of interest as specified in Table 2.1.7. Samples were washed with 3 times TBS-T the next days and finally incubated in secondary antibody solution of similar make-up of TBS, 10% normal donkey (or goat) serum, and relevant dilution of secondary antibody of interest as specified in Table 2.1.8. A secondary antibody-only staining for each newly acquired antibody was tested on both MSN culture and hMLO sections as negative immunocytochemical controls.

MSN images were acquired on the Opera Phenix High-content Screening system (PerkinElmer) (for quantification) or the Invitrogen EVOS ™ FL Auto (ThermoFisher) (for visualisation) cell imaging system and subsequently processed on Harmony and ImageJ, respectively. ICC images to be counted were captured at 20x water-immersion, 30 fields/96 half-well plate, in Z-stack of 4 plan at 1.0 µm step. At 20x objective, 30 imaging field covers almost the entirety of 96 half-wells except the central region at which cells tend to peel away. All channels were captured in sequential order at 80% power and 40 ms exposure for most target except visualisation of DARPP32 which was set at 100ms. Each staining combination for each cell line was imaged and analysed in triplicate. Image analysis and quantification of neurons expressing specific markers

of cultures on polystyrene plates were performed automatically on Harmony using custom analysis pipelines. Positive signals were considered on the basis of signal intensity, morphology and co-colocalisation with other essential markers.

Similarly, images of hMLO sections were acquired on the Opera Phenix High-content Screening system (PerkinElmer) (for quantification) or the Invitrogen EVOS ™ FL Auto (ThermoFisher) (for visualisation) cell imaging system and subsequently processed on Harmony and ImageJ, respectively. The whole of each hMLO section staining for TH, MAP2 and FOXA2 to be counted were captured at 20x water-immersion, in Z-stack of 3 plan at 1.0 µm step. All channels were captured in sequential order at 80% power and 40 ms exposure for both FOXA2 and MAP2 but at 100ms for TH. 2-3 hMLOs derived from the same cell line were aligned to fit on a single paraffin-embedded section; each slide was mounted with 4-6 sections (of all 2-3 hMLOs of the same cell line) of 5.0 µm each taken at approximately 250 µm from one another. Cells of interest was counted and averaged across the 4-6 sections of the same hMLOs. Image analysis and quantification of neurons expressing specific markers were performed automatically on Harmony using custom analysis pipelines. Positive signals were considered on the basis of signal intensity, morphology and co-colocalisation with other essential markers. For example, a true TH-positive neurons counted on immunostained hMLO sections were considered to express nuclear DAPI, cytosolic MAP2 and overlapping cytosolic TH. Fluorescent intensity threshold for selection of positive signals were arbitrarily determined at the gain of 1 and with an arbitrary intensity unit (on Harmony) of no less than 1000. Segmentation of bulk positive signals into individual cells was also automatically performed by Harmony-based segmentation module which executes segmentation based on custom inputs of expected cell size, morphology, and density.

2.2.11. Fontana-Mason staining

hMLO paraffin-embedded sections of 5 μm thick were stained for presence of neuromelanin using the Fontana-Masson Stain Kit (Sigma HT200) as per manufacturer's instructions. Briefly, hMLO sections were first dewaxed and hydrated. Afterwards, they were incubated in pre-warmed Ammoniacal Silver for 60 mins top stain for neuromelanin. Samples were further incubated with gold chloride, sodium thiosulfate, and lastly counter-stained with nuclear fast red solution. Stained sections were dehydrated in ethanol, cleared in xylenes and finally mounted with synthetic resin. Visualisation of neuromelanin-positive cells were detected under Leica DMR fluorescence phase contrast microscope as black to brown cells against pink cellular background.

2.2.12. RNA extraction and Reverse transcription-quantitative polymerase chain reaction (RT-qPCR)

Cell medium was first fully aspirated, and culture was then washed with PBS once. Cells were lysed with Buffer LTE added with 1% β-mercaptoethanol and harvested into Eppendorf tubes. Total RNA of MSN culture over time was extracted and purified from cell lysates using RNeasy Mini kit (Qiagen) according to manufacturer's instructions. Extracted RNA was quantified and assessed on a Nanodrop (DS-11, Denovix). RNA was reversed transcribed into cDNA using superscript III reverse transcriptase kit (Life Technologies) in a 2-step protocol: firstly, 20 μl sample mixtures containing 500 ng of RNA, random primers, 10 mM dNTP mix and ddH2O were first heated to 65ºC for 5 mins followed by 1 min incubation on ice; and secondly, sample mixtures supplemented with 200 U/μl Superscript III reverse transcriptase, 1x first strand buffer, 0.1 M DTT, and 40 U/μl RnaseOut were cooled at 25ºC for 5 mins, heated up at 55ºC for 1 hour then 70ºC for another 15 mins. cDNA were stored at -20ºC till future amplification.

PCR was performed with standard SYBR green (ThermoFisher) in StepOnePlus thermal cycler (Life Technologies). The thermocycling conditions started with DNA denaturation at 94ºC for 2 minutes, followed by primer annealing at 60ºC for 30 seconds and extension at 72ºC for 45 seconds, and a final extension at 68ºC for 10 minutes. The PCR products were run by gel electrophoresis on a 1 % w/v agarose in 1x TAE buffer (40 mM Tris acetate, 1 mM EDTA) containing 1x SYBR Safe (Catalogue No.: S33102) at 100-120 V. DNA fragments were compared against a 1 kb or 500 bp DNA ladder (both from Invitrogen) and visualised with ChemiDoc™ Imaging System (Bio-Rad). The full list of primers used are tabled in Table 2.1.6.

2.2.13. Electrophysiology

Whole-cell recordings of MSN on coverslips were done at 27ºC with constant replacement of pre-warmed external solution which contained: 2.4 mM KCl, 167 mM NaCl, 10 mM Glucose, 10 mM HEPES, 1 mM $MgCl_2$, and 2 mM $CaCl_2$ adjusted to 300 mOsmol/l and pH 7.36 with NaOH. Neurons were patched with a borosilicate glass pipette (8-12MΩ) pulled using a Sutter P-97 Flaming Brown puller (Sutter Instrument Company) and filled with an internal solution consisting of: 140 mM $C_6H_{11}KO_7$, 6 NaCl, 1 mM EGTA, 4 mM MgATP, 0.4 mM Na_3GTP, 10 mM HEPES, and 0.01% Neurobiotin (SP-1120) adjusted to 290 mOsmol/l and pH 7.3 using KOH. Data were acquired with MultiClamp 700B amplifier (Molecular Devices) and Digidata 1550B digitiser (Molecular Devices) and analysed in Clampfit 10.7 (Molecular Devices). Cells were always clamped at -70 mV unless otherwise stated. Access resistance was constantly monitored; cells with access resistance greater than 50MΩ were excluded. All recordings were made within two hours of coverslip preparation.

Cell capacitance and input resistance were automatically reported from Clampex membrane test sampled at 33 kHz. Resting membrane potentials (RMP) were acquired immediately upon

successful break-in in current clamp with zero current injection. Liquid junction potential was estimated at 12 mV using JPCal (Barry, 1994) and adjusted for in RMP recordings.
Na_V and K_V currents were recorded in voltage clamp using a series of 400 ms square voltage steps of 10mV increments from -70 mV to +70 mV. Signals were sampled at 10 kHz and filtered at 2 kHz. Leak subtraction was applied with 4 sub-sweeps and a settling time of 250 ms. Evoked action potentials were recorded in current clamp by injecting 500ms current steps in 10 pA increments from -10 pA to +130 pA. Na_v peak currents are identified as the maximum negative current at each membrane potential within the first 50 ms. Fast A-type K_v peak currents are identified as the maximum positive current at each membrane potential within the first 50 ms. Slow activating K_v peak currents are identified as the average positive current at each membrane potential of the last 50 ms. Current density at each membrane potential is calculated by diving the peak current to the cell capacitance.

Induced action potential (iAP) was recorded in current clamp using clamp using a series of 500 ms square current steps of 10 mA increments from -10 mA to +150 mA. Recording cells were held at -70 mV at the beginning and in-between steps. At each current injection, an action potential is determined as a significant upward deflection of at least 20 mV that overshoot 0. Rheobase current is determined as the minimal current amplitude that results in the depolarization of the cell membranes and generation of an action potential.

Spontaneous EPSC and IPSC were recorded in voltage-clamp mode with 20x gain at reversal potential for inward inhibitory post-synaptic current (i.e. mostly via chloride-based channel) and inward excitatory post-synaptic current (i.e. mostly via AMPA receptors) i.e. -70 mV and 0 mV, respectively. The internal solution for spontaneous synaptic activity recordings was Cs-based containing 140 mM $C_6H_{11}CsO_7$, 6 mM NaCl, 1 mM EGTA, 4 mM MgATP, 0.4 mM Na_3GTP, mM 10 HEPES, and 0.01% Neurobiotin adjusted to 290 mOsmol/l and pH 7.3 using CsOH. All

sEPSC and sIPSC recordings were 1-4 min in duration and low-pass Bessel 8-pole filtered post-hoc. Spontaneous post-synaptic events and event magnitude were automatically detected based on absolute magnitude difference from the baseline (>10pA for sEPSCs and >15pA for sIPSCs) using threshold search function on Clampfit. Putative EPSC or IPSC events were excluded based on template-dependent criteria including rise time and half-width (<4ms and <1.2ms, respectively) and manually validated to reject false-positive events.
H89 (Tocris) was dissolved in dH2O and media applied to the middle (striatal) chamber to the final concentrations of 10 μM for 15 mins prior to recording.

All patched neurons were post-hoc labelled with Streptavidin-Alexa Fluor 488 conjugate (ThermoFisher) and DARPP32 (Sigma) to ascertain their MSN identity. Only neurobiotinylated neurons that co-expressed DARPP32 were selected for analysis.

2.2.14. Dendritic spine visualisation and quantification

Patched coverslip of MSN was immunolabelled for DARPP32 (as described above) and mounted onto SlowFade ™ Diamond Antifade mountant (ThermoFisher). Detection and imaging of DARPP32-positive Neurobiotin™-filled neurons were captured under Olympus FluoView FV1000 confocal microscope with argon and solid-state laser with 488 nm and 559 nm excitation, respectively. Z-stacks of images were sampled sequentially at resolution of 1024 * 1024 pixels, with 60x oil-immersion objective (NA = 1.40), at 1.05 μm steps as optimised by Nyquist sampling theorem. Dendritic branches of biotinylated neurons were captured at 3x software zoom. Images were segmented, reconstructed and automatically rendered using filament and spine detection module in Imaris 9.6.0 (Bitplane, South Windsor, CT, USA) which identified dendrites and detect protrusions along the dendritic filament length. Putative spines at branch points or disconnected dots were manually excluded.

2.2.15. PKA activity assay

Samples representative of each line or condition were lysed and pooled from 3 microfluidic devices. PKA activity was measured using the PKA Colorimetric Activity Kit (ThermoFisher) according to manufacturer's guidelines. Briefly, 40 μL of either cell lysate or lysis buffer standard was added into 96-well microtiter plate that had been pre-coated with an immobilised PKA substrate. Each well was supplemented with 10 μL of reconstituted ATP so as to facilitate PKA-mediated phosphorylation of the substrate. Phosphorylated substrate was detected by donkey anti-rabbit IgG HRP secondary antibodies treated with TMB. Absorbance indicative of phosphorylated substrate was read on PHERAstar® microplate reader (BMG Labtech) at 450 nm.

Protein concentrations of the same samples were quantified using Pierce™BCA Protein Assay Kit (ThermoFisher) following manufacturer's instructions. Briefly, 12 μL of either bovine serum albumin (BSA) standard or cell lysates was added into 96-well plate followed by 100 μL of BCA reagents. The plate was incubated at 37ºC for 30 mins before being read for BCA absorbance at 562 nm wavelength in a PHERAstar® microplate reader (BMG Labtech).

Protein concentration and PKA activity values were inferred from their respective standard curves. Final PKA activity read-outs were normalised against the sample protein concentrations and presented as U/ml. One unit (U) is defined as the amount of PKA required to catalyse the transfer of 1 pmol phosphate from ATP to substrate at 30ºC.

2.2.16. Cloning

All viruses were cloned using in-fusion technology with In-Fusion HD Cloning Kit®.

i. Vector linearisation

5 μg of lentiviral backbone vector (Figure 2.1) was first linearised with two relevant restriction enzymes overnight. Linearised vector solution was then incubated in Bio-Rad T100

thermocycler at enzyme-specific temperature (as recommended by the manufacturer) to deactivate restriction enzymes.

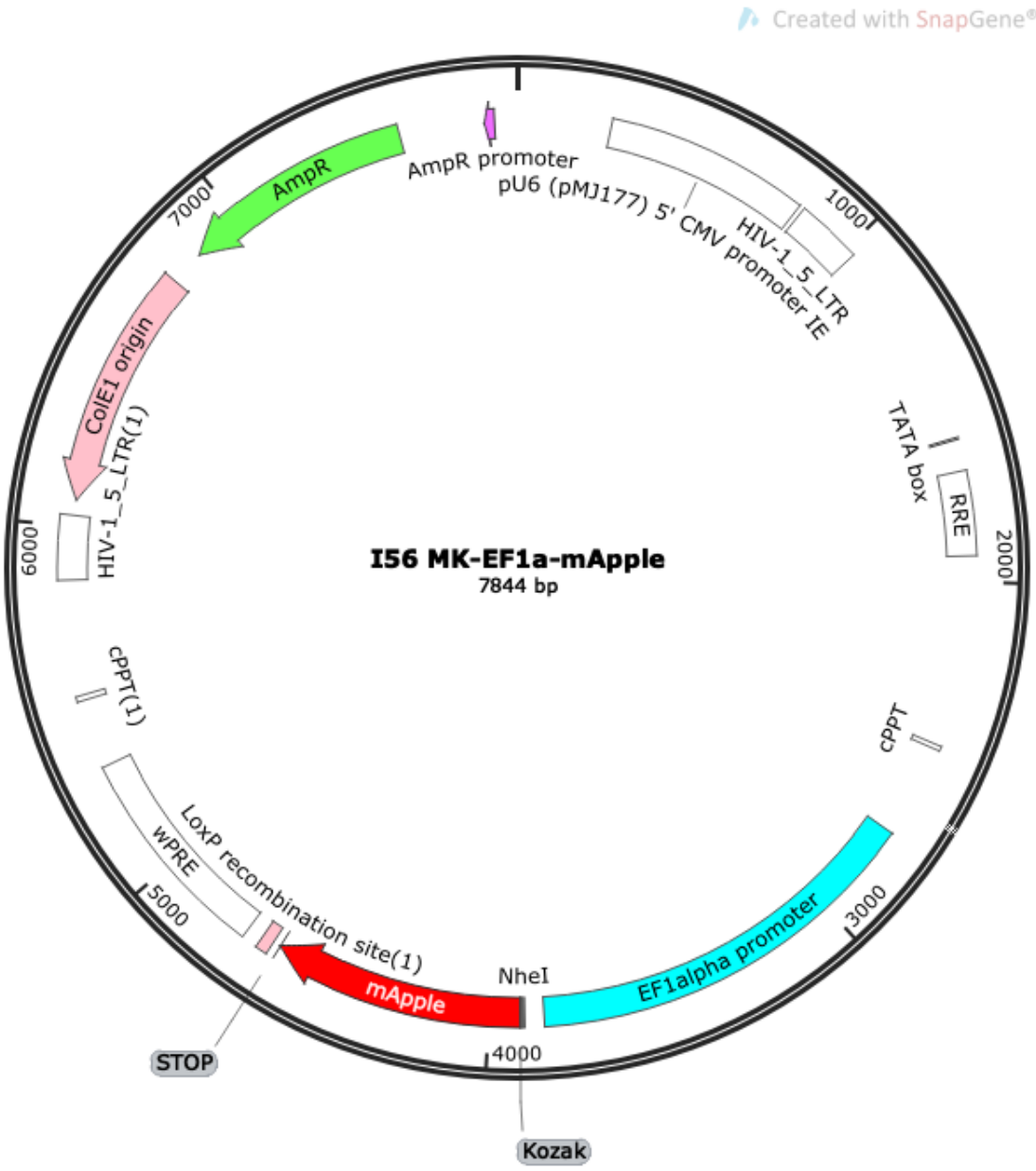

Figure 2.1: Map of lentiviral backbone used in the production of custom human TH promoter.

ii. Insert polymerase chain reaction

Inserts were ordered from IDT as Geneblock (< 2500 bp) or custom DNA oligos (> 2500 bp) depending on insert size. Corresponding forward and reverse primers were generated on

SnapGene such that they were 20 nucleotides homologous overlapping with digested vector on both ends. Amplification of inserts was performed with Q5® Hot Start High-Fidelity 2x Master Mix (NEB) mixed with 200 μM forward and reverse primer, 1 ng/μL template DNA, and nuclease free H2O to make up a final solution of 25 μl per sample. The thermocycler condition was as follows: 30 seconds at 98ºC for denaturation; 35 cycles of annealing starting with 10 seconds at 98ºC, followed by 30 seconds at gradient temperature 56-72ºC, and ending with 45 seconds at 72ºC; 2 mins at 72ºC for final extension; and infinity hold at 12ºC.
PCR reactions were subsequently treated with Dpnl for 1 hour at 37ºC to digest plasmid template DNA and run on gel electrophoresis at 1% w/v agarose in 1x TAE buffer (40 mM Tris acetate, 1 mM EDTA) containing 1x SYBR Safe at 100V. DNA fragments were compared against a 1 kb or 500 bp DNA ladder (both from Invitrogen) and visually inspected for accurate fragment length under the Chemidoc™ Imaging System (Bio-Rad). PCR products were purified using Macherey-Nagel gel and PCR clean-up kit (Catalogue No.: 740609.50) and quantified on Nanodrop.

iii. In-Fusion HD reaction

Insert PCR and 100 ng linearised vector were added in 2:1 ratio, supplemented with 1 μL of 2x NEBuilder(R) HiFi DNA Assembly Master Mix (New England Biolabs, E2621S) and mili-Q® water to make up a 5 μl reaction mix. Exact amount of insert PCR to be added was calculated using In-Fusion molar ratio online calculator. Reaction was performed in thermocycler at 50ºC for 15 mins and cooled to 4ºC.

iv. Transformation

One shot™ Stbl3™ chemically competent cells were purchased from Life Technologies (Catalogue No. C737303) and made readily competent for transformation in the absence of

heat-shocking and related procedure using the Mix&Go! E.Coli Transformation Kit and Buffer Set (Zymo Ressearch) as per manufacturer's instructions. In brief, Sbtl3™ was grown overnight in lysogeny broth (LB) and 0.5 ml of that culture was used to inoculate 50 ml ZymoBroth™ until the OD_{600nm} is 0.4-0.6. The culture was transferred to ice, centrifuged to obtain cell pellet which was then washed and resuspended in proprietary competent buffer. Competent cell suspension was aliquoted into single-use volume and stored at -80ºC.

On the date of transformation, competent Stbl3™ bacteria suspension was thawed on ice for 10 mins while LB agar plates supplemented with 100 μg/ml ampicillin was pre-warmed to 37ºC. 5 μl of In-Fusion reaction was added to 100 μl of Stbl3 and mixed gently by flicking. Reaction was incubated on ice for 5 mins for transformation to take place. Transformed bacteria was then spread onto pre-warmed plate and grown overnight at 37ºC.

v. Colony screening

Selected colonies from overnight transformed bacteria were amplified with a primer pair flanking segment of the backbone and the insert of no more than 500bp so as to identify positive colonies of correct insertion.

Firstly we prepared a PCR plate containing 10 μl reaction per well of MyTaq Red Master Mix, 200 μM of forward and reverse primers and water. Additionally, a U-bottom 96-well plate containing 100 μl LB and ampicillin per well was made in advance. 5-7 single colonies were picked from transformed bacteria plate with a 20 μl pipette tips which in turn was pipetted up and down into PCR plate for screening before being transferred into U-bottom 96-well plate for further growth in 37ºC incubator while PCR was running. PCR conditions for colony screening was as follows: 2 mins at 95ºC for denaturation; 34 cycles of annealing starting with 45 seconds at 95ºC, followed by 30 seconds at 55ºC, and ending with 1 min at 72ºC; 5 mins at 72ºC for final extension; and infinity hold at 12ºC. PCR products were run on gel

electrophoresis at 1% w/v agarose in 1x TAE buffer (40 mM Tris acetate, 1 mM EDTA) containing 1x SYBR Safe (Catalogue No.: S33102) at 100V. DNA fragments were compared against a 1 kb or 500 bp DNA ladder (both from Invitrogen) and visually inspected under Chemidoc™ imaging systems (Bio-Rad). Clones with correct band were further inoculated from the corresponding U-bottom well into 1 ml LB plus ampicillin and cultured until cloudy. Bacterial culture was centrifuged to collect cell pellets and bacterial plasmids were extracted using QIAgen Spin Miniprep Kit as per manufacturer's instructions.

vi. DNA sequencing

Selected plasmids were firstly amplified in BigDye Sequencing reaction. Single reactions were made up of 0.5 μL BigDye, 1.75 μL 5x sequencing buffer, 1 μL primer, 100 ng/μL DNA template mixed in water to the final volume of 10 μL. The PCR condition was as follows: 1 mins at 96ºC for denaturation; 30 cycles of annealing starting with 10 seconds at 96ºC, followed by 5 seconds at 50ºC, and ending with 4 mins at 60ºC; and infinity hold at 4ºC. Amplified DNA was purified with 4 μl of Precipitating Master Mix (125Mm EDTA, 3M NaAc), followed by 50 μl of 100% Ethanol. Plates were then spun at 3000 g 4°C, for 30 minutes, emptied and then washed again with 70 μl of 70% Ethanol. All ethanol content was subsequently removed after 1650 x g spinning at 4°C, for 15 minutes. Residual ethanol was further discarded by another spin at 185 x g, for 10 seconds. Samples were left to dry and sent off for Sanger sequencing at Department of Zoology sequencing service, University of Oxford. Samples were run on an Applied Biosystem 3730XL DNA analyser calibrated for BigDye V3.1. prior to sequencing

2.2.17. Axotomy on fluid-walled microfluidics (FWM)

All experimental steps involving fluid-walled microfluidics were performed together with Federico Nebuloni from the Cook and Walsh lab.

i. Fabrication of fluid-walled microfluidics

On DIV -07, 6 cm petri dishes were pre-coated with 7ml of Poly-L-ornithine overnight. On the following day, petri dishes were then washed with PBS twice, loaded with a thin layer of NMM followed by FC40* (special recipe made from the commercial FC40 by Federico and made propriety. FC40* was empirically found to make more stable wall), and subsequently jetted into an array of 3*7 dumbbells (3*3 cm) using an in-house fluid printer. The jetting mechanism has been previously reported (Soitu *et al.*, 2018). Dumbbell was coated with 2 µl of 0.46 mg/ml of Geltrex ™ (ThermoFisher) overnight.

ii. Establishment of human corticostriatal pathway

On Day -05, DIV 32 post-puromycin selection CN were finally replated into the cortical chambers of all dumbbells at the replating density of 13,000 cells/dumbbell. CN were deposited in 1 µl of cell suspension while 3 µl of cortical maturation media was deposited into the striatal chamber so as to create a positive fluid pressure gradient toward the cortical chamber, restricting movement of CN cell bodies away from the chamber. 2 days later, CN were transduced with LV-Ngn2-GFP, 50 µl of viral stock/2 µl of fresh cortical media to be deposited into the cortical chamber. Empty striatal chamber was also topped up with 2 µl of fresh cortical media, albeit without lentiviruses. On DIV 0, medium from the striatal chamber was removed and replaced with 1 µl of either MSN cell suspension (13,000 cells/dumbbell) or standard cortical media (i.e. DcMM) or cortical media supplemented with 10-fold BDNF (i.e. DcMM with 100 ng/ml BDNF). Fluorescent live images of all dumbbell conduits were taken just prior to MSN replating to serve as initial normalising timepoint. Images were taken on a digital SLR camera (Nikon D7100 DSLR) connected to an epi-fluorescence microscope (Olympus IX53; 1.25×, 4×, 10×, 25× objectives) equipped with a translation stage and an overhead illuminator

(Olympus IX3 with filters). Medium was changed every other day from now on for the next 20 days

iii. Directed axotomy on FWM

On DIV 20, fluorescent live images of all dumbbell conduits were taken again just prior to axotomy for the investigation of axon outgrowth using the same microscope setup. FC40* fluid walls were then washed away by gently pouring the FC40* out of the dish; the whole petri dish was washed again twice with NMM. All washing steps were done with great care to avoid cell peeling. Directed axotomy on corticostriatal axon tract was performed automatically and systematically using the in-house fluid printer as previously described (Soitu *et al.*, 2021). Following axotomy, petri dishes were loaded with fresh FC40* and new dumbbell was jetted around the margins of the previous ones. The new dumbbells were 4*4 in dimension to avoid physical damage to the cell materials. Fresh medium was deposited into their respective chamber as per their experimental conditions. Axon regeneration was visually monitored and microscopically captured at 36, 60, 84 hours post-axotomy. Images were analysed using Cell Profiler 3.8 (McQuin *et al.*, 2018) to describe and quantify ensuing events.

2.2.18. Statistical analysis

All data were presented as mean ± Standard error of the mean (SEM) unless otherwise stated. Raw data were tested for normality and statistical comparison of the means was performed using unpaired Student's t-test, two-way ANOVA with Bonferroni post-hoc test, Karuskal-Wallis test or Friedman corrected with Dunn's multiple comparison test when appropriate. Significance difference was considered at $p < 0.05$. All statistical analyses were performed on GraphPad Prism 6.0 (GraphPad Software).

Chapter 3: Investigating effects of an all iPSC-derived cortico-striato-nigral micro-circuit on the functional maturation of MSN using custom 3-chamber microfluidics.

3.1. Introduction

3.1.1. *In vivo* development of medium spiny neurons (MSN)

The striatum, the primary input nucleus of the basal ganglia, comprises of GABAergic neurons among which 90% are medium-sized spiny projection neurons (MSN) intermingled by a diverse group of cholinergic, fast-spiking and low threshold-spiking interneurons (Tepper and Bolam, 2004). Developmentally, the striatum arises from the ventral telencephalon (subpallium) which subsequently subdivides into distinct molecular structures: the medial, lateral and caudal ganglionic eminence (MGE, LGE and CGE, respectively) (Schuurmans and Guillemot, 2002). While the LGE gives rise to MSN, and hence the majority of the striatum, MGE and CGE are major sources of neocortical interneurons in human and primates (Hansen *et al.*, 2013; Ma *et al.*, 2013). MGE also contributes towards the pallidal projection neurons and the small population of striatal interneurons (Marin, Anderson and Rubenstein, 2000). As the results, development of MSN *in vitro* has been directed towards mimicking the specification of subpallial and LGE progenitors.

Post-mitotic MSN in the striatum are morphologically characterized by their medium-sized cell bodies (10-15 μm), substantially large and highly complex dendritic network, and spiny dendritic networks. Electrophysiological recordings reported MSN relatively 'quiescent' nature at rest with hyperpolarized resting membrane potential, delayed and long latency to fire and low intrinsic excitability (Lahiri and Bevan, 2020). MSN can be further categorically subdivided

into two main subtypes based on their molecular signatures and axonal projections: the direct pathway and indirect pathway MSN (Gerfen and Young, 1988; Gerfen *et al.*, 1990). The former constitutes mostly MSN preferentially projecting to the substantial nigra reticulata (SNr) or the internal globus pallidus (GPi) and expressing dopamine 1 receptor (D1R) and substance P and/or dynorphin. Meanwhile, the indirect pathway preferentially projects to the external globus pallidus (GPe) and expresses dopamine 2 receptor and enkephalin. Few other studies have also suggested a smaller proportion of D1R and D2R co-expressing MSN in both the nucleus accumben shell (17%) and the dorsal striatum (6%) (Bertran-Gonzalez *et al.*, 2008; Matamales *et al.*, 2009). Interestingly, due to the differential molecular composition including expression of dopamine receptors and releasable neurotransmitters, MSN subtypes exhibited slightly different electrophysiological and physiological properties (Cepeda *et al.*, 2008; Gertler, Chan and Surmeier, 2008), exerting differential role in orchestrating basal ganglia output. Generation of specific human subtypes of MSN *in vitro* to study their respective properties and functions, however, remains a challenge considering their close ontogeny.

3.1.2. Architecture of the striatal presynaptic microcircuit

The basal ganglia play a critical role in enacting and regulating decision making and selection of action. The striatum, the largest and most complex structure of the basal ganglia housing almost 2 million neurons, is the important hub of integrating, encoding and relaying information from both intrastriatal and afferent inputs from various brain regions (Rosen and Williams, 2001). Specifically, the striatum receives converging glutamatergic and dopaminergic inputs from the cortex and thalamus, and the midbrain respectively. Cortical and dopaminergic afferents form characteristic synaptic triad with MSN dendrites, specifically on MSN dendritic spine head and neck, respectively (Freund, Powell and Smith, 1984; Smith *et al.*, 1994). Corticostriatal terminals represent the major source of glutamatergic inputs to regulate striatal

GABAergic output while dopamine is thought to exert a modulatory influence on the responsiveness of MSN to excitatory synaptic signals via cell intrinsic excitability state (Nicola, Surmeier and Malenka, 2000). Previous *in vitro* works using primary striatal-cortical co-cultures demonstrated the essential role of cortical presence in facilitating functional and morphological maturation of striatal neurons (Segal, Greenberger and Korkotian, 2003; Penrod *et al.*, 2015). However, these studies were unable to capture the directionality of cortical and striatal connectivity critical for neural communication. Neither has there been successful attempt at recapitulating the striatal presynaptic triad in its endogenous presentation.

3.1.3. Microfluidic technology for cell culture

Since its inception approximately 30 years ago, microfluidics has matured into a much sought-after technology to advance our approach to biological research. The use of bio-compatible and relatively inert polydimethylsiloxane (PDMS) permits long-term culturing of cell cultures. Additionally, advancement in microfluidic fabrications and operations renders it versatile to various experimental design needs and interests. As the result, microfluidic platform has tremendously assisted efforts in modelling and understanding various biological systems, primarily enabling custom and precise control on neurite isolation (Bengoa-Vergniory *et al.*, 2020) as well as orchestrated neuronal circuitry (Virlogeux *et al.*, 2018; Iannielli *et al.*, 2019).

3.1.4. Aims

In this chapter, I aimed to:

- Generate an optimised and robust differentiation protocol of human MSN from healthy control iPSC.
- Recreate the striatal presynaptic microcircuit using custom microfluidics.

- Dissect the physiological relevance of modelling MSN *in vitro* in a circuitry manner.

3.2. Results

3.2.1. Generation and characterisation of iPSC-derived MSN from iPSC

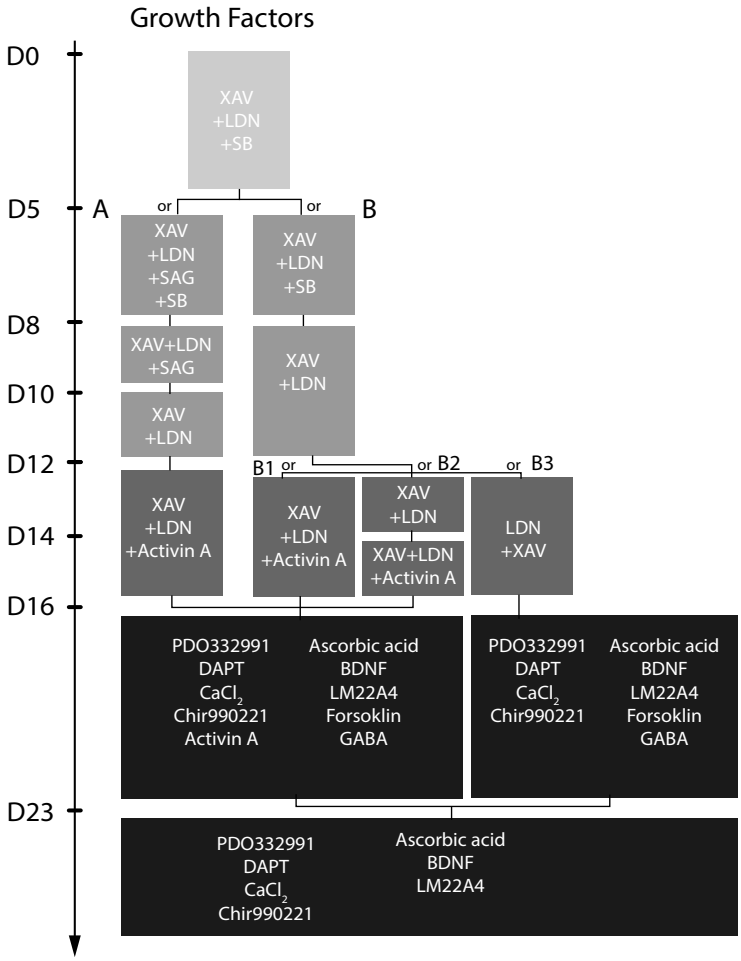

Figure 3.1: Schematics of iPSC-derived MSN differentiation paradigms. The vertical arrow represents timeline of cell cultures by days *in vitro*, i.e. D0 = day 0 *in vitro* . A, B, B1, B2, and B3 represent different paradigms. Different shade represents different stages of the differentiation at which point there are changes in the media make-up. XAV: Wnt signalling pathway inhibitor, LDN: inhibitor of the bone morphogenetic (BMP) pathway, SB: inhibitor of TGFß superfamily type I activin receptor-like kinase (ALK) receptor, SAG: SHH agonist, Activin A: TGFß family protein, PD0332991: inhibitor of CDK4/6, DAPT: inhibitor of γ-secretase; CaCl2: calcium chloride, Chir990221: glycogen synthase kinase 3 inhibitor, BDNF: brain-derived neurotrophic factor, LM22A4: tropomyosin-related kinase B (TrkB) agonist, Forsoklin: stimulates adenylate cyclase, GABA: γ-Aminobutyric acid.

MSN could be directed from the iPSC stage via neural induction of the forebrain followed by mild ventralisation towards the lateral ganglionic eminence (LGE) lineage – neural progenitors of MSN which are terminally committed toward post-mitotic MSN identity. We applied defined cocktails of small molecules so as to recreate the temporal *in vivo* development of MSN reflecting its telencephalic and LGE lineage (Figure 3.1A.). Firstly, neural induction of two-dimensional adherent culture was robustly directed using dual-SMAD inhibitors, LDN193189 and SB431542 (Chambers *et al.*, 2009). Additionally, inhibition of the beta-catenin/Wnt signalling, alone or in combination with low level of ventralising morphogen sonic hedghodge (SHH) was shown to be critical to promote specification of subpallium and LGE, often at the expense of the neighbouring medial ganglionic eminence (MGE) (Gulacsi and Anderson, 2008; Nicoleau *et al.*, 2013). Meanwhile, Arber et al. independently reported that activin A, a TGFβ family protein, could specifically induce LGE development in a SHH-independent manner under adherent culture condition (Arber *et al.*, 2015). Therefore, we explored various paradigms of SHH agonist, SAG, small molecular inhibitor of beta-catenin/Wnt, XAV, and activin A (Figure 3.1) to determine the most optimal condition to direct MSN differentiation.

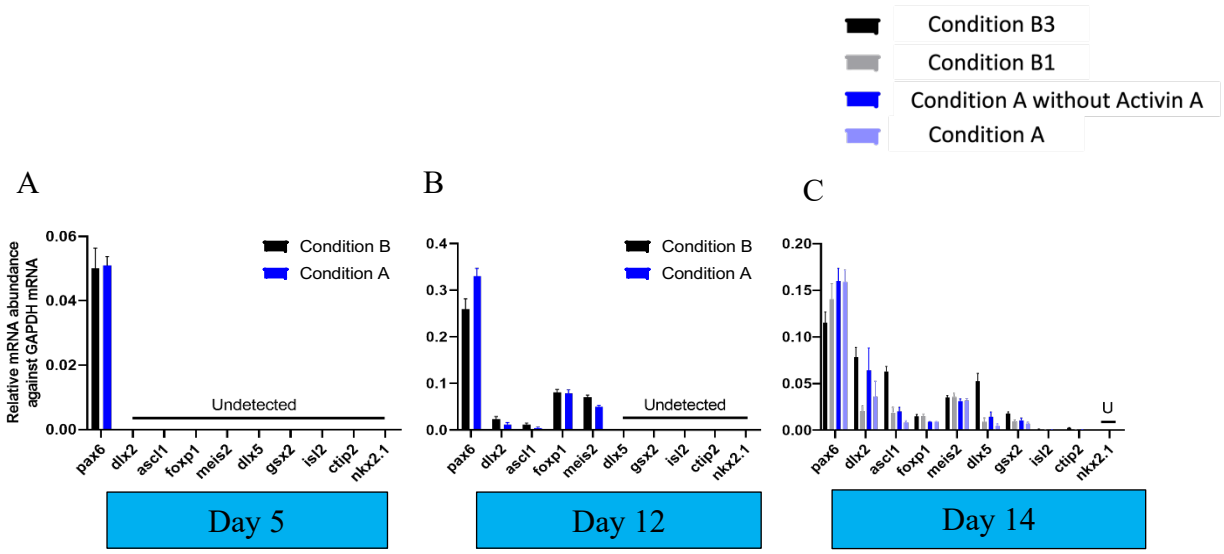

Figure 3.2: **Relative expression profile of cultures from different differentiation paradigms at DIV 5, 12, and 14.** Relative expression of selected genes were assessed against endogenous level of GAPDH at various time points using RT-qPCR. **A**. DIV 5 cultures expressed PAX6, the early telencephalic marker but no genes specific for LGE or MSN progenitors. **B**. On DIV 12, Pax6 expression persisted and expression of pan-GE markers, DLX2 and ASCL1, as well as of LGE markers, FOXP1 and MEIS2, was also detected. **C**. All DIV 14 cultures displayed expression of PAX6, DLX2, ASCL1, FOXP1, MEIS2 as DIV 12 cultures. MSN progenitor-specific genes, ISL1 and CTIP2, were undetectable on DIV 12 but detected on DIV 14. NKX2.1, marker of the MGE, was not found at any timepoint. Interestingly, GSX2, the subpallial marker was only detected in DIV 14 but not DIV 12. All data were presented as mean ± SEM. 'U' or 'Undetected' represented expression out of the detectable range i.e. Ct value was greater than 35 and/or its melting curve exhibited multiple peaks. n=2 differentiations, 4 healthy control lines/differentiation. Healthy control iPS cell lines used in here were SFC156-03, SFC856-03, JR053 and 840. GE, ganglionic eminence, LGE, lateral ganglionic eminence; MGE, medial ganglionic eminence.

Culture development in response to various small molecules was examined at various developmental timepoints by determining the expression profile of marker genes relative to the housekeeping GAPDH level (Figure 3.2). Genes of interest were considered present if their Ct values were smaller than 35 and their melting curves exhibited a single peak below 90°C. I found that at DIV 5, 12 and 14, all differentiation paradigms expressed the same set of transcript markers: PAX6, the early telencephalic marker, was expressed early at DIV 5, suggesting the forebrain lineage (Figure 3.2A); expression of pan-GE progenitor-specific genes, DLX2 and ASCL1, together with that of early LGE progenitor markers FOXP1 and MEIS2, were only detected on DIV 12 and persisted on DIV 14 (Figure 3.2B), suggesting commitment toward GE specification at this stage. Importantly, I found emerging expression of another LGE progenitor maker, DLX5, and early MSN progenitor markers, ISL1 and CTIP2, in minute amounts since DIV 14 (Figure 3.2C). Interestingly, the expression of GSX2, the subpallial markers, was only detected since DIV 14. NKX2.1, the MGE-specific protein, was undetectable at all three checkpoints. Taken together, the transcript expression profile in all culture conditions suggested a directed developmental trajectory towards MSN potentially via telencephalic and LGE intermediates with negligible MGE-driven identity.

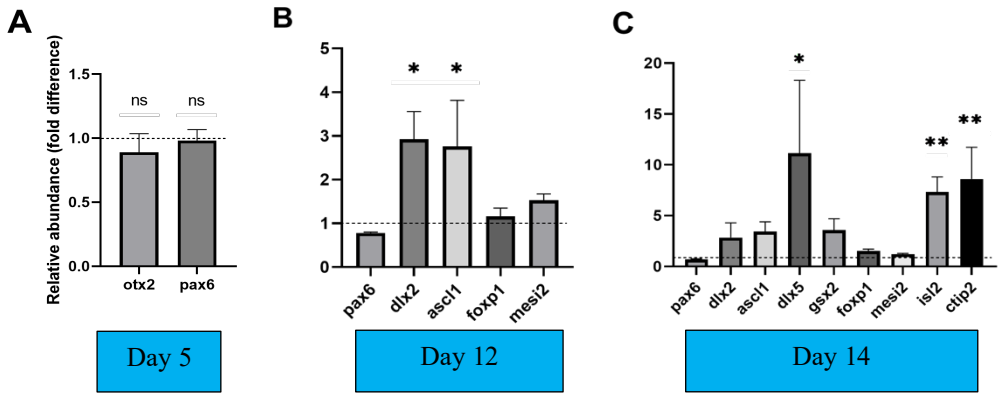

Figure 3.3: Relative expression of selected genes of cultures from differentiation condition B1 as compared to differentiation condition A. DIV 5 PAX6 expression was similar between both conditions, prior to SAG addition. B. Culturing in the absence of SAG exhibited significantly increased expression of pan-GE markers DLX2 and ASCL1 in D12 cultures. **C.** 2 days after Activin A introduction, condition B cultures still showed increased expression of all selected genes, significantly the LGE-progenitor marker DLX5 and MSN progenitor markers, ISL1 and CTIP2. All data were presented as mean ± SEM. Dotted line represent the Day 0 level which was used as the control timepoint against which transcript expression in other days will be normalised so as to show relative transcription expression changes overtime. * $p < 0.05$; ** $p < 0.005$. n=2 differentiations, 4 healthy control lines/differentiation. Healthy control iPS cell lines used in here were SFC156-03, SFC856-03, JR053 and 840 GE, ganglionic eminence; LGE, lateral ganglionic eminence.

To examine the effect of SHH signalling on LGE specification, expression of selected genes between condition A and B was compared. Although PAX6 levels from both conditions were similar on DIV 5 (Figure 3.3A), expression of all subpallial and LGE progenitor markers, particularly DLX2 and ASCL1, was greater in condition B than A, suggesting the undesirable effect of 100 nM SAG from DIV 5-10 coupled with XAV in limiting the directed specification toward MSN identity (Figure 3.3B). Consequently, DIV 14 condition B culture generally expressed higher level of LGE and MSN progenitor markers, particularly DLX5, ISL2, and CTIP2, than condition A cultures of similar DIV (Figure 3.3C). The effect of DIV 12 Activin A was also assessed from the relative abundance of selected genes in cultures with and without Activin A. Regardless of SAG conditioning, Activin A promoted expression of all selected markers for pan-GE, LGE or MSN progenitors, particularly CTIP2, as early as 2 days post Activin A treatment

(p<0.05) (Figure 3.4), suggesting the utility of activin A in striatal development from iPSC independent of SHH signalling.

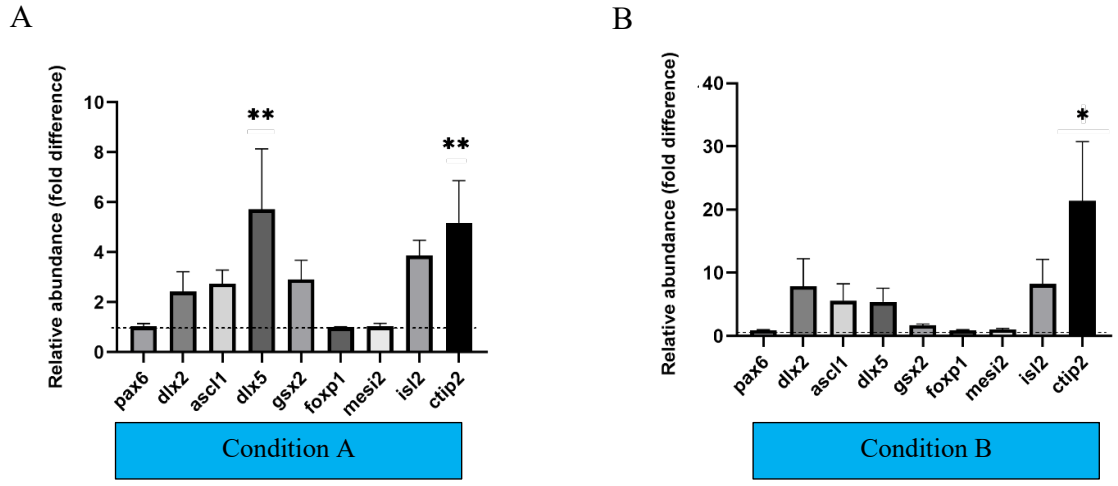

Figure 3.4: Effect of Activin A at DIV 12 on expression of selected genes on DIV 14 cultures in differentiation condition A and B illustrated by relative abundance of selected genes of each condition with the addition of Activin A at DIV 12 (i.e. B1) normalised against that of the same condition in the absence of Activin A (i.e. B3). A-B. Activin A generally promoted expression of all pan-GE, LGE and MSN progenitor markers. Statistically different expression was seen with DLX5, CTIP2 and ISL1 in condition A and only Ctip2 in condition B. All data were presented as mean ± SEM. Dotted line represent the Day 0 level which was used as the control timepoint against which transcript expression in other days will be normalised so as to show relative transcription expression changes overtime. * $p < 0.05$; ** $p < 0.005$. n=2 differentiations, 4 healthy control lines/differentiation. Healthy control iPS cell lines used in here were SFC156-03, SFC856-03, JR053 and 840. GE, ganglionic eminence; LGE, lateral ganglionic eminence; MSN, medium spiny neuron.

Efficiency of the different MSN differentiation paradigms was characterised on DIV 35 by examination of MAP2 expression together with CTIP2 and DARPP32 co-expression across four different healthy control iPS cell lines (Figures 3.5A and B). The mean percentage of CTIP2 and DARPP32 double-positive postmitotic (i.e. MAP2+) neurons was greatest in the absence of SAG with Activin A added on DIV 12 (Condition B1) (26.5% ± 3.1) |(Figure 3.5C). More importantly, average CTIP2 and DARPP32 co-expression at this condition was similar across all experimental lines, demonstrating the robustness of this protocol in multiple healthy control iPS cell lines

also routinely used in the lab for differentiation into other neuronal types such as DaN and CN. MSN was further characterized across four different healthy control iPS cell lines by the expression of other MSN-specific proteins such as dopamine 1 receptor (D1R), Calbindin (CB), and GAD67 (58.8% ± 8.5), GABAergic neuron marker (Figures 3.6A). Almost all differentiated neurons in all conditions displayed D1R (93.4% ± 4.8, 95.5% ± 2.2, 94.6% ± 3.8, and 94.1% ± 1.7 in condition A, B1, B2, and B3, respectively), GAD67 (81.2% ± 12.8, 74.8% ± 18.1, 78.3% ± 8.4, and 54.7% ± 13.2 in condition A, B1, B2, and B3, respectively), and Calbindin (56.5% ± 5.1, 43.8% ± 10.2, 44.3% ± 8.2, and 50.7% ± 7.6 in condition A, B1, B2, and B3, respectively) (Figures 3.6D-F). Likewise, expression of all three markers was comparable between all four healthy control iPS cell lines derived from each differentiation condition. Taken together, these data pointed towards the most optimal differentiation condition of MSNs from iPSC via the coordination of XAV-induced inhibition of WNT signalling pathway and timely activation of TGFβ signalling via Activin A at DIV 12 in the absence of SHH signalling (Figure 3.7A). This protocol from thereon was used as the final optimized differentiation condition for our generation of iPSC-MSN from any of the healthy control iPS cell lines available in our repository.

RT-qPCR to examine temporal transcript abundance of LGE and MSN progenitor markers of cells derived from this differentiation paradigm (Figure 3.7A) suggested a gradual patterning of iPSC towards MSN reminiscent *in vivo* developmental trajectory (Figure 3.7B-D). Specifically, LGE-specific genes such as DLX2, ASCL1, and GSX2 were enriched in early cultures and such enrichment was subsequently reduced in post-mitotic MSN (Figure 3.7B). Meanwhile, expression of selected markers of MSN progenitors including ISL1, DLX5, FOXP1, and MEIS2 increased over time and remained abundant in post-mitotic MSN cultures (Figure 3.7C). CTIP2, GAD67, and DARPP32, which are indicative of post-mitotic MSN, were virtually absent in early cultures and only subsequently expressed in great abundance since DIV 14 (Figure 3.7D).

Notably, expression of NKX2.1, the medial ganglionic eminence marker, was not detected throughout the culture development (Figure 3.7B); TH transcript was found present (Figure 3.7D), suggesting the cellular heterogeneity of the resulting iPSC-MSN culture.

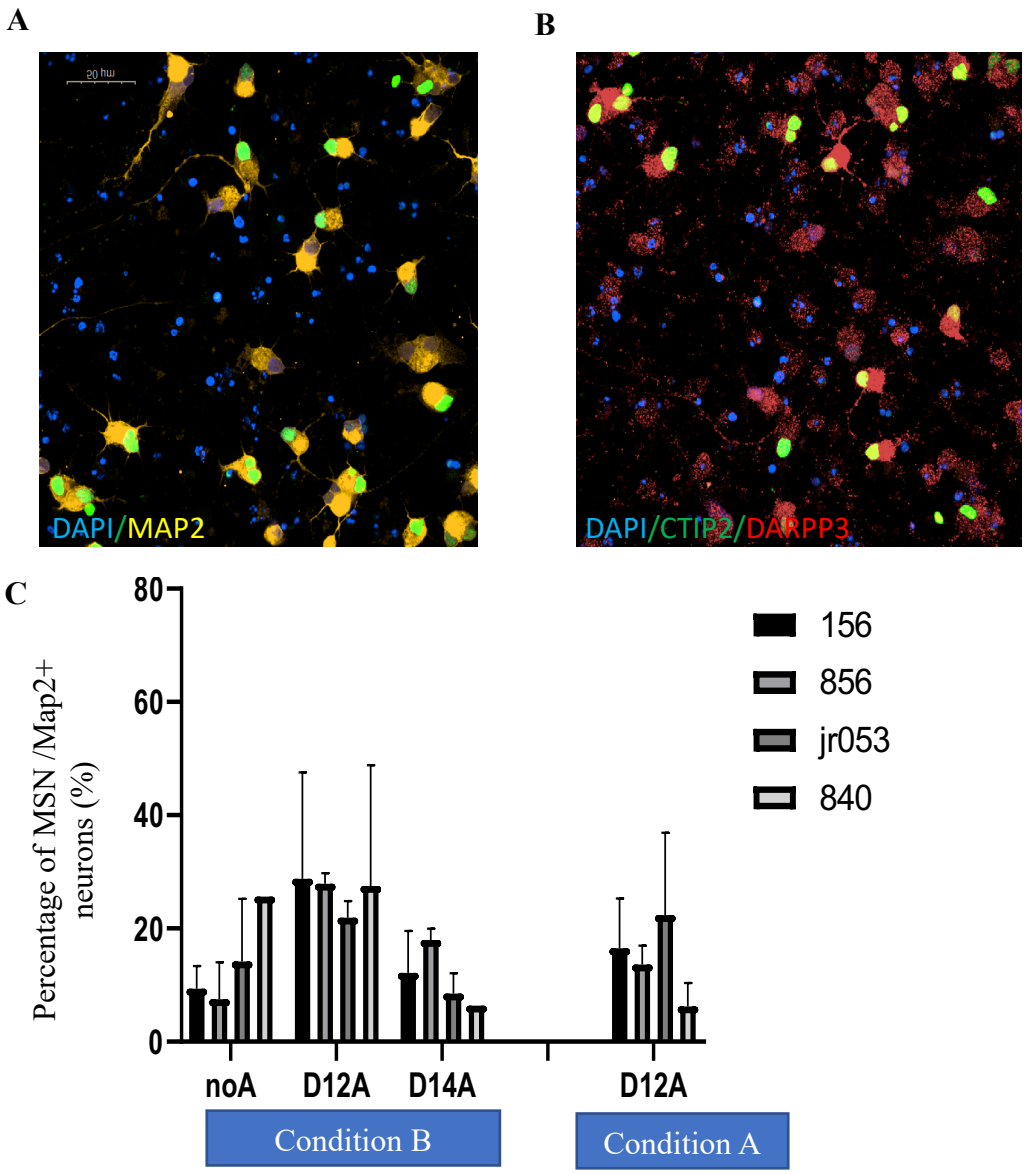

Figure 3.5: DIV 35 MSN characterisation by CTIP2 and DARPP32 co-expression across four different healthy control iPS cell lines. A) Representative images of MSN double-positive for CTIP2 and DARPP32 in condition B2. B) Percentage of MAP2-positive MSN is the greatest in condition B with Activin A addition on day 12 (i.e. D12A), albeit not to a statistically significantly level. NoA, D12A and D14A mean no Activin A added (condition B3), Activin A added on DIV 12 (condition B2) and on DIV 14 (condition B1), respectively. All data were presented as mean ± SEM. n=2 differentiations, 4 healthy control iPS cell lines/differentiation. Healthy control iPS cell lines used in here were SFC156-03 (i.e. 156), SFC856-03 (i.e. 856), JR053 (i.e. jr053) and 840.

Immunostaining of MSN at DIV 35 produced from the optimised differentiation protocol

confirmed the presence of MAP2^{+} neurons which were GABAergic in nature (GAD67^{+}) and co-expressed canonical markers DARPP32 and CTIP2 (Figure 3.7E-F). I also observed expression of selected markers specific to both the direct- and indirect-pathway MSN at DIV 35 (Figure 3.8A-B). Interestingly, the expression profile of sub-type marker exhibited similar temporal pattern, suggesting that there was no directed differentiation towards one subtype at the expense of the other. Immunostaining confirmed expression of MSN-subtype specific neurotransmitter and neurotransmitter precursors including PENK, PDYN and SUBSTANCE P at DIV 45 (Figure 3.8C). Quantification of GABAergic neurons co-expressing either PKEN or PDYN or SUBSTANCE P suggested the dominant presence of direct pathway MSN intermingled by modest population of indirect pathway MSN within my cultures (Figure 3.8D).

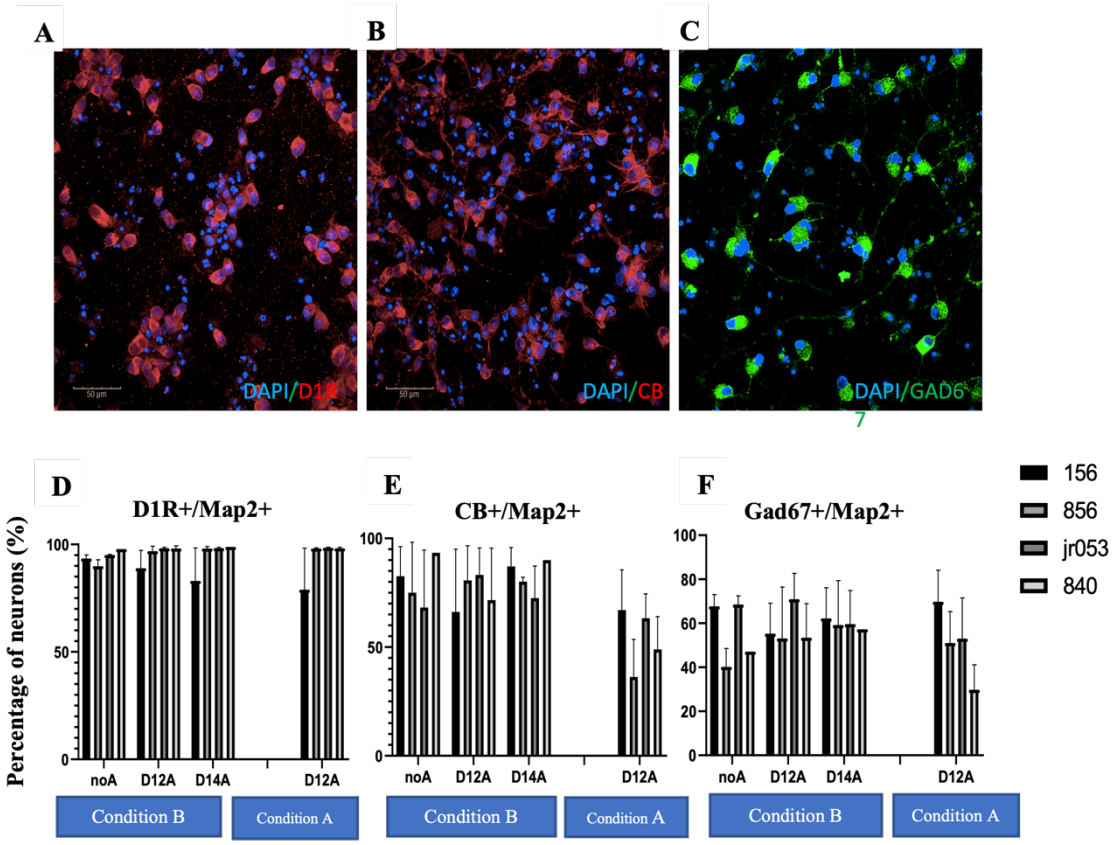

Figure 3.6: Characterisation of DIV 35 MSN derived from four different healthy control iPS cell lines across various differentiation conditions by expression of Dopamine 1 receptor (D1R), Calbindin (CB), and GAD67. A-C) Representative immuostaining images of DIV 35 MSN expressing A) D1R,) CB and C) GAD67. D-F) Average percentages of DIV 35 MSN neurons co-expressing D) D1R and MAP2,) CB and MAP2, and C) GAD67 and MAP2 across different iPS cell lines and differentiation conditions. NoA, D12A and D14A mean no addition of Activin A (condition B3), addition of Activin A on D12 (condition B2) and on D14 (condition B1), respectively. All data were presented as mean ± SEM. N=2 differentiations/cell line.

I next performed whole cell patch-clamping to examine functional maturation of DARPP32-positive iPSC-MSN (Figure 3.7H). Our iPSC-MSN displayed hyperpolarised resting membrane potential (DIV 40-45: -51.2 ± 1.62 mV, n = 25 neurons; DIV 55-60: -53.3 ± 1.47, n = 43 neurons; DIV 70-75: -55.1 ± 1.36 mV, n = 29 neurons), large cell capacitance (DIV 40-45: 24.0 ± 1.26 pA, n = 24 neurons; DIV 55-60: 28 ± 1.11 pA, n = 42 neurons; DIV 70-75: 31.6 ± 2.31 pA, n = 26 neurons), and large input resistance (R_{in}) (DIV 40-45: 1.39 ± 0.15 GΩ, n = 20 neurons; DIV 55-60: 1.29 ± 0.10 GΩ, n = 41 neurons; DIV 70-75: 1.0 ± 0.08 GΩ, n = 27 neurons) (Figure 1I-K). There was no significant improvement of these intrinsic properties of MSN from DIV 40-75 (RMP: p = 0.265; R_{in}: p = 0.09; all were analysed with one-way ANOVA with Bonferroni multiple comparison correction test) with the exception of cell capacitance between DIV 40-45 and DIV 70-75 (p = 0.009). Moreover, I observed firing of action potentials (APs) with the characteristic delayed first spike upon current injections (Figure 3.7G). The proportion of functionally mature neurons that displayed evoked APs to those that were unresponsive increased as the culture aged (DIV 40-45: 7/10 neurons; DIV 55-60: 20/14; DIV 70-75: 14/6) (Figure 3.7L). These data indicated robust generation of electrophysiologically active MSN monoculture that stay electrophysiologically stable between DIV 40-75.

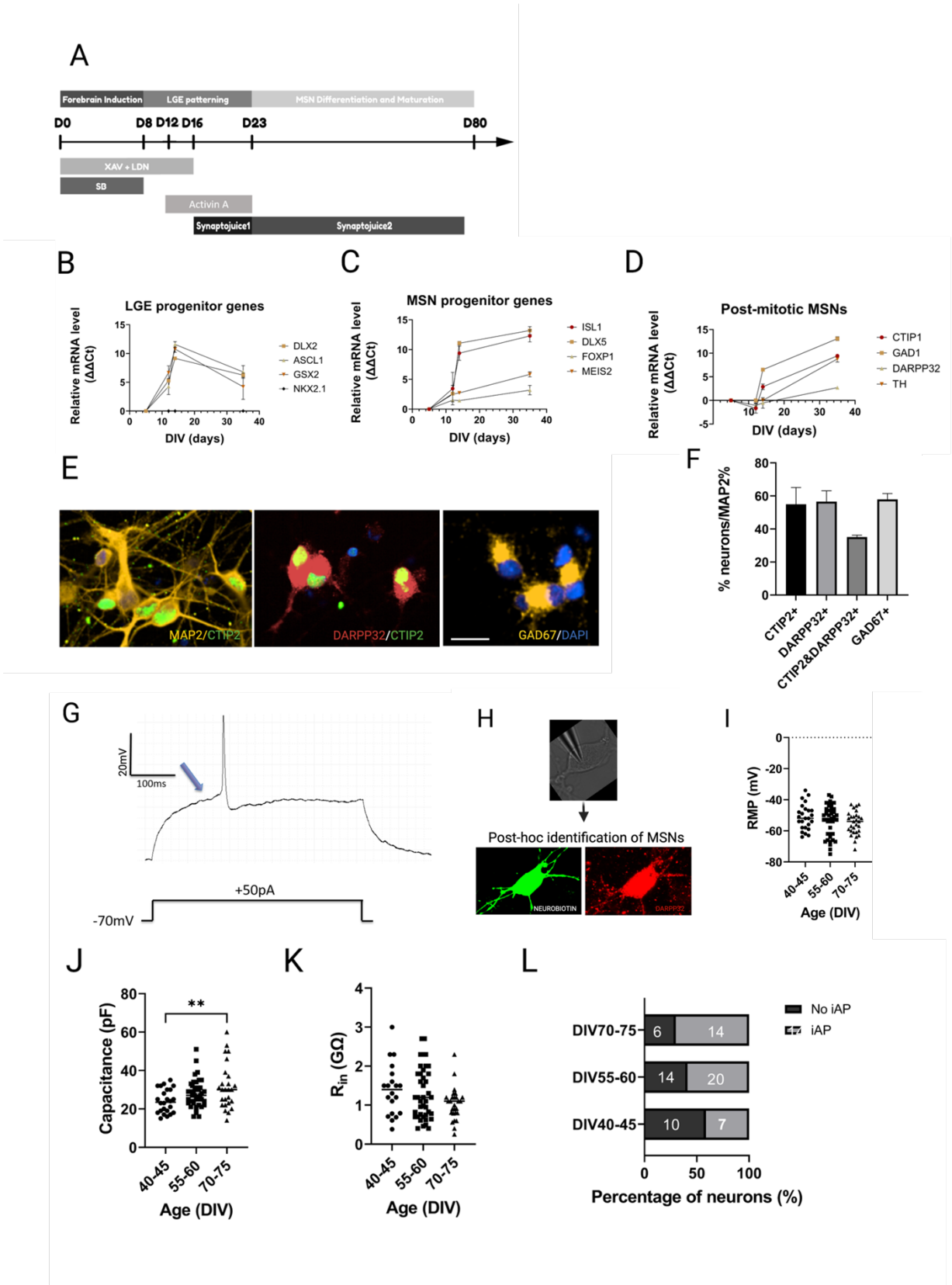
A
Forebrain Induction
LGE patterning
MSN Differentiation and Maturation
D0
D8 D12 D16
D23
D80
XAV + LDN
SB
Activin A
Synaptojuice1
Synaptojuice2
B
LGE progenitor genes
Relative mRNA level (ΔΔCt)
DIV (days)
DLX2
ASCL1
GSX2
NKX2.1
C
MSN progenitor genes
ISL1
DLX5
FOXP1
MEIS2
D
Post-mitotic MSNs
CTIP1
GAD1
DARPP32
TH
E
MAP2/CTIP2
DARPP32/CTIP2
GAD67/DAPI
F
% neurons/MAP2%
CTIP2+
DARPP32+
CTIP2&DARPP32+
GAD67+
G
20mV
100ms
+50pA
-70mV
H
Post-hoc identification of MSNs
NEUROBIOTIN
DARPP32
I
RMP (mV)
Age (DIV)
J
Capacitance (pF)
**
Age (DIV)
K
R_{in} (GΩ)
Age (DIV)
L
No iAP
iAP
DIV70-75
DIV55-60
DIV40-45
Percentage of neurons (%)

Figure 3.7: Generation and characterisation of iPSC-derived MSN. (A) Differentiation condition of medium spiny neurons (MSN) from iPSC. (B-D) Temporal expression of selected markers of LGE progenitors (B), MSN progenitors (C) and post-mitotic MSN (D) from DIV 0 till DIV 35. (E) Immunostaining for MAP2 (yellow), CTIP2 (green), DARPP32 (red), GAD67 (yellow) and DAPI (blue) and (F) quantification of their expression in percentage term at DIV 40-45, Scale bar = 20 μm. G) Representative traces of evoked APs (iAP) showing slow-ramp depolarisation of MSN. Blue arrow indicates delayed first spikes. (H) Whole-cell patch-clamp recording and subsequent post-hoc identification of neurobiotin-filled DARPP32+ neurons for electrophysiological analysis. (I-K) (I) Resting membrane potential (RMP), (I) cell capacitance (J), and (K) input resistance of iPSC-derived MSN over time from DIV 40-75. Each dot represents a single neuron, 2-way ANOVA corrected with Bonferroni post-hoc test, **p<0.01, ns p>0.05. (L) Number of MSN that displayed evoked action potential upon current injection (iAP) and MSN that did not (no iAP) over time. All data were presented as mean ± SEM, N = 3 differentiation experiments of 3 iPS cell lines, unless otherwise stated.

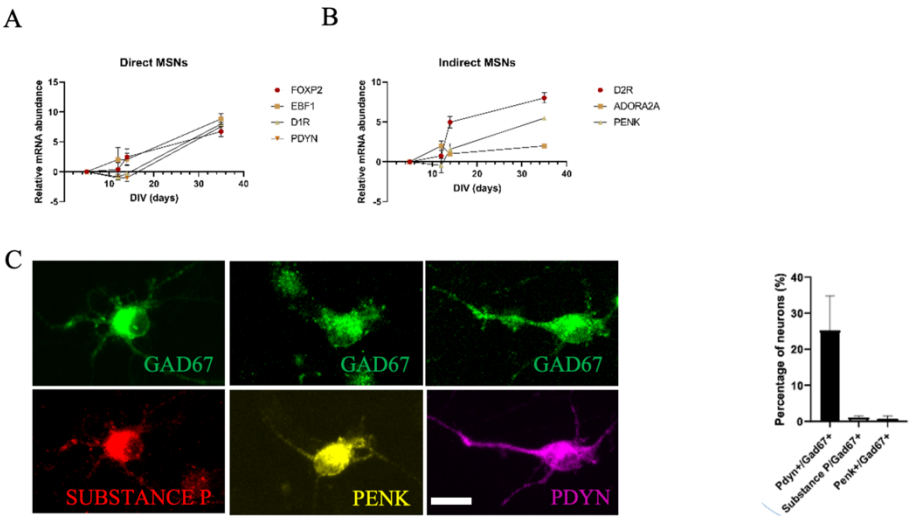

Figure 3.8: Characterisation of MSN subtypes. Cultures contained a mixture of both direct and indirect MSN. (A-B) Transcript abundance of selected marker of (A) direct MSN and (B) indirect MSN over time at DIV 35. Expression was averaged from 2 differentiations of 3 independent iPS cell lines. (C) Immunostaining for GAD67 (green), SUBSTANCE P (red), PKEN (yellow), and PDYN (magenta) at DIV 45 (D) Proportion of GAD67+ cell co-expressing different MSN subtype-specific neurotransmitters at DIV 50, scale bar = 20 μm. All data are presented as mean ± SEM, N = 2 differentiation experiments of 3 iPS cell lines.

3.2.2. Establishment of the striatal presynaptic microcircuit

i. Directed coculturing of iPSC- cortical neurons, MSN, and dopaminergic neurons on open 3-chamber microfluidic platform

Despite the functionally active status of iPSC-derived MSN in monoculture, I still noted a more depolarised RMP and larger R_{in} relative to *in vivo* MSN (Penrod *et al.*, 2015; Lieberman *et al.*, 2018). I hypothesised that such discrepancy was principally due to the lack of non-autologous synapses that endogenously provided valuable developmental cues to modulate MSN functional maturation. To address the lack of maturational signalling within MSN monoculture, I reconstructed *in vitro* the striatal microcircuit mimicking part of the pre-synaptic complexity neighbouring MSN using polydimethylsiloxane – based open three-chamber microfluidic chips. The device consisted of three rectangle chambers (4*10mm) connected via an array of 20 microgrooves of 5 µm wide, 500 µm long and 5 µm high (Figure 3.9A). The narrow width of microchannels compartmentalised neuronal soma in their respective chambers while DaN and CN elongated axons, and not their dendrites, traversed the full 1 mm length of the microchannels to make connections with MSN in the middle chamber (Figure 3.9C).

iPSC-DaN, CN, MSN and rat astrocytes were sequentially plated into their respective chambers so as to recapitulate the cortico-striato-nigral microcircuit in the striatum (Figure 3.9D). I differentiated CNs from iPSC according to protocol optimised by a fellow lab member Bryan Ng who himself has adopted the protocol from previous lab member Emma Whiteley. Emma also provided electrophysiological evidences of functional advantages of coculturing of the resulting iPSC-derived CNs with rat astrocytes is depicted in Figure 3.9. DaN differentiation is routinely performed in large quantity in the lab and those used in this project are generously donated by fellow lab members. Molecular characterisation of the resulting DaN culture

expressing canonical markers of midbrain DaNs including TH and FOXA2 is illustrated by Figure 3.10. As each vial of frozen iPSC was thawed, expanded and shared among a few lab members each of whom performs differentiation of either DaNs and CNs of their individual experimental interests, we reported to one another at meetings and discussion sessions if there is suspicious and/or substantial cell death, unhealthy cell by morphological examination, and strange phenotypes from various biological assays. This exchange of information allows everyone to be readily informed if there is suspicion on potential cell stock-specific issues. Each cell type was replated onto the microfluidic device on their final replating day as per their individual differentiation protocol (Figure 3.11D). Axons were physically guided toward the middle MSN chamber via flow pressure driven by volume difference across chambers (Figure 3.11B). Since BDNF and laminin were shown to be selectively critical for axon differentiation and development (Turney and Bridgman, 2005; Cheng *et al.*, 2011), I set up an artificial BDNF and laminin gradients across the channels to chemically attract axonal projections from the CN and DaN chambers into the middle MSN chambers (Figure 3.11B) prior to MSN deposition. Dopaminergic and cortical axons took approximately 10 days *in vitro* to fully cross and occupy all twenty available microgrooves. I restricted MSN axons travelling out to the DaN and CN chambers by delaying seeding of MSN till after all microgrooves had been populated with DaN or CN axons (Figure 3.11C). By DIV 0 of the microcircuit culture, axons of both DaN and CN densely projected the MSN chamber, poised to regulate MSN progenitor development. In addition to attaining directed connectivity, the culturing schedule was also coordinated to incorporate known temporal features of these neurons characterised in their respective monoculture. Two main objectives include i) DIV 16 MSN progenitors are circuited with post-mitotic and functionally active DaN and CN and ii) at our experimental timepoints (i.e. DIV 40-70 MSN) all three neuronal populations should be individually electrically active (see Figure 3.7H-M, (Hartfield *et al.*, 2014; Hedegaard *et al.*, 2020)) .

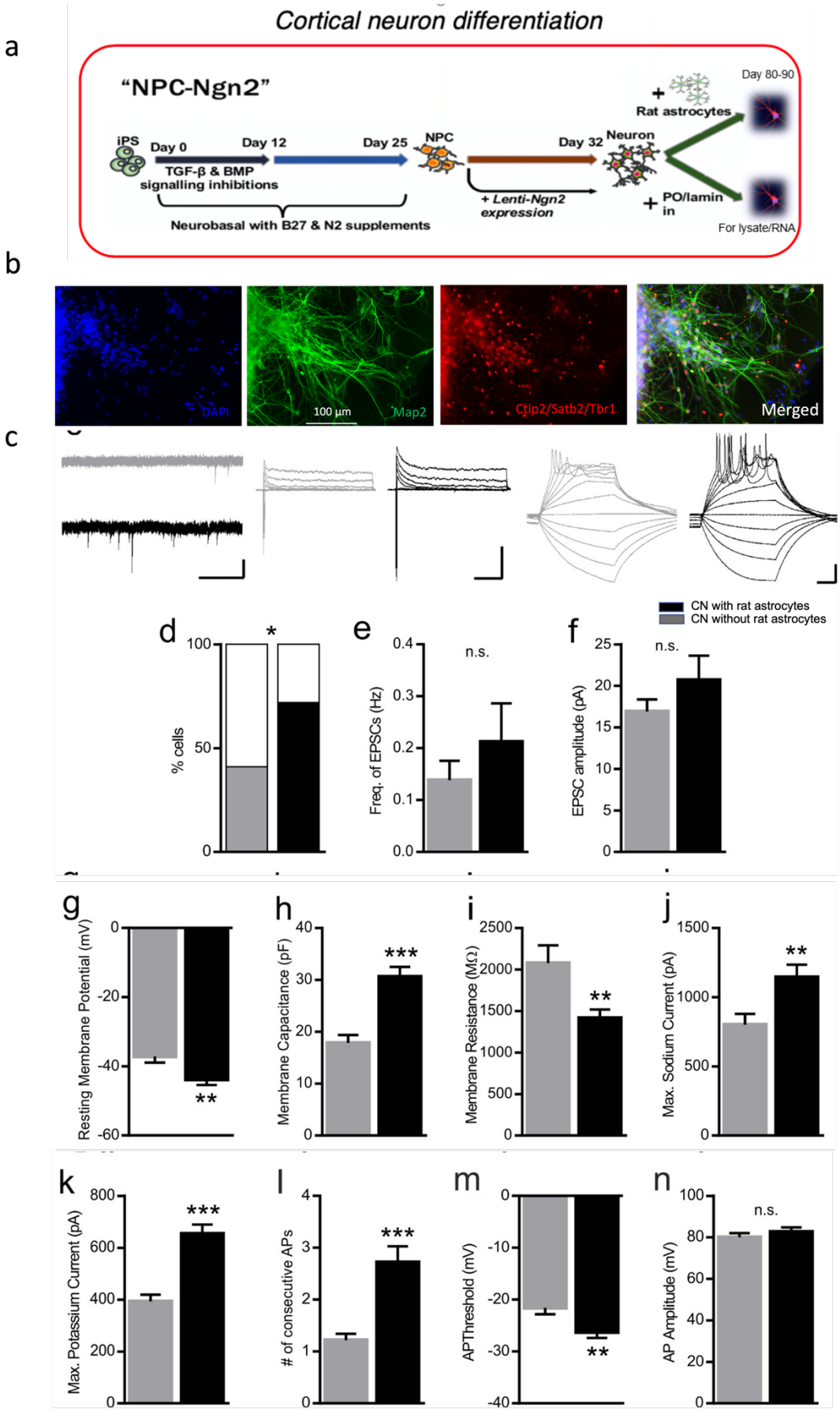
a
Cortical neuron differentiation
"NPC-Ngn2"
iPS
Day 0
Day 12
Day 25
NPC
Day 32
Neuron
Day 80-90
+ Rat astrocytes
TGF-β & BMP signalling inhibitions
Neurobasal with B27 & N2 supplements
+ Lenti-Ngn2 expression
+ PO/lamin in
For lysate/RNA
b
DAPI
100 µm
Map2
Ctip2/Satb2/Tbr1
Merged
c
CN with rat astrocytes
CN without rat astrocytes
d
% cells
*
e
Freq. of EPSCs (Hz)
n.s.
f
EPSC amplitude (pA)
n.s.
g
Resting Membrane Potential (mV)
**
h
Membrane Capacitance (pF)
***
i
Membrane Resistance (MΩ)
**
j
Max. Sodium Current (pA)
**
k
Max. Potassium Current (pA)
***
l
# of consecutive APs
***
m
APThreshold (mV)
**
n
AP Amplitude (mV)
n.s.

Figure 3.9: Characterisation of iPSC-derived cortical neurons. (a) Schematic of cortical neuron differentiation from iPSCs employing dual SMAD inhibitor for neural induction coupled with late Dox-dependent NGN2 overexpression and antibiotic selection for homogenous generation of CNNs. (b) Representative fluorescent images of iPSC-derived post-mitotic neuronal culture expressing cortical layer 4-6 markers Tbr1, Ctip2 and Satb2 – cortical layer 2-4 marker. c) representative traces of CN cocultured with rat astrocytes (grey) versus CN in monoculture (black). (d-n) Quantification of electrophysiological readouts of CNs cocultured with rat astrocyte compared against those in monocultures in terms of d) percentage of cortical neurons, e) frequency of excitatory post synaptic current (EPSC), f) magnitude of EPSC, g) resting membrane potential, h) cell capacitance, i) membrane resistance, j) maximal sodium current, k) maximal potassium current, l) percentage of consecutive action potentials (APs), m) action potential threshold and n) action potential amplitude. Panel a is image courtesy of Bryan Ng, results from panel c-n are obtained by Emma Whiteley.

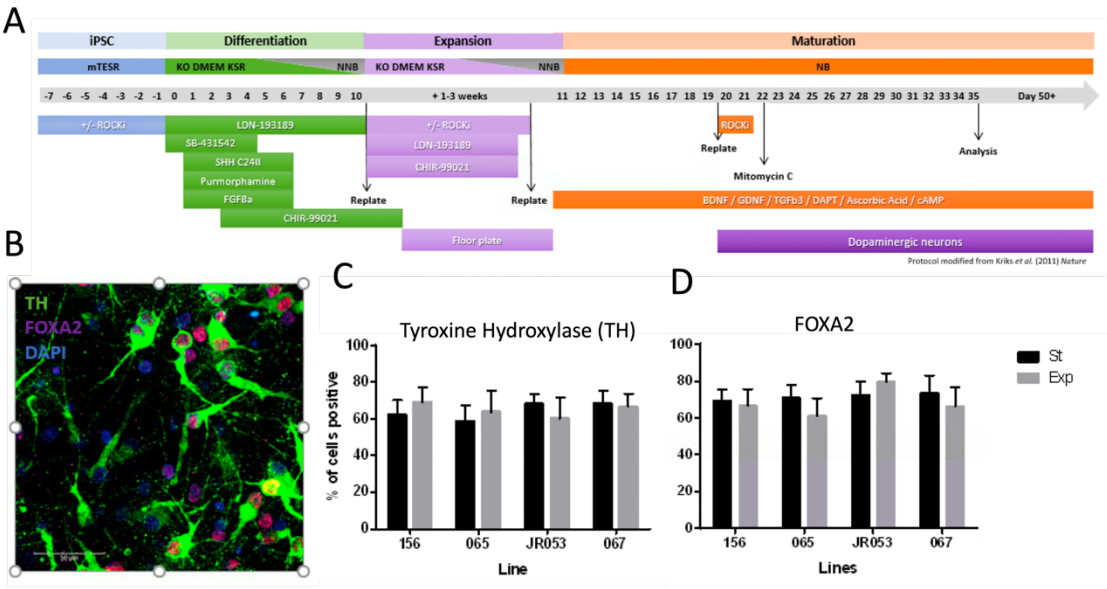

Figure 3.10: Characterisation of iPSC-derived dopaminergic neurons. (A) Schematic of dopaminergic neuron differentiation modified from Kriks et.al. with 3-week expansion of DaN progenitors after DIV 10. B) Representative fluorescent images of resulting iPSC-derived DaNs expressing TH (green) and floorplate marker – FOXA2 (purple). C-D) Quantification of the percentage of C) TH-positive neurons and D) FOXA2-positive neurons in resulting DaN cultures. Image courtesy of Ana Belen Malpartida.

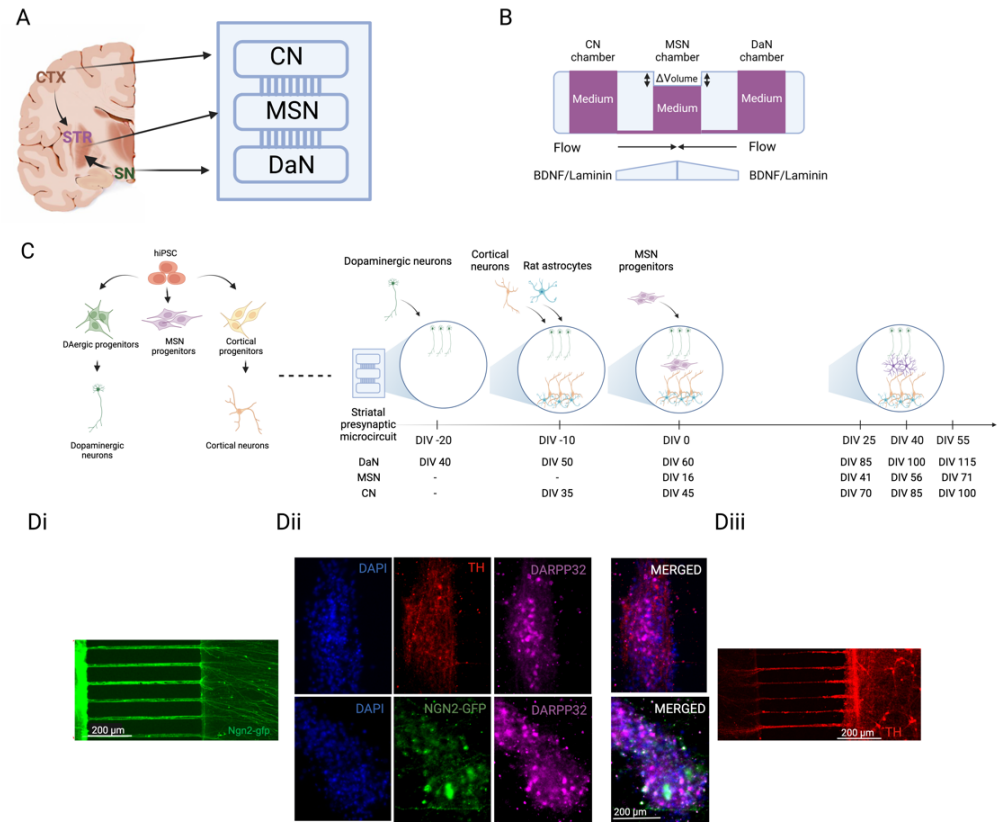

Figure 3.11: In vitro recapitulation of directed striatal presynaptic triad using microfluidics. (A) Schematic of custom microfluidic device which mimics orientation of the cortico-striato-nigral micro-circuit. (B) Side view schematics of fluid and growth factor-driven culturing paradigm of the cortico-striato-nigral micro-circuit. (C) Representative image showing compartmentalisation of (Ci) cortical neurons, (Cii) MSN and (Ciii) dopaminergic neurons in their respective chamber and uni-directional traversing of axons through microchannels. (D) Experimental design schematic showing the culturing workflow from iPSC stage to reconstruct the directional connectivity of striatal presynaptic connectivity.

ii. Effects of cortical glutamatergic inputs on MSN maturation *in vitro*

To examine the physiological role of cortical collaterals onto MSN in my *in vitro* microcircuit, I compared various electrophysiological parameters between MSN grown on coverslips in monoculture (i.e. CN^{-}MSN) versus those cocultured with CN (i.e. CN^{+}MSN) on two-chamber microfluidic devices (Figure 3.12A). Each biological pair of corticostriatal pathway was derived from the same healthy control cell line (SFC067-03, SFC856-03, SFC156-03) and compared against pairs derived from different healthy control lines. Firstly, I found no differences in

intrinsic excitability across time or between culture conditions over the period from DIV 40 – 70. Both RMP and rheobase current did not change significantly (RMP: cortical p = 0.46; DIV p = 0.29, interaction p = 0.58; rheobase current: culture condition p = 0.019 ; DIV p = 0.096, interaction p = 0.69) (Figure 3.12B and C). Interestingly, the fraction of MSNs capable of firing AP upon current injections while circuited with CNs, particular in later cultures between DIV 55-75 was greater than that of MSNs in monocultures. Given the relatively high rheobases of CN^{-}MSN, this result likely implies an increase in maturity as well as cell viability of MSNs in coculture with CNs . Meanwhile, there was a significant cortical effects on both magnitudes and frequency of spontaneous excitatory post-synaptic currents (sEPSCs), particularly more pronounced in late cultures (Figure 3.12F-I). CN^{+}MSN also displayed subtle increase in spontaneous inhibitory post-synaptic current (sIPSCs) (Figure 3.10D,E, and H). These results suggested that our microcircuit setup enabled cortical afferents to make functional synapses with MSN and to enhance MSN excitatory synaptic activities.

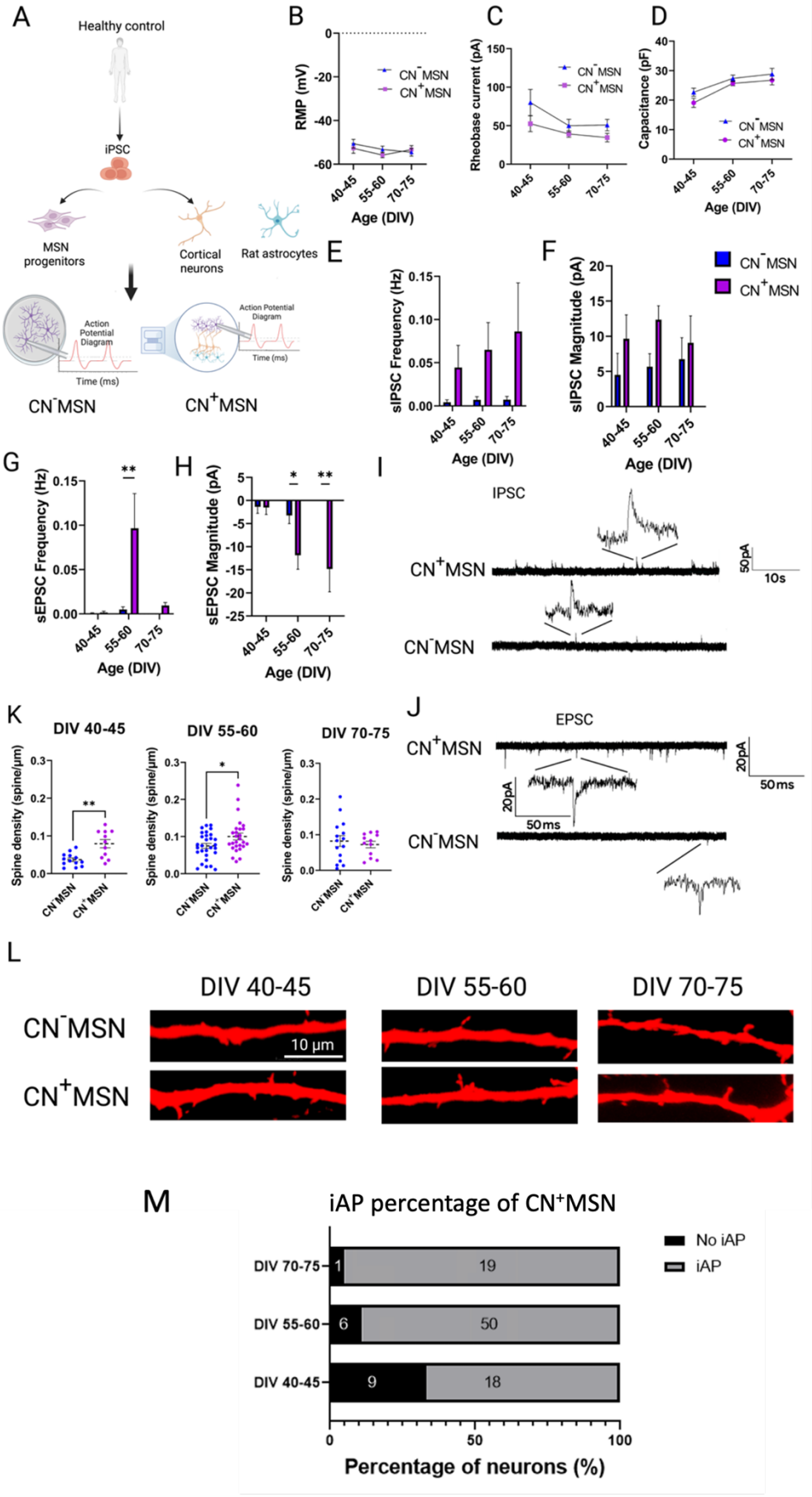
A
Healthy control
iPSC
MSN progenitors
Cortical neurons
Rat astrocytes
Action Potential Diagram
Time (ms)
CN-MSN
CN+MSN
B
RMP (mV)
C
Rheobase current (pA)
D
Capacitance (pF)
Age (DIV)
E
sIPSC Frequency (Hz)
F
sIPSC Magnitude (pA)
G
sEPSC Frequency (Hz)
H
sEPSC Magnitude (pA)
I
IPSC
50pA
10s
J
EPSC
20pA
50ms
K
DIV 40-45
DIV 55-60
DIV 70-75
Spine density (spine/μm)
L
10 μm
M
iAP percentage of CN+MSN
No iAP
iAP
DIV 70-75
DIV 55-60
DIV 40-45
Percentage of neurons (%)

Figure 3.12: Coculturing with iPSC-derived cortical neurons improved synaptic activities and dendritic spine morphology of iPSC-derived MSN. (A) Schematic illustrating the generation and whole cell patch-clamp recording of iPSC-derived MSN in monoculture (CN^-MSN) or in co-culture with cortical neurons in microfluidic devices (CN^+MSN). (B-C) (B) Resting membrane potential (RMP) and (C) rheobase current of CN^-MSN and CN^+MSN, n=14-44 recording MSN per condition. (D-E) Quantification of spontaneous inhibitory post-synaptic current (sIPSC) (D) frequency (E) and magnitude over time from DIV 40-D75, n = 10-37 recording MSN per condition. (F) Representative traces of IPSC of DaN^-CN^-MSN and DaN^-CN^+MSN. (G-H) Quantification of spontaneous excitatory post-synaptic current (sEPSC) (G) frequency and (H) magnitude of CN^-MSN and CN^+MSN over time from DIV 40-D75. n= 9-21 recording MSN per condition. (I) Representative trace of EPSC of DaN^-CN^-MSN and DaN^-CN^+MSN. (J) Pair-wise comparative quantification between CN^-MSN and CN^+MSN from DIV 40-75, each dot represents a recording neuron, n=11-29 recording MSN per condition, two-tailed Student's t-test. (K) Representative images of dendritic spines in neurobiotin-filled DARPP32+ MSN. (L) Representative fluorescent images of dendritic spines between two different culture conditions over time. (M) Number of CN^+MSN that displayed evoked action potential upon current injection (iAP) and MSN that did not (no iAP) over time. Number of MSN that displayed evoked action potential upon current injection (iAP) and MSN that did not (no iAP) over time. All data were presented as mean ± SEM, N = 3 differentiation experiments of 3 iPS cell lines, 2-way ANOVA with Bonferroni post-hoc correction test unless otherwise stated. *p<0.05, **p<0.01.

Dendritic spines are principal sites of synaptic integration and their architecture is highly dynamic reflecting the complex synaptic communication between neurons. Knowing that glutamatergic input profoundly modulates dendritic morphology of MSN (Segal, Greenberger and Korkotian, 2003), I examined whether there existed a differential phenotype of dendritic spines in the presence of cortical glutamatergic innervation. I found that cortical excitatory afferents promoted early dendritic spine formation in MSN which remained stabilised until DIV 75 (Figure 3.12J). On the contrary, dendritic spines were virtually absent in early culture of MSN devoid of cortical projections, but emerged gradually over time and attained a similar density as in CN^+MSN at DIV 70-75 despite CN^-MSN remaining relatively synaptically more quiescent (DIV 40-45: p = 0.001; DIV 55-60: p = 0.0254, DIV 70-75: p = 0.607 CN^-MSN vs. CN^+MSN) (Figure 3.12K)

Taken together, these results suggested the importance of cortical afferents in facilitating synaptic maturation of MSN by prompting not only early formation but also the maturation of

dendritic spines of striatal neurons, indicating the utility of our microcircuit in mimicking functional significance of the network connectivity.

iii. Effects of dopaminergic projections on corticostriatal neuron maturation *in vitro*

To delineate the effect of dopaminergic projections onto corticostriatal neurons, comparison was made between CN^+MSN (DaN^-CN^+MSN) and those circuited with DaN (i.e. DaN^+CN^+MSN) (Figure 3.13A). Each microcircuit consisted of 3 neuronal types derived from the same healthy control lines (SFC067-03, SFC856-03, SFC156-03) and comparison was made between microcircuits derived from different healthy control lines. I found that RMP of corticostriatal neurons became significantly more hyperpolarised with the long-term presence of DaN projections ($p = 0.046$ for DIV 40-45 DaN^+CN^+MSN vs. D70-75 DaN^+CN^+MSN), resulting in a significantly more hyperpolarised RMP of DaN^+CN^+MSN in late, but not early, cultures (DIV 70-75: $p = 0.043$ for DaN^-CN^+MSN RMP vs. DaN^+CN^+MSN RMP) (Figure 3.13B). That was associated with the greater, albeit not statistically significant, rheobase currents of MSN receiving dopaminergic inputs (Figure 3.13C). The fraction of CN^+MSNs capable of firing AP upon current injections while circuited with healthy control-derived DaNs was smaller across all three time points than that of MSN devoid of DaN (i.e. DaN^-CN^+MSNs). Observing the trend toward reduced intrinsic excitability produced by dopaminergic afferents, I delved into the constituent voltage-gated currents of sodium (Na_v) and potassium (K_v) to dissect specific ionic channels responsible for the intrinsic differences. The former underlies membrane depolarisation and hence, firing probability (Hogkin and Huxley, 1952) while the extensive expression of K_v is fundamental for the resting hyperpolarised state of *in vivo* MSN (Wilson and Kawaguchi, 1996). Indeed, I found an increase in both the fast A-type and slow-activating K_v in late cultures at DIV 70-75 (Figure 3.13E-G) but no significant temporal changes in Na_v currents, in agreement with

the more hyperpolarised RMP but similar rheobase current. Difference in K_v can be resulted from either increased K_v of DaN^+CN^+MSN or decreased K_v of DaN^-CN^+MSN or both. When examining each condition independently over the period of DIV 40-70, I observed a gradual increase in K_v among DaN^+CN^+MSN while K_v of DaN^-CN^+MSN increased gradually between DIV 40-65 but subsequently plummeted at DIV 70-75. These data suggested that MSN excitability matured in DA-independent (early) and DA-dependent (late) stages of which the latter was likely to be regulated via extensive DA-mediated K_v conductance.

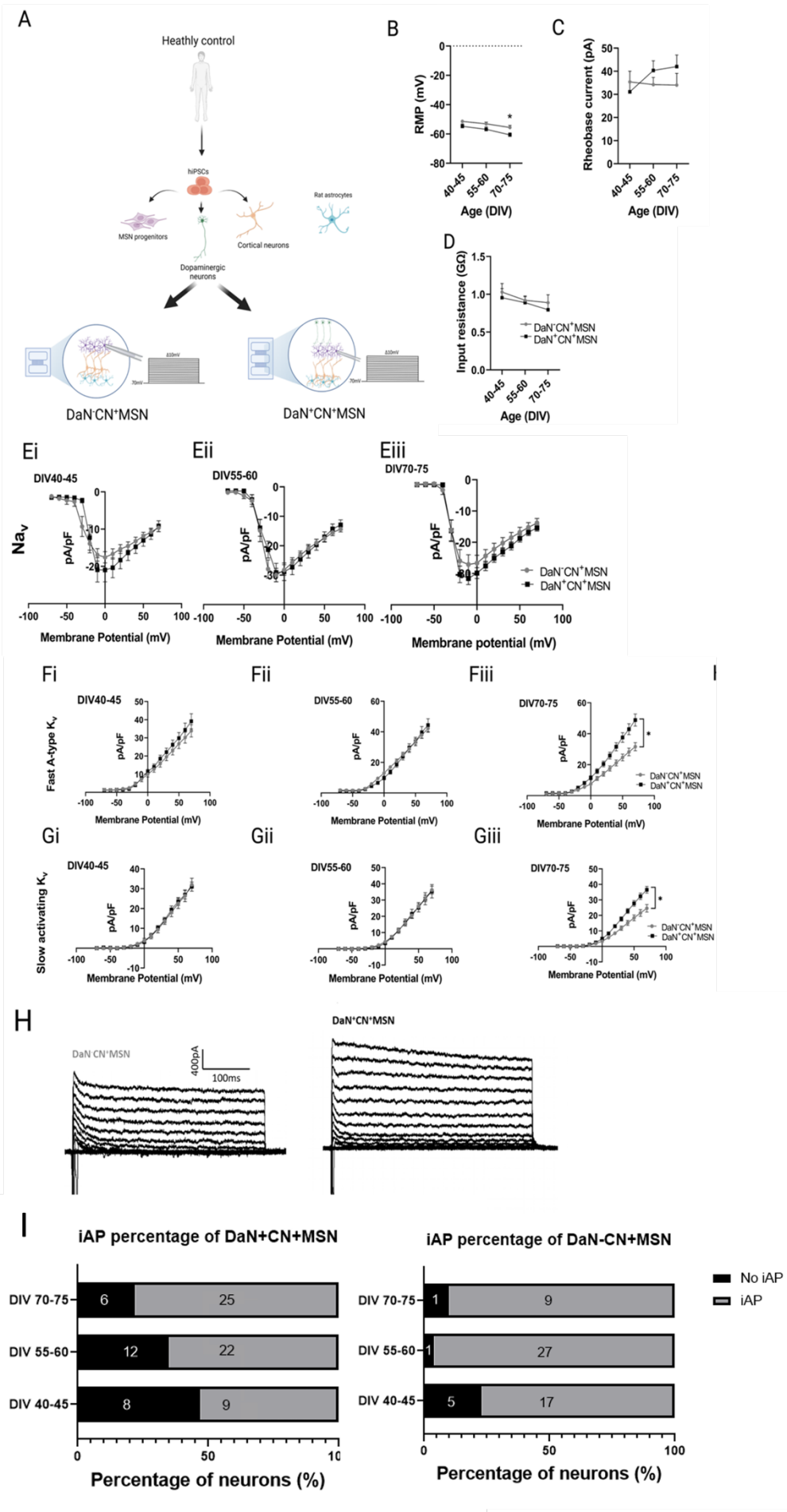
A
Heathly control
hiPSCs
MSN progenitors
Cortical neurons
Rat astrocytes
Dopaminergic neurons
DaN⁻CN⁺MSN
DaN⁺CN⁺MSN
B
RMP (mV)
Age (DIV)
C
Rheobase current (pA)
Age (DIV)
D
Input resistance (GΩ)
DaN⁻CN⁺MSN
DaN⁺CN⁺MSN
Age (DIV)
Ei
Eii
Eiii
DIV40-45
DIV55-60
DIV70-75
Nav
pA/pF
Membrane Potential (mV)
Membrane potential (mV)
Fi
Fii
Fiii
Fast A-type Kv
Gi
Gii
Giii
Slow activating Kv
H
DaN⁻CN⁺MSN
DaN⁺CN⁺MSN
400pA
100ms
I
iAP percentage of DaN+CN+MSN
iAP percentage of DaN-CN+MSN
DIV 70-75
DIV 55-60
DIV 40-45
6
25
12
22
8
9
1
9
1
27
5
17
No iAP
iAP
Percentage of neurons (%)

Figure 3.13: Dopaminergic neurons triggered the intrinsic maturation of iPSC-derived MSN during a critical period. (A) Schematic illustrating the generation and whole cell patch-clamp recording of corticostriatal neurons in the presence or absence of DaN, i.e. $DaN^{-}CN^{+}$MSN and $DaN^{+}CN^{+}$MSN, respectively, on microfluidic devices. (B-D) (B) Resting membrane potential (RMP), (C) rheobase current, and (D) input resistance over time. (E-G) Current density curves of (E) voltage-gated sodium channels, (F) fast A-type voltage-gated potassium, and (G) slow activating voltage-gated potassium channels over time. n= 15-31 recording MSN per condition. (H) Representative fast A-type and and slow activating K_v currents of $DaN^{-}CN^{+}$MSN and $DaN^{+}CN^{+}$MSN at DIV 70-75. All data were presented as mean ± sem, N = 2 differentiation experiments of 3 iPS cell lines, n=21-32 recording MSN per condition, 2-way ANOVA with Bonferroni post-hoc test, *p<0.05, **p<0.001. (I) Number of MSN that displayed evoked action potentials upon current injections (iAP) and MSN that did not (no iAP) in $DaN^{-}CN^{+}$MSN and $DaN^{+}CN^{+}$MSN over time.

3.3. Discussion

3.3.1. Generation of iPSC-MSN

iPSC-MSN provides a useful cellular model to investigate the physiology of motor circuit as well as the pathophysiology of motor disorders such as PD and Huntington's Disease. Here, I reported a useful differentiation protocol to generation adherent iPSC-MSN culture via neurogenesis followed by LGE specification leveraging on time-sensitive coordination of dual SMAD inhibition, WNT signalling inhibition and Activin A-mediated TGF-β signalling. While dual SMAD inhibition has been effectively and routinely used to promote neural induction (Chambers *et al.*, 2009), inhibition of the WNT signalling and activation of the TGF-β signalling via Activin A were often independently employed to generate iPSC-MSN in monoculture (Delli Carri *et al.*, 2013; Arber *et al.*, 2015; Telezhkin *et al.*, 2016), including at the time when I embarked on this project. Only recently did more studies report the efficient concerted use of both BMP/Wnt signalling modulator and Activin A in producing iPSC-derived striatal organoid (Miura *et al.*, 2020) or adherent 2D culture (Iannielli *et al.*, 2019; Tam and Keung, 2022). It is challenging to directly correlate the exact DIV between different differentiation protocols; however, the consensus exposure of Activin A following dual SMAD inhibition and prior to final maturation agrees conceptually with the timeframe Activin A was also introduced in my protocol. Altogether, this lends support to the reproducibility of Activin A usefulness in specifying striatal fate. Recent study suggested that Activin A indeed mediated MSN patterning exclusive via ALK4/5 receptors, a mechanism also replicated by an alternative activator of TGFβ-SMAD2/3 signalling such as Alantolactone (Fjodorova, Noakes and Li, 2020).

Meanwhile, in the developing telencephalon, regionalisation is regulated by opposing gradient of the ventralising morphogen SHH and its repressor GLI3 which gives rise to the ventral subpallium with the basal ganglia and dorsal pallium with the cerebral cortex, respectively (Kuschel, Rüther and Theil, 2003). The dorsal pallium development, in turn, is dependent on the BMP and WNT signalling (Furuta, Piston and Hogan, 1997; Hébert, Mishina and McConnell, 2002; Gulacsi and Anderson, 2008). As the result, a combination of SHH induction and BMP/WNT inhibition was thought to be useful for specifying pan subpallial progenitors, a strategy successfully reported in previous reports of generating iPSC-MSN (Delli Carri *et al.*, 2013; Stanslowsky *et al.*, 2016; Wu *et al.*, 2018; Amimoto *et al.*, 2021). In this project, I recapitulated the activation of the SHH-dependent signalling pathway using SHH agonist, SAG. A dose-dependent effect of SAG on promoting the development of LGE progenitors has been previously reported with the maximal pro-LGE progenitor effect observed at 100 nM, and hence, our choice of SAG concentration in differentiation condition A (Wu *et al.*, 2018). The replacement of SHH with SAG removes the potential variability introduced by recombinant protein components of variable quality in the media mixes, contributing towards more consistent differentiation outcomes. However, my results suggested that the additional exposure to SHH from DIV 5 to 10, in the presence of WNT inhibitor XAV, in fact reduced the expression abundance of LGE/MSN-progenitor transcripts (Figure 3.3) and offered no marginal benefit in terms of expression of postmitotic MSN-specific protein (Figure 3.5 and 3.6). Considering the slight differences in the exact timing of exposure to these different factors in different studies, including mine, this suggested potentially a very fine balance between SHH induction and BMP/WNT inhibition in a highly time-sensitive fashion. Notably, effect of Activin A was found independent of exposure to DIV 5-10 SHH (Figure 3.4), suggesting potentially the sequential effect of these on subpallial development and hence, shedding light on future studies looking at Activin-A/ TGF-β mediated signalling in striatal development.

It worths noting that cellular heterogeneity existed in my iPSC-MSN cultures. Presence of TH-positive cells confirmed by both RT-qPCT and immunostaining (Figure 3.7 and 6.3) is not all surprising. TH-expressing cells have been observed in both human (Porritt *et al.*, 2000; Cossette, Lecomte and Parent, 2005; Cossette, Lévesque and Parent, 2005), rodents (Meredith *et al.*, 1999; Robinson, Heien and Wightman, 2002; Ibáñez-Sandoval *et al.*, 2010), and primates (Dubach *et al.*, 1987) striatum. Interestingly, these TH-expressing interneurons were later found to be of GABAergic nature, receiving both cortical and striatal inputs and discharging inhibitory tone on MSN (Ibáñez-Sandoval *et al.*, 2010; Xenias *et al.*, 2015). Future thorough molecular characterisation of this TH-positive population, and other non-striatal neurons within my culture, using transcriptomic analysis, will provide more insights into the robustness of this proposed MSN differentiation protocol. So far this knowledge is still lacking in the current literature of adherent iPSC-MSN; only Miura et al., (2020) has characterised the diversity of the their striatal organoid using single-cell RNA sequencing technology. Considering the cellular heterogeneity apparent within my iPSC-MSN culture, coupling post-hoc identification with whole-cell patch clamping was sensible to fine-tune the electrophysiological phenotypes to the DARPP32-positive striatal neurons.

3.3.2. Modular microcircuit model to dissect neurotransmitter functions

The present study demonstrated the first attempt at recapitulating *in vitro* the human presynaptic striatal triad consisting of cortical glutamatergic and dopaminergic projections onto MSN. Previous approaches to investigate human striatal neuron (patho)physiology remain largely limited in monoculture of a single neuronal type (Smith-Geater *et al.*, 2020), with more recent success in developing a neuronal network architecture (Miura *et al.*, 2020). To date, there is no cellular model that captures the complexity of both glutamatergic and dopaminergic synapses onto striatal neurons both of which are critical for the emergence of

functional characteristics of MSN. Indeed, although my MSN in monoculture displayed temporal marker expression profile reminiscent of human developmental trajectory reported from the Human Brain Transcriptome, electrophysiological readouts of our iPSC-derived MSN, as compared to those reported from *in vivo* mouse, suggest an immature functional state depicted by depolarising RMP (MSN DIV 75 RMP = -55.1 mV versus < -70 mV in postnatal mouse) and large input resistance (MSN DIV 75 R_{in} = 1.0 GΩ versus < 400 MΩ in postnatal mouse) (Lieberman *et al.*, 2018). Meanwhile, both *in vivo* and *ex vivo* recordings indicated that MSNs remain hyperexcitable at birth and subsequently mature into their adult-like state within the first four postnatal weeks (Tepper *et al.*, 1998; Gertler, Chan and Surmeier, 2008; Peixoto *et al.*, 2016) .

My results demonstrated that combinatorial cortical glutamatergic and dopaminergic inputs further facilitated maturation of the intrinsic membrane properties and synaptic activity of MSN beyond the benefits of long-term culturing. This corroborated the relevance of cortical neurons in promoting both inhibitory and excitatory synaptic maturity of MSN (Tu *et al.*, 2016; Paraskevopoulou, Herman and Rosenmund, 2019) as well as time-sensitive influence of dopaminergic transmission on MSN excitability maturation previously reported in rodent (Lieberman *et al.*, 2018). Because the average spine density between CN-MSN cocultures and that of MSN monocultures was no longer significantly different from each other, it suggests that the absence of cortical projections might delay but did not affect overall formation of dendritic spines. It worths noting that other than spine density, spine morphology is also a critical metrics informative of spine maturity, and hence spine functions. The spine detection module from Imaris used in this work could not reliably categorise the selected spines into their different specific subtypes morphology. Therefore, I hypothesise that the precocious increase in spine density observed in the cortico-striatal coculture between DIV 40-60, relative to their delayed increase in sEPSC from DIV 55 to 75, is likely attributed to the differential

spine maturity in different cultures. This suggests that while monocultured MSN could still form dendritic spines, cortical projections exert a more significant impact on physiologic maturation of striatal dendritic spines, as demonstrated by the frequency and magnitude of excitatory synaptic activities. Future study employing more robust classifications of spine subtypes will be useful to resolve this slight temporal mix-match between sEPSC and spine density measurements

It worths noting that while my microcircuit-based culturing approach promoted electrophysiological maturation of iPSC-derived MSN, these MSN have yet display adult-like membrane properties (in term of RMP and input resistance) as reported in mouse/rat. This could be attributed to the potential electrophysiological differences between human and non-human MSN but more likely to be immature phenotypes given the incomplete recapitulation of the neural microenvironment surrounding MSN. For example, glutamatergic input onto MSN originates from not only the cortex but also the thalamus which makes up ~40% of glutamatergic synapses on MSN dendrites and converges with corticostriatal afferents indiscriminately onto both MSN subtypes (Groenewegen and Berendse, 1994; Smith *et al.*, 2004; Doig, Moss and Bolam, 2010). Future investigation should complete the presynaptic landscape of striatal neurons with iPSC-derived thalamic neurons on a four-chamber microfluidics to examine if thalamostriatal synapses further potentiate MSN maturity.

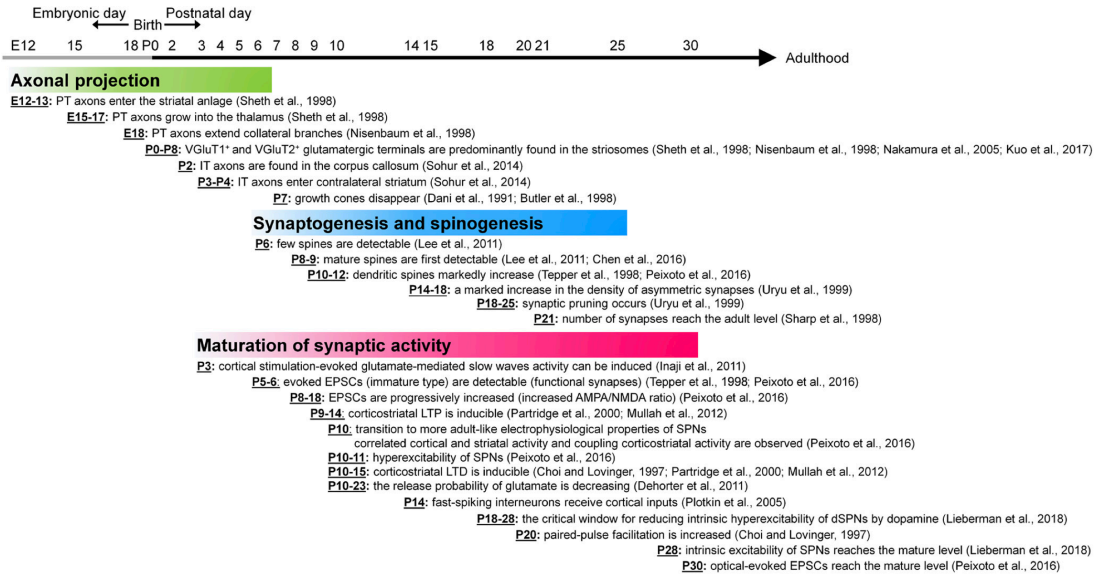

Figure 3.14: Developmental timeline of corticosynaptogenesis in mouse. AMPA: α-amino-3-hydroxy-5-methyl-4-isoxazolepropionic acid; dSPN; direct striatonigral pathway neuron; EPSC: excitatory postsynaptic current; iSPN: indirect striatopallidal pathway neuron; IT: intratelencephalic; LTD: long-term depression; LTP: long-term potentiation; NMDA: N-methyl-D-aspartate; PT: pyramidal tract; SPN: striatal projection neuron; VGluT1: vesicular glutamate transporter 1; VGluT2: vesicular glutamate transporter 2. Adapted from Kuo et.al., 2019 (Kuo and Liu, 2019).

Both corticofugal and dopaminergic axons innervate the striatum in embryonic stage, as early as E12 and E17, respectively (Figure 3.14) (Voorn *et al.*, 1988; Kuo and Liu, 2019). However, excitatory synaptogenesis in the striatum continues postnatally and terminates around P18; EPSCs are progressively increased during the same period (Peixoto *et al.*, 2016). Likewise, dopamine release dynamic continue to mature, manifested by increasing dopamine synthesis as well as quantal size of dopamine release during vesicle fusion, over the P8-30 period, albeit with the most dramatic increase taking place around P20 preceding the reduction MSN intrinsic excitability toward adult-like phenotype. This relative developmental progression of physiological maturation of MSN *in vivo* matches the relatively effect of CNs and DaNs on early and late MSN, respectively, observed in my microcircuit cultures. However, it worths noting that direct temporal correlation between *in vivo* and in iPSC-derived model *in vitro* is rather challenging with the current *status quo*.

A significant highlight of this approach is its customisability. The modular nature of this setup allows immense flexibility on reconstructing the compartmentalisation of different neuronal populations and the directionality of their specific connectivity. Hence, virtually any microcircuit can be established applying the similar design concept. Targeted manipulation to specific compartments is also permitted with great ease. Although future studies with more comprehensive orthogonal mapping is necessary, immunostaining and electrophysiological results indicate that our approach captured some extent of the oriented connectivity resembling that *in vivo* and there existed functional glutamate and dopamine transmission. Furthermore, although it is essential to measure effect of neurotransmitters in an intact neural circuit, a modular reductionistic model such as the one established here proved to be useful to facilitate delineation of selective effect of specific neurotransmitters.

Chapter 4: Investigating temporal changes of striatal electrophysiological properties synapsed with dopaminergic neurons harbouring PD-related GBA-N370S mutation.

4.1. Introduction

4.1.1. *GBA1* mutation in PD

Mutation in the glucocerebrosidase (*GBA*) gene is one of the most common risk factors in PD and among them N370S (the c.1226A > G) variant is one of the most common worldwide (Riboldi and Di Fonzo, 2019). Approximately 2-9% of PD patients carried heterozygous *GBA* mutations, whereas this incidence was reported to be as high as 10-31% in Ashkenazi Jewish PD patients. PD patients carrying *GBA* mutations exhibited similar clinical phenotype of motor and non-motor symptoms (Riboldi and Di Fonzo, 2019), albeit at the earlier age of onset and with modestly more severe motor symptoms than non-carrier (Clark *et al.*, 2007; Gan-Or *et al.*, 2008).

GBA gene is located in chromosome 1 (1q13) and encodes for the lysosomal hydrolyse enzyme glucocerebrosidase (GCase). GCase in turns cleaves glycosphingolipids (GSLs) GlcCer and GlcSph into glucose and ceramide, and glucose and sphingosine, respectively. The mechanism underlying GBA mutation-driven PD pathology remains elusive. Mutant GBA generated misfolded GCase and the resulting reduced GCAse enzymatic activity was often attributed as pathogenic mechanism. GCase activity was found substantially and uniquely reduced in the SNpc in both human brains or dried blood spot from *GBA*-PD patients (Gegg *et al.*, 2012; Alcalay *et al.*, 2015). Reduced GCase activity subsequently results in accumulation of GSLs which play an important role in structural properties of cell/organelle membrane bilayer and

are also key regulators of multiple biological processes including but not limited to autophagy, cell growth, senescence, ER stress (Garcia-Ruiz, Morales and Fernández-Checa, 2015). Indeed, Multiple previous studies using human neurons supported autonomous mechanistic link between loss of GCase activity with reduced DaN viability due to failure of the mitochondria and endolysosomal pathway (Fernandes *et al.*, 2016; Kim *et al.*, 2021; Grigor'eva *et al.*, 2023), dysregulation of calcium homeostasis and subsequent increased susceptibility to stress responses (Schondorf *et al.*, 2014), destabilisation of α-syn tetramers and increase DaN susceptibility to cytotoxicity induced by pathologic α-syn fibrils (Kim *et al.*, 2018; Yun *et al.*, 2018). Single-cell transcriptomics of *GBA-N370S* DaNs identified an increased in ER stress and alpha-synuclein release, together with synaptic, autophagic and lysosomal perturbation (Lang *et al.*, 2019). Studies on monozygotic twins impaired alpha-synuclein clearance and reduced DA release in *GBA-N370S* DaNs (Woodard *et al.*, 2014). However, most homozygous *GBA* did not develop into PD and *GBA* heterozygotes displayed greater PD risk than non-carriers (Rosenbloom *et al.*, 2011; Alcalay *et al.*, 2014). These findings suggested a multifactorial pathophysiology induced by *GBA* mutant DaN, thereby implying the inevitable challenge in identifying singly effective modifiable therapeutic targets against impacted DaN. I hypothesised that an alternative approach to understand DaN neurodegeneration is to investigate pathology of the striatal output neurons so as to predict the overall pathogenic effects of *GBA* mutation on presynaptic DaN. In doing so, it is also possible to dissect potential modifiable therapeutic targets to directly preserve the integrity of the striatum physiology.

4.1.2. Striatal pathology in Parkinson's Disease

Dysfunction of the striatum has been implicated in various motor disorders including PD although the exact mechanisms remain much debated due to accumulation of conflicting findings (Liang, DeLong and Papa, 2008; Kita and Kita, 2011; Deffains *et al.*, 2016; Singh *et al.*,

2016; Salvadores *et al.*, 2017; Parker *et al.*, 2018; Dittmer, Dell'Acqua and Sather, 2019; Valsky *et al.*, 2020; Cruz *et al.*, 2022). The consensus from mouse works suggested that the characteristic and selective degeneration of substantia nigra par compacta (SNpc) DaN resulted in aberrant striatal activity patterns which subsequently altered basal ganglia balanced output governing motor behaviours (Parker *et al.*, 2018; McGregor and Nelson, 2019). Studies from nonhuman primates showed contradictory results, showing both increased MSN firing (Liang, DeLong and Papa, 2008) and no change (Deffains *et al.*, 2016). It worths nothing that these findings relied on chemical toxin-based PD animal models of unphysiologically harsh and abrupt ablation of DaN or their terminals deprived of the temporal and genetic nature of PD pathophysiology. Interestingly, striatal single-unit recording of PD patients undergoing unanesthetized deep brain stimulation showed increased in MSN spontaneous firing (Singh *et al.*, 2016). As far as I am aware, there has been no other report of striatal electro-pathology in human model of PD. The specific effects on the two parallel principle striatal pathways, the direct pathway and indirect pathway, is also contentious. The classical premises suggested their functionally opposed roles in regulating action and their diametrical changes in firing rate in PD (Parker *et al.*, 2018) although more recent observation of co-activation of both pathways at the initiation of movement has challenged this view (Cui *et al.*, 2013) .

4.1.3. Protein kinase A and striatum and PD

Protein kinase A (PKA) is a principal regulator of a plethora of signalling molecules critical for various cellular pathways including synaptic signalling and neuronal excitability, to name a few (Goldsmith and Abrams, 1992; Ehlers, 2000; Choi *et al.*, 2002). Increasing concentration of intracellular cAMP activates PKA which in turn phosphorylates multiple different proteins. For example, the electrophysiological activity of many cellular channels including voltage-gated sodium and potassium channels is robustly regulated by PKA-mediated phosphorylation of

channel subunits. In MSN both Kv4.2 and Kv1.2, the principal channel contributors towards fast A-type and slowly inactivating potassium current, respectively (Shen et al. 2004; Tkatch, Baranauskas, and Surmeier 2000), as well as Nav, are negatively modulated by PKA activation (Scheuer 2011; Schrader et al. 2002; Surmeier and Kitai 1993). Interestingly, DARPP32, the canonical protein marker differentially enriched in MSN and also the signalling hub of MSN, is bi-directionally regulated by PKA. Activation of PKA stimulates DARPP32 phosphorylation at Thr34, rendering DARPP32 an inhibitor of protein phosphatase 1 (PP-1). On the other hand, activation of DARPP32 by Cdk5-dependend phosphorylation at Thr75 converts DARPP32 into an inhibitor of PKA. The intertwined signalling network between DARPP32 and PKA suggests the important role of PKA in regulating cellular physiology of MSN in both healthy and disease state.

Mechanistic evidence relating PKA and PD, including familial PD, remains scarce. Muda et al., (2014) reported PKA phosphorylation-dependent modulation of LRRK2 kinase activity which was reduced in the major PD-related LRRK2 mutations R1441C/G/H, the region belongs to the consensus PKA recognition site (Muda *et al.*, 2014). In addition, activation of PKA rescued mitochondria respiratory deficits in the PINK1-deficent models of SH-SY5Y cell line and primary cortical neurons, potentially via A kinase anchoring protein 1 (AKAP1) – a scaffold protein that recruits PKA to the mitochondria (Dagda *et al.*, 2011). Interestingly, mutation of PKA subunits was found to be associated with body tremor in genetic mouse model and parkinsonism-like motor deficits in a novel neurodegenerative disorder (Wong *et al.*, 2014; Hoang Trung *et al.*, 2021). These findings lend support to the potential involvement of PKA in PD.

4.1.4. Aims

In this chapter, I aimed to:

- Recapitulate the striatal microcircuit burdened with *GBA-N370S* DaN.
- Investigate striatal electrophysiological pathology synapsed with *GBA-N370S* DaN.
- Investigate the involvement of PKA in striatal pathology in microcircuit with *GBA-N370S* DaN (if any).

4.2. Results

4.2.1. Establishment of striatal presynaptic triad with mutant *GBA-N370s* dopaminergic neurons

The modular nature of our micro-circuit setup permits mix and match of neuronal populations of different genetic background so as to delineate impact of specific genetic burden from a single population. To dissect impacts of *GBA-N370S* DaN on the physiology of corticostriatal output neurons, I established the striatal microcircuit using iPSC-derived CN and MSN from healthy controls connected with iPSC-derived DaN from either healthy controls or PD patients carrying *GBA-N370S* mutations (Figure 12A). Healthy control microcircuits consisted of CN, DaN and MSN derived from the same healthy control of SFC856-03-04, SFC156-03-01 or SFC067-03 and PD-relevant microcircuit comprised of DaN derived from *GBA N370S*-habouring cell lines, namely MK071, MK082 or MK088 with CN-MSN pair derived from either SFC856-03-04 or SFC156-03-01.

4.2.2. Impact of mutant *GBA-N370S* dopaminergic neurons on MSN functional properties

To delineate the effect of *GBA-N370S* DaN on post-synaptic MSN, I made comparisons of electrophysiological properties between corticostriatal neurons in microcircuit with either healthy DaN (DaN^+CN^+MSN) or *GBA-N370S* DaN (*GBA-N370S* DaN^+CN^+MSN) (Figure 4.1A). I found that while both groups exhibited increasingly hyperpolarised RMP over time, RMP of DaN^+CN^+MSN was always more hyperpolarised that that of *GBA-N370S* DaN^+CN^+MSN, particularly statistically pronounced in early culture (D40-45: $p = 0.0033$, two-way ANOVA with Bonferroni multiple correction test) (Figure 4.1B). Similarly, a significant genotype effect was observed for rheobase current at DIV 40-45 but not in later cultures (DIV 40-45: $p = 0.0248$, two-way ANOVA with Bonferroni multiple correction test) (Figure 4.1C). Interestingly, while more depolarised RMPs of *GBA-N370S* DaN^+CN^+MSNs, relative to DaN^+CN^+MSNs, imply hyperexcitability of MSNs circuited with *GBA-N370S* DaNs, the greater rheobase observed in *GBA-N370S* DaN^+CN^+MSN indicate lower likelihood to fire AP i.e. hypoexcitability. The fractions of neurons capable of eliciting AP upon current injections between the DaN^+CN^+MSN *GBA-N370S* DaN^+CN^+MSN are not significantly different from each other (iAP/no iAP neurons among *GBA-N370S* DaN^+CN^+MSN and DaN^+CN^+MSN 20/9 and 28/11)

Neuronal excitability is tightly controlled by coordinated activity of both Na_v and $K_{v.,}$ The inward flux of sodium ions depolarises cell membrane toward action potential threshold and trigger spontaneous firing while outward currents generated K_v underly resting membrane potentials and action potential afterhyperpolarisation (Hogkin and Huxley, 1952). Hence, I next explored whether the altered intrinsic excitability was coupled with relevant ionic channel changes. Unsurprisingly, I observed a substantial reduction in current density of both Na_v and K_v among the *GBA-N370S* DaN^+CN^+MSN (DIV 40-45: Na_v and slow activating $K_{v,}$ DaN genotype $p < 0.0001$, membrane potential $p < 0.0001$, interaction $p < 0.0001$; fast A-type K_v, DaN genotype $p =$

0.0001, membrane potential p <0.0001, interaction p <0.0001) (Figure 4.1Di, Ei, Fi, and G). Such reduction in sodium current was matched with an increase in rheobase current and seemingly suggestive of hypoexcitability while decrease in potassium currents likely contribute to the depolarisation of MSN RMP indicative of hyperexcitability at the same timepoint. While these findings seem to contradict each other, it worths noting that small peak sodium currents at approximately -20 pA/pF (see Figure 3.13E) and high rheobase could also be indicative of immature MSNs which trend toward being hyperexcitable relative to their adult counterparts (see Figure 3.14 and (Lieberman *et al.*, 2018). Hence, if taken together, these findings suggest an overall hyperexcitable state of MSNs cultured in circuit with *GBA-N370S* DANs. Interestingly, recordings of MSN from intermediate and late cultures between DIV 55-70 revealed resolution of genotypic effects previously observed at DIV 40-45 (Figure 4.1D-F). These data suggested the early pathological role of *GBA-N370S* mutation in DaN in altering striatal GABAergic output via early hyperexcitability of post-synaptic MSN independent of overt degeneration of dopaminergic afferents.

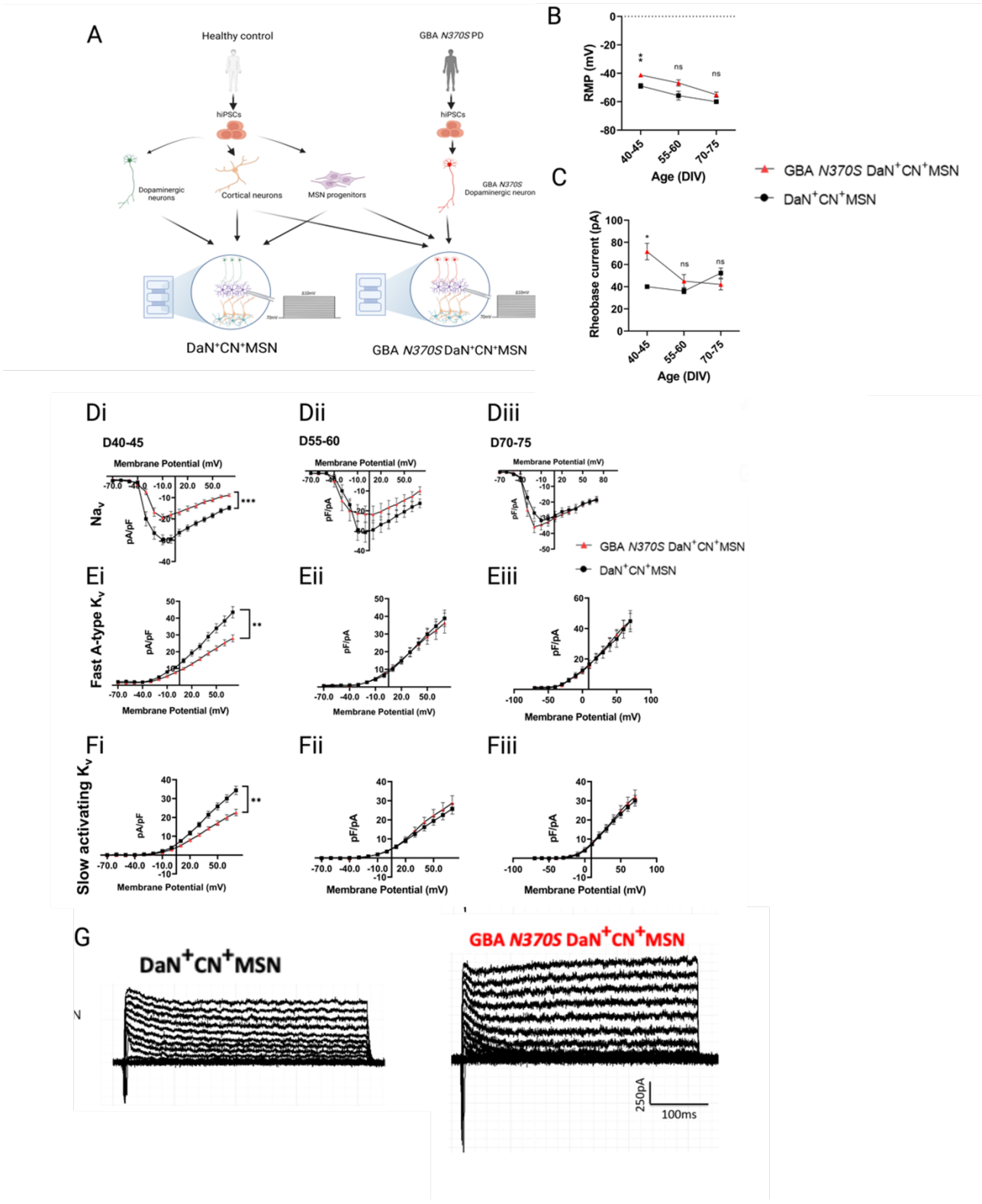
A
Healthy control
GBA N370S PD
hiPSCs
hiPSCs
Dopaminergic neurons
Cortical neurons
MSN progenitors
GBA N370S Dopaminergic neuron
DaN+CN+MSN
GBA N370S DaN+CN+MSN
B
RMP (mV)
Age (DIV)
40-45
55-60
70-75
ns
C
Rheobase current (pA)
Age (DIV)
GBA N370S DaN+CN+MSN
DaN+CN+MSN
Di
D40-45
Dii
D55-60
Diii
D70-75
Membrane Potential (mV)
Nav
pA/pF
pF/pA
Ei
Eii
Eiii
Fast A-type Kv
Fi
Fii
Fiii
Slow activating Kv
G
DaN+CN+MSN
GBA N370S DaN+CN+MSN
250pA
100ms

Figure 4.1: Early but transient current deficits and altered excitability of MSN circuited with *GBA-N370S* DaN. (A) Schematic illustrating the generation and whole cell patch-clamp recording of $DaN^{+}CN^{+}$MSN and *GBA-N370S* $DaN^{+}CN^{+}$MSN. (B-C) (B) Resting membrane potential (RMP), and (C) rheobase current of $DaN^{-}CN^{+}$MSN and *GBA-N370S* $DaN^{-}CN^{+}$MSN over time, n=14-40 recording MSN per condition. (D-F) Current density curves of (D) voltage-gated sodium channels, (E) fast A-type voltage-gated potassium, and (F) slow activating voltage-gated potassium channels over time. (G) Representative differential fast A-type and and slow activating K_v currents of $DaN^{+}CN^{+}$MSN and *GBA-N370S* $DaN^{+}CN^{+}$MSN at DIV 40-45. All data were presented as mean ± sem, N= 3 differentiation experiments of 3 iPS cell lines, n = 27-33 recording MSN at DIV40-45, N = 3 differentiation experiments of 3 iPS cell lines, n= 14-17 recording MSN per condition at DIV 55-60 and DIV 70-75. 2-way ANOVA with Bonferroni post-hoc test, ns $p>0.05$, *$p<0.05$, **$p<0.01$, ***$p<0.001$

4.2.3. Involvement of protein kinase A signalling in modulating striatal pathology

To examine whether PKA activity is involved in the early deficits of corticostriatal neurons effected by *GBA-N370S* DaN, I applied cell-permeable PKA antagonist H89, a competitive inhibitor of adenosine triphosphate site on PKA catalytic subunit, directly to MSN chambers of the striatal microcircuit and perform whole-cell patch clamping of MSN at DIV 40-45 (Figure 4.2A and B). Relative PKA activity was quantified in figure 4.2B-C, in which lower values of U/ml indicate less PKA is needed to mediate transfer of phosphate from PKA to substrate and thus, that the PKA is more active. PKA activity assay suggested intrinsic increase in PKA activity among *GBA-N370S* $DaN^{+}CN^{+}$MSN which then reduced to the control level upon administration of 10 µM H89 for 15 mins (Figure 4.2C). These data suggested the phenotypic increase in PKA activity of MSN synapsed with *GBA-N370S* DaN and the utility of H89 in normalising striatal PKA activity *in vitro*. Interestingly, upon collecting lysates of DaN from the corresponding devices from which striatal lysates were gathered, I also found a significant reduction in PKA activity of *GBA-N370S* DaN relative to healthy control-derived DaN. Such *GBA N370S*-induced deficit remained in the mutant DaN synapsed with MSN treated with H89, demonstrating the fluid isolation of different neuronal compartments (Figure 4.2D). I found that treatment of MSN with H89 resolved the genetic effect of *GBA-N370S* on MSN Na_v and K_v current density at

DIV 40-45 to healthy control levels (Figure 4.2F-H), indicating the involvement of PKA in mediating intrinsic excitability of corticostriatal neurons via ionic conductance. This phenotypic rescue was, importantly, independent of PKA activity within *GBA-N370* DaN (Figure 4.2D).

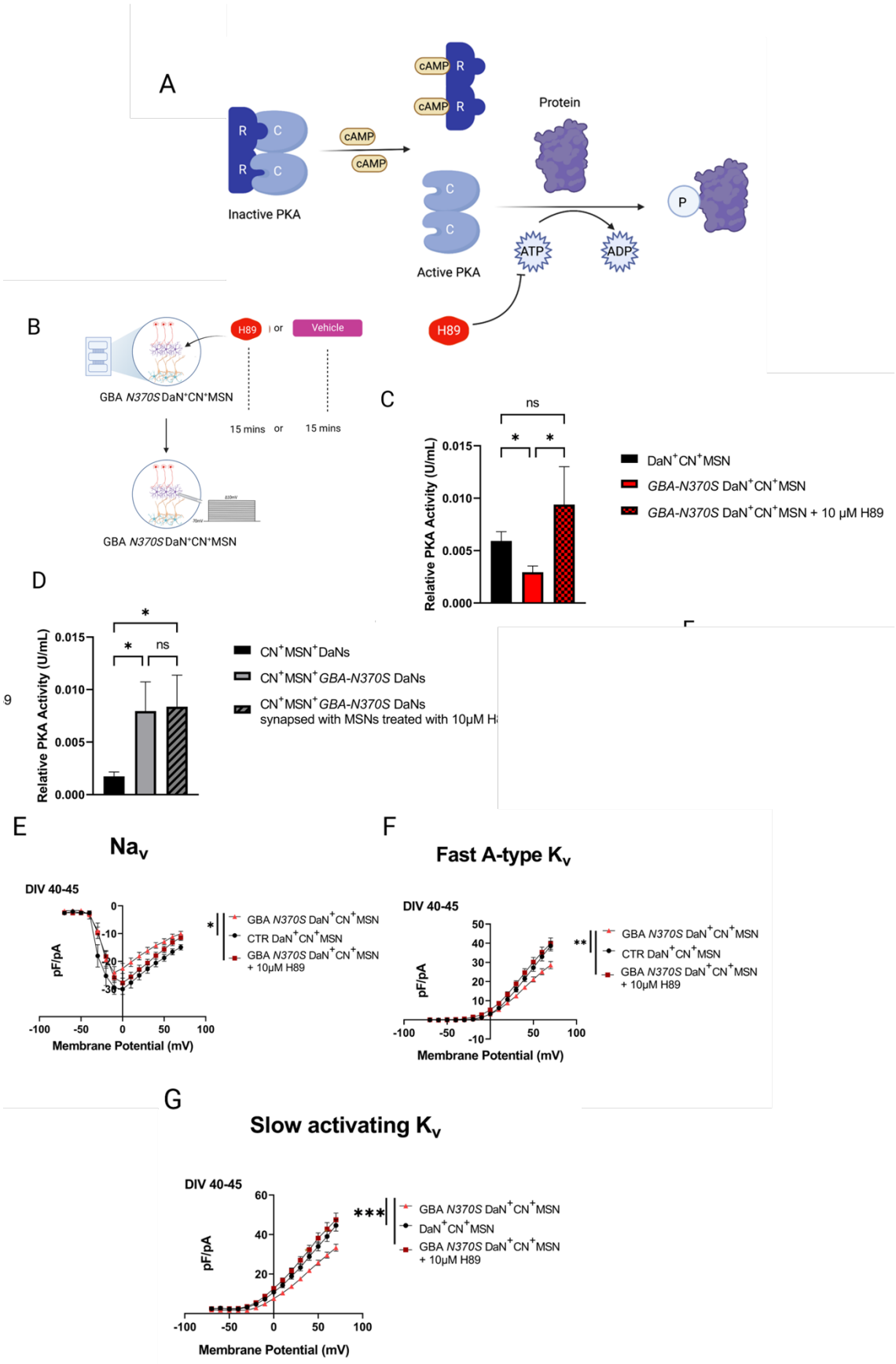
A
cAMP
R
C
Inactive PKA
Active PKA
Protein
P
ATP
ADP
H89
B
or
Vehicle
GBA N370S DaN+CN+MSN
15 mins
or
15 mins
GBA N370S DaN+CN+MSN
C
ns
*
*
Relative PKA Activity (U/mL)
0.015
0.010
0.005
0.000
DaN+CN+MSN
GBA-N370S DaN+CN+MSN
GBA-N370S DaN+CN+MSN + 10 µM H89
D
*
*
ns
Relative PKA Activity (U/mL)
CN+MSN+DaNs
CN+MSN+GBA-N370S DaNs
CN+MSN+GBA-N370S DaNs
synapsed with MSNs treated with 10µM H
E
Nav
DIV 40-45
pF/pA
Membrane Potential (mV)
*
GBA N370S DaN+CN+MSN
CTR DaN+CN+MSN
GBA N370S DaN+CN+MSN
+ 10µM H89
F
Fast A-type Kv
DIV 40-45
pF/pA
Membrane Potential (mV)
**
GBA N370S DaN+CN+MSN
CTR DaN+CN+MSN
GBA N370S DaN+CN+MSN
+ 10µM H89
G
Slow activating Kv
DIV 40-45
pF/pA
Membrane Potential (mV)
***
GBA N370S DaN+CN+MSN
DaN+CN+MSN
GBA N370S DaN+CN+MSN
+ 10µM H89

Figure 4.2: PKA antagonist rescued early current deficits of MSN circuited with *GBA-N370S* DaN. (A) Schematic demonstrating antagonistic mechanism of H89 in PKA-mediated phosphorylation signalling cascade. (B) Schematic illustrating treatment of PKA antagonist H89 on MSN in the striatal presynaptic microcircuit. (C-D) Quantitative measure of PKA activity of (C) $DaN^{+}CN^{+}MSN$,*GBA-N370S* $DaN^{+}CN^{+}MSN$ and *GBA-N370S* $DaN^{+}CN^{+}MSN$ treated with PKA antagonist H89, Kruskal-Wallis test with Dunn's correction test, and (D) healthy DaN, mutant *GBA-N370S* DaN synapsed with healthy control MSN or mutant *GBA-N370S* DaN synapsed with MSN treated with H89, in the corresponding microcircuit; Friedman test with Dunn's correction test; values were measured by PKA colorimetric activity kit and normalised against total protein level extrapolated from BSA assays. Each unit per ml (U/ml) was defined as the amount of PKA needed to mediate the transfer of 1.0pmol phosphate from ATP to substrate at 30°C as per manufacturer's instructions. (E-G) Current density curves of (E) Na_v, (F) fast A-type K_v, and (G) slowly activating K_v of DIV 40-45 MSN. All data were presented as mean ± SEM, N = 2 differentiation experiments of 3 iPS cell lines, n= 17-30 recording MSN per condition. 2-way ANOVA with Bonferroni post-hoc test unless otherwise stated, ns $p>0.05$, *$p<0.05$, **$p<0.01$, ***$p<0.001$.

4.3. Discussion

I am reporting here an early electrophysiological deficit of intrinsic properties of MSNs, in terms of RMP, excitability, and voltage-gated sodium and potassium currents, when circuited with *GBA-N370S* DaNs, as compared an all-healthy control-derived microcircuit. Such deficit is correlated with increased striatal PKA activity, reduced PKA activity among *GBA-N370S* DaNs, and independent of DaN degeneration. Interestingly, these deficits were also quickly resolved in later cultures or with PKA inhibition to the early cultured MSNs.

4.3.1. Putative compensative mechanism of striatal micro-circuit

In our study, because ATP competitive analogue produced similar amplification of both Na_v and $K_{v,,}$ it is likely that the observed elevation of striatal PKA activity has been resulted from upstream of PKA from cAMP in the PKA signalling cascade. Activation of PKA is initiated by binding of cAMP to the regulatory subunits of PKA, thereby inducing the dissociation of the regulatory from the catalytic subunits and activate the latter (Figure 4.2A). The intracellular level of cAMP, in turn, is regulated by balanced activity of adenyl cyclase (AC) and cyclic nucleotide phosphodiesterase (PDE). The ontogenic source of elevated PKA activity could implied an increase in cAMP concentration and hence, AC activity. One potential source of elevating adenylyl cyclase/cAMP is the excessive D1R activation which stimulates the AC-cAMP-PKA cascade via G_s-mediated activation of AC (Gerfen and Surmeier, 2011). Meanwhile, previous voltage clamp study confirmed that D1R stimulation reduced Na_v currents by limiting channel availability (Surmeier and Kitai, 1993) while lessening K_v peak current amplitude through altering channel inactivation kinetics (Schrader *et al.*, 2002). Likewise, D1R agonist SFK81297 reversibly reproduced the reduction in Na_v and K_v current amplitude, through PKA-mediated phosphorylation of channel subunits, and improved striatal firing probability (Kitai

and Surmeier, 1993; Schiffmann, Lledo and Vincent, 1995). Given that the majority of our cultures was of direct pathway MSN (dMSN) expressing mainly Substance P or Pro-dynorphin (Figure 3.8), implicating D1R as a plausible inference. Future experiment employing pharmacological manipulation of D1R using its agonist SFK81297 might lend greater support to this hypothesis. Also, it remains to be explored whether the increased D1R signalling is due to altered channel kinetics, increased channel expression, or increased striatal DA content. Considering that the striatal deficit did not phenocopy the striatal excitability in the absence of dopaminergic projections at the same timepoint, I speculated that increased, rather than reduced, tonic DA content at the nigrostriatal synapses is a more logical explanation of D1R over-stimulation. This hypothesis aligns with previous works on other models of PD-related familial mutations reporting early cell-autonomous hyperexcitability of midbrain DaN prior to overt neurodegeneration (Bishop *et al.*, 2010; Subramaniam *et al.*, 2014; Carola *et al.*, 2021) but contrasts with a single report on *GBA N370*-associated reduced spontaneous firing and basal DA release by Woodard and colleagues (Woodard *et al.*, 2014). Woodard's findings, however, were observed from monoculture DaN dearth of circuit-dependent synaptic inputs so as to faithfully recapitulate the physiological dynamics of DaN excitability.

It could also be argued that the early deficits of MSN circuited with *GBA-N370S* DaNs demonstrated a delayed development rather than a case of compensative mechanism. It has been previously proposed that developmental component plays a role in the aetiology of PD whereby developmental defects are constantly compensated for for a long time but increase the susceptibility of carrier to disease onset in later life (Schwamborn, 2018). iPSC-derived models like one described in this work, with all cell types habouring the same mutation/genetic signature, could offer an early window to the investigation of early disease pathology. Additionally, given the inherent skepticism around iPSC-derived neurons being developmentally immature as compared to their *in vivo* counterpart, a transgenic mouse

model carrying similar mutation could be explored in parallel to further corroborate *in vitro* findings. Preliminary evidence from a *GBA-N370S* transgenic mouse model currently developed in the lab suggested significant deficit in evoked dopamine release and motor behaviour at 3-month old which was then subsided at 6-month old. This finding seems to favour the hypothesis of early dysfunction and subsequent compensation although more experiments are still required to determine whether this observation is consistent and if so, what the mechanism is.

Epidemiological data suggested that only about 9.1% of *GBA* mutation carriers would develop PD with relatively earlier age of onset and more modest motor impairment as compared to non-carriers (Riboldi and Di Fonzo, 2019). This seems to be in agreement with the early striatal pathology I observed in this study which was subsequently resolved in later DIVs. As the deficit normalisation was likely to be intrinsic to non-mutant MSN, I proposed that *GBA1* mutation-driven deficits in DaN emerged early but in itself were insufficient to induce long-term dysfunction in the motor circuit regulated by the basal ganglia. This evidence of potential compensative capacity suggests that it may be possible to interfere therapeutically to ameliorate pathology at an early stage. While major therapeutic effort has been channelled toward reversing DaN pathology, my results suggested that concomitant direct rescue of the striatal deficits is an attractive complementation so as to preserve the integrity of the basal ganglia output. Future studies should mimic the full genetic landscape of *GBA-N370S* carriers by deriving all three neuronal populations of the microcircuit from the same *GBA-N370S* cell lines. Pairwise comparisons of striatal functions from all mutant *GBA*-affected microcircuit with mixed healthy controls and mutant *GB*A-derived microcircuit would delineate contributing pathological roles of different neuronal populations of the striatal presynaptic circuitry to the net debilitating burden of *GBA* mutation on the striatum.

4.3.2. Putative pathological mechanism of *GBA-N370S* mutation.

The mechanism by which mutant *GBA-N370S* DaN induced early hyperexcitability of healthy control-derived MSN preceding neurodegeneration remains unclear. Here, I observed a reduction in PKA activity in *GBA-N370S* DaN relative to healthy control-derived DaN (Figure 4.2D) which is consistent with the previously reported downregulation of PKRACB transcript expression from DaN monoculture harbouring the same genetic burden (Lang *et al.*, 2019). Mutation of PKA regulatory subunit *PRKAR1B* has been reported in novel familial neurodegenerative condition with parkinsonism and dementia (Wong *et al.*, 2014) and *Prkar1b*-knockout rat exhibited body tremor (Hoang Trung *et al.*, 2021). Moreover, reduced PKA activity in DaN has been implicated in PD pathophysiology in other PD-related mutation model such *LRRK2 R1444C/G/H* (Muda *et al.*, 2014; Parisiadou *et al.*, 2014) and *PINK1* (Dagda *et al.*, 2014). Likewise, increased PKA activity was thought to be protective against PD (Yang *et al.*, 2008; Hwang *et al.*, 2014). However, mechanistic link between *GBA1* mutations and PKA activity in nigral neurons has never been identified. Nevertheless, it is well documented that the large network of lysosome genes including *GBA* is moderated by a master regulator transcription factor EB (TFEB) (Sardiello *et al.*, 2009) which in turn is the downstream substrate of PKA-mediated phosphorylation via mTORC1 (Martina *et al.*, 2012). Considering in parallel our previous observation indicating dysregulation of lysosomal/autophagic signalling in monocultured DaN carrying *GBA-N370S* (Fernandes *et al.*, 2016; Lang *et al.*, 2019), I speculated that the plethora of cellular perturbations in nigral DaN burdened by *GBA-N370S* mutation might be initiated by reduced activity of the master kinase PKA which disrupts various associated neuronal functions potentially via lysosomes and/or lysosomal-related organelles.

Alternatively, PKA was also thought to positively modulate neurotransmitter release in most synapses via a combination of factors including phosphorylation of various proteins involved in

synaptic vesicle exocytosis (Lonart *et al.*, 2003; Nagy *et al.*, 2004; Cho *et al.*, 2015). To a much lesser extent, it was also noted that blockade of PKA signalling did not lead to reduced neurotransmitter release in some synapses including hippocampal CA1 neurons (Weisskopf *et al.*, 1994). Direct observation bridging PKA signalling and DA release in midbrain DaN has not been reported although *in vivo* studies suggested PKA phosphorylation-mediated increase in DA release via activation of TH enzymatic activity (Campbell, Hardie and Vulliet, 1986; Wu *et al.*, 1992). Given the multifactorial multi-staged nature of the synthesis, packaging, and release of neurotransmitter, it is challenging to predict the net striatal DA content from TH activity dynamics. Taking into account the putative mechanistic link concerning striatal hyperexcitability and striatal D1R over-activation, it is tempting to hypothesise an increase in net extracellular DA at the nigrostriatal synapses which warrants future investigation. Nevertheless, the involvement of PKA in neurotransmitter release machineries offers an alternative hypothesis whereby mutant *GBA-N370S* DaN can affect DA striatal content, indicating the potentially complex multitude of the pathophysiology of *GBA-N370S* variant-mediated PD converging on tight modulation of PKA activity.

Chapter 5: Generation and characterisation of healthy control and familial PD-patient iPSC-derived human midbrain-like organoid (hMLO).

5.1. Introduction

5.1.1. Cerebral organoid

The first attempts at neural organoid were to generate cerebral organoid in the absence of exogenously added cues so as to drive intrinsic progression of cellular spheroids (Lancaster *et al.*, 2013). This organoid displayed a surprisingly diverse molecular signature reflecting a plethora of cellular ontology from the forebrain, hindbrain, and even non-ectodermal cells, both neurons and glial cells such as astrocytes. However, dearth of instructional developmental cues presented a major challenge of consistency and hence, reproducibility that is critical for modelling of specific diseases and/or biological phenomenon. An alternative strategy which was inspired from 2D directed differentiation and utilize patterning power of exogenous known morphogens or small molecules to drive specific cellular identity was subsequently developed. This approach not only improves reproducibility across lines but also permits specification of sub-brain regions of similar developmental trajectory (Birey *et al.*, 2017; Yoon *et al.*, 2019).

The broad panel of molecular, cellular, electrophysiological and computational tools allows robust identification of cellular signature of cerebral/cortical organoid (Quadrato *et al.*, 2017; Fleck *et al.*, 2021). These reports suggested high degree of similarities in cytoarchitectural and functional features of cortical organoid reminiscent of cerebral cortex (Uzquiano *et al.*, 2022). Interestingly, cortical organoid culturing over extended period of time exhibited spontaneously active neuronal network (Quadrato *et al.*, 2017) and replicated complex oscillatory activities

resembling the neural network in human preterm neonatal brain (Trujillo *et al.*, 2019). Such mature and physiologically relevant model has permitted uncovering of many insights into both human corticogenesis (Li *et al.*, 2017; Pollen *et al.*, 2019; Uzquiano *et al.*, 2022) and human cortical developmental abnormality (Qian *et al.*, 2016; Paulsen *et al.*, 2022). Parallel with refinement of organoid development, concurrent effort was directed at merging of organoid of cerebral cortex with those of different brain regions to form assembloids, expanding the available modelling palette and elevating organoid model utility (Andersen *et al.*, 2020; Miura *et al.*, 2020; Birey *et al.*, 2022). While still in its infancy, human assembloids exhibited functional circuits mimicking endogenous connectivity (Andersen *et al.*, 2020).

5.1.2. Midbrain organoid

The selective vulnerability of SNpc DaN in PD renders the necessity for a human cellular model such as midbrain organoid. Leveraging on the similar conceptual strategy of cortial organoid development, understanding of *in vivo* midbrain development was employed to generate midbrain organoid. Unlike cerebral organoid, organoid recapitulating the human midbrain which is not a default pathway of neurogenesis are always guided by well-defined and exogenously supplemented morphogens/small molecules within a well-established timeframe. Albeit sporadic and incomplete, existing evidence suggested that the resulting physiologically-relevant architecture of SNpc DaN in human midbrain-like organoid (hMLO) indeed facilitated emergence of more physiological features on the single-cell level and of late-stage developmental properties (Jo *et al.*, 2016; Fiorenzano *et al.*, 2021) as similarly observed in cortical organoid. Therefore, hMLO represents a promising model to shed light on complex human-specific endogenously spontaneous pathology that has largely been elusive in alternative modelling approach such as synucleinopathies in PD.

5.1.3. α-synuclein pathology in familial Parkinson's Disease

Synucleinopathy is one of the canonical molecular markers of PD (Araki *et al.*, 2019). In PD, α-synuclein converts from a soluble synaptic protein into insoluble fibrils aggregating within the affected neurites and cell bodies of midbrain DaN (Spillantini *et al.*, 1997; Stefanis, 2012). The conversion of unfolded monomer into insoluble aggregates was found to involve hyperphosphorylation of monomeric α-synuclein which exhibits intrinsic cellular toxicity as well as increased propensity to polymerization to form toxic fibrils (Goedert, 2001; Killinger *et al.*, 2019). However, the exact aetiology of synucleinopathy remains elusive. Much of the current insights into potential mechanism of synucleinopathy rely on various models of artificial induction of synucleinopathy employing the deliberate introduction of pre-formed fibrils (PFF) which in turns facilitate amyloid formation via 'seeded polymerization' (Soto, 2003; Awa *et al.*, 2022). It is hypothesized that a more physiologically relevant model of human neurons such as human organoid would permit investigation of synucleinopathy via recapitulation of spontaneous α-synuclein pathology in a genetically-related model of PD.

5.1.4. Aims

Within this chapter, I aimed to:

- Determine an optimized and robust differentiation of hMLO from iPSC of both healthy and familial PD patients
- Investigate potential spontaneous α-synuclein pathology in the context of familial PD-related mutation including *SNCA* Triplication and GNA *N370S* using the hMLO model.

5.2. Results

5.2.1. Characterisation of iPSC-derived hMLO.

Adapted from (Jo *et al.*, 2016), my first two differentiations generating hMLO from our healthy controls-derived lines produced organoid with TH-expressing cells but virtually no co-expression of FOXA2 (Figure 5.1). This prompted a need to optimise Jo's protocol using our cells lines with the key objectives in not only generating DaN but also recreating its floorplate ontology. To do so, I examined multiple hMLO differentiation paradigms on control iPSC by varying initial cell seeding density, SHH sub-types, and SHH and fibroblast growth factor 8a (FGF8a) (SF) exposure period (Figure 5.2). Previous works reported that early treatment with a GSK-3 inhibitor (CHIR99021), in combination of SB431542 and LDN193189, promotes neuroectodermal differentiation. Subsequent exposure to SHH and FGF8a concurrently was found to induce mesencephalic specification (Joksimovic and Awatramani, 2014). In addition, variable cell seeding density, SHH sub-type, and SF treatment duration could influence the differentiation efficiency of early embryoid bodies toward the midbrain. Multiple differentiation protocols in each of which each of those contributing factors were applied individually and pair-wise comparisons were made to dissect their individual impacts on differentiation efficiency in term of i) midbrain patterning probability via expression of FOXA2, floor-plate progenitor marker, and ii) subsequent development of TH-expressing dopaminergic neurons (Figure 5.2).

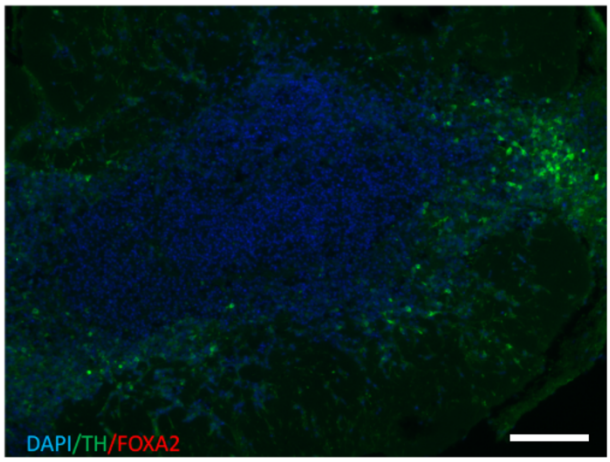

Figure 5.1: Representative immunostaining image of hMLO differentiation batch 1 at DIV 46. TH-expressing cells were present but no FOXA2 signal was detected, Scale bar = 200 μm.

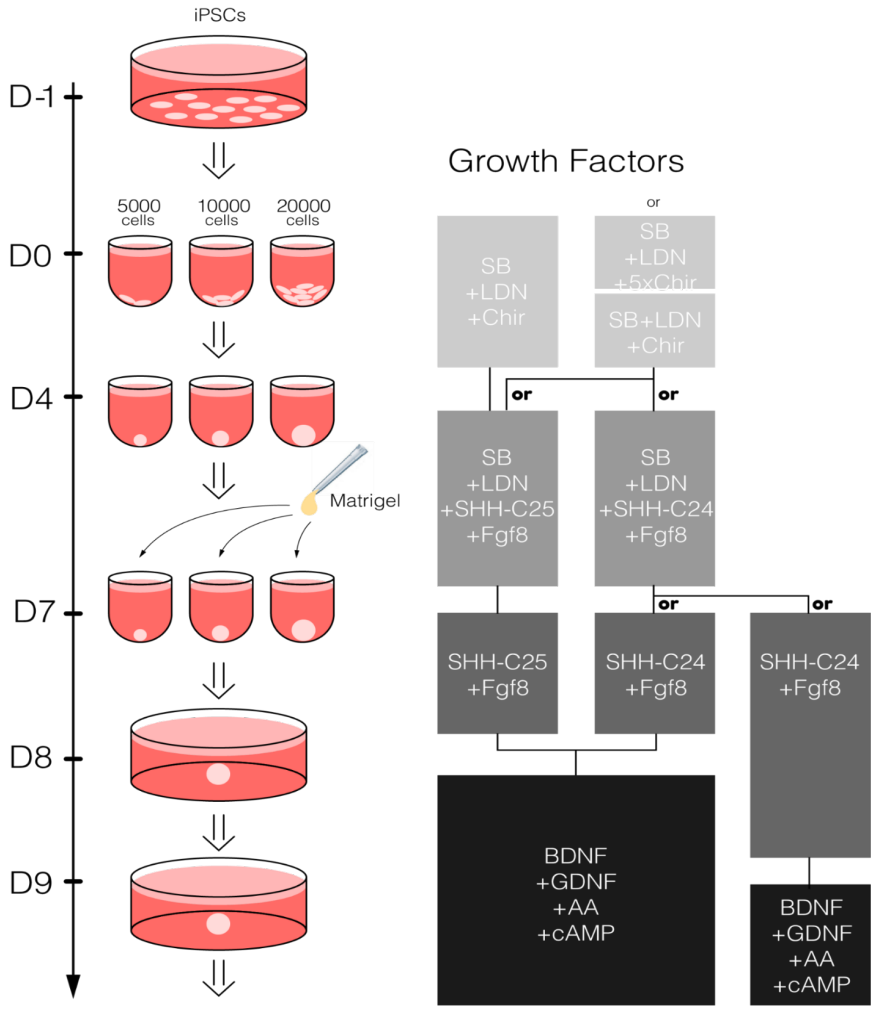

Figure 5.2: Schematics of differentiation conditions of iPSC-derived hMLO. The vertical arrow represents timeline of cell cultures by days *in vitro*, i.e. D0 = day 0 *in vitro*. Different shade represents different stages of the differentiation at which point there are changes in the media make-up. Key differences of different differentiation strategies include: different seeding cell numbers (5000, 10000 or 20000 cells/well); CHIR exposure between D0-2 (0.8 µM or 4.0 µM), subtype of recombinant SHH (mouse SHH-C25II or human SHH-C24II) and exposure duration of the duo SHH and Fgf8 (4 or 5 days) XAV: Wnt signalling pathway inhibitor, LDN: inhibitor of the bone morphogenetic (BMP) pathway; SB: inhibitor of TGFß superfamily type I activin receptor-like kinase (ALK) receptor; Fgf8: fibroblast growth factor 8, SHH-C24: recombinant human sonic hedghog; SHH-C25II: recombinant mouse sonic hedgehog; Chir: Chir990221, glycogen synthase kinase 3 inhibitor; BDNF: brain-derived neurotrophic factor; GDNF: glia-derived neurotrophic factor; AA: ascorbic acid.

Qualitative observation of all immunostained hMLO section revealed abundant expression of FOXA2, MAP2 and TH in most hMLO generated (Figure 5.3). Upon quantitatively comparing immunohistochemical staining of hMLO sections produced from various differentiation

strategies at DIV 46, the expression of FOXA2 was shown to be the greatest in hMLO seeded with of 20,000 cells and subjected to 5-day SF independently (Figure 5.3A). At 5,000 and 10,000 cells/hMLO, neither 5-day SF nor increased CHIR99021 nor SHH-C25 improved FOXA2 expression. However, at higher seeding density of 20,000 cells/hMLO, FOXA2 expression was abundant in the absence of increased CHIR99021 and augmented by SHH-C25, a more potent SHH sub-type (Figure 5.3A). Similarly, expression of tyrosine hydroxylase (TH), the rate limiting enzyme of DA synthesis and concomitantly the principal marker of DaN, was enhanced by extended exposure of early embryoids to SF for 5 days or with low concentration of CHIR99021. High initial cell seeding of 20,00 cells/hMLO also led to the most abundant TH expression in late organoid at DIV 96. However, more potent SHH-C25 did not seem to confer advantageous edge in term of TH expression over the milder isotype SHH-C24 (Figure 5.4). Nevertheless, it worths noting that TH-expressing neurons constituted 5-10% of the human midbrain (La Manno *et al.*, 2016). Taken together, this finding suggested that iPSC could be differentiated into hMLO via floorplate patterning with LDN193189, SB431542, CHIR99021, SHH-C25 and FGF8a at defined timepoints and concentrations (Figure 5.4).

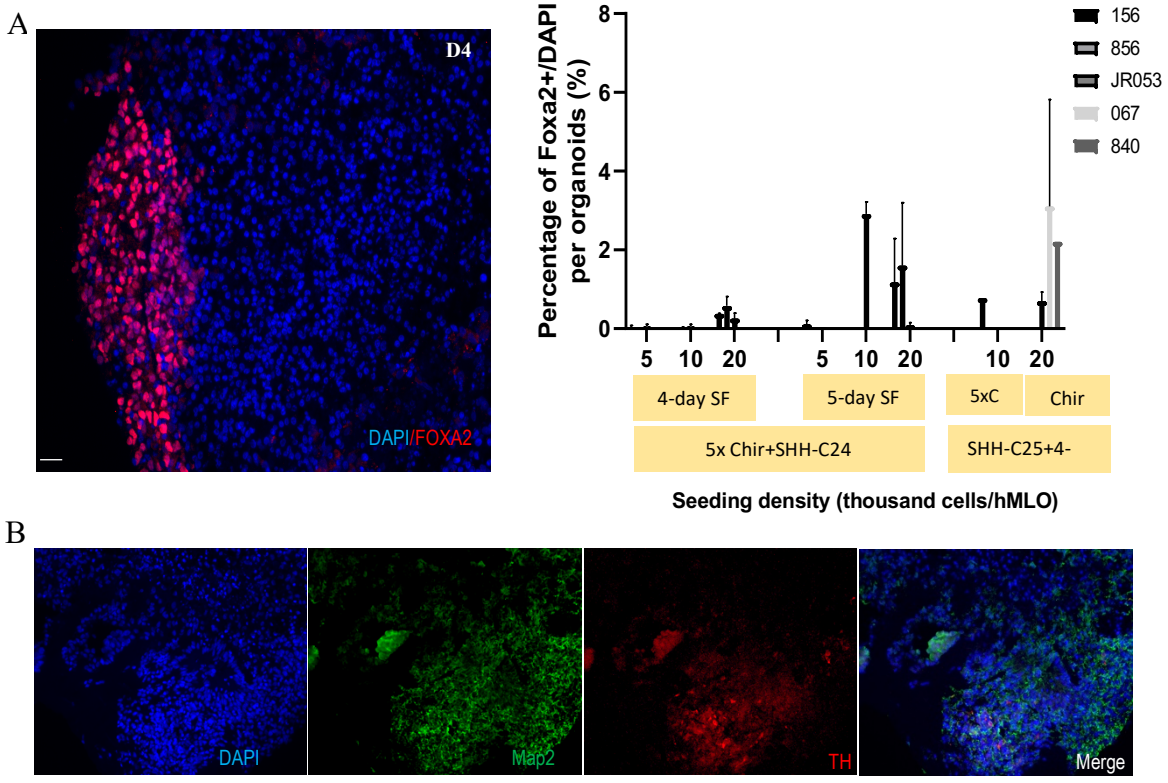

Figure 5.3: Immunohistochemical characterisation of midbrain origin by FOXA2 expression in paraffin-embedded hMLO on DIV 46. A. Generally, FOXA2 expression is greatest with extended SHH and FGF8a patterning and SHH-C25 with high seeding density of 20,000 cells/hMLO. B. Tyrosine hydroxylase expression remained sparse on DIV 46. All data were presented as mean ± SEM. n=1 differentiations, 4 control lines/differentiation, 2 hMLO/iPS cell line. SF = SHH + FGF8, Chir = CHIR99021

Efficiency of floorplate patterning and subsequent expression of midbrain DaN was, however, independently modulated by ventralising potency of SHH, starting cell number, and treatment duration of SHH and FGF8a. Although each differentiation condition was only performed once, the results was informative of effects of individual contributing factors to hMLO generation for me to single out an optimised protocol to move forward with. Specifically, a combination of high starting cell number at 20,000 cells/hMLO, highly potent SHH-C25, and 5-day treatment of SHH and FGF8 substantially promoted the greatest efficiency of the development of floorplate precursors (i.e. FOXA2-positive cells) and subsequently post-mitotic midbrain DaN (i.e. MAP2 and TH co-expression) reminiscent key features of the human midbrain that is of interest to PD modelling (Figure 5.4). The optimized hMLO differentiation was illustrated in Figure 5.5A, which generated hMLO expressing abundant neurons including floor-plate specific DaNs

(Figure 5.5C-D). These hMLO expressed molecularly identifiable and mature DaN, expressing dopamine transporter (DAT) and G-protein-regulated inward-rectifier potassium channel 2 (GIRK2) (DAT- and GIRK2-positive cells; Figure 5.6A-E), of potentially diverse dopaminergic subtypes (Calbindin-positive and -negative; Figure 5.6G and H) intermingled with neural precursors (Nestin-positive cells, Figure 5.6F). Moreover, within the hMLO nested astrocytes (S100β-positive cells, Figure 5.6I). Interestingly, using Fontana-Mason assay, I was able to detect spontaneous formation of dark-pigmented neuromelanin, a characteristic insoluble granular pigments that accumulate in the A9 midbrain in human and primate (Sulzer *et al.*, 2000), in DIV 96 hMLO derived from healthy controls (Figure 5.5E).

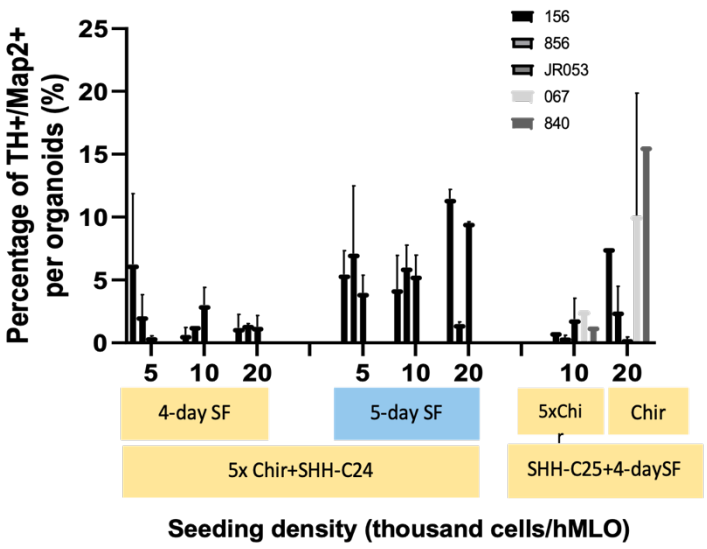

Figure 5.4: Quantification of differential TH expression in corresponding differentiation conditions at DIV 96. All data is presented as mean ± standard error of the mean (SEM). n=1 differentiation, 2 hMLOs/line/condition. SF = SHH + FGF8, Chir = CHIR99021

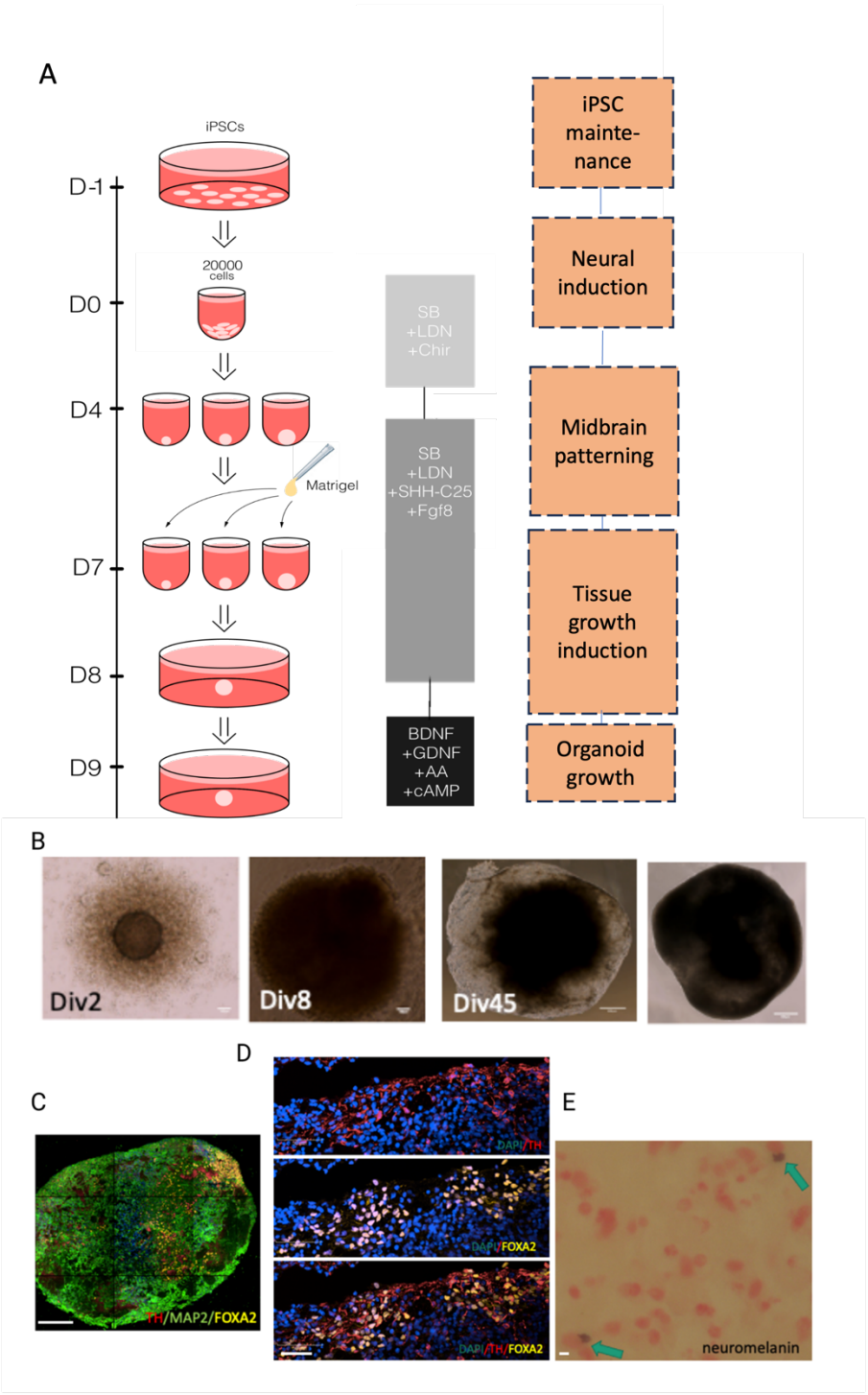

Figure 5.5: Characterisation of hMLO derived from selected optimised differentiation protocol. A) Schematic of differentiation timeline of iPSC-derived hMLO adapted and modified from Jo et al., 2016. Photo adapted and modified from Jo et. al., 2016. B) Representative bright field images of hMLO over time reflecting their morphological development, scale bar = 500 μm. C-D) Representative immunohistochemical images of hMLO section with MAP2 (green), TH (red), and FOXA2 (yellow) at C) low (scale bar = 200 μm), and D) high magnification (scale bar = 50 μm). E) Representative image of Fontana-Masson staining of black-pigmented neuromelanin present in hMLO sections (scale bar = 50 μm).

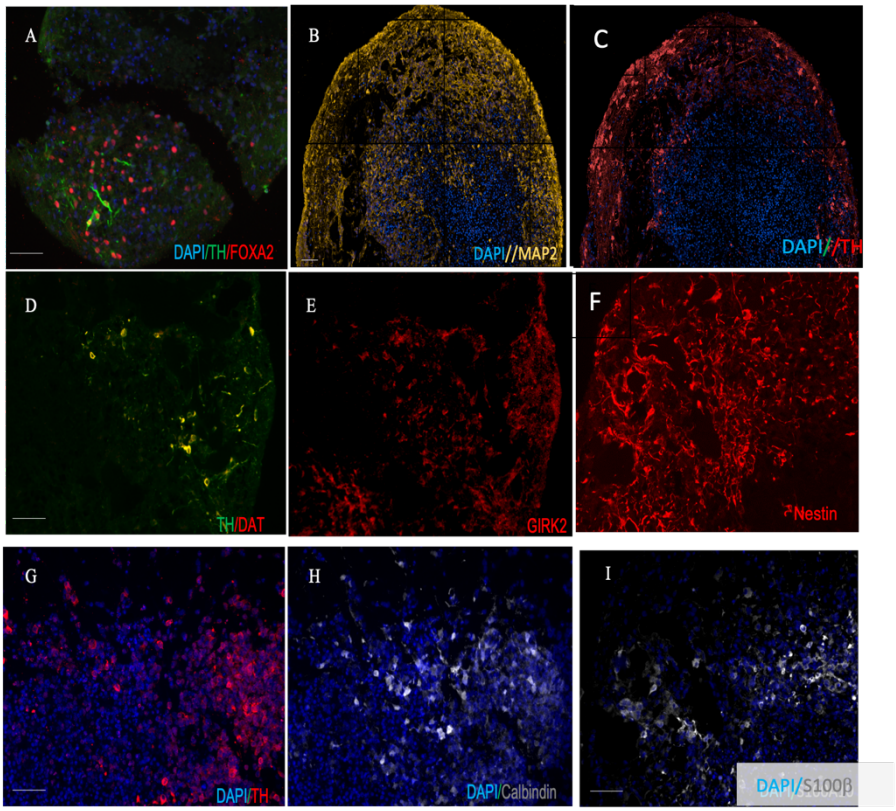

Figure 5.6: Representative ICC images of DIV 96 hMLO reflecting their diverse neuronal and neural make-up. (A-C) Abundant post-mitotic (MAP2-positive) neurons in hMLO many of which was DaN. D. True identity of DaN was confirmed by co-localisation of TH with Dopamine transporter (DAT). (E, G&H) Presence of diverse dopaminergic neuron subtypes suggested by combinatorial expressiom of FOXA2, of G-protein-regulated inward-rectifier potassium channel 2 (GIRK2) and calbindin (CB) intermingled with (F) NESTIN-positive neural precursors and (I) S100β-expressing astrocytes. Scale bar =200μm.

5.2.2. Disease-modelling of familial PD patients-specific hMLO.

Applying the optimised hMLO differentiation protocol, I generated hMLO from iPSC-derived from both healthy controls and other PD patients carrying PD-related mutations, including *SNCA A53T*, *SNCA* Triplication, and *GBA-N370S*, so as to investigate potential pathology conferred by these mutations in this model. Although I was able to observe both expression of FOXA2 and TH in most hMLO, the former was absent among hMLO derived from iPSC habouring *SNCA A53T* in the first round of differentiation (Table 5.2.2.). These iPS cell lines, however, were amenable to our routine 2-dimensional DaN differentiation at a comparable

efficiency to the remaining iPSC lines. This suggested still a potentially limited robustness of this hMLO differentiation protocol in patterning floor-plate identity. Moving forward with the other responsive cell lines (i.e. *GBA-N370S* and *SNCA*-Triplication lines), I repeated the experiment 2-3 times and quantified FOXA2 and TH expression following immunohistochemistry of 5 μm hMLO paraffin-embedded sections. Interestingly, neither *SNCA* Triplication nor *GBA-N370S* mutation affected the net expression abundance of both FOXA2 and TH at DIV 46 or DIV 96, respectively, relative to healthy control-derived hMLO (Figure 5.7A and B). This lack of genetic mutation-driven discrepancy was independent of the chosen measurement parameter given the linear relationship between the percentage of TH-positive neurons over MAP2-positive neurons and that of TH-positive area over MAP2-positive area (Figure 5.7C).

It was speculated that a more physiologically relevant model such as organoid might permit emergence of spontaneous α-synuclein pathology reminiscent that found in post-mortem human tissue. However, preliminary immunostaining of total α-synuclein as well as phosphorylated α-synuclein at the residue S129 in TH-positive neurons revealed no presence of either altered α-synuclein expression or α-synuclein phosphorylation in *SNCA* Triplication-habouring hMLO relative to healthy control-derived ones. Furthermore, preliminary proximity ligation assay (performed by Nora Bengoa-Vergniory, N = 1 differentiation, n = 1 hMLO/iPSC line) also reported no difference in the number of α-synuclein puncta per TH-expressing neuron (Figure 5.7D).

Table 5.2.2: Quality control on robustness of hMLO differentiated from various iPS cell lines of various genetic background across differentiations. opB1/2/3 = optimised differentiation batch 1/2/3, Y= yes, N = no, ND = not done

Mutations	iPSC lines	Presence of FOXA2 immunopositivity (Y or N or NA)			Presence of TH immunopositivity (Y or N or NA)		
Differentiation Batch No.		opB1	opB3	opB4	opB1	opB3	opB4
SNCA A53T	SFC828-03	N	ND	ND	Y	ND	ND
	SFC829-03	N	ND	ND	Y	ND	ND
	SFC830-04	N	ND	ND	Y	ND	ND
SNCA Triplication	SFC831-1	Y	Y	ND	Y	Y	ND
	SFC831-3	Y	Y	ND	Y	Y	ND
	SFC831-3	Y	Y	ND	Y	Y	ND
GBA N370S	MK082	Y	Y	Y	Y	Y	Y
	SFC871-03	Y	N	N	Y	Y	Y
	MK071	N	Y	Y	Y	Y	Y
	MK088	ND	N	Y	Y	Y	Y

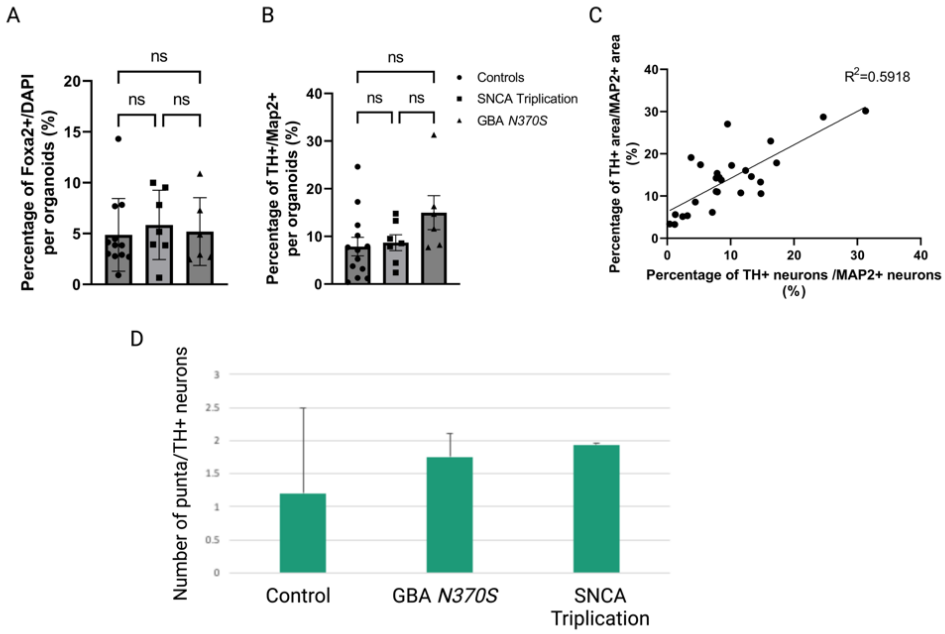

Figure 5.7: Neither overt neurodegeneration nor alpha-synuclein pathology observed in hMLO of different genetic burdens. Quantification of FOXA2- and TH-expressing cells at A) DIV 46 and B) DIV 96, respectively. C) Positively linear correlation between quantitative parameters, TH-positive area and TH-positive neurons. Each dot represents a cell line from one differentiation. All data wereb presented as mean ± standard error of the mean (SEM). n=2-3 differentiation, 2-3 line/genetic condition, 3-4 hMLO/line. ns p>0.05, Kruskal Wallis test followed by Dunn's multiple comparisons test. D) Quanifification of alpha-synuclein punctas in hMLO habouring different genetic burdens, N=1 differentiation, 1-2 line/genetic condition, 1 hMLO/line, Nora Bengoa-Vergniory performed experiments and analysed the data.

5.3. Discussion

Adapting from a published protocol, I modified several key elements previously reported to contribute toward midbrain patterning and development so as to optimise differentiation of hMLO from iPSC derived from healthy controls and familial PD patients. Using immunostaining, I confirmed that the resulting hMLO expressed floor-plate progenitors prior to emergence of various neuronal subtypes, including A9 DaN negative for calbindin but positive for its specific transporter and G protein-coupled rectifying potassium channel GIRK2. Notably, these hMLO also expressed astrocytes intermingled with neurons. However, hMLO derived from familial PD patients displayed comparable differentiation potential with neither overt neurodegeneration nor distinguishable spontaneous alpha-synuclein pathology. This suggested that while this

model was able to recapitulate some key molecular features of midbrain, it remains physiologically limited in permitting spontaneous PD pathology reminiscent that occurring in human.

5.3.1. Generation of hMLO from iPSC

Being a more recent success as compared to cerebral organoid, generation of midbrain organoid recapitulating their ontological floorplate identity has been reported only from a number of research groups (Fiorenzano et al. 2021; Jo et al. 2016; Kim et al. 2019; Kwak et al. 2020; Qian et al. 2016; Smits et al. 2019; Tieng et al. 2014). Each of these was inspired from previous 2D successful derivation of midbrain DaN: Smit et al., (2019) was developed from Reinhart et al., (2013) (Reinhardt et al. 2013) while all the remaining learned from Kriks et al., (2011) (Kriks et al. 2011). Despite minute discrepancy in the exact temporal timepoints and durations of the administration of various patterning factors, these approaches shared striking conceptual resemblance including initial neural patterning with dual -SMAD inhibitor, coupled with early activation of SHH, FGF8 and WNT (using CHIR99021). However, only hMLO reported by Qian et al., (2016) and Kim et al., (2019) were derived from iPSC with an approximate yield of 50% of all cells expressing TH. At the commencement of this project in late 2018, only Jo et al., (2016), Qian et al., (2016) and Tieng et al., (2014) were published among which only Jo and colleagues reported a comprehensive characterisation panel of the resulting hMLO by transcriptomic, molecular and electrophysiological assays. As the result, I decided to employ Jo et.al.'s approach of generating hMLO from iPSC via floorplate patterning (Jo et al. 2016).

It worths noting that Jo et al., (2016) protocol to generate hMLO was employed on human pluripotent cells (hPSCs) and not iPSC. Despite important similarities between the two cell types in terms of self-renewing capability and pluripotency, reports suggested intrinsic

differences in differentiation potential stemming from epigenetic memory of somatic cells of origin (Kim *et al.*, 2010; Polo *et al.*, 2010) and single cell heterogeneity post-reprogramming of iPSC (Narsinh *et al.*, 2011). In fact, iPSC differentiated into neural cells at much lower and greater variable efficiency than hPSCs did, independent of reprogramming approach (Hu *et al.*, 2010). Similar phenomena were also observed in generation of other cell types such as hemangioblasts (Feng *et al.*, 2010) and cardiovascular progenitors (Narsinh *et al.*, 2011). Hence I had hypothesised that extended treatment of SHH and FGF8 would address the intrinsic limitation in differentiation potential of iPSC as compared to that of hPSC reported by Jo et al.(2016). Another recently published work from Kim and colleagues (2019) demonstrated similar conceptual approach in which hMLO was directed from iPSC in the presence of prolonged SHH and FGF8 for 10 days (versus 4 days in Jo et al., 2019 and 5 days in this report) followed by continued exposure to SHH for another 5 days (Kim *et al.*, 2019). Such strong telencephalic patterning might have accounted for the substantially large proportion of approximately 32% TH+/MAP2+ neurons found in their hMLO. Nevertheless, neither Kim nor I performed comprehensive transcriptomic profiling of cellular composition within the resulting hMLO in comparison with that of human midbrain so as to validate the physiological relevance of the resulting iPSC-derived hMLO models. A recent single-cell transcriptomics study on the identifying temporal neuronal diversity within the human midbrain, in direct comparison with mouse midbrains or other independent reports on mouse midbrain (Poulin *et al.*, 2014), have reported a number of differences in mouse and human dopaminergic neuron development and concurrently informed useful markers of various DaN subtypes specific in the human midbrain through various developmental stages to be considered for future characterisation of hMLOs (La Manno *et al.*, 2016). For example, *Aldh1a1* and the transcriptional co-regulator *Lmo3*, are specifically expressed in human embryonic DaNs that are precursor of DaNs in both VTA and SNc. However, in postnatal stage *ALDH1A1*, and *SOX6* distinguish SNc cells from *CALB1*-positive VTA cells. Up to date, such knowledge gap remains to be filled so as to lend

greater confidence in the existing midbrain organoid generation strategy. As a result, it is challenging to conclude whether the absence of PD-related α-synuclein pathology is characteristic of the genetic mutations I was looking at or symptom of a physiologically irrelevant/immature models.

5.3.2. Synucleinopathy in hMLO-based modelling of PD

Our results suggested lack of spontaneous abnormalities in term of alpha-synuclein expression, its phosphorylation at serin 129 (pS129) as well as aggregation in DIV 96 hMLO derived from familial PD patients. Despite being one of the characteristic pathological hallmarks of PD found in human tissue of the midbrain, only three studies reported spontaneous synucleinopathy in *in vitro* human models using iPSC (Kim *et al.*, 2019; Jo *et al.*, 2021; Mohamed *et al.*, 2021). When using hMLO derived from iPSC lines engineered by CRISPR-Cas9 technology to carry heterozygous *LRRK2-G2019S* point mutation or isogenic controls, Kim and colleagues observed in the mutant line aberrant localisation of pS129-α-synuclein with autophagic and mitophagy markers without any difference in total amount of pS129-α-synuclein (Kim *et al.*, 2019). It, hence, seems logical to imply that the abnormal positioning of phosphorylated α-synuclein is secondary manifestation of perturbed autophagy and mitophagy which in turn are widely reported as pathological features of mutant DaN (Pischedda *et al.*, 2021; Singh *et al.*, 2021). Likewise, Mohamed et al., (2021) reported elevated levels of α-synuclein and a time-dependent increase in α-synuclein aggregation, both in the oligomeric and phosphorylated forms of α-synuclein, also in DIV 100 hMLO derived from patients carrying *SNCA* Triplication mutation relative to their isogenic controls. This highlighted the necessity of performing isogenic control experiments in a highly variable modelling system as organoid and implied that any potential α-synuclein phenotype in mutant hMLO might have been masked in the absence of isogenic controls. Jo et al., (2021) also reported recapitulation of PD

synucleinopathological hallmarks using hMLO models from genetically modified embryonic cell lines. Their findings included significant loss of midbrain DaN and accumulation of α-synuclein aggregates in both *GBA*$^{-/-}$ and dox-inducible *SNCA*-overexpressing hMLO as compared to wild-type controls hMLO (Jo *et al.*, 2021). Although their *GBA*$^{-/-}$ and *SNCA*-overexpressing hPSC lines were not patient-specific, this results demonstrated the fundamental genetic-to-phenotype relationship of PD-related mutations and synucleinopathy which has not been previously observed in PD animal models or 2-dimensional monoculture of human midbrain DaN.

Chapter 6: Generation and characterisation of a custom human tyrosine-hydroxylase promoter-specific reporter in a viral expression system.

6.1. Introduction

6.1.1. Brief biology of human tyrosine hydroxylase promoter.

Tyrosine hydroxylase is an enzyme encoded by the TH gene on human chromosome 11p15 (Craig *et al.*, 1986). Expression of TH is selective in catecholamine-expressing neurons, particularly DaN, and responsible for catalysing amino acid L-tyrosine into L-3,4-dihydroxyphenylalanine (L-DOPA) which in turn is the precursor of dopamine (Nagatsu *et al*, 1964) . The sequence of human TH promoter (phTH) is more than 10 kb and made up of various conserved regions (Kessler *et al.*, 2003; Wang, Fones and Cave, 2018) as well as important motifs critical for binding of factors/activators/repressors driving specific expression of TH in cell-type specific manner. The huge interest in studying DaN has triggered much greater interest in understanding the biological makeup and activity of phTH

6.1.2. Current status quo of human TH promoter-driven reporter

A TH reporter is instrumental in fine-tuning iPSC-DaN specific phenotypes given the lack of DaN homogenous culture differentiated from iPSC using any of the current differentiation protocols. As more emphasis is placed on generating advanced *in vitro* cultures such as organoid or co-cultures of different neural and neuronal cell types so as to better recapitulate the *in vivo* cellular physiology, a TH reporter is also valuable to facilitate cell-type specific investigation. However, a useful TH reporter that could specifically label human neurons remains a topic of ongoing effort. Majority of mouse-derived TH reporters showed poor specificity in robustly identifying iPSC-DaN in cultures. This is likely to surface from dissimilarities between the sequence of mouse/rat TH promoter and that of human promoter. A more recently reported TH reporter that tagged DaN with 95% specificity in non-human primates such as monkey (Stauffer *et al.*, 2016) displayed minimally specific labelling of iPSC-DaN *in vitro* (Preliminary data obtained by Tara Caffery). In fact, attempts at generating custom human TH promoters were met with variable success (Kaneda *et al.*, 1991; Gardaneh *et al.*, 2000; Kim *et al.*, 2003), albeit mostly in cell lines and often with long promoter construct of a few kb. These studies shed light on critical regions of functionality, informing following up attempts of functionally useful regions.

The choice of lentiviral vector (LV), rather than the traditional adenosine-associated virus commonly used for *in vivo* transfection, was preferred following empirical evidence of superior transduction efficiency of LV-based vector over both adenosine-associated viruses type nine and five (Figure 6.1). Hence, all viruses made in this work for the purpose of transducing iPSC-DaN would be cloned into the LV vector backbone for higher transduction efficiency.

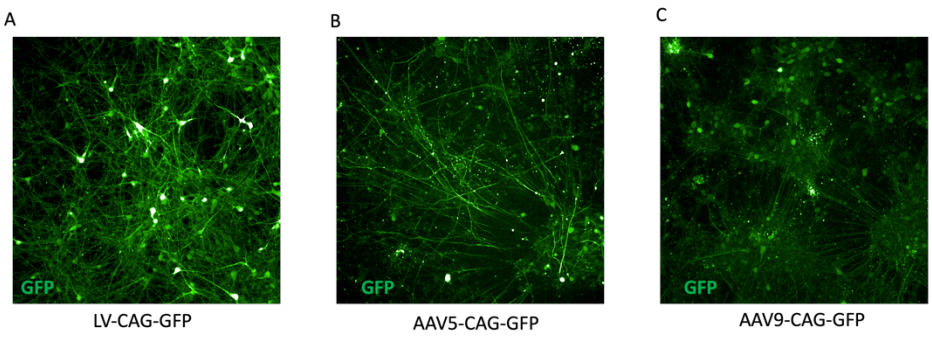

Figure 6.1: Characterisation of transduction efficiency of different viral vectors. Representative live fluorescent images of iPSC-DaN transduced with A) lentiviruses B) adenovirus-associated viruses type 5 or C) adenovirus-associated viruses type 9 expressing GFP (green) under the generic universal promoter CAG. (Images were taken Tara Caffery).

6.1.3. Aims

In this chapter, I aimed to

- Conceptualise and design an abridged phTH that are amenable to the lentiviral system
- Characterise various custom promoter designs so as to validate the feasibility of such design approach as well as to identify a functional custom promoter.

6.2. Results

6.2.1. *In silico* generation of a custom human promoter TH.

The full-sized human TH promoter (approximately 11 kb) is too large to be packed into a lentivirus together with reporter genes of interest without significantly compromising transduction efficiency. To single out important sequences that contribute towards proper functionality of the human TH promoter and DA specification, I identified all known binding domains from previous literature and annotated them along the length of the full human TH

promoter (NICB GRCH38.p13(GCF_000001405.39)) (Figure 6.1). Key motifs that are essential to transcription initiation universal to majority of proteins including: the transcription start site (TSS) (Kessler *et al.*, 2003; Romano *et al.*, 2005), the first 124 bp upstream from TSS, the cAMP-response element (CRE) (Cha-Molstad *et al.*, 2004), and the RNA polymerase binding site, the TATA box (Horikoshi *et al.*, 1992; Nikolov *et al.*, 1996). Considering the high similarity in molecular, cellular and functional features of TH across different species, it is sensible to also identify evolutionarily conserved regions (CRs). Five CRs were consistently and independently reported in two different publications (Romano *et al.*, 2005; Wang, Fones and Cave, 2018). The reported lengths of all five CRs from Wang et. al. were greater than but inclusive of that of CRs in Romano et. al. Therefore, I included the longer contigs to avoid potential loss of important segments. Interestingly, Wang et al. also found one CR that was not reported elsewhere. This contig, similar to the other CRs, housed binding motifs of many TH-specific transcription factors. Moreover, Banerjiee et.al. found two GC-rich regions conserved in tetrapod vertebrates encoding ribonucleoprotein (hnRNP) transactivator of TH transcription (Banerjee *et al.*, 2014).

I also identified and annotated sequences bound by transcription factors known to be critical in specifying DA neurogenesis: MEIS-PBX1 (Schulte and Geerts, 2019), four bicoid binding elements (BBE) signalling attachment of PTIX3, MTA1 and DJ1 (Lebel *et al.*, 2001; Kessler *et al.*, 2003; Reddy *et al.*, 2011), FOXA2 (Wang, Fones and Cave, 2018) , NURR1 (Wang, Fones and Cave, 2018), MEIS2 (Wang, Fones and Cave, 2018), PAX6 (Wang, Fones and Cave, 2018), GLI (Kessler *et al.*, 2003; Kim *et al.*, 2003), transcription factor activator protein 1 (AP-1) (Hess, Angel and Schorpp-Kistner, 2004), the Neuron-Restrictive Silencer Factor/RE1-Silencing Transcription factor (NRSF/REST) (Wang, Fones and Cave, 2018). Moreover, the first intron downstream of the human TH promoter contained the scaffold or matrix attachment region (S/MAR) repeat (TCAT) found essential toward specific expression of TH (Lenartowski *et al.*,

2003) . Interestingly, this S/MAR repeat shared great resemblance to the first intron of EF1-α gene . Insertion of this intron to the human EF-1 alpha gene behind the MCMV and the HCMV promoter greatly enhanced the gene expression in transfected cell lines through increasing RNA transcription and/or RNA stability, driving greater and more stable gene expression surpassing the CMV promoter (Wang *et al.*, 2017)

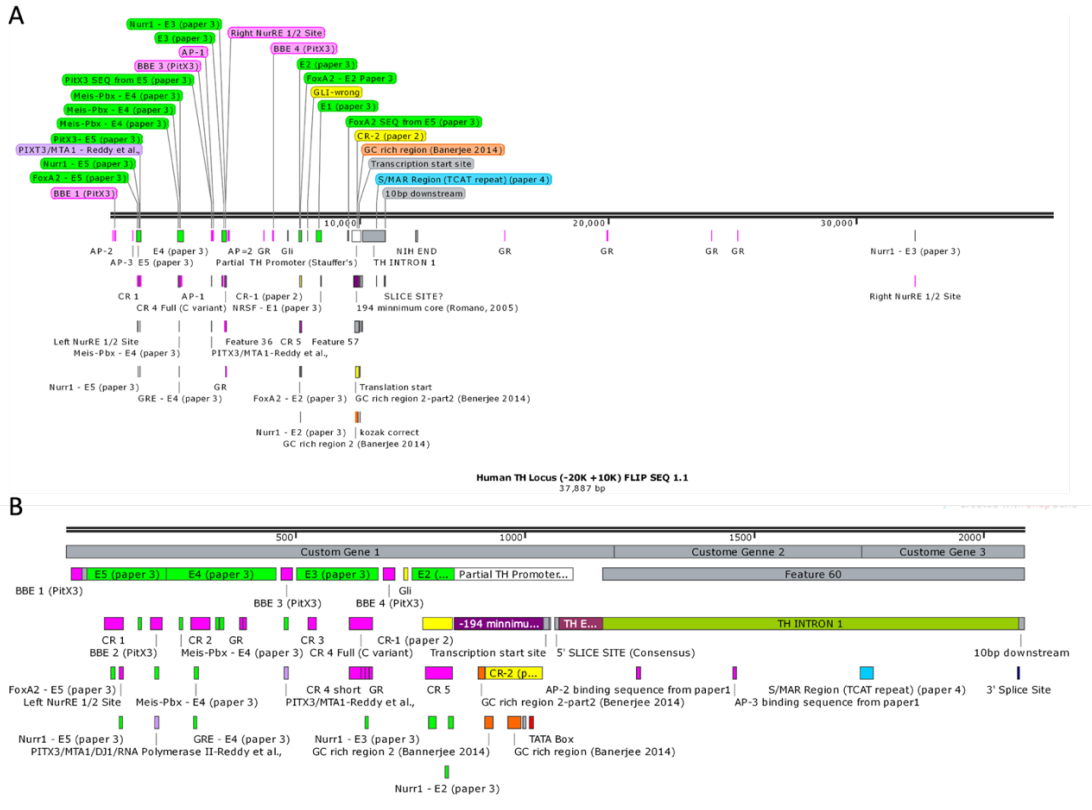

Figure 6.2: human TH promoter annotations. A) the full-length human TH gene was annotated with functional binding domains previously reported. Different colour represented different studies. B) Abridged custom human TH promoter (abridged-pcTH) generated from extracting and concatenating known functional contigs, together with the sequences of exon 1, intron 1 and part of exon 2. Paper 1 is (Kessler *et al.*, 2003), paper 2 is (Banerjee *et al.*, 2014) , paper 3 (Wang, Fones and Cave, 2018), and paper 4 is (Lenartowski and Goc, 2002). BBE = bicoid binding element, CR = conserved region, GRE = glucocorticoid receptor activation. E1-5 = evolutionary conserved region 1-5.

The final abridged custom human TH promoter (abridged-pcTH) was generated from extracting and concatenating i) all annotated domains along the entire length of human TH promoter that were reported independently in at least two different studies, ii)10 bp sequence flanking either side of each binding region which acted as spacer region to minimize potential steric hindrance

due to binding of multiple protein complexes, iii) 300 bp sequence upstream of the transcription start site previously characterised to be useful in specifically labelling DaN in monkey (Stauffer *et al.*, 2016) (Figure 6.1B). Given the unique role of the S/MAT region in driving specific TH expression, the full-length exon 1 and intron 1 were also considered in some of the experimental variants (Figure 6.1B).

6.2.2. Generation and characterisation of a custom human TH promoter-specific reporter in lentiviruses.

In the first round of custom human TH promoter (pcTH) generation, three variants of pcTH (pcTHv1.0, pcTH c1.2, pcTH v2.0; Figure 6B-D) were designed (see Appendix for exact sequences), each of which was cloned upstream of the red fluorescent protein mApple using In-Fusion technology and packaged into a lentiviral backbone (Figure 1.2A). pcTH v1.0 consisted of the abridged human TH promoter, exon 1, intron 1, the first 12 bp of exon 2 and the consensus GDPPVAT protein linker. The first 12 bp of exon 2 encompassed the 3' slice site, allowing proper splicing of intron 1 prior to translation while keeping the sequence read in-frame. Due to the presence of the short amino acid sequence translated from exon 1 and 2 upstream of the mApple sequence, a consensus protein linker was included to facilitate proper folding of the resulting polycistronic protein. Following the similar design concept, pcTH v1.2 was made with the addition of the Kozak sequence downstream of the GDPPVAT protein linker and immediately upstream of the mApple sequence. Kozak consensus sequence is a nucleic acid motif of a consensus sequence "GCCACC" occurring naturally in most eukaryotic mRNA and play a significant role in initiating translation. This Kozak sequence was artificially introduced upstream of mApple so as pre-empt the potential lack of/limited mApple expression downstream of the bulky Exon1-protein linker complex.

To investigate the necessity of the S/MAR repeat in our design, pcTH v2.0 was made up of only the abridged human TH promoter plus the first 12 bp of the first exon to maintain in-frame translation.

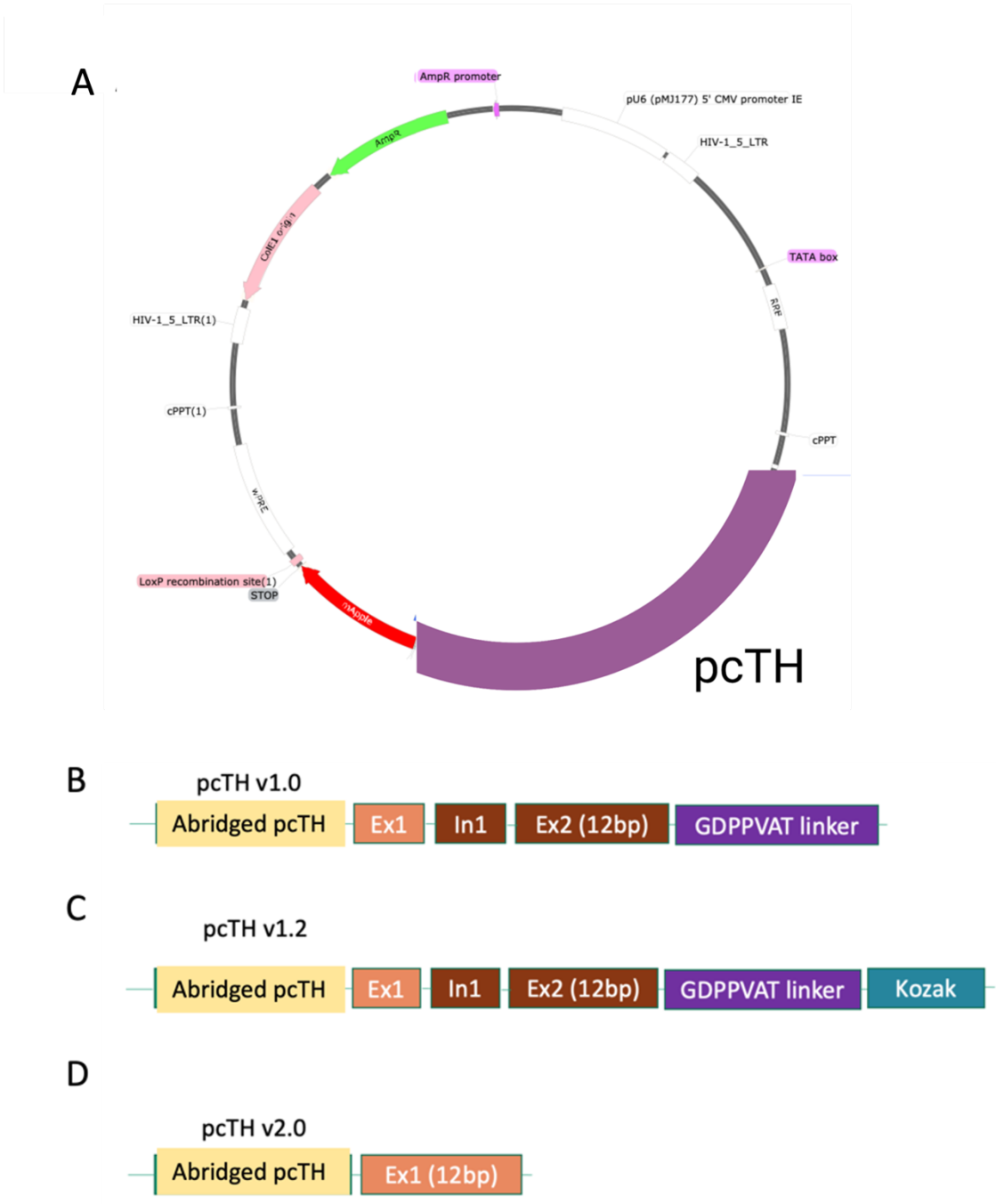

Figure 6.3: Generation of custom human TH promoter (pcTH) reporter. A) Schematics representing the final lentiviruses containing the pcTH of interest driving expression of the fluorescent protein mApple. B-D) Schematics of the three versions of pcTH to be investigated.

pcTH constructs driving expression of mApple were packaged into lentiviral vectors (Figure 6.1A) which in turn were used to transduce post-mitotic iPSC-DaN and iPSC-MSN. iPSC-DaN exhibited abundant expression of TH-expressing cells (Figure 6.3A) and hence a non-TH specific but functional promoter could still stochastically drive expression of the fluorescent reporter. Hence, transduction of the iPSC-MSN, which contained a smaller proportion of TH-positive cells (Figure 6.3B), with the same viral titre could provide another positive but titrated control to determine the specificity of the custom promoter. Live cultures were examined under the Evos ™ fluorescent microscope to examine mApple expression 7 days post-transduction. Following that, culture was immunostained so as to validate mApple expression with that of TH. Interestingly, DaN culture displayed abundant mApple expression with many of mApple-positive cells were also TH-expressing while a few of mApple-positive cells were false positive. Similar trend was observed in iPSC-MSN culture containing a small population of TH-expressing neurons, potentially of striatal interneuron identity (discussed in Chapter 3), suggesting the selective driver effect of this custom promoter. This result was from a qualitative pilot transduction experiment; robust quantification was not performed due to the mix match between live imaging of mApple and immunostained imaging of TH expression. Much to my dismay, neither LV-pcTH-mApple v1.0 nor v1.2-mApple displayed any expression in either iPSC-cortical neurons, -DaN or -MSN. Considering the differential mApple expression between LV-pvTH-mApple v1.0/1.2 and v2.0 in light of the differences in their promoter constructs, it is likely that the lack of mApple signal was due to failure of translation and/or proper protein folding.

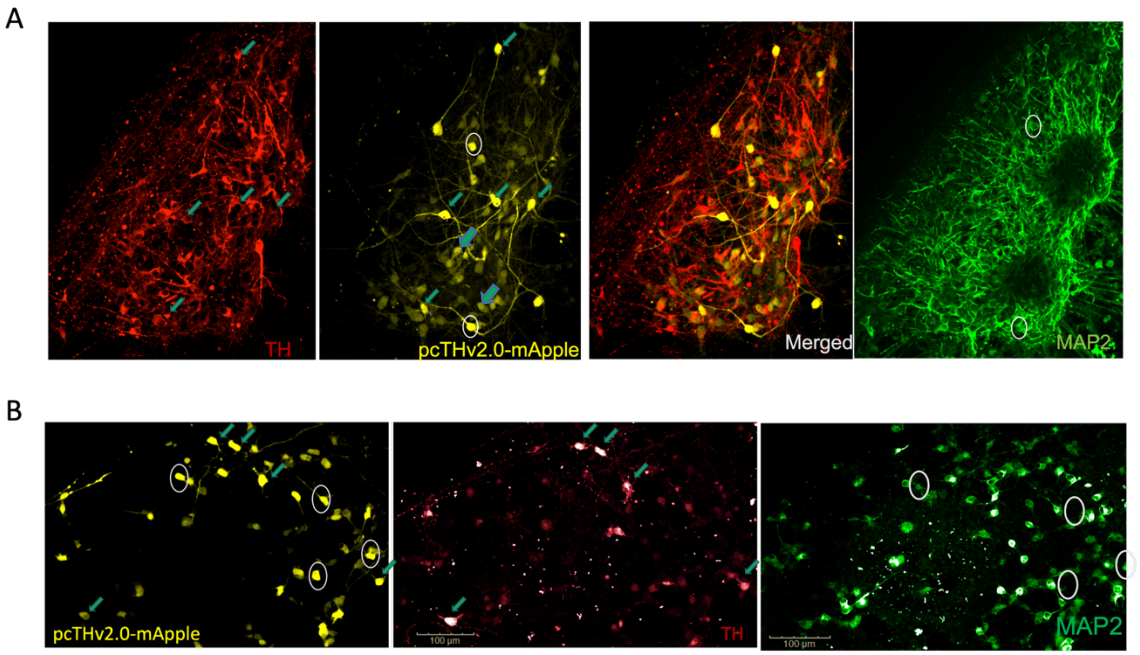

Figure 6.4: Characterisation of mApple expression driven by pcTH v2.0 in transduced iPSC-neurons 7 days post-transduction in A) iPSC-DaN and B) iPSC-MSN. Green arrow = TH, MAP2 and mApple co-expressing cells i.e. positive neurons. White circle = MAP2 and mApple-positive but TH-negative cells i.e. false positive. Scale bar =100 μm.

6.3. Discussion

I reported here the feasibility to design and generate a custom human TH promoter that is small enough to be packaged into a lentiviral system while retaining its effective functionality, permitting quick labelling of iPSC-DaN for various experimental designs and in complex culture systems. However, this effort is still very preliminary considering the observation of many unlabelled TH-expressing cells using my best working version pcTH v2.0. Elements and contigs that were reported to be essential for selective TH expression in full length human *TH* genes such as the S/MAR region have been identified in previous works and annotated in my *in silico* design but yet be successfully included to effectively drive reporter gene expression. The immediate step would entail successful incorporation of these contigs into pcTH v2.0 so as to

further enhance the promoter specificity. For instance, the 3' untranslated region of multiple genes, including *TH* gene, has been suggested to include enhancer element regulating tissue-specific gene expression (Beck *et al.*, 1991). Previous works showed that particularly in the human *TH* gene the sequence of 760 bp immediately downstream of the last 14th exon exhibited transactivating properties to drive reporter gene expression when used either alone or synergistically with the 5' kb sequence immediately prior of the TSS (Gandelman *et al.*, 1990; Wong *et al.*, 1995; Gardaneh *et al.*, 2000). pcTH v2.0-mApple DNA insert is slightly under 2 kb long; and considering the theoretical packaging limit of this lentiviral system at approximately 4 kb (i.e the difference between the 9 kb being maximal recommended length of 5' to 3' LTR and the 5-3-LTR length of this lentivirus), this suggested an ample space available to augment the current pcTH v2.0 with more useful binding motifs without compromising on packaging efficiency.

An optimised human TH promotor-specific reporter could offer significant improvements to many current experimental regimes and permit application of new experimental strategies using DaN cultures *in vitro* by directly labelling TH-expressing DaNs with either a fluorescent protein or an actuator/sensor protein of interest. For example, given the inherent neuronal heterogeneity within most iPSC-derived monocultures such as that of DaNs, a human TH promoter-specific reporter could greatly facilitate the fine-tuning of high-throughput biological assays and the subsequent analyses, such as cellular/organelle calcium fluctuations or optogenetic stimulation to name a few, which were otherwise likely confounded by non-DaN-specific responses. Such reporter could also be of great help to accurately identify DaNs in real-time for low throughput experiments such as patch-clamping of hMLO sections.

Chapter 7: Advanced modelling neuronal microcircuit with fluid-walled microfluidic (FWM) platform

7.1. Introduction

7.1.1. Axon pathology and its relevance to PD

Based on the observation of dopamine deficiency more than 60 years ago (EHRINGER and HORNYKIEWICZ, 1960), Oleh Hornykiewicz was first to propose the cellular aetiology of PD as a dying-back degeneration. Early works in toxin-induced models of PD using MPTP reported substantially greater diminishing of striatal dopaminergic terminal field preceding that of nigral cell bodies in both non-human primates (Herkenham *et al.*, 1991; Meissner *et al.*, 2003) and mouse (Serra *et al.*, 2002) . The development of familial models of PD has facilitated the study of early pathogenic events in the disease course. In fact, increasing understanding of various PD-relevant genetic risks many of which produced synaptically localised proteins such as LRRR2 and α-synuclein fuelled further interest in axonal pathology in PD. For example, immunohistochemical staining of post-mortem brain tissues of patients suffering from dementia with Lewy bodies (DBL) revealed greater abundance of small α-syn aggregates (and only a few Lewy bodies) in pre-synaptic axonal terminals than in cell bodies (Kramer and Schulz-Schaeffer, 2007). This was coincided with the substantial loss of post-synaptic dendritic spines, rendering it a plausible explanation of cognitive impairment observed in DBL. In mouse transgenic model expressing truncated α-syn (α-synuclein (1–120)), or carrying *LRRK2-G2019S* or *LRRK2-L1444G* axonal pathology was observed early and associated with motor deficits despite the absence of cell loss at the same age (Tofaris *et al.*, 2006; Li *et al.*, 2009; Parisiadou *et al.*, 2009). Interestingly, mechanisms governing axonal pathology could be distinct from that

of neuronal cell loss (Raff, Whitmore and Finn, 2002), implying axonal pathology as a separate pathogenic process of PD rather than a repercussion of dying cell soma.

The two classical examples of axonal degeneration are Wallerian degeneration and dying back (or Wallerian-like) degeneration. The former is injury-induced (Conforti, Gilley and Coleman, 2014) while the latter is associated with neurodegenerative conditions (Salvadores *et al.*, 2017) such as ALS (Moloney, de Winter and Verhaagen, 2014), SMA (Rahmanzadeh *et al.*, 2021), AD (Adalbert and Coleman, 2013), and PD (Volpicelli-Daley *et al.*, 2011) although recent data also implied the involvement of Wallerian degeneration in neurodegeneration (Coleman and Höke, 2020; Krauss *et al.*, 2020). Previous mechanistic studies proposed converging pathways between the two forms of degeneration (Raff, Whitmore and Finn, 2002; Conforti, Gilley and Coleman, 2014; Yaron and Schuldiner, 2016), suggesting that understanding of either can inform the knowledge of the other. In the central nervous system, axon regeneration from both forms of degeneration is possible but limited due to concurrent effects of inhibitory surrounding environment (Huebner and Strittmatter, 2009; Fawcett, 2020) and intrinsic regenerative capacity (Mahar and Cavalli, 2018). Hence, one of the outstanding physiological questions is that how target-derived factors influence axon sprouting and regeneration post-axotomy. Regeneration of the injured CN, unlike that of the injured PNS, is much more challenging and once deemed an unattainable goal. Considering the limited regenerative capacity intrinsic to CN neurons, it follows that a permissive extrinsic signals, be it physiological post-synaptically target-derived or externally introduced, could be deterministic to rescue reinnervation and consequently, functional regeneration. Hence, understanding of external environment that is permissive to axon regeneration can greatly improve their reconnections towards their relevant targets.

7.1.2. Axon injury and regeneration models on microfluidic platform *in vitro*

Attempts to model and study axonal injury and their regeneration have been revolutionised by compartmentalised microfluidic chambers that allow segregation of cell bodies and their axons (Neto *et al.*, 2016; Bengoa-Vergniory *et al.*, 2020). Previous studies using this model enabled axon-specific injury as well as subsequent assessment of ensuing regeneration so as to reveal important intrinsic pathways of regeneration (Taylor *et al.*, 2005; Hur *et al.*, 2011; Klim *et al.*, 2019; Melamed *et al.*, 2019; Hofmann *et al.*, 2022). Additionally, compartmentalised coculture platform is amenable to testing of factors acting specifically on distal axons (Taylor *et al.*, 2005; Bengoa-Vergniory *et al.*, 2020) so as to explore potential extrinsic regulators affecting axon sprouting and regeneration.

Axotomy *in vitro* is traditionally performed with sharp objects or chemicals dearth of reproducibility. Such brute-force technique is also often destructive to the coating substrate, thereby limiting and confounding axon regeneration . The improved microfluidic design in recent years allows for more high throughput mechanical axotomy via vacuum aspiration (Tong *et al.*, 2015; Klim *et al.*, 2019; Melamed *et al.*, 2019). However, axotomy in all of these different PDMS-based microfluidic platform, due to the apparent physical obstruction above the axonal microchannels associated with these devices, is limited within the distal axons in the distal chambers and offers little to no flexibility on mimicking endogenous neuronal circuits. Moreover, the plastic wall is impermissible to other physical manipulations such as electrophysiological experiment, for instance, to assess functional regeneration, rendering the attempts at investigating axon reinnervation incomplete.

7.1.3. Fluid-walled microfluidic technology

First reported in 2017, microfluidics with fluid walls was touted as an attractive addition to the panel of conventional plastic-walled counterparts given its immense ease of fabrication and customisability (Walsh *et al.*, 2017). This approach leverages on fluid immiscibility between cell medium and hydrophilic bio-compatible fluorocarbon (FC40). These fluid walls are interfaces between immiscible liquids, made by mechanical pinning of FC40 onto flat un-patterned substrate, and proven compatible for cell culture (Soitu *et al.*, 2019). This approach offers a quick and viable solution to reconstruct neuronal circuits with accessibility to all circuit compartments. In addition, subsequent studies from the same lab reported optimised methodologies to re-pattern existing circuit (Soitu *et al.*, 2019) and to automatically create highly reproducible injury (Soitu *et al.*, 2021). Taken together, fluid-walled microfluidics (FWM) seems an attractive platform to recapitulate neuronal circuit, model axon injury and assess ensuing events *in vitro.*

7.1.4. Aims

In this chapter working in collaboration with Federico Nebuloni, an engineering DPhil candidate from Walsh and Cook lab from the University of Oxford, I aimed to:

- Establish iPSC-derived corticostriatal pathway on fluid-walled microfluidics (FWM).
- Optimise a high throughout and reproducible mechanical axotomy using microjet for neuronal circuit cultured on FWM.
- Investigate the role of diffusible target-derived factors on i) axon outgrowth, and ii) axon regeneration of the human iPSC-cortical neurons on the FWM platform.

7.2. Results

7.2.1. Fabrication and principles of fluid-walled dumbbell-shaped microfluidic

In collaboration with Walsh Lab at the University of Oxford leveraging on their previously published novel freestyle microfluidic technology (Walsh *et al.*, 2017; Soitu *et al.*, 2018), we designed and fabricated fluid-walled (FW) dumbbells within which iPSC-derived neurons were to be cultured in an open-access manner (Figure 7.1A and B). Using an in-house printer which operated much like drawing on a piece of paper with a hydrophobic and fluorophilic stylus, we patterned a circuit-relevant design of dumbbells. Each dumbbell was a pair of two 3*3 mm squares connected by a thin conduit of 0.2*1 mm (Width*Length); a 3*7 array of dumbbells was printed on a single 6 cm petri dish (Figure 7.1B). This platform was compatible for long-term culturing of iPSC-derived neurons and hence was applied to reconstruct the corticostriatal network *in vitro*.

Current PDMS-based neural microcircuit models involves plastic barriers shielding parts or whole of the neuronal circuit, rendering these areas inaccessible to wider experimental interests such as imaging or direct physical manipulation such as axonal tract damage, or complex patch-clamping (Figure 7.1C). The fluid-walled microcircuit offered multiple unique advantages that were unconceivable with standard plastic-walled microcircuit. Specifically, it provided unrestricted access to all compartments, axonal and cell bodies alike (figure 7.1Cii). Furthermore, the microfluidic arrangement was reconfigurable on demand during

experimental assays: fluid walls could be built, destroyed and rebuilt (Soitu *et al.*, 2019) (Figure 7.1Cii).

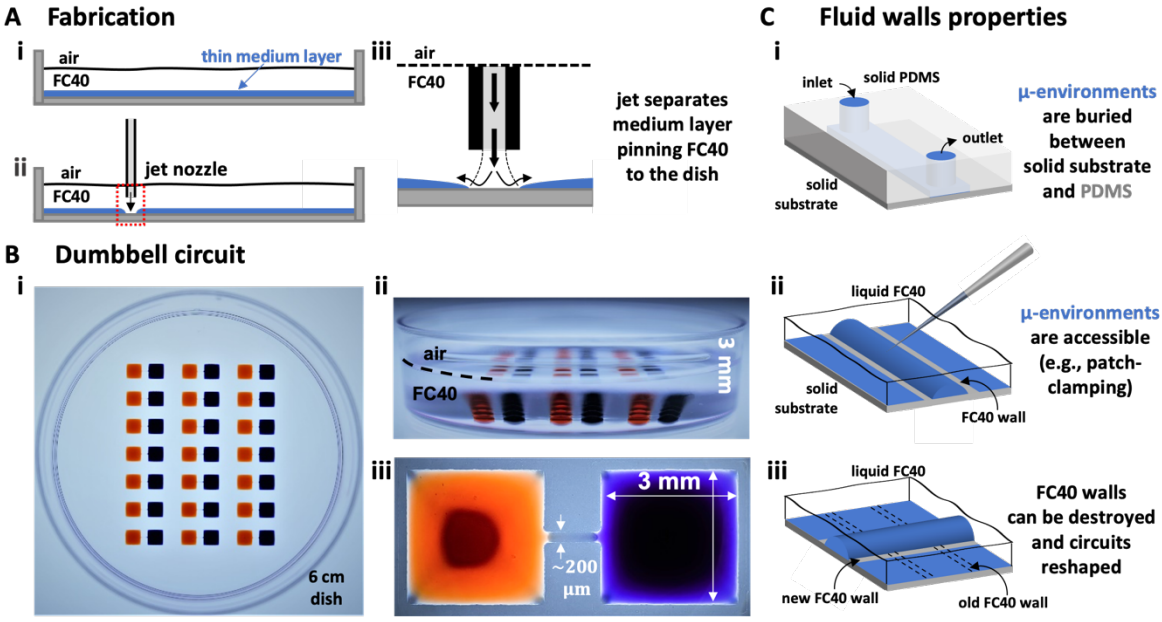

Figure 7.1: Generation of fluid-walled microfluidic-based circuit. A) Principles and making of fluid-walled microfluidics. i) immiscible aqueous cell medium was overlayed with inert hydrophobic fluorocarbon (FC40). ii) Making of fluid wall was performed by jetting a Teflon-coated nozzle which concurrently iii) replaced aqueous medium and pinned FC40 . B) Design of fluid-walled dumbbell-shaped circuits for cell culturing on petri dish with i) front view, ii) side view and iii) zoomed-in view on individual dumbbells. C) Unique advantages of fluid-walled circuit over i) PDMS-based cell circuit being ii) easy accessibility to all segments of the circuit and ii) on-demand reconfigurability.

7.2.2. Recapitulation of the human corticostriatal pathway on fluid-walled dumbbells.

CN were seeded into empty cortical chamber in small volume suspension in the presence of high-volume pressure exerted from the opposite chambers (i.e. striatal chamber) (Figure 7.2A). This initial positive pressure toward cell chambers was essential to attain unidirectional fluid flow (Figure 7.2B). In doing so, we restricted cell movements into the conduits, allowing compartmentalisation of cell bodies of GFP-expressing cortical neuron cell bodies within the cortical chambers and extension of neurites across the conduit (Figure 7.2C). The continuous

fluid flow across the thin conduit would eventually re-establish the volume equilibrium between the two chambers, consequently permitting bidirectional fluid exchange as well as undeterred neurite projection across the conduits (Figure 7.2C). Immunostaining of cortical chamber (i.e. DIV 60 iPSC-CN) confirmed the presence of only MAP2-positive post-mitotic cortical neurons negative for DARPP32 but expressing GFP under the influence of NGN2 promoter (Figure 7.2Di). Immunostaining of the striatal chamber (i.e. DIV 40 iPSC-MSN) revealed similar confinement of cell bodies of MAP2-positive post-mitotic MSN expressing their canonical marker DARPP32 but not GFP (Figure 7.2Ei). Interestingly, immunostaining of neurites traversing across the conduits suggested that only SMI 312-positive axons, and not MAP2-positive dendrites projected from the cortical chamber across the conduits to the striatal chambers. Collectively, we were able to recreate the corticostriatal pathway mimicking the endogenous connectivity.

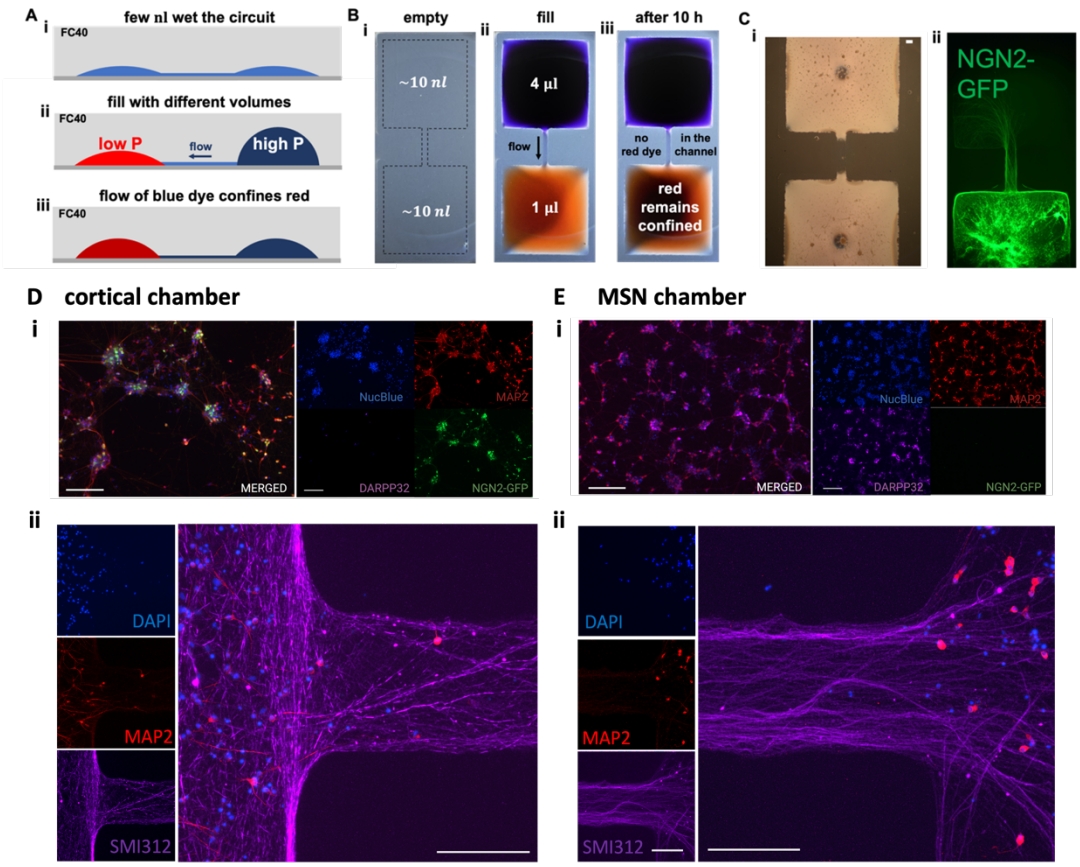

Figure 7.2: Recapitulation of the human cortiostriatal pathway on fluid-walled microfluidics. A -B) Principles of fluid isolation in fluid-walled circuits demonstrated in A) schematics and B) representative dye isolation experiment over time. C) Representative images of iPSC-derived GFP-expressing cortical neurons on fluid-walled dumbbells in i) bright field and ii) fluorescence microscope. D-E) Representative immunostaining images confirming compartmentalisation of different neuronal populations (Di and Ei) and neurites (Dii and Eii) in D) cortical chamber and E) striatal chamber. Separation of postmitotic cortical neurons Di) NGN2-GFP (green)/MAP2+ (red)/DAPI-positive and DARPP32 (purple)-negative in the cortical chamber from postmitotic MSN Ei) DARPP32 (purple)/MAP2+ (red)/DAPI-positive and NGN2-GFP(green)-negative. Immunostaining of neurites projecting out from the Dii) cortical chamber into the conduit into the Eii) striatal chamber suggested neurite isolation of axon (SMI-312-positive, purple) and dendrites (MAP2-positive, red) within the conduits and cell chambers, respectively. Scale bar 150 µm.

7.2.3. Independency of cortical axon outgrowth on target-derived signals.

In addition to offering easy accessibility to all culture compartments and reconfigurability of the circuit, FWM also permits long-term live microscopic monitoring without optical distortion given the similar refractive index between FC40 and that of water (1.29 versus 1.33).

Moreover, the instrumentation is capable of generating cellular damage in a custom, precise and high throughput fashion (Soitu *et al.*, 2021). Taken together, FW microcircuit represents an attractive platform for the investigation of axon physiology *in vitro* and axotomy modelling.

During development, following migration along the radial glia to their final location postmitotic CN extend axons toward their appropriate synaptic partners. Such pathfinding of axon growth cones is orchestrated by a plethora of molecular cues both intrinsically (Yu and Bargmann, 2001) and target-derived (Davis, 2000). While understanding of the intrinsic factors in axonal physiology has been supported by dissociated culture of neurons *in vitro* (Klim *et al.*, 2019; Melamed *et al.*, 2019), the specific role of target-derived signals remains elusive due to the dearth of useful human models encompassing the complex microenvironment surrounding these neurons. We cultured iPSC-derived GFP-expressing CN in cortical chambers of FWM dumbbells (Figure 7.3A) and exposed them to different target 'sources' in the striatal chamber, be it standard cortical maturation medium (i.e. CN-CN condition) or cortical maturation medium supplemented with 10-fold concentration of BDNF (100 ng/ml) (i.e. CN-BDNF condition) or MSN (i.e. CN-MSN condition) (Figure 7.3Bi). Axon outgrowth was quantified as the difference in area covered by GFP-expressing neurites within the conduits between DIV 0 (i.e. Area(t_{D0})) and DIV 20 (i.e. Area(t_{D20})), ΔArea(t_{D20-0}). Axon outgrowth index was calculated by dividing ΔArea(t_{D20-0}) by Area(t_{D0}) so as to normalise for confounding difference in cell numbers between dumbbells. We presented the differential cortical axon outgrowth among different culture conditions as fold difference against axon outgrowth index of the control CN-CN Medium condition to account for variability between batches of iPSC differentiation. Interestingly, we found that neither increased BDNF nor MSN induced statistically significant outgrowth of cortical axons ($p>0.05$, one-way ANOVA with Bonferroni correction test for multiple comparison), implying that cortical axon outgrowth was independent of exogenously supplied BDNF and target-derived molecules (figure 7.3Bii and C).

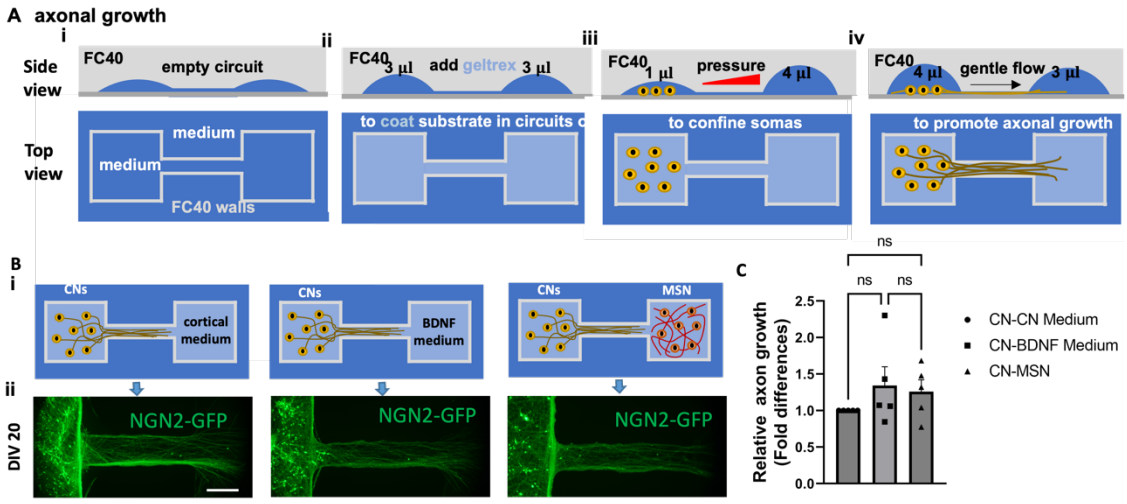

Figure 7.3: Cortical axon outgrowth is independent of target-derived signals. A) Schematics of neuronal culturing on fluid-walled dumbbells starting from i) jetting the circuit, ii) coating the culture dish, iii) cell plating and iv) long term culturing. B) i) Schematics of different culturing conditions of cortical neurons and ii) representative corresponding fluorescent images of their axon expressing NGN2-GFP at DIV 20. C) Quantification of relative axon outgrowth across different culture conditions. Each dot represents a healthy control-derived iPS cell line from one differentiation. N = 2 iPS cell lines, n = 2-3 differentiations per line. One-way ANOVA with Bonferroni correction test. ns $p > 0.05$. Scale bar = 200 µm.

7.2.4. The effect of target-derived signals on regeneration of axotomized cortical axons.

Likewise, regeneration of post axonal tract damage is thought to involve both cell autonomous and target-derived signallings (Mahar and Cavalli, 2018; Fawcett, 2020). Employing our FWM-based circuit platform, we investigated and compared the physiological impact of exogenously supplied neurotrophic factor such as BDNF and cortical endogenous post-synaptic target, MSN from the striatum, post axonal trauma. Directed axotomy was performed at pre-defined coordinates along the conduit at DIV 20 using the in-house fluid printer as described earlier (Figure 7.4Ai-Aii and Bi-Bii), following which a new circuit was printed. The newly printed dumbbells had bigger chambers and wider conduits than the original dumbbells so as to avoid physical damage to cells residing close the previous borders (Figure 7.4Aiii and Bii). Axon

regeneration from the point of axotomy within the conduits was monitored and recorded at 36, 60 and 84 hours post-axotomy (Figure 7.4Aiv and Biii).

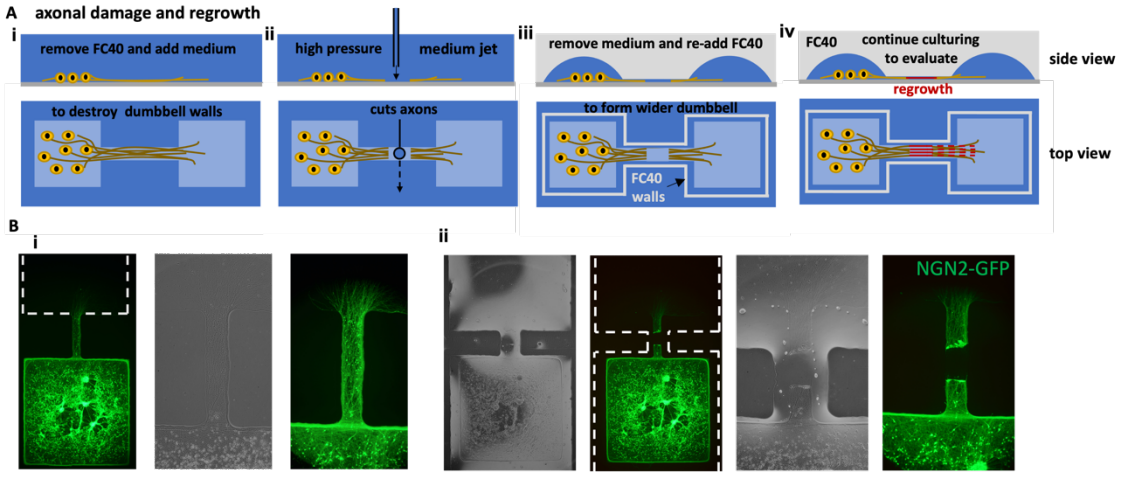

Figure 7.4: Directed axotomy and regeneration of human cortical neurons. A) Schematics of DIV 20 culture just prior to axon damage followed by ii) directed axon severing, iii) re-jetting of the dumbbell circuits and iv) monitoring of axon regeneration. B) Representative fluorescent and bright-field images of cortical axon tracts expressing NGN2-GFP i) prior to axon cut and ii) after axon cut.

Axon regeneration was quantified as the difference in area covered by GFP-expressing neurites within the conduits at DIV 20 right after axotomy (i.e. Area(t_{D20})) and 36, 60, 84 and 100 hours after axotomy. Axon regeneration was normalised against Area(t_{D20}) so as to account for differential level of axon damage. We found that regeneration of cortical axon generated from two different iPS cell lines was enhanced by both BDNF and MSN (Figure 7.5). Such increased axon regeneration was observed as early as 36 hours post axonal cut and remained significantly greater 100 hours post-axotomy (SFC156-03: CN-CN medium versus CN-BDNF medium, $p > 0.05$ at 36 and 60 hours, $p < 0.01$ at 84 hours; CN-CN medium versus CN-MSN, $p < 0.0001$ at 36 hours, $p < 0.001$ at 60 and 84 hours; SFC856-03: CN-CN medium versus CN-BDNF medium, $p < 0.001$ at 36 hours, $p < 0.05$ at 60 and 84 hours; CN-CN medium versus CN-MSN, $p < 0.01$ at 36 and 84 hours, $p < 0.05$ at 60 hours; two-way ANOVA with Bonferroni correction

test). The rate of axon regeneration, however, was similar regardless of the target sources (for both lines, $p > 0.05$, two-way ANOVA with Bonferroni correction test). Interestingly, axon regeneration in the presence of BDNF or MSN remained on an upward trajectory from our last recorded timepoints, suggesting a potential continued regeneration (For all conditions in both line except SFC856-03 CN-CN Medium: $p < 0.05$ between different timepoints, two-way ANOVA with Bonferroni correction test). On the other hand, SFC856-03 axons did not regenerate significantly more from 36 hours post-axotomy ($p > 0.05$ between different timepoints two-way ANOVA with Bonferroni correction test) (Figure 7.5C). These results suggested that environmental cues such as relevant post-synaptic target and neurotrophic factor BDNF promoted axonal regeneration after severing.

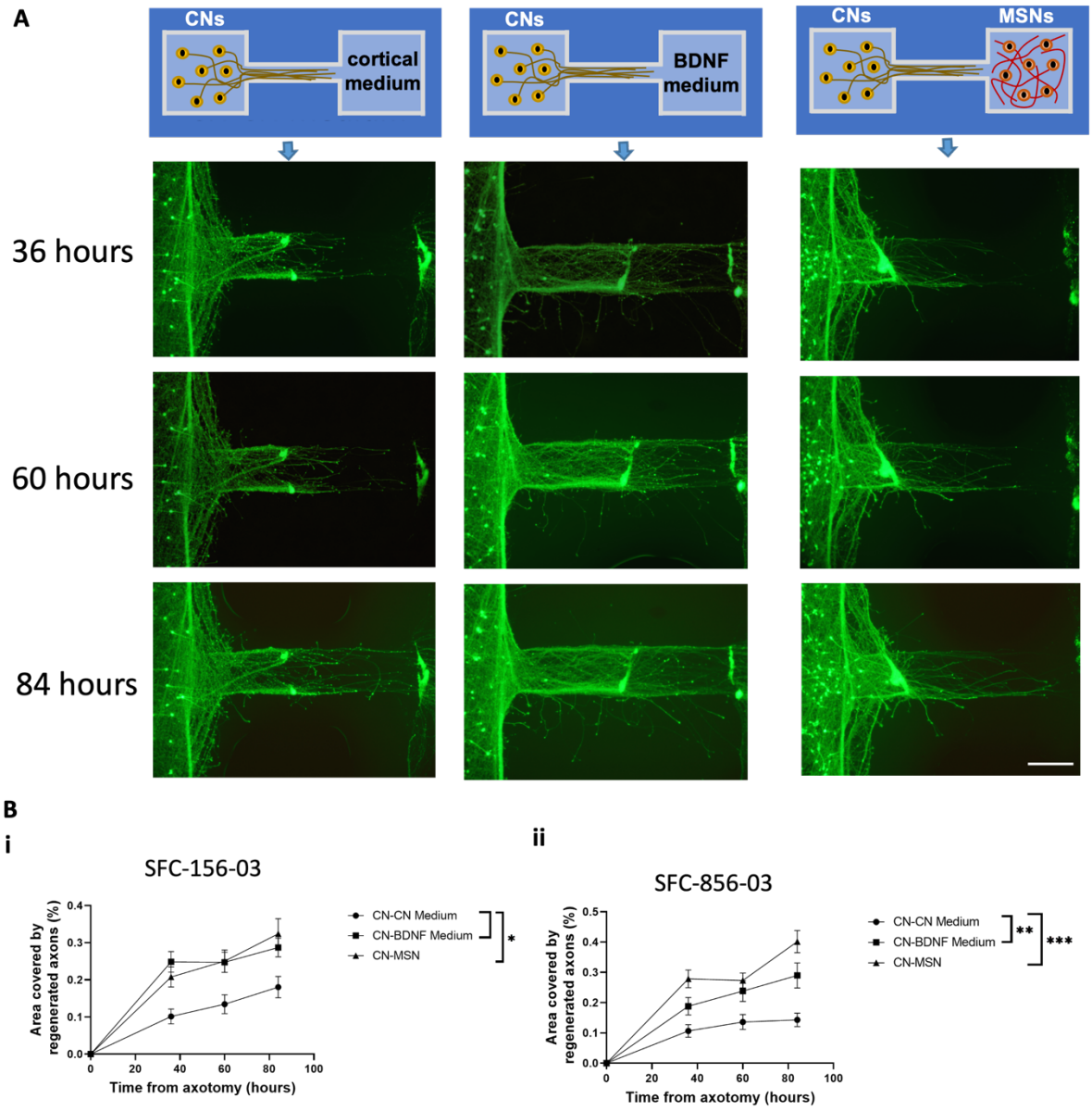

Figure 7.5: Dependency of axon regeneration on target-derived signals post axotomy. A) Representative fluorescent images of axon regeneration in different culture conditions over time. B) Quantification of axon regeneration as percentage of total axonal area in the conduit prior to axon damage in 2 healthy controls-derived iPS cell lines, i) SFC-156-003 and ii) SFC-856-03. N =2-3 differentiations per iPSC line, * p <0.05, ** p < 0.01, *** p < 0.001, two-way ANOVA with Bonferroni correction test. Scale bar = 200 μm.

7.3. Discussion

Leveraging on the advanced fluid-walled microfluidic technology, I was able to recreate the human corticostriatal pathway *in vitro* which was amenable to physical interventions. Directed axotomy followed by assessment of subsequent axon regeneration revealed a target-

dependent regeneration of the human corticostriatal axons, demonstrating the importance of modeling axotomy in a circuit-based manner and of creating permissive external environment for axon regeneration.

7.3.1. Fluid-walled circuit for neuronal circuit modelling

FWM represents an attractive alternative platform from the traditional PDMS-based to recapitulate neuronal circuits in a highly physiological manner. FWM offers unique strength unattainable by the PDMS-based microfluidics: i) unrestricted accessibility to all circuit compartments and ii) on-demand configurability and reconfigurability. The former is desirable to be coupled with physical manipulations such as patch-clamping. Electrophysiological experiments of MSN cultured in microcircuit in chapter 3 and 4 were performed following manual removal of microfluidic devices from the coverslips where cells were attached. Successful detachment of microfluidic devices with minimal shear stress due to high risk of peeling of cells and/or severing of axonal arrays was challenging. Hence, manual experience was desirable and even so, success was not always certain with two-chamber devices. Unsurprisingly, this problem became increasingly pronounced as the circuit became increasingly complex with more connecting chambers. As the results, recording of highly dynamic events such as post-synaptic currents, long-term potentiation/depression was not feasible in microcircuit with three or more connecting chambers in which preservation of all connecting neuronal populations and their axonal tracts was unlikely following attempts at uncoupling the devices and cell coverslips. Other than patch-clamping, high resolution live imaging of various circuit compartments could also be facilitated in the absence of physical barriers hindering up-close access of optical objectives to the culture. Moreover, the configurable nature of the FWM platform permitted custom design and jetting of circuits of interest with ease within minutes, offering great potential to recreate any circuits *in vitro* of

variable patterns mimicking the diverse connectivity *in vivo*. Interestingly, these fluid walls could be easily demolished and reconstructed into completely different patterns. It worths noting, however, that some level of C++ language and familiarisation with the operating software are required to customize design algorithm at one's own wish.

Another significant highlight of FWM was its high throughput that was enabled by streamlined and automatic workflows so as to attain reproducible and consistent results. The low reagent consumption and cell requirement were other attractive advantages of the FWM approach for the application of large-scale cell culturing in screening of potential drug candidates, for instance.

7.3.2. Automatic axotomy assay using micro-jet on FWM

We described an automatic method to sever human cortical axon tracts in monolayer culture in a systemic and high throughput fashion. This assay enhanced reproducibility and consistency of axon cut across cultures and experimental batches relative to alternative axotomy model such as neurite scratch. It worths noting, however, that the cut parameters, including nozzle speed, cut speed, cut power, and number of cut repeat, required fine-tuning to specific cell cultures. The cut dimensions used in this work were optimized for human cortical axons at DIV 55 and cultured in the dumbbell circuit for 20 days at the seeding density of 13,000 cells/chamber. The thickness of axonal tract, which in turn was a function of cell density, DIV, and axon outgrowth rate, could result in variability in the quality of micro-jet cut. Without careful calibration and optimization, this could be a potential confounding factor in achieving similar axon damages across culture conditions which produced variable axon outgrowth. We excluded in our analysis axon tracts that were incompletely severed so as to avoid potential differences in axonal damage.

7.3.3. Target-dependent axonal physiology in health and PD

Contrary to many previous works, high BDNF seems to offer no relative enhancement to axon outgrowth in our model. This could be attributed to the different neuronal subtypes and species. As far as we are aware, this is the first report on the influence of external diffusible factors on human cortical axon outgrowth *in vitro*. While BDNF signalling pathway, as well as majority of intrinsic pathways regulating axon sprouting, is conserved across species, some others are mammalian or human-specific (Mahar and Cavalli, 2018). Collectively, these human-specific features can differentially modulate BDNF effect on human cortical axons, necessitating the need for human axon model. Discrepancy in BDNF impact could also be explained due to the experimental choice of BDNF concentration. Ji et. al. suggested that maximal phosphorylation-dependent activation of TrkB, the major receptor of BDNF expressed on cortical neurons, was achieved within 5 mins by 25 ng/ml BDNF in primary rat hippocampal neuron (Ji *et al.*, 2005, 2010). This implied that it is possible that we had introduced almost maximally useful BDNF concentration in the standard human cortical maturation medium (10 ng/ml); extra BDNF did not confer significant marginal benefit on axon outgrowth as illustrated by our results. It worths noting that 10-20 ng/ml BDNF is commonly used in neuronal media of various subtypes, likely also based on its maximally acting concentration.

Diffusible factors such as netrin-1 releasable from the LGE were shown to have strong instructive effects on the outgrowth of corticofugal axons (Métin *et al.*, 1997; Taylor, Menon and Gupton, 2015). However, our results suggested lack of iPSC-MSN-derived impact on iPSC-cortical neurons. Possible explanation would be mix-match between neuron developmental stages. Findings reported in both Metin et. al., and Taylor et. al., were observed in embryonic cortical neurons and embryonic LGE, the progenitors of MSN. It remains a challenge to

accurately align specifically days *in vitro* with development stages *in vivo*. iPSC-cortical neurons used in our assay were postmitotic. As the result, it is possible that the role of target-derived releasable factors on axon outgrowth of iPSC-cortical neurons was significantly diminished at post-mitotic stage.

Supplementation of exogenous neurotrophic factors has been hailed as a potential therapeutic strategy to enhance nerve regeneration. BDNF, in particular, has shown promising effect on restoring neuronal connectivity in PNS (Kobayashi *et al.*, 1997; Brock *et al.*, 2010; Li *et al.*, 2020), potentially via directing upregulation of outgrowth-associated genes and pathways (Cai *et al.*, 1999; Lu *et al.*, 2012). The heightened demand of BDNF following axon injury might explain the emergence of BDNF-dependent positive effect on axon regeneration despite its neutral effect on axon outgrowth in our model. Interestingly, BDNF exerted its regenerative power independent of its ontological sources, be it endogenous from upregulation of neuronal BDNF or secreted by non-neuronal sources such as Schwann cells (Song *et al.*, 2008; Wilhelm *et al.*, 2012). One limitation of our current model is that it is difficult to identify the exact cellular location of BDNF biology: whether BDNF bound directly to TrkB receptors at the proximal cut ends or it diffused into the cortical chamber and exerted it effect there on cell bodies or a combination of both.

BDNF was found to be upregulated following peripheral nerve injury (Funakoshi *et al.*, 1993; Grosheva *et al.*, 2016). Independent studies in the PNS also showed dose-dependent improvement of axon regeneration with exogenously applied BDNF, either by autocrine or paracrine source (Boyd and Gordon, 2003). In our setup, although BDNF was supplied in 10-fold concentration of what was otherwise used in cortical maturation medium (i.e. 100 ng/ml) directly in the distal chamber, the constant fluid exchange within the dumbbell would eventual equilibrate across both chambers. As the result, the high extracellular BDNF probably exerted

acute autocrine effect on axonal distal terminals but also gradual paracrine effect on cortical cell bodies as BDNF dissipated down the concentration gradient towards the cortical chambers. This mimicked the postsynaptic neuron activity-dependent secretion of BDNF (Tao *et al.*, 2002) to instruct presynaptic axon physiology. Interestingly, our coculture of CN with their relevant postsynaptic target MSN also promoted axon regeneration post-axotomy, an effect comparable to that induced by exogenous BDNF. This observation suggested that distant postsynaptic target could have released some pro-regeneration factors that dynamically acted on retrograde axons to facilitate reinnervation. Future experiment investigating culture media could shed light on the potential releasable factors beneficial to axon regeneration secreted from non-autologous targets. Furthermore, my results also demonstrated the importance of modelling axotomy and subsequent axon regeneration investigation in a neuronal pathway/microcircuit manner. Marginal benefit of therapeutic candidate can only be accurately assessed in the absence of confounding influence by endogenous neuronal target.

Chapter 8: Discussion

This thesis aims to develop and establish advanced approaches for culturing iPSC-neurons in a highly physiological manner namely i) two-dimensional neuronal circuit on PDMS-based open-chambered microfluidic, ii) three-dimensional human midbrain-like organoid and iii) two-dimensional neuronal circuit on fluid-walled microfluidics. In doing so, I investigated various physiological phenomenon as well as PD-relevant cellular pathology that has been challenging to obtain otherwise. In this chapter, I will briefly summarise the culture models of interest and key emerging biological findings enabled by these different strategies. I will discuss the strengths and limitations of each approach and suggest how this panel of different culturing strategies can complement each other to broaden the scope of available experimental assays in understanding PD pathogenesis. I will also elaborate on the significance of the observed striatal pathology in PD and its implications.

8.1. Advanced iPSC-derived cultures *in vitro*

8.1.1. Neuronal circuits on open-chambered microfluidics

The use of open-chambered microfluidics permits modelling of neurons with their endogenous connectivity which is critical for neuronal maturation and novel disease mechanism manifestation. In Chapter 3, I showed proof-of-principle the feasibility of establishing a neuronal microcircuit, specifically the striatal presynaptic microcircuit consisting of iPSC-DaN, iPSC-CN and iPSC-MSN. The converging cortical and dopaminergic projections onto iPSC-MSN mimic the concurrent inputs received onto MSN *in vivo* and facilitated the enhancement of electrophysiological properties of iPSC-MSN in the microcircuit setup as compared to iPSC-MSN in monoculture. It worths noting that this circuit-driven maturation of MSN even surpassed the benefits of long-term culturing in monoculture, corroborating the importance of

modelling neurons *in vitro* in a physiological fashion with their non-autologous connections. This is particularly pertinent for network-dependent phenotypes such as electrophysiological properties, synaptic profile or neurotransmitter release, to name a few.

One highlight of this platform is the modularity of the microfluidic devices. Virtually any neuronal circuit could be reconstructed *in vitro* leveraging this conceptual approach. Different players of the circuit can be incrementally introduced into the system and examined in a pairwise manner so as to delineate their specific role. In doing so, my results, for the first time as far as I am aware, provided direct experimental proof toward the physiological contribution of human cortical and dopaminergic inputs onto MSN synaptic and intrinsic maturation, respectively. Compartmentalised modules also permit compartment-specific treatments that are necessary to inform specific population-driven observations. However, this advantage comes at the cost of chamber accessibility, particularly to the axonal microgrooves, due to the presence of a physical plastic wall obstructing close approach toward neurons attaching on the coverslip bottoms. As the results, it remains challenging to couple within this platform high resolution imaging or duo electrophysiological patch-clamping experiments.

8.1.2. Human midbrain-like organoid (hMLO).

In Chapter 5, I set out to establish an optimised protocol to generate iPSC-derived hMLO from which PD pathogenesis centered on DaN could be investigated. Modified from existing literature (Jo *et al.*, 2016), I reported an optimised protocol to generate hMLO from iPS cell lines with relevant cellular signatures of the floor plate ontology, A9 DaN, and a diverse group of other neural and neuronal cells typically found within the human midbrain. Moreover, DIV 96 hMLO was found to produce neuromelanin spontaneously. It worths noting that whilst the cell type diversity and general expression profile were consistent across different hMLO

derived from various iPS cell line, there was significant variability in the absolute number of FOXA2 or TH-expressing neurons between iPS cell lines of similar genetic burden, between batches of differentiation and even among hMLO derived from the same cell lines. Such variability was not unusual with the organoid system built upon self-assembly and hence, remains a significant limitation of this approach. Ongoing effort to address the limited reproducibility of this system has brought about some initial success at reducing variation between organoid using bioengineered scaffold (Fiorenzano *et al.*, 2021).

Having established the differentiation protocol, I generated hMLO from healthy controls as well as familial PD patient iPS cell lines and investigated potential cellular pathology induced by familial PD mutations *SNCA-Triplication* and *GBA-N370S*. However, at DIV 96 hMLO derived from iPS cell lines habouring either *SNCA-Triplication* or *GBA-N370S* exhibited comparable expression of both FOXA2 and TH. Nor was there apparent difference in the number of α-synuclein puncta within TH-expressing neurons among hMLO with different genetic burden. No other potential phenotypes have been looked at. However, the absence of spontaneous α-synucleinopathy, even in hMLO carrying *SNCA* Triplication mutation implied that the current hMLO might not be primed to model human midbrain and/or PD. It is likely that prolonged culturing might be necessary for hMLO to manifest age-related disease phenotypes such as α-synucleinopathy. It is also probable that the current hMLO model was not sufficiently representative of the human midbrain considering that I have yet performed comprehensive transcriptomic analysis on the resulting hMLO to affirm their midbrain-like identity.

Another apparent limitation of the organoid system is its limited capacity to model neuronal circuits. The relative positioning and connections of cells emerged spontaneously through inherent self-assembly within individual organoid are not comparable to the *in vitro* conditions. It is still possible to capture some extent of endogenous connectivity by generating

patterned organoid recapitulating small brain regions followed by guided fusion to form assembloids (Miura *et al.*, 2020). Custom directionality of neural connections can potentially be permissible by incorporating degradable bio-compatible scaffold to provide instructive directional guidance.

8.1.3. Neural circuit on fluid-walled microfluidics (FWM).

In Chapter 7, I reported a successful collaboration with Federico Nebuloni from the Walsh and Cook lab to establish a neural circuit model leveraging on their novel free-style microfluidics technology. Similar to the PDMS-based microfluidics, FWM permitted compartmentalisation of neuronal populations and directed neuronal connections based on differential fluid pressure, enabling recapitulation of the human corticostriatal network *in vitro*. Overcoming the limited accessibility apparent of plastic-walled microfluidic as well as the lack of directed neuronal connectivity associated with the organoid system, FWM presents an attractive alternative for studying circuit-related topics in an open-access manner. All circuit compartments were freely accessible for immediate high-resolution imaging and/or sophisticated electrophysiological experiments. Moreover, FWM presented an unprecedented opportunity in creatively custom circuit design to suit variable experimental needs within minutes which, otherwise, would take a significant amount of time and consumable cost to fabricate using PDMS. Taken together, this methodology could be extensively employed to reconstruct neuronal circuit of any shape and form with ease which subsequently could be amenable to a wide range of biological assays.

To highlight the key advantages of the FWM platform, we designed and performed directed axotomy assays on the resulting iPSC-derived corticostriatal tract and subsequently investigated axon regeneration affected by target-derived cues using live imaging of

fluorescent protein-tagged axons. In doing so, we provided proof-in-concept the feasibility of attaining i) systemic, direct and highly reproducible axon damage specifically to the axon compartment, ii) long-term live imaging of any compartment of the circuit with ease, and iii) great flexibility of circuit configuration and reconfiguration. Surprisingly, neither distal BDNF nor endogenous post-synaptic neurons exert positive influence on axon outgrowth in our cultures, suggesting the greater contribution of intrinsic signalling towards axon outgrowth. However, our results suggested empirically the beneficially pro-regeneration effect of exogenously supplied BDNF on axotomized axons. This initial success encourages development of micro-assays to screen for drug candidates that can promote regeneration after axon injury. However, BDNF pro-regeneration effect was comparable to that exerted by relevant postmitotic neuronal target, corroborated the necessity of a microcircuit-based culture to better understand the marginal therapeutic effect of potential drug candidates in the *in vivo* system.

The unique conceptual advantages of the FWM technology also render it useful for highly challenging experimental paradigm such as the investigation of synaptic plasticity within a microcircuit culture. Despite being one of the few unique features of neurons, synapses and their network-dependent properties such as synaptic plasticity have often been looked at principally within *in vivo* or organotypic slices which retain certain level of neuronal connectivity. Attempts looking at neuronal synapses in the absence of directed non-autologous inputs would undoubtedly receive scepticism on the physiological relevance of the resulting outcomes.

Wider adoption of FWM is currently restricted due to limited availability of the specific toolkit required to perform fluid jetting. Being a relatively new technology, its instrumentation remains under-popularised and in short supply. Our success in modelling axotomy in a circuit-

dependent manner hopefully would fuel more interests in considering using then for similar purposes and beyond.

8.1.4. Adoption of bioengineered tools to improve neural culture model.

Neuroscience pursuit has been met by parallel improvement in the toolkit and methodology developed to help enhance our biological experimental needs. Microfluidics chambers, spider-silk microfibers, and FWM are just a few examples explored and/or discussed in this work. Each of them offers unique strength unattainable by the other so as to cater to the broadly different experimental paradigms. Their applications often are complementary to one another's to inform more comprehensive understanding of biological processes and hence, sound knowledge of their utility and fundamental working mechanism is required prior to their employment. These necessitate greater and closer collaboration across disciplines to address increasingly sophisticated questions.

8.1.5. Future directions

Altogether, this work highlighted the importance and usefulness of modelling neurons in a highly physiological fashion, both in healthy and disease state. While current reductionistic model of neuron monoculture has offered great insights towards the understanding of both neuronal physiology and pathophysiology, thorough characterisation of molecular signature using transcriptomic analysis often revealed mixed maturation efficiency post neuronal differentiation with some iPSC-derived neurons such as iPSC-CN displaying immature or fetal-like identity of some iPSC-derived neurons (Handel *et al.*, 2016; Yao *et al.*, 2017) but others such as iPSC-DaN, once accounted for cellular heterogeneity, exhibiting similar expression profile as that of mature laser-captured human dopaminergic neurons isolated from post-

mortem tissue (Sandor *et al.*, 2017). This lack of consistent maturity of certain iPSC-derived cell models often invite scepticism toward their capacity to model aging-related disorders such as PD in which pathology slowly accumulates over the course of a few decades in the human brain. The significant discrepancy between the biological age of disease onset and functional maturity of iPSC-derived cell models might have accounted for missing spontaneous disease-associated cellular phenotypes such as synucleinopathy. The pursuit for more physiologically mature model of iPSC-derived neurons is, hence, justified and, in fact, highly-sought after. 3D organoid model which conceptually permits not only recapitulation of tissue-specific architecture but also long-term culturing of neurons for gradual emergence of mature cellular phenotypes offers an efficient solution to generate more mature neuronal models (Sloan *et al.*, 2017; Trujillo *et al.*, 2019). Coculture of neurons with supporting glia cells has also been employed to aid *in vitro* maturation of iPSC-derived neurons (Burke *et al.*, 2020; Hedegaard *et al.*, 2020). Neuron-neuron coculture, specifically with consideration of their connectivity, should be another major step of improvement towards more functionally mature neuronal model *in vitro.* Considering that neurogenesis precedes gliogenesis *in vivo* (Lenroot and Giedd, 2006; Miller and Gauthier, 2007), one would imagine that co-culturing of neurons with relevant neurons such as a neuronal microcircuit presented in this work would exert even more pronounced effect on functional identity and maturation of these iPSC-derived neurons for meaningful disease modelling. Future investigations looking at disease-specific phenotypes on monoculture should therefore be further validated on advanced co-culture to consolidate the validity of observed phenotypes.

Whilst each of the abovementioned approach offers unique strength complementary to one another, the ambitious goal remains to consolidate all of their respective strengths into a single platform i.e. a three dimensional circuit with open-access. Unsurprisingly, such an advanced culturing platform would open up opportunities to a plethora of biological assays

from a highly relevant biological models. More importantly, a unified modelling platform would minimize confounding technical factors emerging from different experimental setups and hence, facilitate experimental interpretation across different modelling strategies.

8.2. Striatal pathology in PD

8.2.1. Early human striatal pathology in PD and striatal compensatory phenomenon.

I set out in Chapter 4 to investigate the effect of the consequences on the MSN in the presence of altered pre-synaptic DaN inputs. This approach shifted the attention of PD pathogenesis away from neurodegeneration classically affected DaN onto functional maintenance of the striatal circuit so as to preserve the functional integrity of the motor-controlling center basal ganglia. While DaN pathology and degeneration is the canonical hallmark of PD and remains a great topic of research interest, addressing striatal pathology would be the ultimate goal of delaying/improving motor symptoms. Considering that striatal pathology emerged early when synapsed with *GBA-N370S* DaN independent of DaN neurodegeneration, reversing striatal pathology is an attractive early therapeutic target to slow down PD progression and/or alleviate PD symptoms. Interestingly, as such early striatal hyperexcitability was normalised spontaneously over time, it suggested that a heathy striatal genetic landscape can potentially augment their capacity to overcome debilitating signals released by mutant DaN. This can be confirmed in future work by comparing striatal electrophysiological properties of those derived from heathy control iPS cell lines versus those derived from *GBA-N370S* iPS cell lines cultured in the same microcircuit with *GBA-N370S* DaN.

Human striatal pathology in iPSC-derived model like what was described here could benefit greatly from development of new tools that allow identification of direct and indirect pathway.

New reporter cell lines which can specifically label D1R- or D2R-expressing neurons, Patch-seq, or new antibody combinations of concurrent MSN-specific and subtype-specific immunostaining are some examples of useful approaches to fine-tune striatal pathology.

It is interesting to explore the mechanistic signalling underlying the striatal regeneration as potential therapeutic target. In this work, I reported an increased PKA activity in iPSC-MSN upon connection with *GBA-N370S* DaN, demonstrating a dynamic interaction between the MSN and DaN population within the microcircuit culture, most likely due to diffusible elements released by the mutant DaN. I also observed the concurrent deficit in sodium and potassium ionic conductance and rescue of that deficit upon pharmacologically-induced normalisation of striatal PKA activity. It worths noting that such rescue of MSN ionic conductance deficit occurred despite the persistence of the phenotypic reduction in PKA activity in *GBA-N370S DaN* in the same microcircuit where MSN were treated with the PKA antagonist. This positioned MSN-autonomous signalling pathways as potential therapeutic targets to alleviate the overall burden of DaN pathology on the striatum and likely, also the basal ganglia by virtue of the striata connectivity. Considering PKA being the common drug target in many different medical conditions, one can be optimistic on the readily available bank of drug candidates that could be quickly repurposed to correct striatal hyperexcitability observed in my PD model.

8.2.2. Future directions

The modular microcircuit described in this work is a new methodology which holds great potential in dissecting individual contribution of different neuronal populations towards the eventual circuit phenotype. Future experiments with this model should establish a complete genetic landscape of PD patients by deriving all cell types of the microcircuit from the same *GBA-N370S* iPS cell lines. Pairwise comparisons of striatal phenotypes as different neuronal

populations being subsequently replaced in the *in vitro* microcircuit can shed light on the individual contribution of each cell type and/or how their genetic makeup affects PD manifestation in the context of *GBA-N370S (*or any other mutation of interest). Previous work on *GBA-N370S* DaN monoculture suggested multiple cell-autonomous deficits which could be linked toward the observed MSN hyperexcitability. Hence, it would be interesting to investigate if such phenomenon could be replicated in *GBA-N370S* DaN in my microcircuit culture and if so, how DaN pathology could influence the striatal physiology. On the other hand, more detailed molecular investigation on PKA-dependent signalling on normalising striatal pathology could also open up new therapeutic opportunity window and target.

While the genetic focus of this microcircuit work has been on *GBA-N370S*, striatal pathology in the context of microcircuit could also be investigated using neurons derived from other PD-related mutations. It would be interesting to assess whether the striatal pathology observed in this work is common across PD-related mutations or unique to *GBA N370S* variants. Despite the common preferential loss of SNpc DaN, PD patients often present with a diverse profile of motor symptoms and severity, suggesting variable degree of striatal dysfunction. Different variants exhibited have also been suggested to be associated with different panel of cellular autonomous perturbations (Byers *et al.*, 2011; Nguyen *et al.*, 2011; Fernandes *et al.*, 2016; Zambon *et al.*, 2019; Carola *et al.*, 2021). Therefore, knowledge of mutation-specific striatal pathology would be useful to stratify relevant therapeutic approach.

Reference

Adalbert, R. and Coleman, M. P. (2013) 'Review: Axon pathology in age-related neurodegenerative disorders.', *Neuropathology and applied neurobiology*. England, 39(2), pp. 90–108. doi: 10.1111/j.1365-2990.2012.01308.x.

Alcalay, R. N. *et al.* (2014) 'Comparison of Parkinson risk in Ashkenazi Jewish patients with Gaucher disease and GBA heterozygotes.', *JAMA neurology*. United States, 71(6), pp. 752–757. doi: 10.1001/jamaneurol.2014.313.

Alcalay, R. N. *et al.* (2015) 'Glucocerebrosidase activity in Parkinson's disease with and without GBA mutations.', *Brain : a journal of neurology*, 138(Pt 9), pp. 2648–2658. doi: 10.1093/brain/awv179.

Alexander, G. E. and Crutcher, M. D. (1990) 'Functional architecture of basal ganglia circuits: neural substrates of parallel processing.', *Trends in neurosciences*. England, 13(7), pp. 266–271. doi: 10.1016/0166-2236(90)90107-l.

Alexander, G. E., DeLong, M. R. and Strick, P. L. (1986) 'Parallel organization of functionally segregated circuits linking basal ganglia and cortex.', *Annual review of neuroscience*. United States, 9, pp. 357–381. doi: 10.1146/annurev.ne.09.030186.002041.

Amimoto, N. *et al.* (2021) 'Generation of striatal neurons from human induced pluripotent stem cells by controlling extrinsic signals with small molecules', *Stem Cell Research*, 55, p. 102486. doi: https://doi.org/10.1016/j.scr.2021.102486.

Andersen, J. *et al.* (2020) 'Generation of Functional Human 3D Cortico-Motor Assembloids.', *Cell*. United States, 183(7), pp. 1913-1929.e26. doi: 10.1016/j.cell.2020.11.017.

Araki, K. *et al.* (2019) 'Parkinson's disease is a type of amyloidosis featuring accumulation of amyloid fibrils of α-synuclein.', *Proceedings of the National Academy of Sciences of the United States of America*. United States, 116(36), pp. 17963–17969. doi: 10.1073/pnas.1906124116.

Arber, C. *et al.* (2015) 'Activin A directs striatal projection neuron differentiation of human pluripotent stem cells.', *Development (Cambridge, England)*, 142(7), pp. 1375–1386. doi: 10.1242/dev.117093.

Awa, S. *et al.* (2022) 'Phosphorylation of endogenous α-synuclein induced by extracellular seeds initiates at the pre-synaptic region and spreads to the cell body', *Scientific Reports*, 12(1), p. 1163. doi: 10.1038/s41598-022-04780-4.

Badanjak, K. *et al.* (2021) 'iPSC-Derived Microglia as a Model to Study Inflammation in Idiopathic Parkinson's Disease.', *Frontiers in cell and developmental biology*. Switzerland, 9, p. 740758. doi: 10.3389/fcell.2021.740758.

Banerjee, K. *et al.* (2014) 'Regulation of tyrosine hydroxylase transcription by hnRNP K and DNA secondary structure.', *Nature communications*. England, 5, p. 5769. doi: 10.1038/ncomms6769.

Barbera, G. *et al.* (2016) 'Spatially Compact Neural Clusters in the Dorsal Striatum Encode Locomotion Relevant Information.', *Neuron*. United States, 92(1), pp. 202–213. doi: 10.1016/j.neuron.2016.08.037.

Barry, P. H. (1994) 'JPCalc, a software package for calculating liquid junction potential corrections in patch-clamp, intracellular, epithelial and bilayer measurements and for correcting junction potential measurements.', *Journal of neuroscience methods*. Netherlands, 51(1), pp. 107–116. doi: 10.1016/0165-0270(94)90031-0.

Beck, I. *et al.* (1991) 'Enhancer element at the 3'-flanking region controls transcriptional response to hypoxia in the human erythropoietin gene.', *The Journal of biological chemistry*. United States, 266(24), pp. 15563–15566.

Beloozerova, I. N. *et al.* (2003) 'Activity of different classes of neurons of the motor cortex during postural corrections.', *The Journal of neuroscience : the official journal of the Society for Neuroscience*. United States, 23(21), pp. 7844–7853. doi: 10.1523/JNEUROSCI.23-21-07844.2003.

Bengoa-Vergniory, N. *et al.* (2020) 'CLR01 protects dopaminergic neurons in vitro and in mouse models of Parkinson's disease.', *Nature communications*, 11(1), p. 4885. doi: 10.1038/s41467-020-18689-x.

Bertero, A., Verrillo, L. and Apicella, A. junior (2022) 'A Novel Layer 4 Corticofugal Cell Type/Projection Involved in Thalamo-Cortico-Striatal Sensory Processing', *The Journal of Neuroscience*, 42(8), pp. 1383 LP – 1405. doi: 10.1523/JNEUROSCI.1738-21.2021.

Bertran-Gonzalez, J. *et al.* (2008) 'Opposing patterns of signaling activation in dopamine D1 and D2 receptor-expressing striatal neurons in response to cocaine and haloperidol.', *The Journal of neuroscience : the official journal of the Society for Neuroscience*. United States, 28(22), pp. 5671–5685. doi: 10.1523/JNEUROSCI.1039-08.2008.

Birey, F. *et al.* (2017) 'Assembly of functionally integrated human forebrain spheroids.', *Nature*,

545(7652), pp. 54–59. doi: 10.1038/nature22330.

Birey, F. *et al.* (2022) 'Dissecting the molecular basis of human interneuron migration in forebrain assembloids from Timothy syndrome', *Cell Stem Cell*, 29(2), pp. 248-264.e7. doi: https://doi.org/10.1016/j.stem.2021.11.011.

Bishop, M. W. *et al.* (2010) 'Hyperexcitable substantia nigra dopamine neurons in PINK1- and HtrA2/Omi-deficient mice.', *Journal of neurophysiology*, 104(6), pp. 3009–3020. doi: 10.1152/jn.00466.2010.

Björklund, A. and Dunnett, S. B. (2007) 'Dopamine neuron systems in the brain: an update', *Trends in Neurosciences*, 30(5), pp. 194–202. doi: https://doi.org/10.1016/j.tins.2007.03.006.

Bohnen, N. I. *et al.* (2006) 'Positron emission tomography of monoaminergic vesicular binding in aging and Parkinson disease.', *Journal of cerebral blood flow and metabolism : official journal of the International Society of Cerebral Blood Flow and Metabolism*. United States, 26(9), pp. 1198–1212. doi: 10.1038/sj.jcbfm.9600276.

Bolam, J. P. *et al.* (1983) 'A type of aspiny neuron in the rat neostriatum accumulates [3H]gamma-aminobutyric acid: combination of Golgi-staining, autoradiography, and electron microscopy.', *The Journal of comparative neurology*. United States, 213(2), pp. 121–134. doi: 10.1002/cne.902130202.

Bolam, J. P. *et al.* (1985) 'Glutamate decarboxylase-immunoreactive structures in the rat neostriatum: a correlated light and electron microscopic study including a combination of Golgi impregnation with immunocytochemistry.', *The Journal of comparative neurology*. United States, 237(1), pp. 1–20. doi: 10.1002/cne.902370102.

Boyd, J. G. and Gordon, T. (2003) 'Neurotrophic factors and their receptors in axonal regeneration and functional recovery after peripheral nerve injury.', *Molecular neurobiology*. United States, 27(3), pp. 277–324. doi: 10.1385/MN:27:3:277.

Brichta, L. and Greengard, P. (2014) 'Molecular determinants of selective dopaminergic vulnerability in Parkinson's disease: an update.', *Frontiers in neuroanatomy*. Switzerland, 8, p. 152. doi: 10.3389/fnana.2014.00152.

Britt, J. P. *et al.* (2012) 'Synaptic and behavioral profile of multiple glutamatergic inputs to the nucleus accumbens.', *Neuron*. United States, 76(4), pp. 790–803. doi: 10.1016/j.neuron.2012.09.040.

Brittain, J.-S., Sharott, A. and Brown, P. (2014) 'The highs and lows of beta activity in cortico-

basal ganglia loops.', *The European journal of neuroscience*. France, 39(11), pp. 1951–1959. doi: 10.1111/ejn.12574.

Brock, J. H. *et al.* (2010) 'Local and remote growth factor effects after primate spinal cord injury.', *The Journal of neuroscience : the official journal of the Society for Neuroscience*. United States, 30(29), pp. 9728–9737. doi: 10.1523/JNEUROSCI.1924-10.2010.

Brown, P. and Williams, D. (2005) 'Basal ganglia local field potential activity: character and functional significance in the human.', *Clinical neurophysiology : official journal of the International Federation of Clinical Neurophysiology*. Netherlands, 116(11), pp. 2510–2519. doi: 10.1016/j.clinph.2005.05.009.

Burke, E. E. *et al.* (2020) 'Dissecting transcriptomic signatures of neuronal differentiation and maturation using iPSCs.', *Nature communications*. England, 11(1), p. 462. doi: 10.1038/s41467-019-14266-z.

Byers, B. *et al.* (2011) 'SNCA triplication Parkinson's patient's iPSC-derived DA neurons accumulate α-synuclein and are susceptible to oxidative stress.', *PloS one*. United States, 6(11), p. e26159. doi: 10.1371/journal.pone.0026159.

Cai, D. *et al.* (1999) 'Prior exposure to neurotrophins blocks inhibition of axonal regeneration by MAG and myelin via a cAMP-dependent mechanism.', *Neuron*. United States, 22(1), pp. 89–101. doi: 10.1016/s0896-6273(00)80681-9.

Campbell, D. G., Hardie, D. G. and Vulliet, P. R. (1986) 'Identification of four phosphorylation sites in the N-terminal region of tyrosine hydroxylase.', *The Journal of biological chemistry*. United States, 261(23), pp. 10489–10492.

Carbon, M. *et al.* (2004) 'Caudate nucleus: influence of dopaminergic input on sequence learning and brain activation in Parkinsonism.', *NeuroImage*. United States, 21(4), pp. 1497–1507. doi: 10.1016/j.neuroimage.2003.12.014.

Carola, G. *et al.* (2021) 'Parkinson's disease patient-specific neuronal networks carrying the LRRK2 G2019S mutation unveil early functional alterations that predate neurodegeneration', *npj Parkinson's Disease*, 7(1), p. 55. doi: 10.1038/s41531-021-00198-3.

Cepeda, C. *et al.* (2008) 'Differential electrophysiological properties of dopamine D1 and D2 receptor-containing striatal medium-sized spiny neurons.', *The European journal of neuroscience*. France, 27(3), pp. 671–682. doi: 10.1111/j.1460-9568.2008.06038.x.

Cha-Molstad, H. *et al.* (2004) 'Cell-type-specific binding of the transcription factor CREB to the

cAMP-response element.', *Proceedings of the National Academy of Sciences of the United States of America*. United States, 101(37), pp. 13572–13577. doi: 10.1073/pnas.0405587101.

Chambers, S. M. *et al.* (2009) 'Highly efficient neural conversion of human ES and iPS cells by dual inhibition of SMAD signaling.', *Nature biotechnology*, 27(3), pp. 275–280. doi: 10.1038/nbt.1529.

Chang, D. *et al.* (2017) 'A meta-analysis of genome-wide association studies identifies 17 new Parkinson's disease risk loci.', *Nature genetics*. United States, 49(10), pp. 1511–1516. doi: 10.1038/ng.3955.

Cheng, P.-L. *et al.* (2011) 'Self-amplifying autocrine actions of BDNF in axon development.', *Proceedings of the National Academy of Sciences of the United States of America*, 108(45), pp. 18430–18435. doi: 10.1073/pnas.1115907108.

Cho, R. W. *et al.* (2015) 'Phosphorylation of Complexin by PKA Regulates Activity-Dependent Spontaneous Neurotransmitter Release and Structural Synaptic Plasticity', *Neuron*, 88(4), pp. 749–761. doi: https://doi.org/10.1016/j.neuron.2015.10.011.

Choi, E. Y., Yeo, B. T. T. and Buckner, R. L. (2012) 'The organization of the human striatum estimated by intrinsic functional connectivity.', *Journal of neurophysiology*. United States, 108(8), pp. 2242–2263. doi: 10.1152/jn.00270.2012.

Choi, J. *et al.* (2002) 'Phosphorylation of stargazin by protein kinase A regulates its interaction with PSD-95.', *The Journal of biological chemistry*. United States, 277(14), pp. 12359–12363. doi: 10.1074/jbc.M200528200.

Clark, L. N. *et al.* (2007) 'Mutations in the glucocerebrosidase gene are associated with early-onset Parkinson disease.', *Neurology*. United States, 69(12), pp. 1270–1277. doi: 10.1212/01.wnl.0000276989.17578.02.

Coleman, M. P. and Höke, A. (2020) 'Programmed axon degeneration: from mouse to mechanism to medicine', *Nature Reviews Neuroscience*, 21(4), pp. 183–196. doi: 10.1038/s41583-020-0269-3.

Conforti, L., Gilley, J. and Coleman, M. P. (2014) 'Wallerian degeneration: an emerging axon death pathway linking injury and disease.', *Nature reviews. Neuroscience*. England, 15(6), pp. 394–409. doi: 10.1038/nrn3680.

Cossette, M., Lecomte, F. and Parent, A. (2005) 'Morphology and distribution of dopaminergic neurons intrinsic to the human striatum.', *Journal of chemical neuroanatomy*. Netherlands,

29(1), pp. 1–11. doi: 10.1016/j.jchemneu.2004.08.007.

Cossette, M., Lévesque, D. and Parent, A. (2005) 'Neurochemical characterization of dopaminergic neurons in human striatum.', *Parkinsonism & related disorders*. England, 11(5), pp. 277–286. doi: 10.1016/j.parkreldis.2005.02.008.

Cowan, R. L. *et al.* (1990) 'Parvalbumin-containing GABAergic interneurons in the rat neostriatum.', *The Journal of comparative neurology*. United States, 302(2), pp. 197–205. doi: 10.1002/cne.903020202.

Craig, S. P. *et al.* (1986) 'Localization of the human tyrosine hydroxylase gene to 11p15: gene duplication and evolution of metabolic pathways.', *Cytogenetics and cell genetics*. Switzerland, 42(1–2), pp. 29–32. doi: 10.1159/000132246.

Cruz, B. F. *et al.* (2022) 'Action suppression reveals opponent parallel control via striatal circuits', *Nature*, 607(7919), pp. 521–526. doi: 10.1038/s41586-022-04894-9.

Cui, G. *et al.* (2013) 'Concurrent activation of striatal direct and indirect pathways during action initiation.', *Nature*. England, 494(7436), pp. 238–242. doi: 10.1038/nature11846.

Dagda, R. K. *et al.* (2011) 'Mitochondrially localized PKA reverses mitochondrial pathology and dysfunction in a cellular model of Parkinson's disease', *Cell Death & Differentiation*, 18(12), pp. 1914–1923. doi: 10.1038/cdd.2011.74.

Dagda, R. K. *et al.* (2014) 'Beyond the mitochondrion: cytosolic PINK1 remodels dendrites through protein kinase A.', *Journal of neurochemistry*, 128(6), pp. 864–877. doi: 10.1111/jnc.12494.

Davis, G. W. (2000) 'The making of a synapse: target-derived signals and presynaptic differentiation.', *Neuron*. United States, 26(3), pp. 551–554. doi: 10.1016/s0896-6273(00)81190-3.

Deffains, M. *et al.* (2016) 'Subthalamic, not striatal, activity correlates with basal ganglia downstream activity in normal and parkinsonian monkeys.', *eLife*. England, 5. doi: 10.7554/eLife.16443.

Delli Carri, A. *et al.* (2013) 'Human pluripotent stem cell differentiation into authentic striatal projection neurons.', *Stem cell reviews and reports*. United States, 9(4), pp. 461–474. doi: 10.1007/s12015-013-9441-8.

DeLong, M. R. and Wichmann, T. (2007) 'Circuits and Circuit Disorders of the Basal Ganglia',

Archives of Neurology, 64(1), pp. 20–24. doi: 10.1001/archneur.64.1.20.

Deng, H., Wang, P. and Jankovic, J. (2018) 'The genetics of Parkinson disease.', *Ageing research reviews*. England, 42, pp. 72–85. doi: 10.1016/j.arr.2017.12.007.

Deng, Y.-P., Lei, W.-L. and Reiner, A. (2006) 'Differential perikaryal localization in rats of D1 and D2 dopamine receptors on striatal projection neuron types identified by retrograde labeling.', *Journal of chemical neuroanatomy*. Netherlands, 32(2–4), pp. 101–116. doi: 10.1016/j.jchemneu.2006.07.001.

Deng, Y. *et al.* (2015) 'Differential organization of cortical inputs to striatal projection neurons of the matrix compartment in rats ', *Frontiers in Systems Neuroscience* . Available at: https://www.frontiersin.org/articles/10.3389/fnsys.2015.00051.

Dittmer, P. J., Dell'Acqua, M. L. and Sather, W. A. (2019) 'Synaptic crosstalk conferred by a zone of differentially regulated Ca(2+) signaling in the dendritic shaft adjoining a potentiated spine.', *Proceedings of the National Academy of Sciences of the United States of America*, 116(27), pp. 13611–13620. doi: 10.1073/pnas.1902461116.

Doig, N. M., Moss, J. and Bolam, J. P. (2010) 'Cortical and Thalamic Innervation of Direct and Indirect Pathway Medium-Sized Spiny Neurons in Mouse Striatum', *The Journal of Neuroscience*, 30(44), pp. 14610 LP – 14618. doi: 10.1523/JNEUROSCI.1623-10.2010.

di Domenico, A. *et al.* (2019) 'Patient-Specific iPSC-Derived Astrocytes Contribute to Non-Cell-Autonomous Neurodegeneration in Parkinson's Disease.', *Stem cell reports*. United States, 12(2), pp. 213–229. doi: 10.1016/j.stemcr.2018.12.011.

Dorsey, E. R. *et al.* (2018) 'The Emerging Evidence of the Parkinson Pandemic.', *Journal of Parkinson's disease*. Netherlands, 8(s1), pp. S3–S8. doi: 10.3233/JPD-181474.

Dorst, M. C. *et al.* (2020) 'Polysynaptic inhibition between striatal cholinergic interneurons shapes their network activity patterns in a dopamine-dependent manner', *Nature Communications*, 11(1), p. 5113. doi: 10.1038/s41467-020-18882-y.

Dräger, N. M. *et al.* (2022) 'A CRISPRi/a platform in human iPSC-derived microglia uncovers regulators of disease states', *Nature Neuroscience*, 25(9), pp. 1149–1162. doi: 10.1038/s41593-022-01131-4.

Drori, E., Berman, S. and Mezer, A. A. (2022) 'Mapping microstructural gradients of the human striatum in normal aging and Parkinson's disease.', *Science advances*. United States, 8(28), p. eabm1971. doi: 10.1126/sciadv.abm1971.

Dubach, M. *et al.* (1987) 'Primate neostriatal neurons containing tyrosine hydroxylase: immunohistochemical evidence.', *Neuroscience letters*. Ireland, 75(2), pp. 205–210. doi: 10.1016/0304-3940(87)90298-9.

Edvardson, S. *et al.* (2012) 'A deleterious mutation in DNAJC6 encoding the neuronal-specific clathrin-uncoating co-chaperone auxilin, is associated with juvenile parkinsonism.', *PloS one*. United States, 7(5), p. e36458. doi: 10.1371/journal.pone.0036458.

Van Den Eeden, S. K. *et al.* (2003) 'Incidence of Parkinson's Disease: Variation by Age, Gender, and Race/Ethnicity', *American Journal of Epidemiology*, 157(11), pp. 1015–1022. doi: 10.1093/aje/kwg068.

Ehlers, M. D. (2000) 'Reinsertion or degradation of AMPA receptors determined by activity-dependent endocytic sorting.', *Neuron*. United States, 28(2), pp. 511–525. doi: 10.1016/s0896-6273(00)00129-x.

EHRINGER, H. and HORNYKIEWICZ, O. (1960) '[Distribution of noradrenaline and dopamine (3-hydroxytyramine) in the human brain and their behavior in diseases of the extrapyramidal system].', *Klinische Wochenschrift*. Germany, 38, pp. 1236–1239. doi: 10.1007/BF01485901.

Ekman, U. *et al.* (2012) 'Functional brain activity and presynaptic dopamine uptake in patients with Parkinson's disease and mild cognitive impairment: a cross-sectional study.', *The Lancet. Neurology*. England, 11(8), pp. 679–687. doi: 10.1016/S1474-4422(12)70138-2.

Farrer, M. *et al.* (1998) 'Low frequency of alpha-synuclein mutations in familial Parkinson's disease.', *Annals of neurology*. United States, 43(3), pp. 394–397. doi: 10.1002/ana.410430320.

Fawcett, J. W. (2020) 'The Struggle to Make CNS Axons Regenerate: Why Has It Been so Difficult?', *Neurochemical research*. United States, 45(1), pp. 144–158. doi: 10.1007/s11064-019-02844-y.

Feng, Q. *et al.* (2010) 'Hemangioblastic derivatives from human induced pluripotent stem cells exhibit limited expansion and early senescence.', *Stem cells (Dayton, Ohio)*. England, 28(4), pp. 704–712. doi: 10.1002/stem.321.

Fernandes, H. J. R. *et al.* (2016) 'ER Stress and Autophagic Perturbations Lead to Elevated Extracellular α-Synuclein in GBA-N370S Parkinson's iPSC-Derived Dopamine Neurons.', *Stem cell reports*, 6(3), pp. 342–356. doi: 10.1016/j.stemcr.2016.01.013.

Fieblinger, T. *et al.* (2014) 'Cell type-specific plasticity of striatal projection neurons in parkinsonism and L-DOPA-induced dyskinesia.', *Nature communications*, 5, p. 5316. doi:

10.1038/ncomms6316.

Fiorenzano, A. *et al.* (2021) 'Single-cell transcriptomics captures features of human midbrain development and dopamine neuron diversity in brain organoids.', *Nature communications*. England, 12(1), p. 7302. doi: 10.1038/s41467-021-27464-5.

Fjodorova, M., Noakes, Z. and Li, M. (2020) 'A role for TGFβ signalling in medium spiny neuron differentiation of human pluripotent stem cells.', *Neuronal signaling*. England, 4(2), p. NS20200004. doi: 10.1042/NS20200004.

Fleck, J. S. *et al.* (2021) 'Resolving organoid brain region identities by mapping single-cell genomic data to reference atlases', *Cell Stem Cell*, 28(6), pp. 1148-1159.e8. doi: https://doi.org/10.1016/j.stem.2021.02.015.

French, S. J. and Totterdell, S. (2003) 'Individual nucleus accumbens-projection neurons receive both basolateral amygdala and ventral subicular afferents in rats.', *Neuroscience*. United States, 119(1), pp. 19–31. doi: 10.1016/s0306-4522(03)00150-7.

Freund, T. F., Powell, J. F. and Smith, A. D. (1984) 'Tyrosine hydroxylase-immunoreactive boutons in synaptic contact with identified striatonigral neurons, with particular reference to dendritic spines.', *Neuroscience*. United States, 13(4), pp. 1189–1215. doi: 10.1016/0306-4522(84)90294-x.

Funakoshi, H. *et al.* (1993) 'Differential expression of mRNAs for neurotrophins and their receptors after axotomy of the sciatic nerve.', *The Journal of cell biology*. United States, 123(2), pp. 455–465. doi: 10.1083/jcb.123.2.455.

Furuta, Y., Piston, D. W. and Hogan, B. L. (1997) 'Bone morphogenetic proteins (BMPs) as regulators of dorsal forebrain development.', *Development (Cambridge, England)*. England, 124(11), pp. 2203–2212. doi: 10.1242/dev.124.11.2203.

Fusaki, N. *et al.* (2009) 'Efficient induction of transgene-free human pluripotent stem cells using a vector based on Sendai virus, an RNA virus that does not integrate into the host genome.', *Proceedings of the Japan Academy. Series B, Physical and biological sciences*. Japan, 85(8), pp. 348–362. doi: 10.2183/pjab.85.348.

Galvan, A. and Wichmann, T. (2008) 'Pathophysiology of parkinsonism.', *Clinical neurophysiology : official journal of the International Federation of Clinical Neurophysiology*. Netherlands, 119(7), pp. 1459–1474. doi: 10.1016/j.clinph.2008.03.017.

Gan-Or, Z. *et al.* (2008) 'Genotype-phenotype correlations between GBA mutations and

Parkinson disease risk and onset.', *Neurology*. United States, 70(24), pp. 2277–2283. doi: 10.1212/01.wnl.0000304039.11891.29.

Gandelman, K. Y. *et al.* (1990) 'Species and regional differences in the expression of cell-type specific elements at the human and rat tyrosine hydroxylase gene loci.', *Journal of neurochemistry*. England, 55(6), pp. 2149–2152. doi: 10.1111/j.1471-4159.1990.tb05811.x.

Garcia-Ruiz, C., Morales, A. and Fernández-Checa, J. C. (2015) 'Glycosphingolipids and cell death: one aim, many ways.', *Apoptosis : an international journal on programmed cell death*. Netherlands, 20(5), pp. 607–620. doi: 10.1007/s10495-015-1092-6.

Gardaneh, M. *et al.* (2000) 'Synergy between 5' and 3' flanking regions of the human tyrosine hydroxylase gene ensures specific, high-level expression in neuroblastoma cells.', *Neuroscience letters*. Ireland, 292(3), pp. 147–150. doi: 10.1016/s0304-3940(00)01474-9.

Gasser, T. (2005) 'Genetics of Parkinson's disease.', *Current opinion in neurology*. England, 18(4), pp. 363–369. doi: 10.1097/01.wco.0000170951.08924.3d.

Gegg, M. E. *et al.* (2012) 'Glucocerebrosidase deficiency in substantia nigra of parkinson disease brains.', *Annals of neurology*. United States, 72(3), pp. 455–463. doi: 10.1002/ana.23614.

Gerfen, C. R. *et al.* (1990) 'D1 and D2 dopamine receptor-regulated gene expression of striatonigral and striatopallidal neurons.', *Science (New York, N.Y.)*. United States, 250(4986), pp. 1429–1432. doi: 10.1126/science.2147780.

Gerfen, C. R. and Surmeier, D. J. (2011) 'Modulation of striatal projection systems by dopamine.', *Annual review of neuroscience*, 34, pp. 441–466. doi: 10.1146/annurev-neuro-061010-113641.

Gerfen, C. R. and Young, W. S. 3rd (1988) 'Distribution of striatonigral and striatopallidal peptidergic neurons in both patch and matrix compartments: an in situ hybridization histochemistry and fluorescent retrograde tracing study.', *Brain research*. Netherlands, 460(1), pp. 161–167. doi: 10.1016/0006-8993(88)91217-6.

Gertler, T. S., Chan, C. S. and Surmeier, D. J. (2008) 'Dichotomous Anatomical Properties of Adult Striatal Medium Spiny Neurons', *Journal of Neuroscience*, 28(43), pp. 10814–10824. doi: 10.1523/jneurosci.2660-08.2008.

Giguère, N., Burke Nanni, S. and Trudeau, L.-E. (2018) 'On Cell Loss and Selective Vulnerability of Neuronal Populations in Parkinson's Disease.', *Frontiers in neurology*. Switzerland, 9, p. 455.

doi: 10.3389/fneur.2018.00455.

Gladkov, A. *et al.* (2017) 'Design of Cultured Neuron Networks in vitro with Predefined Connectivity Using Asymmetric Microfluidic Channels', *Scientific Reports*, 7(1), p. 15625. doi: 10.1038/s41598-017-15506-2.

Goedert, M. (2001) 'Alpha-synuclein and neurodegenerative diseases.', *Nature reviews. Neuroscience*. England, 2(7), pp. 492–501. doi: 10.1038/35081564.

Goldberg, J. A. *et al.* (2004) 'Spike synchronization in the cortex/basal-ganglia networks of Parkinsonian primates reflects global dynamics of the local field potentials.', *The Journal of neuroscience : the official journal of the Society for Neuroscience*. United States, 24(26), pp. 6003–6010. doi: 10.1523/JNEUROSCI.4848-03.2004.

Goldsmith, B. A. and Abrams, T. W. (1992) 'cAMP modulates multiple K+ currents, increasing spike duration and excitability in Aplysia sensory neurons.', *Proceedings of the National Academy of Sciences of the United States of America*. United States, 89(23), pp. 11481–11485. doi: 10.1073/pnas.89.23.11481.

Graves, S. M. and Surmeier, D. J. (2019) 'Delayed Spine Pruning of Direct Pathway Spiny Projection Neurons in a Mouse Model of Parkinson's Disease.', *Frontiers in cellular neuroscience*, 13, p. 32. doi: 10.3389/fncel.2019.00032.

Grigor'eva, E. V *et al.* (2023) 'Biochemical Characteristics of iPSC-Derived Dopaminergic Neurons from N370S GBA Variant Carriers with and without Parkinson's Disease.', *International journal of molecular sciences*. Switzerland, 24(5). doi: 10.3390/ijms24054437.

Groenewegen, H. J. and Berendse, H. W. (1994) 'The specificity of the "nonspecific" midline and intralaminar thalamic nuclei.', *Trends in neurosciences*. England, 17(2), pp. 52–57. doi: 10.1016/0166-2236(94)90074-4.

Grosheva, M. *et al.* (2016) 'Comparison of trophic factors' expression between paralyzed and recovering muscles after facial nerve injury. A quantitative analysis in time course.', *Experimental neurology*. United States, 279, pp. 137–148. doi: 10.1016/j.expneurol.2016.02.020.

Gulacsi, A. A. and Anderson, S. A. (2008) 'Beta-catenin-mediated Wnt signaling regulates neurogenesis in the ventral telencephalon.', *Nature neuroscience*, 11(12), pp. 1383–1391. doi: 10.1038/nn.2226.

Guo, Q. *et al.* (2015) 'Whole-brain mapping of inputs to projection neurons and cholinergic

interneurons in the dorsal striatum.', *PloS one*. United States, 10(4), p. e0123381. doi: 10.1371/journal.pone.0123381.

Haber, S. N., Fudge, J. L. and McFarland, N. R. (2000) 'Striatonigrostriatal pathways in primates form an ascending spiral from the shell to the dorsolateral striatum.', *The Journal of neuroscience : the official journal of the Society for Neuroscience*. United States, 20(6), pp. 2369–2382. doi: 10.1523/JNEUROSCI.20-06-02369.2000.

Handel, A. E. *et al.* (2016) 'Assessing similarity to primary tissue and cortical layer identity in induced pluripotent stem cell-derived cortical neurons through single-cell transcriptomics', *Human Molecular Genetics*, 25(5), pp. 989–1000. doi: 10.1093/hmg/ddv637.

Hansen, D. V *et al.* (2013) 'Non-epithelial stem cells and cortical interneuron production in the human ganglionic eminences.', *Nature neuroscience*. United States, 16(11), pp. 1576–1587. doi: 10.1038/nn.3541.

Hartfield, E. M. *et al.* (2014) 'Physiological characterisation of human iPS-derived dopaminergic neurons.', *PloS one*. United States, 9(2), p. e87388. doi: 10.1371/journal.pone.0087388.

Hébert, J. M., Mishina, Y. and McConnell, S. K. (2002) 'BMP signaling is required locally to pattern the dorsal telencephalic midline.', *Neuron*. United States, 35(6), pp. 1029–1041. doi: 10.1016/s0896-6273(02)00900-5.

Hedegaard, A. *et al.* (2020) 'Pro-maturational Effects of Human iPSC-Derived Cortical Astrocytes upon iPSC-Derived Cortical Neurons.', *Stem cell reports*, 15(1), pp. 38–51. doi: 10.1016/j.stemcr.2020.05.003.

Heman-Ackah, S. M. *et al.* (2017) 'Alpha-synuclein induces the unfolded protein response in Parkinson's disease SNCA triplication iPSC-derived neurons.', *Human molecular genetics*. England, 26(22), pp. 4441–4450. doi: 10.1093/hmg/ddx331.

Hendrickx, D. M. *et al.* (2021) 'A New Synuclein-Transgenic Mouse Model for Early Parkinson's Reveals Molecular Features of Preclinical Disease', *Molecular Neurobiology*, 58(2), pp. 576–602. doi: 10.1007/s12035-020-02085-z.

Herkenham, M. *et al.* (1991) 'Selective retention of MPP+ within the monoaminergic systems of the primate brain following MPTP administration: an in vivo autoradiographic study.', *Neuroscience*. United States, 40(1), pp. 133–158. doi: 10.1016/0306-4522(91)90180-v.

Hernandez, D. G., Reed, X. and Singleton, A. B. (2016) 'Genetics in Parkinson disease: Mendelian versus non-Mendelian inheritance.', *Journal of neurochemistry*. England, 139

Suppl(Suppl 1), pp. 59–74. doi: 10.1111/jnc.13593.

Hess, J., Angel, P. and Schorpp-Kistner, M. (2004) 'AP-1 subunits: quarrel and harmony among siblings', *Journal of Cell Science*, 117(25), pp. 5965 LP – 5973. doi: 10.1242/jcs.01589.

Hjorth, J. J. J. *et al.* (2020) 'The microcircuits of striatum in silico', *Proceedings of the National Academy of Sciences*, 117(17), pp. 9554 LP – 9565. doi: 10.1073/pnas.2000671117.

Hoang Trung, H. *et al.* (2021) 'Deficiency of the RIβ subunit of protein kinase A causes body tremor and impaired fear conditioning memory in rats', *Scientific Reports*, 11(1), p. 2039. doi: 10.1038/s41598-021-81515-x.

Hofmann, M. *et al.* (2022) 'Cytoskeletal assembly in axonal outgrowth and regeneration analyzed on the nanoscale', *Scientific Reports*, 12(1), p. 14387. doi: 10.1038/s41598-022-18562-5.

Hogkin, A. L. and Huxley, A. F. (1952) 'A quantitative description of membrane current and its application to conduction and excitation in nerve.', *The Journal of physiology*, 117(4), pp. 500–544. doi: 10.1113/jphysiol.1952.sp004764.

Horikoshi, M. *et al.* (1992) 'Transcription factor TFIID induces DNA bending upon binding to the TATA element.', *Proceedings of the National Academy of Sciences of the United States of America*. United States, 89(3), pp. 1060–1064. doi: 10.1073/pnas.89.3.1060.

Horowitz, M. and Zimran, A. (1994) 'Mutations causing Gaucher disease.', *Human mutation*. United States, 3(1), pp. 1–11. doi: 10.1002/humu.1380030102.

Hruska, K. S. *et al.* (2008) 'Gaucher disease: mutation and polymorphism spectrum in the glucocerebrosidase gene (GBA).', *Human mutation*. United States, 29(5), pp. 567–583. doi: 10.1002/humu.20676.

Hu, B.-Y. *et al.* (2010) 'Neural differentiation of human induced pluripotent stem cells follows developmental principles but with variable potency.', *Proceedings of the National Academy of Sciences of the United States of America*. United States, 107(9), pp. 4335–4340. doi: 10.1073/pnas.0910012107.

Huebner, E. A. and Strittmatter, S. M. (2009) 'Axon regeneration in the peripheral and central nervous systems.', *Results and problems in cell differentiation*. Germany, 48, pp. 339–351. doi: 10.1007/400_2009_19.

Huh, Y. E. *et al.* (2020) 'β-Glucocerebrosidase activity in GBA-linked Parkinson disease: The

type of mutation matters.', *Neurology*. United States, 95(6), pp. e685–e696. doi: 10.1212/WNL.0000000000009989.

Hur, E.-M. *et al.* (2011) 'Engineering neuronal growth cones to promote axon regeneration over inhibitory molecules', *Proceedings of the National Academy of Sciences*. Proceedings of the National Academy of Sciences, 108(12), pp. 5057–5062. doi: 10.1073/pnas.1011258108.

Hwang, R.-D. *et al.* (2014) 'The neuroprotective effect of human uncoupling protein 2 (hUCP2) requires cAMP-dependent protein kinase in a toxin model of Parkinson's disease.', *Neurobiology of disease*. United States, 69, pp. 180–191. doi: 10.1016/j.nbd.2014.05.032.

Iannielli, A. *et al.* (2019) 'Reconstitution of the Human Nigro-striatal Pathway on-a-Chip Reveals OPA1-Dependent Mitochondrial Defects and Loss of Dopaminergic Synapses.', *Cell reports*, 29(13), pp. 4646-4656.e4. doi: 10.1016/j.celrep.2019.11.111.

Ibáñez-Sandoval, O. *et al.* (2010) 'Electrophysiological and morphological characteristics and synaptic connectivity of tyrosine hydroxylase-expressing neurons in adult mouse striatum.', *The Journal of neuroscience : the official journal of the Society for Neuroscience*. United States, 30(20), pp. 6999–7016. doi: 10.1523/JNEUROSCI.5996-09.2010.

Janezic, S. *et al.* (2013) 'Deficits in dopaminergic transmission precede neuron loss and dysfunction in a new Parkinson model', *Proceedings of the National Academy of Sciences*. Proceedings of the National Academy of Sciences, 110(42), pp. E4016–E4025. doi: 10.1073/pnas.1309143110.

Jankovic, J. (2008) 'Parkinson's disease: clinical features and diagnosis.', *Journal of neurology, neurosurgery, and psychiatry*. England, 79(4), pp. 368–376. doi: 10.1136/jnnp.2007.131045.

Ji, Y. *et al.* (2005) 'Cyclic AMP controls BDNF-induced TrkB phosphorylation and dendritic spine formation in mature hippocampal neurons.', *Nature neuroscience*. United States, 8(2), pp. 164–172. doi: 10.1038/nn1381.

Ji, Y. *et al.* (2010) 'Acute and gradual increases in BDNF concentration elicit distinct signaling and functions in neurons.', *Nature neuroscience*. United States, 13(3), pp. 302–309. doi: 10.1038/nn.2505.

Jin, X., Tecuapetla, F. and Costa, R. M. (2014) 'Basal ganglia subcircuits distinctively encode the parsing and concatenation of action sequences.', *Nature neuroscience*. United States, 17(3), pp. 423–430. doi: 10.1038/nn.3632.

Jo, J. *et al.* (2016) 'Midbrain-like Organoids from Human Pluripotent Stem Cells Contain

Functional Dopaminergic and Neuromelanin-Producing Neurons.', *Cell stem cell*. United States, 19(2), pp. 248–257. doi: 10.1016/j.stem.2016.07.005.

Jo, J. *et al.* (2021) 'Lewy Body-like Inclusions in Human Midbrain Organoids Carrying Glucocerebrosidase and α-Synuclein Mutations.', *Annals of neurology*. United States, 90(3), pp. 490–505. doi: 10.1002/ana.26166.

Jokinen, P. *et al.* (2009) 'Impaired cognitive performance in Parkinson's disease is related to caudate dopaminergic hypofunction and hippocampal atrophy.', *Parkinsonism & related disorders*. England, 15(2), pp. 88–93. doi: 10.1016/j.parkreldis.2008.03.005.

Joksimovic, M. and Awatramani, R. (2014) 'Wnt/beta-catenin signaling in midbrain dopaminergic neuron specification and neurogenesis.', *Journal of molecular cell biology*. United States, 6(1), pp. 27–33. doi: 10.1093/jmcb/mjt043.

Kamath, T. *et al.* (2022) 'Single-cell genomic profiling of human dopamine neurons identifies a population that selectively degenerates in Parkinson's disease', *Nature Neuroscience*, 25(5), pp. 588–595. doi: 10.1038/s41593-022-01061-1.

Kaneda, N. *et al.* (1991) 'Tissue-specific and high-level expression of the human tyrosine hydroxylase gene in transgenic mice.', *Neuron*. United States, 6(4), pp. 583–594. doi: 10.1016/0896-6273(91)90061-4.

Kelly, R. M. and Strick, P. L. (2004) 'Macro-architecture of basal ganglia loops with the cerebral cortex: use of rabies virus to reveal multisynaptic circuits.', *Progress in brain research*. Netherlands, 143, pp. 449–459. doi: 10.1016/s0079-6123(03)43042-2.

Kessler, M. A. *et al.* (2003) 'The human tyrosine hydroxylase gene promoter', *Molecular Brain Research*, 112(1), pp. 8–23. doi: https://doi.org/10.1016/S0169-328X(02)00694-0.

Killinger, B. A. *et al.* (2019) 'Endogenous alpha-synuclein monomers, oligomers and resulting pathology: let's talk about the lipids in the room', *npj Parkinson's Disease*, 5(1), p. 23. doi: 10.1038/s41531-019-0095-3.

Kim, H. *et al.* (2019) 'Modeling G2019S-LRRK2 Sporadic Parkinson's Disease in 3D Midbrain Organoids.', *Stem cell reports*, 12(3), pp. 518–531. doi: 10.1016/j.stemcr.2019.01.020.

Kim, K. *et al.* (2010) 'Epigenetic memory in induced pluripotent stem cells.', *Nature*. England, 467(7313), pp. 285–290. doi: 10.1038/nature09342.

Kim, S. *et al.* (2018) 'GBA1 deficiency negatively affects physiological α-synuclein tetramers

and related multimers', *Proceedings of the National Academy of Sciences*. Proceedings of the National Academy of Sciences, 115(4), pp. 798–803. doi: 10.1073/pnas.1700465115.

Kim, S. *et al.* (2021) 'Dysregulation of mitochondria-lysosome contacts by GBA1 dysfunction in dopaminergic neuronal models of Parkinson's disease', *Nature Communications*, 12(1), p. 1807. doi: 10.1038/s41467-021-22113-3.

Kim, T. E. *et al.* (2003) 'Cloning and cell type-specific regulation of the human tyrosine hydroxylase gene promoter.', *Biochemical and biophysical research communications*. United States, 312(4), pp. 1123–1131. doi: 10.1016/j.bbrc.2003.11.029.

Kish, S. J. *et al.* (2008) 'Preferential loss of serotonin markers in caudate versus putamen in Parkinson's disease.', *Brain : a journal of neurology*. England, 131(Pt 1), pp. 120–131. doi: 10.1093/brain/awm239.

Kita, H. (1993) 'GABAergic circuits of the striatum.', *Progress in brain research*. Netherlands, 99, pp. 51–72. doi: 10.1016/s0079-6123(08)61338-2.

Kita, H. and Kita, T. (2011) 'Role of Striatum in the Pause and Burst Generation in the Globus Pallidus of 6-OHDA-Treated Rats.', *Frontiers in systems neuroscience*. Switzerland, 5, p. 42. doi: 10.3389/fnsys.2011.00042.

Kitai, S. T. and Surmeier, D. J. (1993) 'Cholinergic and dopaminergic modulation of potassium conductances in neostriatal neurons.', *Advances in neurology*. United States, 60, pp. 40–52.

Klein, C. and Westenberger, A. (2012) 'Genetics of Parkinson's disease.', *Cold Spring Harbor perspectives in medicine*. United States, 2(1), p. a008888. doi: 10.1101/cshperspect.a008888.

Klim, J. R. *et al.* (2019) 'ALS-implicated protein TDP-43 sustains levels of STMN2, a mediator of motor neuron growth and repair', *Nature Neuroscience*, 22(2), pp. 167–179. doi: 10.1038/s41593-018-0300-4.

Kobayashi, N. R. *et al.* (1997) 'BDNF and NT-4/5 prevent atrophy of rat rubrospinal neurons after cervical axotomy, stimulate GAP-43 and Talpha1-tubulin mRNA expression, and promote axonal regeneration.', *The Journal of neuroscience : the official journal of the Society for Neuroscience*. United States, 17(24), pp. 9583–9595. doi: 10.1523/JNEUROSCI.17-24-09583.1997.

Köroğlu, Ç. *et al.* (2013) 'DNAJC6 is responsible for juvenile parkinsonism with phenotypic variability.', *Parkinsonism & related disorders*. England, 19(3), pp. 320–324. doi: 10.1016/j.parkreldis.2012.11.006.

Kouli, A., Torsney, K. M. and Kuan, W.-L. (2018) 'Parkinson's Disease: Etiology, Neuropathology, and Pathogenesis.', in Stoker, T. B. and Greenland, J. C. (eds). Brisbane (AU). doi: 10.15586/codonpublications.parkinsonsdisease.2018.ch1.

Kramer, M. L. and Schulz-Schaeffer, W. J. (2007) 'Presynaptic alpha-synuclein aggregates, not Lewy bodies, cause neurodegeneration in dementia with Lewy bodies.', *The Journal of neuroscience : the official journal of the Society for Neuroscience*. United States, 27(6), pp. 1405–1410. doi: 10.1523/JNEUROSCI.4564-06.2007.

Krauss, R. *et al.* (2020) 'Axons Matter: The Promise of Treating Neurodegenerative Disorders by Targeting SARM1-Mediated Axonal Degeneration.', *Trends in pharmacological sciences*. England, 41(4), pp. 281–293. doi: 10.1016/j.tips.2020.01.006.

Kravitz, A. V *et al.* (2010) 'Regulation of parkinsonian motor behaviours by optogenetic control of basal ganglia circuitry.', *Nature*. England, 466(7306), pp. 622–626. doi: 10.1038/nature09159.

Kriks, S. *et al.* (2011) 'Dopamine neurons derived from human ES cells efficiently engraft in animal models of Parkinson's disease.', *Nature*. England, 480(7378), pp. 547–551. doi: 10.1038/nature10648.

Kubota, Y., Mikawa, S. and Kawaguchi, Y. (1993) 'Neostriatal GABAergic interneurones contain NOS, calretinin or parvalbumin.', *Neuroreport*. England, 5(3), pp. 205–208. doi: 10.1097/00001756-199312000-00004.

Kuo, H.-Y. and Liu, F.-C. (2019) 'Synaptic Wiring of Corticostriatal Circuits in Basal Ganglia: Insights into the Pathogenesis of Neuropsychiatric Disorders.', *eNeuro*. United States, 6(3). doi: 10.1523/ENEURO.0076-19.2019.

Kuschel, S., Rüther, U. and Theil, T. (2003) 'A disrupted balance between Bmp/Wnt and Fgf signaling underlies the ventralization of the Gli3 mutant telencephalon.', *Developmental biology*. United States, 260(2), pp. 484–495. doi: 10.1016/s0012-1606(03)00252-5.

Lahiri, A. K. and Bevan, M. D. (2020) 'Dopaminergic Transmission Rapidly and Persistently Enhances Excitability of D1 Receptor-Expressing Striatal Projection Neurons.', *Neuron*, 106(2), pp. 277-290.e6. doi: 10.1016/j.neuron.2020.01.028.

Lancaster, M. A. *et al.* (2013) 'Cerebral organoids model human brain development and microcephaly.', *Nature*. England, 501(7467), pp. 373–379. doi: 10.1038/nature12517.

Lang, C. *et al.* (2019) 'Single-Cell Sequencing of iPSC-Dopamine Neurons Reconstructs Disease

Progression and Identifies HDAC4 as a Regulator of Parkinson Cell Phenotypes.', *Cell stem cell*. United States, 24(1), pp. 93-106.e6. doi: 10.1016/j.stem.2018.10.023.

Laverne, G. *et al.* (2022) 'Cholinergic interneuron inhibition potentiates corticostriatal transmission in direct medium spiny neurons and rescues motor learning in parkinsonism.', *Cell reports*. United States, 40(1), p. 111034. doi: 10.1016/j.celrep.2022.111034.

Lebel, M. *et al.* (2001) 'Pitx3 activates mouse tyrosine hydroxylase promoter via a high-affinity binding site.', *Journal of neurochemistry*. England, 77(2), pp. 558–567. doi: 10.1046/j.1471-4159.2001.00257.x.

Lenartowski, R. *et al.* (2003) 'The bovine tyrosine hydroxylase gene associates in vitro with the nuclear matrix by its first intron sequence.', *Acta biochimica Polonica*. Poland, 50(3), pp. 865–873. doi: 035003865.

Lenartowski, R. and Goc, A. (2002) 'Tissue-specific association of the human tyrosine hydroxylase gene with the nuclear matrix', *Neuroscience Letters*, 330(2), pp. 151–154. doi: https://doi.org/10.1016/S0304-3940(02)00746-2.

Lenroot, R. K. and Giedd, J. N. (2006) 'Brain development in children and adolescents: insights from anatomical magnetic resonance imaging.', *Neuroscience and biobehavioral reviews*. United States, 30(6), pp. 718–729. doi: 10.1016/j.neubiorev.2006.06.001.

Leroy, E. *et al.* (1998) 'The ubiquitin pathway in Parkinson's disease.', *Nature*. England, pp. 451–452. doi: 10.1038/26652.

Lesage, S. *et al.* (2016) 'Loss of VPS13C Function in Autosomal-Recessive Parkinsonism Causes Mitochondrial Dysfunction and Increases PINK1/Parkin-Dependent Mitophagy.', *American journal of human genetics*. United States, 98(3), pp. 500–513. doi: 10.1016/j.ajhg.2016.01.014.

Leventoux, N. *et al.* (2020) 'Human Astrocytes Model Derived from Induced Pluripotent Stem Cells.', *Cells*. Switzerland, 9(12). doi: 10.3390/cells9122680.

Levy, R. *et al.* (2000) 'High-frequency synchronization of neuronal activity in the subthalamic nucleus of parkinsonian patients with limb tremor.', *The Journal of neuroscience : the official journal of the Society for Neuroscience*. United States, 20(20), pp. 7766–7775. doi: 10.1523/JNEUROSCI.20-20-07766.2000.

Li, R. *et al.* (2020) 'Growth factors-based therapeutic strategies and their underlying signaling mechanisms for peripheral nerve regeneration', *Acta Pharmacologica Sinica*, 41(10), pp. 1289–1300. doi: 10.1038/s41401-019-0338-1.

Li, Y. *et al.* (2009) 'Mutant LRRK2(R1441G) BAC transgenic mice recapitulate cardinal features of Parkinson's disease.', *Nature neuroscience*. United States, 12(7), pp. 826–828. doi: 10.1038/nn.2349.

Li, Y. *et al.* (2017) 'Induction of Expansion and Folding in Human Cerebral Organoids.', *Cell stem cell*. United States, 20(3), pp. 385-396.e3. doi: 10.1016/j.stem.2016.11.017.

Liang, L., DeLong, M. R. and Papa, S. M. (2008) 'Inversion of dopamine responses in striatal medium spiny neurons and involuntary movements.', *The Journal of neuroscience : the official journal of the Society for Neuroscience*. United States, 28(30), pp. 7537–7547. doi: 10.1523/JNEUROSCI.1176-08.2008.

Lieberman, O. J. *et al.* (2018) 'Dopamine Triggers the Maturation of Striatal Spiny Projection Neuron Excitability during a Critical Period.', *Neuron*, 99(3), pp. 540-554.e4. doi: 10.1016/j.neuron.2018.06.044.

Lin, L. *et al.* (2016) 'Molecular Features Underlying Neurodegeneration Identified through In Vitro Modeling of Genetically Diverse Parkinson's Disease Patients.', *Cell reports*. United States, 15(11), pp. 2411–2426. doi: 10.1016/j.celrep.2016.05.022.

Little, S. and Brown, P. (2014) 'The functional role of beta oscillations in Parkinson's disease.', *Parkinsonism & related disorders*. England, 20 Suppl 1, pp. S44-8. doi: 10.1016/S1353-8020(13)70013-0.

Lonart, G. *et al.* (2003) 'Phosphorylation of RIM1alpha by PKA triggers presynaptic long-term potentiation at cerebellar parallel fiber synapses.', *Cell*. United States, 115(1), pp. 49–60. doi: 10.1016/s0092-8674(03)00727-x.

Lu, J. *et al.* (2010) 'Decreased glucocerebrosidase activity in Gaucher disease parallels quantitative enzyme loss due to abnormal interaction with TCP1 and c-Cbl.', *Proceedings of the National Academy of Sciences of the United States of America*. United States, 107(50), pp. 21665–21670. doi: 10.1073/pnas.1014376107.

Lu, P. *et al.* (2012) 'Motor axonal regeneration after partial and complete spinal cord transection.', *The Journal of neuroscience : the official journal of the Society for Neuroscience*. United States, 32(24), pp. 8208–8218. doi: 10.1523/JNEUROSCI.0308-12.2012.

Ma, T. *et al.* (2013) 'Subcortical origins of human and monkey neocortical interneurons', *Nature Neuroscience*, 16(11), pp. 1588–1597. doi: 10.1038/nn.3536.

Ma, Y. *et al.* (2002) 'Parametric mapping of [18F]FPCIT binding in early stage Parkinson's

disease: a PET study.', *Synapse (New York, N.Y.)*. United States, 45(2), pp. 125–133. doi: 10.1002/syn.10090.

MacAskill, A. F. *et al.* (2012) 'Subcellular connectivity underlies pathway-specific signaling in the nucleus accumbens', *Nature Neuroscience*, 15(12), pp. 1624–1626. doi: 10.1038/nn.3254.

Magnin, M., Morel, A. and Jeanmonod, D. (2000) 'Single-unit analysis of the pallidum, thalamus and subthalamic nucleus in parkinsonian patients.', *Neuroscience*. United States, 96(3), pp. 549–564. doi: 10.1016/s0306-4522(99)00583-7.

Mahar, M. and Cavalli, V. (2018) 'Intrinsic mechanisms of neuronal axon regeneration', *Nature Reviews Neuroscience*, 19(6), pp. 323–337. doi: 10.1038/s41583-018-0001-8.

La Manno, G. *et al.* (2016) 'Molecular Diversity of Midbrain Development in Mouse, Human, and Stem Cells.', *Cell*, 167(2), pp. 566-580.e19. doi: 10.1016/j.cell.2016.09.027.

Marin, O., Anderson, S. A. and Rubenstein, J. L. (2000) 'Origin and molecular specification of striatal interneurons.', *The Journal of neuroscience : the official journal of the Society for Neuroscience*. United States, 20(16), pp. 6063–6076. doi: 10.1523/JNEUROSCI.20-16-06063.2000.

Martina, J. A. *et al.* (2012) 'MTORC1 functions as a transcriptional regulator of autophagy by preventing nuclear transport of TFEB.', *Autophagy*, 8(6), pp. 903–914. doi: 10.4161/auto.19653.

Di Martino, A. *et al.* (2008) 'Functional connectivity of human striatum: a resting state FMRI study.', *Cerebral cortex (New York, N.Y. : 1991)*. United States, 18(12), pp. 2735–2747. doi: 10.1093/cercor/bhn041.

Matamales, M. *et al.* (2009) 'Striatal medium-sized spiny neurons: identification by nuclear staining and study of neuronal subpopulations in BAC transgenic mice.', *PloS one*. United States, 4(3), p. e4770. doi: 10.1371/journal.pone.0004770.

Matsuda, W. *et al.* (2009) 'Single nigrostriatal dopaminergic neurons form widely spread and highly dense axonal arborizations in the neostriatum.', *The Journal of neuroscience : the official journal of the Society for Neuroscience*. United States, 29(2), pp. 444–453. doi: 10.1523/JNEUROSCI.4029-08.2009.

McGregor, M. M. and Nelson, A. B. (2019) 'Circuit Mechanisms of Parkinson's Disease.', *Neuron*. United States, 101(6), pp. 1042–1056. doi: 10.1016/j.neuron.2019.03.004.

McQuin, C. *et al.* (2018) 'CellProfiler 3.0: Next-generation image processing for biology.', *PLoS biology*. United States, 16(7), p. e2005970. doi: 10.1371/journal.pbio.2005970.

Meissner, W. *et al.* (2003) 'Time-course of nigrostriatal degeneration in a progressive MPTP-lesioned macaque model of Parkinson's disease.', *Molecular neurobiology*. United States, 28(3), pp. 209–218. doi: 10.1385/MN:28:3:209.

Melamed, Z. *et al.* (2019) 'Premature polyadenylation-mediated loss of stathmin-2 is a hallmark of TDP-43-dependent neurodegeneration', *Nature Neuroscience*, 22(2), pp. 180–190. doi: 10.1038/s41593-018-0293-z.

Meredith, G. E. *et al.* (1999) 'Immunocytochemical characterization of catecholaminergic neurons in the rat striatum following dopamine-depleting lesions.', *The European journal of neuroscience*. France, 11(10), pp. 3585–3596. doi: 10.1046/j.1460-9568.1999.00774.x.

Métin, C. *et al.* (1997) 'A role for netrin-1 in the guidance of cortical efferents.', *Development (Cambridge, England)*. England, 124(24), pp. 5063–5074. doi: 10.1242/dev.124.24.5063.

Miller, F. D. and Gauthier, A. S. (2007) 'Timing Is Everything: Making Neurons versus Glia in the Developing Cortex', *Neuron*, 54(3), pp. 357–369. doi: https://doi.org/10.1016/j.neuron.2007.04.019.

Mink, J. W. (1996) 'The basal ganglia: focused selection and inhibition of competing motor programs.', *Progress in neurobiology*. England, 50(4), pp. 381–425. doi: 10.1016/s0301-0082(96)00042-1.

Mink, J. W. and Thach, W. T. (1993) 'Basal ganglia intrinsic circuits and their role in behavior.', *Current opinion in neurobiology*. England, 3(6), pp. 950–957. doi: 10.1016/0959-4388(93)90167-w.

Miura, Y. *et al.* (2020) 'Generation of human striatal organoids and cortico-striatal assembloids from human pluripotent stem cells.', *Nature biotechnology*, 38(12), pp. 1421–1430. doi: 10.1038/s41587-020-00763-w.

Mohamed, N.-V. *et al.* (2021) 'Midbrain organoids with an SNCA gene triplication model key features of synucleinopathy.', *Brain communications*. England, 3(4), p. fcab223. doi: 10.1093/braincomms/fcab223.

Moloney, E. B., de Winter, F. and Verhaagen, J. (2014) 'ALS as a distal axonopathy: molecular mechanisms affecting neuromuscular junction stability in the presymptomatic stages of the disease.', *Frontiers in neuroscience*. Switzerland, 8, p. 252. doi: 10.3389/fnins.2014.00252.

Muda, K. *et al.* (2014) 'Parkinson-related LRRK2 mutation R1441C/G/H impairs PKA phosphorylation of LRRK2 and disrupts its interaction with 14-3-3.', *Proceedings of the National Academy of Sciences of the United States of America*, 111(1), pp. E34-43. doi: 10.1073/pnas.1312701111.

Muguruma, K. *et al.* (2015) 'Self-organization of polarized cerebellar tissue in 3D culture of human pluripotent stem cells.', *Cell reports*. United States, 10(4), pp. 537–550. doi: 10.1016/j.celrep.2014.12.051.

Muñoz, E. *et al.* (1997) 'Identification of Spanish familial Parkinson's disease and screening for the Ala53Thr mutation of the alpha-synuclein gene in early onset patients.', *Neuroscience letters*. Ireland, 235(1–2), pp. 57–60. doi: 10.1016/s0304-3940(97)00710-6.

Nagatsu, T., Levitt, M. and Udenfriend, S. (1964) 'TYROSINE HYDROXYLASE. THE INITIAL STEP IN NOREPINEPHRINE BIOSYNTHESIS.', *The Journal of biological chemistry*. United States, 239, pp. 2910–2917.

Nagy, G. *et al.* (2004) 'Regulation of releasable vesicle pool sizes by protein kinase A-dependent phosphorylation of SNAP-25.', *Neuron*. United States, 41(3), pp. 417–429. doi: 10.1016/s0896-6273(04)00038-8.

Nakagawa, M. *et al.* (2008) 'Generation of induced pluripotent stem cells without Myc from mouse and human fibroblasts.', *Nature biotechnology*. United States, 26(1), pp. 101–106. doi: 10.1038/nbt1374.

Nalls, M. A. *et al.* (2011) 'Imputation of sequence variants for identification of genetic risks for Parkinson's disease: a meta-analysis of genome-wide association studies.', *Lancet (London, England)*. England, 377(9766), pp. 641–649. doi: 10.1016/S0140-6736(10)62345-8.

Nalls, M. A. *et al.* (2019) 'Identification of novel risk loci, causal insights, and heritable risk for Parkinson's disease: a meta-analysis of genome-wide association studies.', *The Lancet. Neurology*. England, 18(12), pp. 1091–1102. doi: 10.1016/S1474-4422(19)30320-5.

Nambu, A., Tachibana, Y. and Chiken, S. (2015) 'Cause of parkinsonian symptoms: Firing rate, firing pattern or dynamic activity changes?', *Basal Ganglia*, 5(1), pp. 1–6. doi: https://doi.org/10.1016/j.baga.2014.11.001.

Nandhagopal, R. *et al.* (2009) 'Longitudinal progression of sporadic Parkinson's disease: a multi-tracer positron emission tomography study.', *Brain : a journal of neurology*. England, 132(Pt 11), pp. 2970–2979. doi: 10.1093/brain/awp209.

Narsinh, K. H. *et al.* (2011) 'Single cell transcriptional profiling reveals heterogeneity of human induced pluripotent stem cells.', *The Journal of clinical investigation*. United States, 121(3), pp. 1217–1221. doi: 10.1172/JCI44635.

Neto, E. *et al.* (2016) 'Compartmentalized Microfluidic Platforms: The Unrivaled Breakthrough of In Vitro Tools for Neurobiological Research.', *The Journal of neuroscience : the official journal of the Society for Neuroscience*. United States, 36(46), pp. 11573–11584. doi: 10.1523/JNEUROSCI.1748-16.2016.

Nguyen, H. N. *et al.* (2011) 'LRRK2 mutant iPSC-derived DA neurons demonstrate increased susceptibility to oxidative stress.', *Cell stem cell*, 8(3), pp. 267–280. doi: 10.1016/j.stem.2011.01.013.

Nicola, S. M., Surmeier, D. J. and Malenka, R. C. (2000) 'Dopaminergic Modulation of Neuronal Excitability in the Striatum and Nucleus Accumbens', *Annual Review of Neuroscience*. Annual Reviews, 23(1), pp. 185–215. doi: 10.1146/annurev.neuro.23.1.185.

Nicoleau, C. *et al.* (2013) 'Embryonic stem cells neural differentiation qualifies the role of Wnt/β-Catenin signals in human telencephalic specification and regionalization', *STEM CELLS*. John Wiley & Sons, Ltd, 31(9), pp. 1763–1774. doi: 10.1002/stem.1462.

Nikolov, D. B. *et al.* (1996) 'Crystal structure of a human TATA box-binding protein/TATA element complex.', *Proceedings of the National Academy of Sciences of the United States of America*. United States, 93(10), pp. 4862–4867. doi: 10.1073/pnas.93.10.4862.

Okita, K. *et al.* (2013) 'An efficient nonviral method to generate integration-free human-induced pluripotent stem cells from cord blood and peripheral blood cells.', *Stem cells (Dayton, Ohio)*. England, 31(3), pp. 458–466. doi: 10.1002/stem.1293.

Oliveira, L. M. A. *et al.* (2015) 'Elevated α-synuclein caused by SNCA gene triplication impairs neuronal differentiation and maturation in Parkinson's patient-derived induced pluripotent stem cells.', *Cell death & disease*. England, 6(11), p. e1994. doi: 10.1038/cddis.2015.318.

Oswal, A. *et al.* (2021) 'Neural signatures of hyperdirect pathway activity in Parkinson's disease', *Nature Communications*, 12(1), p. 5185. doi: 10.1038/s41467-021-25366-0.

Pan, W. X., Mao, T. and Dudman, J. T. (2010) 'Inputs to the dorsal striatum of the mouse reflect the parallel circuit architecture of the forebrain.', *Frontiers in neuroanatomy*. Switzerland, 4, p. 147. doi: 10.3389/fnana.2010.00147.

Paraskevopoulou, F., Herman, M. A. and Rosenmund, C. (2019) 'Glutamatergic Innervation

onto Striatal Neurons Potentiates GABAergic Synaptic Output.', *The Journal of neuroscience : the official journal of the Society for Neuroscience*, 39(23), pp. 4448–4460. doi: 10.1523/JNEUROSCI.2630-18.2019.

Parisiadou, L. *et al.* (2009) 'Phosphorylation of ezrin/radixin/moesin proteins by LRRK2 promotes the rearrangement of actin cytoskeleton in neuronal morphogenesis.', *The Journal of neuroscience : the official journal of the Society for Neuroscience*. United States, 29(44), pp. 13971–13980. doi: 10.1523/JNEUROSCI.3799-09.2009.

Parisiadou, L. *et al.* (2014) 'LRRK2 regulates synaptogenesis and dopamine receptor activation through modulation of PKA activity.', *Nature neuroscience*, 17(3), pp. 367–376. doi: 10.1038/nn.3636.

Park, J. *et al.* (2018) 'A 3D human triculture system modeling neurodegeneration and neuroinflammation in Alzheimer's disease', *Nature Neuroscience*, 21(7), pp. 941–951. doi: 10.1038/s41593-018-0175-4.

Parker, J. G. *et al.* (2018) 'Diametric neural ensemble dynamics in parkinsonian and dyskinetic states.', *Nature*, 557(7704), pp. 177–182. doi: 10.1038/s41586-018-0090-6.

Parr-Brownlie, L. C. and Hyland, B. I. (2005) 'Bradykinesia Induced by Dopamine D₂ Receptor Blockade Is Associated with Reduced Motor Cortex Activity in the Rat', *The Journal of Neuroscience*, 25(24), pp. 5700 LP – 5709. doi: 10.1523/JNEUROSCI.0523-05.2005.

Paulsen, B. *et al.* (2022) 'Autism genes converge on asynchronous development of shared neuron classes.', *Nature*. England, 602(7896), pp. 268–273. doi: 10.1038/s41586-021-04358-6.

Peixoto, R. T. *et al.* (2016) 'Early hyperactivity and precocious maturation of corticostriatal circuits in Shank3B−/− mice', *Nature Neuroscience*, 19(5), pp. 716–724. doi: 10.1038/nn.4260.

Penrod, R. D. *et al.* (2015) 'The presence of cortical neurons in striatal-cortical co-cultures alters the effects of dopamine and BDNF on medium spiny neuron dendritic development.', *Frontiers in cellular neuroscience*, 9, p. 269. doi: 10.3389/fncel.2015.00269.

Pessiglione, M. *et al.* (2005) 'Thalamic neuronal activity in dopamine-depleted primates: evidence for a loss of functional segregation within basal ganglia circuits.', *The Journal of neuroscience : the official journal of the Society for Neuroscience*. United States, 25(6), pp. 1523–1531. doi: 10.1523/JNEUROSCI.4056-04.2005.

Pischedda, F. *et al.* (2021) 'LRRK2 G2019S kinase activity triggers neurotoxic NSF aggregation.',

Brain : a journal of neurology. England, 144(5), pp. 1509–1525. doi: 10.1093/brain/awab073.

Poewe, W. (2008) 'Non-motor symptoms in Parkinson's disease.', *European journal of neurology*. England, 15 Suppl 1, pp. 14–20. doi: 10.1111/j.1468-1331.2008.02056.x.

Polito, C. *et al.* (2012) 'Interaction of caudate dopamine depletion and brain metabolic changes with cognitive dysfunction in early Parkinson's disease.', *Neurobiology of aging*. United States, 33(1), pp. 206.e29–39. doi: 10.1016/j.neurobiolaging.2010.09.004.

Pollen, A. A. *et al.* (2019) 'Establishing Cerebral Organoids as Models of Human-Specific Brain Evolution.', *Cell*. United States, 176(4), pp. 743-756.e17. doi: 10.1016/j.cell.2019.01.017.

Polo, J. M. *et al.* (2010) 'Cell type of origin influences the molecular and functional properties of mouse induced pluripotent stem cells.', *Nature biotechnology*. United States, 28(8), pp. 848–855. doi: 10.1038/nbt.1667.

Polymeropoulos, M. H. *et al.* (1996) 'Mapping of a gene for Parkinson's disease to chromosome 4q21-q23.', *Science (New York, N.Y.)*. United States, 274(5290), pp. 1197–1199. doi: 10.1126/science.274.5290.1197.

Porritt, M. J. *et al.* (2000) 'New dopaminergic neurons in Parkinson's disease striatum', *The Lancet*, 356(9223), pp. 44–45. doi: https://doi.org/10.1016/S0140-6736(00)02437-5.

Postuma, R. B. *et al.* (2012) 'Identifying prodromal Parkinson's disease: pre-motor disorders in Parkinson's disease.', *Movement disorders : official journal of the Movement Disorder Society*. United States, 27(5), pp. 617–626. doi: 10.1002/mds.24996.

Poulin, J.-F. *et al.* (2014) 'Defining midbrain dopaminergic neuron diversity by single-cell gene expression profiling.', *Cell reports*. United States, 9(3), pp. 930–943. doi: 10.1016/j.celrep.2014.10.008.

Prots, I. *et al.* (2018) 'α-Synuclein oligomers induce early axonal dysfunction in human iPSC-based models of synucleinopathies.', *Proceedings of the National Academy of Sciences of the United States of America*. United States, 115(30), pp. 7813–7818. doi: 10.1073/pnas.1713129115.

Qian, X. *et al.* (2016) 'Brain-Region-Specific Organoids Using Mini-bioreactors for Modeling ZIKV Exposure.', *Cell*. United States, 165(5), pp. 1238–1254. doi: 10.1016/j.cell.2016.04.032.

Quadrato, G. *et al.* (2017) 'Cell diversity and network dynamics in photosensitive human brain organoids.', *Nature*. England, 545(7652), pp. 48–53. doi: 10.1038/nature22047.

Quadri, M. *et al.* (2013) 'Mutation in the SYNJ1 gene associated with autosomal recessive, early-onset Parkinsonism.', *Human mutation*. United States, 34(9), pp. 1208–1215. doi: 10.1002/humu.22373.

Raff, M. C., Whitmore, A. V and Finn, J. T. (2002) 'Axonal self-destruction and neurodegeneration.', *Science (New York, N.Y.)*. United States, 296(5569), pp. 868–871. doi: 10.1126/science.1068613.

Rahmanzadeh, R. *et al.* (2021) 'Myelin and axon pathology in multiple sclerosis assessed by myelin water and multi-shell diffusion imaging.', *Brain : a journal of neurology*. England, 144(6), pp. 1684–1696. doi: 10.1093/brain/awab088.

Ramos-Gonzalez, P. *et al.* (2021) 'Astrocytic atrophy as a pathological feature of Parkinson's disease with LRRK2 mutation', *npj Parkinson's Disease*, 7(1), p. 31. doi: 10.1038/s41531-021-00175-w.

Reddy, S. D. N. *et al.* (2011) 'Multiple coregulatory control of tyrosine hydroxylase gene transcription', *Proceedings of the National Academy of Sciences*, 108(10), pp. 4200 LP – 4205. doi: 10.1073/pnas.1101193108.

Riboldi, G. M. and Di Fonzo, A. B. (2019) 'GBA, Gaucher Disease, and Parkinson's Disease: From Genetic to Clinic to New Therapeutic Approaches.', *Cells*, 8(4). doi: 10.3390/cells8040364.

Robinson, D. L., Heien, M. L. A. V and Wightman, R. M. (2002) 'Frequency of dopamine concentration transients increases in dorsal and ventral striatum of male rats during introduction of conspecifics.', *The Journal of neuroscience : the official journal of the Society for Neuroscience*. United States, 22(23), pp. 10477–10486. doi: 10.1523/JNEUROSCI.22-23-10477.2002.

Romano, G. *et al.* (2005) 'Characterization of five evolutionary conserved regions of the human tyrosine hydroxylase (TH) promoter: implications for the engineering of a human TH minimal promoter assembled in a self-inactivating lentiviral vector system.', *Journal of cellular physiology*. United States, 204(2), pp. 666–677. doi: 10.1002/jcp.20319.

Rosen, G. D. and Williams, R. W. (2001) 'Complex trait analysis of the mouse striatum: independent QTLs modulate volume and neuron number.', *BMC neuroscience*. England, 2, p. 5. doi: 10.1186/1471-2202-2-5.

Rosenbloom, B. *et al.* (2011) 'The incidence of Parkinsonism in patients with type 1 Gaucher disease: data from the ICGG Gaucher Registry.', *Blood cells, molecules & diseases*. United

States, 46(1), pp. 95–102. doi: 10.1016/j.bcmd.2010.10.006.

de Rus Jacquet, A. *et al.* (2021) 'The LRRK2 G2019S mutation alters astrocyte-to-neuron communication via extracellular vesicles and induces neuron atrophy in a human iPSC-derived model of Parkinson's disease', *eLife*. Edited by H. J. Bellen and H. Y. Zoghbi. eLife Sciences Publications, Ltd, 10, p. e73062. doi: 10.7554/eLife.73062.

Salvadores, N. *et al.* (2017) 'Axonal Degeneration during Aging and Its Functional Role in Neurodegenerative Disorders.', *Frontiers in neuroscience*. Switzerland, 11, p. 451. doi: 10.3389/fnins.2017.00451.

Sandor, C. *et al.* (2017) 'Transcriptomic profiling of purified patient-derived dopamine neurons identifies convergent perturbations and therapeutics for Parkinson's disease.', *Human molecular genetics*. England, 26(3), pp. 552–566. doi: 10.1093/hmg/ddw412.

Sardiello, M. *et al.* (2009) 'A gene network regulating lysosomal biogenesis and function.', *Science (New York, N.Y.)*. United States, 325(5939), pp. 473–477. doi: 10.1126/science.1174447.

Schiffmann, S. N., Lledo, P. M. and Vincent, J. D. (1995) 'Dopamine D1 receptor modulates the voltage-gated sodium current in rat striatal neurones through a protein kinase A.', *The Journal of physiology*, 483 (Pt 1(Pt 1), pp. 95–107. doi: 10.1113/jphysiol.1995.sp020570.

Schmidt, R. *et al.* (2013) 'Canceling actions involves a race between basal ganglia pathways.', *Nature neuroscience*. United States, 16(8), pp. 1118–1124. doi: 10.1038/nn.3456.

Schondorf, D. C. *et al.* (2014) 'iPSC-derived neurons from GBA1-associated Parkinson's disease patients show autophagic defects and impaired calcium homeostasis.', *Nature communications*. England, 5, p. 4028. doi: 10.1038/ncomms5028.

Schrader, L. A. *et al.* (2002) 'PKA modulation of Kv4.2-encoded A-type potassium channels requires formation of a supramolecular complex.', *The Journal of neuroscience : the official journal of the Society for Neuroscience*, 22(23), pp. 10123–10133. doi: 10.1523/JNEUROSCI.22-23-10123.2002.

Schrag, A. *et al.* (2003) 'Young- versus older-onset Parkinson's disease: impact of disease and psychosocial consequences.', *Movement disorders : official journal of the Movement Disorder Society*. United States, 18(11), pp. 1250–1256. doi: 10.1002/mds.10527.

Schulte, D. and Geerts, D. (2019) 'MEIS transcription factors in development and disease.', *Development (Cambridge, England)*. England, 146(16). doi: 10.1242/dev.174706.

Schuurmans, C. and Guillemot, F. (2002) 'Molecular mechanisms underlying cell fate specification in the developing telencephalon.', *Current opinion in neurobiology*. England, 12(1), pp. 26–34. doi: 10.1016/s0959-4388(02)00286-6.

Schwamborn, J. C. (2018) 'Is Parkinson's Disease a Neurodevelopmental Disorder and Will Brain Organoids Help Us to Understand It?', *Stem Cells and Development*. Mary Ann Liebert, Inc., publishers, 27(14), pp. 968–975. doi: 10.1089/scd.2017.0289.

Scott, W. K. *et al.* (1997) 'Genetic complexity and Parkinson's disease. Deane Laboratory Parkinson Disease Research Group.', *Science (New York, N.Y.)*. United States, pp. 387–8; author reply 389. doi: 10.1126/science.277.5324.387.

Segal, M., Greenberger, V. and Korkotian, E. (2003) 'Formation of dendritic spines in cultured striatal neurons depends on excitatory afferent activity', *European Journal of Neuroscience*, 17(12), pp. 2573–2585. doi: 10.1046/j.1460-9568.2003.02696.x.

Serra, P. A. *et al.* (2002) 'The neurotoxin 1-methyl-4-phenyl-1,2,3,6-tetrahydropyridine induces apoptosis in mouse nigrostriatal glia. Relevance to nigral neuronal death and striatal neurochemical changes.', *The Journal of biological chemistry*. United States, 277(37), pp. 34451–34461. doi: 10.1074/jbc.M202099200.

Sesack, S. R. and Grace, A. A. (2010) 'Cortico-Basal Ganglia reward network: microcircuitry.', *Neuropsychopharmacology : official publication of the American College of Neuropsychopharmacology*. England, 35(1), pp. 27–47. doi: 10.1038/npp.2009.93.

Sidransky, E. *et al.* (2009) 'Multicenter analysis of glucocerebrosidase mutations in Parkinson's disease.', *The New England journal of medicine*. United States, 361(17), pp. 1651–1661. doi: 10.1056/NEJMoa0901281.

Singh, A. *et al.* (2016) 'Human striatal recordings reveal abnormal discharge of projection neurons in Parkinson's disease.', *Proceedings of the National Academy of Sciences of the United States of America*. United States, 113(34), pp. 9629–9634. doi: 10.1073/pnas.1606792113.

Singh, F. *et al.* (2021) 'Pharmacological rescue of impaired mitophagy in Parkinson's disease-related LRRK2 G2019S knock-in mice.', *eLife*. England, 10. doi: 10.7554/eLife.67604.

Sloan, S. A. *et al.* (2017) 'Human Astrocyte Maturation Captured in 3D Cerebral Cortical Spheroids Derived from Pluripotent Stem Cells.', *Neuron*. United States, 95(4), pp. 779-790.e6. doi: 10.1016/j.neuron.2017.07.035.

Smith-Geater, C. *et al.* (2020) 'Aberrant Development Corrected in Adult-Onset Huntington's Disease iPSC-Derived Neuronal Cultures via WNT Signaling Modulation.', *Stem cell reports*, 14(3), pp. 406–419. doi: 10.1016/j.stemcr.2020.01.015.

Smith, Y. *et al.* (1994) 'Synaptic relationships between dopaminergic afferents and cortical or thalamic input in the sensorimotor territory of the striatum in monkey.', *The Journal of comparative neurology*. United States, 344(1), pp. 1–19. doi: 10.1002/cne.903440102.

Smith, Y. *et al.* (2004) 'The thalamostriatal system: a highly specific network of the basal ganglia circuitry.', *Trends in neurosciences*. England, 27(9), pp. 520–527. doi: 10.1016/j.tins.2004.07.004.

Soitu, C. *et al.* (2018) 'Microfluidic chambers using fluid walls for cell biology.', *Proceedings of the National Academy of Sciences of the United States of America*. United States, 115(26), pp. E5926–E5933. doi: 10.1073/pnas.1805449115.

Soitu, C. *et al.* (2019) 'Raising fluid walls around living cells.', *Science advances*. United States, 5(6), p. eaav8002. doi: 10.1126/sciadv.aav8002.

Soitu, C. *et al.* (2021) 'Creating wounds in cell monolayers using micro-jets.', *Biomicrofluidics*. United States, 15(1), p. 14108. doi: 10.1063/5.0043312.

Song, X.-Y. *et al.* (2008) 'Peripherally-derived BDNF promotes regeneration of ascending sensory neurons after spinal cord injury.', *PloS one*. United States, 3(3), p. e1707. doi: 10.1371/journal.pone.0001707.

Sonninen, T.-M. *et al.* (2020) 'Metabolic alterations in Parkinson's disease astrocytes', *Scientific Reports*, 10(1), p. 14474. doi: 10.1038/s41598-020-71329-8.

Soto, C. (2003) 'Unfolding the role of protein misfolding in neurodegenerative diseases', *Nature Reviews Neuroscience*, 4(1), pp. 49–60. doi: 10.1038/nrn1007.

Spillantini, M. G. *et al.* (1997) 'Alpha-synuclein in Lewy bodies.', *Nature*. England, pp. 839–840. doi: 10.1038/42166.

Stanslowsky, N. *et al.* (2016) 'Neuronal Dysfunction in iPSC-Derived Medium Spiny Neurons from Chorea-Acanthocytosis Patients Is Reversed by Src Kinase Inhibition and F-Actin Stabilization.', *The Journal of neuroscience : the official journal of the Society for Neuroscience*. United States, 36(47), pp. 12027–12043. doi: 10.1523/JNEUROSCI.0456-16.2016.

Stauffer, W. R. *et al.* (2016) 'Dopamine Neuron-Specific Optogenetic Stimulation in Rhesus

Macaques.', *Cell*, 166(6), pp. 1564-1571.e6. doi: 10.1016/j.cell.2016.08.024.

Stefanis, L. (2012) 'α-Synuclein in Parkinson's disease.', *Cold Spring Harbor perspectives in medicine*. United States, 2(2), p. a009399. doi: 10.1101/cshperspect.a009399.

Strauss, K. M. *et al.* (2005) 'Loss of function mutations in the gene encoding Omi/HtrA2 in Parkinson's disease.', *Human molecular genetics*. England, 14(15), pp. 2099–2111. doi: 10.1093/hmg/ddi215.

Subramaniam, M. *et al.* (2014) 'Mutant α-Synuclein Enhances Firing Frequencies in Dopamine Substantia Nigra Neurons by Oxidative Impairment of A-Type Potassium Channels', *The Journal of Neuroscience*, 34(41), pp. 13586 LP – 13599. doi: 10.1523/JNEUROSCI.5069-13.2014.

Sulzer, D. *et al.* (2000) 'Neuromelanin biosynthesis is driven by excess cytosolic catecholamines not accumulated by synaptic vesicles.', *Proceedings of the National Academy of Sciences of the United States of America*. United States, 97(22), pp. 11869–11874. doi: 10.1073/pnas.97.22.11869.

Surmeier, D. J. and Kitai, S. T. (1993) 'Chapter 20 D1 and D2 dopamine receptor modulation of sodium and potassium currents in rat neostriatal neurons', in Arbuthnott, G. W. and Emson, P. C. B. T.-P. in B. R. (eds) *Chemical Signalling in the Basal Ganglia*. Elsevier, pp. 309–324. doi: https://doi.org/10.1016/S0079-6123(08)61354-0.

Svoboda, D. S. *et al.* (2019) 'Human iPSC-derived microglia assume a primary microglia-like state after transplantation into the neonatal mouse brain.', *Proceedings of the National Academy of Sciences of the United States of America*. United States, 116(50), pp. 25293–25303. doi: 10.1073/pnas.1913541116.

Tachibana, Y. *et al.* (2011) 'Subthalamo-pallidal interactions underlying parkinsonian neuronal oscillations in the primate basal ganglia.', *The European journal of neuroscience*. France, 34(9), pp. 1470–1484. doi: 10.1111/j.1460-9568.2011.07865.x.

Taguchi, Y. V *et al.* (2017) 'Glucosylsphingosine Promotes α-Synuclein Pathology in Mutant GBA-Associated Parkinson's Disease.', *The Journal of neuroscience : the official journal of the Society for Neuroscience*, 37(40), pp. 9617–9631. doi: 10.1523/JNEUROSCI.1525-17.2017.

Takahashi, K. and Yamanaka, S. (2006) 'Induction of pluripotent stem cells from mouse embryonic and adult fibroblast cultures by defined factors.', *Cell*. United States, 126(4), pp. 663–676. doi: 10.1016/j.cell.2006.07.024.

Tam, R. W. and Keung, A. J. (2022) 'Human Pluripotent Stem Cell-Derived Medium Spiny

Neuron-like Cells Exhibit Gene Desensitization.', *Cells*. Switzerland, 11(9). doi: 10.3390/cells11091411.

Tao, X. *et al.* (2002) 'A calcium-responsive transcription factor, CaRF, that regulates neuronal activity-dependent expression of BDNF.', *Neuron*. United States, 33(3), pp. 383–395. doi: 10.1016/s0896-6273(01)00561-x.

Taylor, A. M. *et al.* (2005) 'A microfluidic culture platform for CNS axonal injury, regeneration and transport', *Nature Methods*, 2(8), pp. 599–605. doi: 10.1038/nmeth777.

Taylor, A. M., Menon, S. and Gupton, S. L. (2015) 'Passive microfluidic chamber for long-term imaging of axon guidance in response to soluble gradients.', *Lab on a chip*. England, 15(13), pp. 2781–2789. doi: 10.1039/c5lc00503e.

Tecuapetla, F. *et al.* (2014) 'Balanced activity in basal ganglia projection pathways is critical for contraversive movements.', *Nature communications*. England, 5, p. 4315. doi: 10.1038/ncomms5315.

Telezhkin, V. *et al.* (2016) 'Forced cell cycle exit and modulation of GABAA, CREB, and GSK3beta signaling promote functional maturation of induced pluripotent stem cell-derived neurons.', *American journal of physiology. Cell physiology*. United States, 310(7), pp. C520-41. doi: 10.1152/ajpcell.00166.2015.

Tepper, J. M. *et al.* (1998) 'Postnatal development of the rat neostriatum: electrophysiological, light- and electron-microscopic studies.', *Developmental neuroscience*. Switzerland, 20(2–3), pp. 125–145. doi: 10.1159/000017308.

Tepper, J. M. *et al.* (2010) 'Heterogeneity and diversity of striatal GABAergic interneurons.', *Frontiers in neuroanatomy*. Switzerland, 4, p. 150. doi: 10.3389/fnana.2010.00150.

Tepper, J. M. *et al.* (2018) 'Heterogeneity and Diversity of Striatal GABAergic Interneurons: Update 2018.', *Frontiers in neuroanatomy*. Switzerland, 12, p. 91. doi: 10.3389/fnana.2018.00091.

Tepper, J. M. and Bolam, J. P. (2004) 'Functional diversity and specificity of neostriatal interneurons', *Current Opinion in Neurobiology*, 14(6), pp. 685–692. doi: https://doi.org/10.1016/j.conb.2004.10.003.

Tian, Y. *et al.* (2021) 'Transgenic Mice Expressing Human α-Synuclein 1-103 Fragment as a Novel Model of Parkinson's Disease ', *Frontiers in Aging Neuroscience* . Available at: https://www.frontiersin.org/articles/10.3389/fnagi.2021.760781.

Tofaris, G. K. *et al.* (2006) 'Pathological changes in dopaminergic nerve cells of the substantia nigra and olfactory bulb in mice transgenic for truncated human alpha-synuclein(1-120): implications for Lewy body disorders.', *The Journal of neuroscience : the official journal of the Society for Neuroscience*. United States, 26(15), pp. 3942–3950. doi: 10.1523/JNEUROSCI.4965-05.2006.

Tong, Z. *et al.* (2015) 'A microfluidic neuronal platform for neuron axotomy and controlled regenerative studies', *RSC Advances*. The Royal Society of Chemistry, 5(90), pp. 73457–73466. doi: 10.1039/C5RA11522A.

Trujillo, C. A. *et al.* (2019) 'Complex Oscillatory Waves Emerging from Cortical Organoids Model Early Human Brain Network Development.', *Cell stem cell*. United States, 25(4), pp. 558-569.e7. doi: 10.1016/j.stem.2019.08.002.

Tsunemi, T. *et al.* (2020) 'Astrocytes Protect Human Dopaminergic Neurons from α-Synuclein Accumulation and Propagation', *The Journal of Neuroscience*, 40(45), pp. 8618 LP – 8628. doi: 10.1523/JNEUROSCI.0954-20.2020.

Tu, G. *et al.* (2016) 'Influence of cortical synaptic input on striatal neuronal dendritic arborization and sensitivity to excitotoxicity in corticostriatal coculture', *Journal of Neurophysiology*, 116(2), pp. 380–390. doi: 10.1152/jn.00933.2015.

Turner, R. S. and DeLong, M. R. (2000) 'Corticostriatal activity in primary motor cortex of the macaque.', *The Journal of neuroscience : the official journal of the Society for Neuroscience*. United States, 20(18), pp. 7096–7108. doi: 10.1523/JNEUROSCI.20-18-07096.2000.

Turney, S. G. and Bridgman, P. C. (2005) 'Laminin stimulates and guides axonal outgrowth via growth cone myosin II activity.', *Nature neuroscience*. United States, 8(6), pp. 717–719. doi: 10.1038/nn1466.

Uzquiano, A. *et al.* (2022) 'Proper acquisition of cell class identity in organoids allows definition of fate specification programs of the human cerebral cortex.', *Cell*. United States, 185(20), pp. 3770-3788.e27. doi: 10.1016/j.cell.2022.09.010.

Valsky, D. *et al.* (2020) 'What is the true discharge rate and pattern of the striatal projection neurons in Parkinson's disease and Dystonia?', *eLife*. England, 9. doi: 10.7554/eLife.57445.

Vanan, S. *et al.* (2020) 'Altered striatal dopamine levels in Parkinson's disease VPS35 D620N mutant transgenic aged mice', *Molecular Brain*, 13(1), p. 164. doi: 10.1186/s13041-020-00704-3.

Villalba, R. M., Lee, H. and Smith, Y. (2009) 'Dopaminergic denervation and spine loss in the striatum of MPTP-treated monkeys.', *Experimental neurology*. United States, 215(2), pp. 220–227. doi: 10.1016/j.expneurol.2008.09.025.

Virlogeux, A. *et al.* (2018) 'Reconstituting Corticostriatal Network on-a-Chip Reveals the Contribution of the Presynaptic Compartment to Huntington's Disease.', *Cell reports*. United States, 22(1), pp. 110–122. doi: 10.1016/j.celrep.2017.12.013.

Volpicelli-Daley, L. A. *et al.* (2011) 'Exogenous α-synuclein fibrils induce Lewy body pathology leading to synaptic dysfunction and neuron death.', *Neuron*. United States, 72(1), pp. 57–71. doi: 10.1016/j.neuron.2011.08.033.

Voorn, P. *et al.* (1988) 'The pre- and postnatal development of the dopaminergic cell groups in the ventral mesencephalon and the dopaminergic innervation of the striatum of the rat.', *Neuroscience*. United States, 25(3), pp. 857–887. doi: 10.1016/0306-4522(88)90041-3.

Wakabayashi, K. *et al.* (2007) 'The Lewy body in Parkinson's disease: molecules implicated in the formation and degradation of alpha-synuclein aggregates.', *Neuropathology : official journal of the Japanese Society of Neuropathology*. Australia, 27(5), pp. 494–506.

Walsh, E. J. *et al.* (2017) 'Microfluidics with fluid walls', *Nature Communications*, 8(1), p. 816. doi: 10.1038/s41467-017-00846-4.

Wang, M., Fones, L. and Cave, J. W. (2018) 'Conserved Upstream Regulatory Regions in Mammalian Tyrosine Hydroxylase.', *Molecular neurobiology*. United States, 55(9), pp. 7340–7351. doi: 10.1007/s12035-018-0936-9.

Wang, X. *et al.* (2017) 'The EF-1α promoter maintains high-level transgene expression from episomal vectors in transfected CHO-K1 cells.', *Journal of cellular and molecular medicine*. England, 21(11), pp. 3044–3054. doi: 10.1111/jcmm.13216.

Warren, L. *et al.* (2010) 'Highly efficient reprogramming to pluripotency and directed differentiation of human cells with synthetic modified mRNA.', *Cell stem cell*. United States, 7(5), pp. 618–630. doi: 10.1016/j.stem.2010.08.012.

Weisskopf, M. G. *et al.* (1994) 'Mediation of hippocampal mossy fiber long-term potentiation by cyclic AMP.', *Science (New York, N.Y.)*. United States, 265(5180), pp. 1878–1882. doi: 10.1126/science.7916482.

Wichmann, T. and Soares, J. (2006) 'Neuronal firing before and after burst discharges in the monkey basal ganglia is predictably patterned in the normal state and altered in

parkinsonism.', *Journal of neurophysiology*. United States, 95(4), pp. 2120–2133. doi: 10.1152/jn.01013.2005.

Wilhelm, J. C. *et al.* (2012) 'Cooperative roles of BDNF expression in neurons and Schwann cells are modulated by exercise to facilitate nerve regeneration.', *The Journal of neuroscience : the official journal of the Society for Neuroscience*. United States, 32(14), pp. 5002–5009. doi: 10.1523/JNEUROSCI.1411-11.2012.

Wilson, C. J. and Kawaguchi, Y. (1996) 'The origins of two-state spontaneous membrane potential fluctuations of neostriatal spiny neurons.', *The Journal of neuroscience : the official journal of the Society for Neuroscience*, 16(7), pp. 2397–2410. doi: 10.1523/JNEUROSCI.16-07-02397.1996.

Wong, S. C. *et al.* (1995) 'The 3' flanking region of the human tyrosine hydroxylase gene directs reporter gene expression in peripheral neuroendocrine tissues.', *Journal of neurochemistry*. England, 65(1), pp. 23–31. doi: 10.1046/j.1471-4159.1995.65010023.x.

Wong, T. H. *et al.* (2014) 'PRKAR1B mutation associated with a new neurodegenerative disorder with unique pathology', *Brain*, 137(5), pp. 1361–1373. doi: 10.1093/brain/awu067.

Woodard, C. M. *et al.* (2014) 'iPSC-derived dopamine neurons reveal differences between monozygotic twins discordant for Parkinson's disease.', *Cell reports*, 9(4), pp. 1173–1182. doi: 10.1016/j.celrep.2014.10.023.

Wu, J. *et al.* (1992) 'Site-directed mutagenesis of tyrosine hydroxylase. Role of serine 40 in catalysis.', *The Journal of biological chemistry*. United States, 267(36), pp. 25754–25758.

Wu, M. *et al.* (2018) 'A Chemical Recipe for Generation of Clinical-Grade Striatal Neurons from hESCs.', *Stem cell reports*, 11(3), pp. 635–650. doi: 10.1016/j.stemcr.2018.08.005.

Xenias, H. S. *et al.* (2015) 'Are striatal tyrosine hydroxylase interneurons dopaminergic?', *The Journal of neuroscience : the official journal of the Society for Neuroscience*. United States, 35(16), pp. 6584–6599. doi: 10.1523/JNEUROSCI.0195-15.2015.

Xu, R. *et al.* (2020) 'Human iPSC-derived mature microglia retain their identity and functionally integrate in the chimeric mouse brain', *Nature Communications*, 11(1), p. 1577. doi: 10.1038/s41467-020-15411-9.

Yang, L. *et al.* (2008) 'Attenuation of MPTP neurotoxicity by rolipram, a specific inhibitor of phosphodiesterase IV.', *Experimental neurology*, 211(1), pp. 311–314. doi: 10.1016/j.expneurol.2007.02.010.

Yang, W. *et al.* (2020) 'Current and projected future economic burden of Parkinson's disease in the U.S.', *npj Parkinson's Disease*, 6(1), p. 15. doi: 10.1038/s41531-020-0117-1.

Yao, Z. *et al.* (2017) 'A Single-Cell Roadmap of Lineage Bifurcation in Human ESC Models of Embryonic Brain Development.', *Cell stem cell*. United States, 20(1), pp. 120–134. doi: 10.1016/j.stem.2016.09.011.

Yaron, A. and Schuldiner, O. (2016) 'Common and Divergent Mechanisms in Developmental Neuronal Remodeling and Dying Back Neurodegeneration.', *Current biology : CB*. England, 26(13), pp. R628–R639. doi: 10.1016/j.cub.2016.05.025.

Yoon, S.-J. *et al.* (2019) 'Reliability of human cortical organoid generation', *Nature Methods*, 16(1), pp. 75–78. doi: 10.1038/s41592-018-0255-0.

Yu, J. *et al.* (2007) 'Induced pluripotent stem cell lines derived from human somatic cells.', *Science (New York, N.Y.)*. United States, 318(5858), pp. 1917–1920. doi: 10.1126/science.1151526.

Yu, T. W. and Bargmann, C. I. (2001) 'Dynamic regulation of axon guidance.', *Nature neuroscience*. United States, 4 Suppl, pp. 1169–1176. doi: 10.1038/nn748.

Yun, S. P. *et al.* (2018) 'α-Synuclein accumulation and GBA deficiency due to L444P GBA mutation contributes to MPTP-induced parkinsonism.', *Molecular neurodegeneration*, 13(1), p. 1. doi: 10.1186/s13024-017-0233-5.

Zaja-Milatovic, S. *et al.* (2005) 'Dendritic degeneration in neostriatal medium spiny neurons in Parkinson disease', *Neurology*, 64(3), pp. 545 LP – 547. doi: 10.1212/01.WNL.0000150591.33787.A4.

Zambon, F. *et al.* (2019) 'Cellular α-synuclein pathology is associated with bioenergetic dysfunction in Parkinson's iPSC-derived dopamine neurons.', *Human molecular genetics*. England, 28(12), pp. 2001–2013. doi: 10.1093/hmg/ddz038.

Zhou, F.-M., Wilson, C. J. and Dani, J. A. (2002) 'Cholinergic interneuron characteristics and nicotinic properties in the striatum.', *Journal of neurobiology*. United States, 53(4), pp. 590–605. doi: 10.1002/neu.10150.

Zimprich, A. *et al.* (2011) 'A mutation in VPS35, encoding a subunit of the retromer complex, causes late-onset Parkinson disease.', *American journal of human genetics*. United States, 89(1), pp. 168–175. doi: 10.1016/j.ajhg.2011.06.008.

Appendix

1. **Sequences of different variants of abridged human TH promoter-specific construct to be packaged into lentiviral backbone.**

pcTHv1.0

AGGCtcgaggcggccgcGGGTGTGGTAGCCGAGCCTGTAATCCCAGAATTTGGGGAGGCTAAGGACAAGC
TCAGGTGTTGGTAGAGTTCATCCCAGGCCCCAAAGTAATCACATGGCAAACAAGCCCTGTCTAAA
TATCACGGCGGCTGGGGCAGCGGCACGCAGCGGCCTGGAAATGTCAGCCGGGGGTGGGGGCTC
CTCCGAGCCCCGGGATTAGCAGAGGTACCTGAAGTGGGCTGTGGCCTTGCAATGAGATGTGATT
TGCTGTCAAAGCACAGCTGCCGCCTCGGTGAGTGACTAATGAGAACTGAATGCCGCTCTTATTGC
TTTTCACTCGACTAATTTGTCAGAGGCTGTCAAGAGCCAGGGGGAGGGGGCAGAGGGTGGGGA
CCGGAGGTCTGATTGAGTCACCGGCATGGGGGCGAGGCTGGGTGCCCGGAGGGGTCTGCAAGA
AACCAGGAGCACCTGGCAGGAACCACAAGGGCCTGCAACTGCTAATCCCTGATGCCCCCCACTG
TGTCGCTCTGGGCCTGACTTCCAAACACCCAATTATCCCTAAGTGCATCCGATCGACTGGCAGGG
CGGCTGTTCCGGGGCCCACCTCGTCCATGCGCTCCGCCCGCCCTGCTGTGGGGCTCCATCTGATG
GCCTCATTAGGGCTAATTGCTCTGGCATTTGGGTCTGACAGGGACGGCGGAGGCGCAGTGGCTC
ACGCCTGTAATCCCAGCACTTTGGGAGGCCGAGGCTCAATCATGGGTGGTCCAGACTGGAGTGA
AAGCACAACTGGCCCGGCAGGAAACCGAATTAAAAAGCAATATTTGTATCAGTGGAAGACATTT
GCTGAAAGGTTAAATCCACATCCGGACCCTGGCTGTCTCAGCCCCCCGCAGAGCACGAGCCCCTG
GTCCCCGCAAGCCCGCGGGCTGAGGATGATTCAGACAGGGCTGGGGAGTGAAGGCAATTAGAT
TCCACGGACGAGCCCTTTCTCCTGCGCCTCCCTCCTTCCTCACCCACCCCCGCCTCCATCAGGCACA
GCAGGCAGGGGTGGGGGATGTAAGGAGGGGAAGGTGGGGGACCCAGAGGGGGCTTTGACGT
CAGCTCAGCTTATAAGAGGCTGCTGGGCCAGGGCTGTGGAGACGGAGCCCGGACCTCCACACTG
AGCCATGCCCACCCCCGACGCCACCACGCCACAGGCCAAGGGCTTCCGCAGGGCCGTGTCTGAG
CTGGACGCCAAGCAGGCAGAGGCCATCATGGTAAGAGGGCAGGTAGGTGCCCGGCGGCCGCA
GTGGACCGGAGCCCAGGGCTGGTGCCAGCTGCCTCTGCTACTCCCCAGCCTGGCTGGCAGCCCC
AGGCTCAGGGTCCATGCAAACCCCTGGGACGCGGCGTGGATGTGGAGGCCTGGGCACAGCGGC
ATCCCCTGTGCCTGGTGTTTGAGTCCCTGTTGGGGGAGGGTGAGGTGATGCCTGTCCCTGTGTGT
GCCCCTCTTAGGCCGACCTCTCTCGGGGGTCGTGTGGGTCTCTGTGTCTTGTTTCATCTTGAATCT
TAACGATCGGAATGTGGAAACAAATCCATCCAAAAAATCCAAGATGGCCAGAGGTCCCCGGCTG
CTGCACCCAGCCCCCACCCTACTCCCACCTGCCCCTGCCTCCCTCTGCCCCAGCTGCCCTAGTCAGC
ACCCCAACCAGCCTGCCTGCTTGGGGAGGCAGCCCCAAGGCCCTTCCCAGGCTCTAGCAGCAGCT
CATGGTGGGGGGTCCTGGGCAAATAGGGGGCAAAATTCAAAGGGTATCTGGGCTCTGGGGTGA
TTCCCATTGGCCTGTTCCTCCCTTATTTCCCTCATTCATTCATTCATTCATTCATTCACCATGG

AGTCTGTGTTCCCTGTGACCTGCACTCGGAAGCCCTGTGTACAGGGGACTGTGTGGGCCAGGCT
GGATAATCGGGAGCTTTTCAGCCCACAGGAGGGGTCTTCGGTGCCTCCTTGGGCACTCAGAACCT
TGGGCTCCCTGGCACATTTAAAATGGGTTTTTATTTATGGACCTTGATTGAAATGTGGTGTGAGTT
GTAGCAGTGTCATTTCCAGGTACCTTCTCAGGGACACAGGGCGCCCTCCCCCGTCCTCCCCCGCCC
TCCCCTACCCTCCCCCACCAGGCTCCCCATCAGGCATCCCCTCCCCAGGGCGCCCCGGGGGGGGA
TCCACCGGTCGCCACCCGTACGgCTAGC.

pcTHv1.2

AGGCtcgaggcggccgcGGGTGTGGTAGCCGAGCCTGTAATCCCAGAATTTGGGGAGGCTAAGGACAAGC
TCAGGTGTTGGTAGAGTTCATCCCAGGCCCCAAAGTAATCACATGGCAAACAAGCCCTGTCTAAA
TATCACGGCGGCTGGGGCAGCGGCACGCAGCGGCCTGGAAATGTCAGCCGGGGGTGGGGGCTC
CTCCGAGCCCCGGGATTAGCAGAGGTACCTGAAGTGGGCTGTGGCCTTGCAATGAGATGTGATT
TGCTGTCAAAGCACAGCTGCCGCCTCGGTGAGTGACTAATGAGAACTGAATGCCGCTCTTATTGC
TTTTCACTCGACTAATTTGTCAGAGGCTGTCAAGAGCCAGGGGGAGGGGGCAGAGGGTGGGGA
CCGGAGGTCTGATTGAGTCACCGGCATGGGGGCGAGGCTGGGTGCCCGGAGGGGTCTGCAAGA
AACCAGGAGCACCTGGCAGGAACCACAAGGGCCTGCAACTGCTAATCCCTGATGCCCCCCACTG
TGTCGCTCTGGGCCTGACTTCCAAACACCCAATTATCCCTAAGTGCATCCGATCGACTGGCAGGG
CGGCTGTTCCGGGGCCCACCTCGTCCATGCGCTCCGCCCGCCCTGCTGTGGGGCTCCATCTGATG
GCCTCATTAGGGCTAATTGCTCTGGCATTTGGGTCTGACAGGGACGGCGGAGGCGCAGTGGCTC
ACGCCTGTAATCCCAGCACTTTGGGAGGCCGAGGCTCAATCATGGGTGGTCCAGACTGGAGTGA
AAGCACAACTGGCCCGGCAGGAAACCGAATTAAAAAGCAATATTTGTATCAGTGGAAGACATTT
GCTGAAAGGTTAAATCCACATCCGGACCCTGGCTGTCTCAGCCCCCCGCAGAGCACGAGCCCCTG
GTCCCCGCAAGCCCGCGGGCTGAGGATGATTCAGACAGGGCTGGGGAGTGAAGGCAATTAGAT
TCCACGGACGAGCCCTTTCTCCTGCGCCTCCCTCCTTCCTCACCCACCCCCGCCTCCATCAGGCACA
GCAGGCAGGGGTGGGGGATGTAAGGAGGGGAAGGTGGGGGACCCAGAGGGGGCTTTGACGT
CAGCTCAGCTTATAAGAGGCTGCTGGGCCAGGGCTGTGGAGACGGAGCCCGGACCTCCACACTG
AGCCATGCCCACCCCCGACGCCACCACGCCACAGGCCAAGGGCTTCCGCAGGGCCGTGTCTGAG
CTGGACGCCAAGCAGGCAGAGGCCATCATGGTAAGAGGGCAGGTAGGTGCCCGGCGGCCGCA
GTGGACCGGAGCCCAGGGCTGGTGCCAGCTGCCTCTGCTACTCCCCAGCCTGGCTGGCAGCCCC
AGGCTCAGGGTCCATGCAAACCCCTGGGACGCGGCGTGGATGTGGAGGCCTGGGCACAGCGGC
ATCCCCTGTGCCTGGTGTTTGAGTCCCTGTTGGGGGAGGGTGAGGTGATGCCTGTCCCTGTGTGT
GCCCCTCTTAGGCCGACCTCTCTCGGGGGTCGTGTGGGTCTCTGTGTCTTGTTTCATCTTGAATCT
TAACGATCGGAATGTGGAAACAAATCCATCCAAAAAATCCAAGATGGCCAGAGGTCCCCGGCTG
CTGCACCCAGCCCCCACCCTACTCCCACCTGCCCCTGCCTCCCTCTGCCCCAGCTGCCCTAGTCAGC
ACCCCAACCAGCCTGCCTGCTTGGGGAGGCAGCCCCAAGGCCCTTCCCAGGCTCTAGCAGCAGCT

CATGGTGGGGGGTCCTGGGCAAATAGGGGGCAAAATTCAAAGGGTATCTGGGCTCTGGGGTGA
TTCCCATTGGCCTGTTCCTCCCTTATTTCCCTCATTCATTCATTCATTCATTCATTCACCATGG
AGTCTGTGTTCCCTGTGACCTGCACTCGGAAGCCCTGTGTACAGGGGACTGTGTGGGCCAGGCT
GGATAATCGGGAGCTTTTCAGCCCACAGGAGGGGTCTTCGGTGCCTCCTTGGGCACTCAGAACCT
TGGGCTCCCTGGCACATTTAAAATGGGTTTTTATTTATGGACCTTGATTGAAATGTGGTGTGAGTT
GTAGCAGTGTCATTTCCAGGTACCTTCTCAGGGACACAGGGCGCCCTCCCCCGTCCTCCCCCGCCC
TCCCCTACCCTCCCCCACCAGGCTCCCCATCAGGCATCCCCTCCCCAGGGCGCCCCGGGGGGGGA
TCCACCGGTCGCCACCCGTACGgCTAGCGCCACC

pcTHv2.0

AGGCtcgaggcggccgcGGGTGTGGTAGCCGAGCCTGTAATCCCAGAATTTGGGGAGGCTAAGGACAAGC
TCAGGTGTTGGTAGAGTTCATCCCAGGCCCCAAAGTAATCACATGGCAAACAAGCCCTGTCTAAA
TATCACGGCGGCTGGGGCAGCGGCACGCAGCGGCCTGGAAATGTCAGCCGGGGGTGGGGGCTC
CTCCGAGCCCCGGGATTAGCAGAGGTACCTGAAGTGGGCTGTGGCCTTGCAATGAGATGTGATT
TGCTGTCAAAGCACAGCTGCCGCCTCGGTGAGTGACTAATGAGAACTGAATGCCGCTCTTATTGC
TTTTCACTCGACTAATTTGTCAGAGGCTGTCAAGAGCCAGGGGGAGGGGGCAGAGGGTGGGGA
CCGGAGGTCTGATTGAGTCACCGGCATGGGGGCGAGGCTGGGTGCCCGGAGGGGTCTGCAAGA
AACCAGGAGCACCTGGCAGGAACCACAAGGGCCTGCAACTGCTAATCCCTGATGCCCCCCACTG
TGTCGCTCTGGGCCTGACTTCCAAACACCCAATTATCCCTAAGTGCATCCGATCGACTGGCAGGG
CGGCTGTTCCGGGGCCCACCTCGTCCATGCGCTCCGCCCGCCCTGCTGTGGGGCTCCATCTGATG
GCCTCATTAGGGCTAATTGCTCTGGCATTTGGGTCTGACAGGGACGGCGGAGGCGCAGTGGCTC
ACGCCTGTAATCCCAGCACTTTGGGAGGCCGAGGCTCAATCATGGGTGGTCCAGACTGGAGTGA
AAGCACAACTGGCCCGGCAGGAAACCGAATTAAAAAGCAATATTTGTATCAGTGGAAGACATTT
GCTGAAAGGTTAAATCCACATCCGGACCCTGGCTGTCTCAGCCCCCCGCAGAGCACGAGCCCCTG
GTCCCCGCAAGCCCGCGGGCTGAGGATGATTCAGACAGGGCTGGGGAGTGAAGGCAATTAGAT
TCCACGGACGAGCCCTTTCTCCTGCGCCTCCCTCCTTCCTCACCCACCCCCGCCTCCATCAGGCACA
GCAGGCAGGGGTGGGGGATGTAAGGAGGGGAAGGTGGGGGACCCAGAGGGGGCTTTGACGT
CAGCTCAGCTTATAAGAGGCTGCTGGGCCAGGGCTGTGGAGACGGAGCCCGGACCTCCACACTG
AGCCATGCCCACCCCCGACGCCACCACGCCACAGGCCAAgCTAGCGCCACC